Enhancing Thermal Comfort in a Room Using Natural Ventilation, Phase Change Materials and Green Wall Biofilters

By

Peter Abdo

A thesis submitted in fulfillment of the requirements for the degree of

Doctor of Philosophy

School of Mechanical and Mechatronic Engineering

Faculty of Engineering and Information Technology

University of Technology Sydney

June 2019

Certificate of Original Authorship

I, Peter Abdo declare that this thesis, is submitted in fulfilment of the requirements for the award of Doctor of Philosophy, in the School of Mechanical and Mechatronic Engineering / Faculty of Engineering and Information Technology at the University of Technology Sydney.

This thesis is wholly my own work unless otherwise reference or acknowledged. In addition, I certify that all information sources and literature used are indicated in the thesis.

This document has not been submitted for qualifications at any other academic institution.

Signature   Production Note:
                 Signature removed prior to publication.

Date:

June 26, 2019

Acknowledgements

I would like to express my deep respect and appreciation for my supervisor Dr. B. Phuoc Huynh. He has provided me with efficient guidance, continuous support and constant encouragement. I also appreciate the help and advice provided by my co-supervisor Dr. Thanh Nguyen.

I would like to thank Mrs. Rahil Taghipour for her help with the computational work using Ansys Fluent. Her significant contribution is highly regarded and appreciated.

I would like to acknowledge the cooperation with Dr. Fraser Torpy and Dr. Peter Irga of the Plants and Environmental Quality Research Group, Faculty of Science, University of Technology Sydney. Our work together with the green wall modules has been successful and had generated several journal articles and peer reviewed conference proceedings. I would also like to thank Mr. Jock Gammon of Junglefy Pty Ltd. (www.junglefy.com.au) for providing the green wall modules and fans needed for experiments.

It is my pleasure to express my warm thanks to the mechanical engineering laboratory staff for their help and support with my experimental work, namely Mr. Vahik Avakian, Mr. Laurence Stonard and Mr. Jack Liang. I also acknowledge the help of Mr. Peter Tawadros, the mechanical engineering laboratory manager.

I would like to express my gratitude to all those who helped me throughout my PhD study specially Dr. Ali Braytee for his contribution with the statistical analysis, Dr. Yuhan Huang for his advice during the preparation of the three dimensional models for computations and Mr. Kyle Gabriel for creating the Raspberry Pi software and adjusting it several times as per our needs.

Finally, this research is supported by an Australian Government Research Training Program Scholarship.

To my parents and my brothers

List of publications

Following is a list of journal articles, peer reviewed conference proceedings and reports associated with my PhD research study:

Journal articles

1. **Abdo, P.**, Taghipour, R. & Huynh, B. P. (2019). Three Dimensional Simulation of Wind Driven Ventilation through a Windcatcher with Different Inlet Designs, *ASME Journal of Thermal Science and Engineering Applications*. **(Revision Under review)**

2. **Abdo, P.**, Huynh, B. P., Irga, P. J., & Torpy, F. R. (2019). Evaluation of air flow through an active green wall biofilter. *Urban Forestry and Urban Greening*, *41*, 75-84. doi:10.1016/j.ufug.2019.03.013

3. Pettit, T., Irga, P. J., **Abdo, P.**, & Torpy, F. R. (2017). Do the plants in functional green walls contribute to their ability to filter particulate matter?. *Building and Environment*, *125*, 299-307. doi:10.1016/j.buildenv.2017.09.004

4. Irga, P. J., Paull, N. J., **Abdo, P.**, & Torpy, F. R. (2017). An assessment of the atmospheric particle removal efficiency of an in room botanical biofilter system. *BUILDING AND ENVIRONMENT*, *115*, 281-290. doi:10.1016/j.buildenv.2017.01.035

5. Irga, P. J., **Abdo, P.**, Zavattaro, M., & Torpy, F. R. (2017). An assessment of the potential fungal bioaerosol production from an active living wall. *BUILDING AND ENVIRONMENT*, *111*, 140-146. doi:10.1016/j.buildenv.2016.11.004

Peer Reviewed Conference Proceedings

6. **Abdo, P.**, Huynh, B. P., Braytee A., & Taghipour, R. (2019). EFFECT OF PHASE CHANGE MATERIAL ON TEMPERATURE IN A ROOM FITTED WITH A WINDCATCHER. In *Proceedings of the ASME 2019 International Mechanical Engineering Congress and Exposition (IMECE2019)*. Salt Lake City, UT, USA: The American Society of Mechanical Engineers (ASME).

7. **Abdo, P.**, Taghipour, R., & Huynh, B. P. (2019). THREE DIMENSIONAL SIMULATION OF THE EFFECT OF WINDCATCHER`S INLET SHAPE. In *Proceedings of the ASME - JSME - KSME Joint Fluids Engineering Conference 2019*. San Francisco, CA, USA

8. **Abdo, P.**, Taghipour, R., & Huynh, B. P. (2019). THREE DIMENSIONAL SIMULATION OF VENTILATION FLOW THROUGH A SOLAR WINDCATCHER. In *Proceedings of the ASME - JSME - KSME Joint Fluids Engineering Conference 2019*. San Francisco, CA, USA.

9. **Abdo, P.**, Taghipour, R., & Huynh, B. P. (2018). Simulation of Buoyancy Driven and Winddriven Ventilation Flow in a Three Dimensional Room Fitted with a Windcatcher. In T. C. W. Lau, & R. M. Kelso (Eds.), *Proceedings of the 21st Australasian Fluid Mechanics Conference*. Adelaide, Australia: The Australasian Fluid Mechanics Society.

10. **Abdo, P.**, Huynh, B. P., & Avakian, V. (2018). EFFECT OF GREEN WALL MODULES ON AIR TEMPERATURE AND HUMIDITY. In *Proceedings of the ASME 2018 5th Joint US-European Fluids Engineering Division Summer Meeting (FEDSM2018)*. Montreal, Quebec, Canada: The American Society of Mechanical Engineers (ASME). doi:10.1115/FEDSM2018-83139

11. Taghipour, R., **Abdo, P.**, & Huynh, B. P. (2018). Effect of Wind Speed on Ventilation Flow Through a Two Dimensional Room Fitted With a Windcatcher. In *Proceedings of the ASME 2018 International Mechanical Engineering Congress and Exposition (IMECE2018)*. Pittsburgh, PA, USA: The American Society of Mechanical Engineers (ASME). doi:10.1115/imece2018-88666

12. **Abdo, P.**, Taghipour, R., & Huynh, B. P. (2018). EFFECT OF WINDCATCHER'S INLET SHAPE ON VENTILATION FLOW THROUGH A TWO DIMENSIONAL ROOM. In *Proceedings of the ASME 2018 5th Joint US-European Fluids Engineering Division Summer Meeting (FEDSM2018)*. Montreal, Quebec, Canada: The American Society of Mechanical Engineers (ASME). doi:10.1115/FEDSM2018-83141

13. **Abdo, P.**, Huynh, B. P., & Avakian, V. (2018). Effect of Fan Speed on Air Flow through a Green Wall Module. In *Proceedings of the ASME 2018 5th Joint US-European Fluids Engineering Division Summer Meeting (FEDSM2018)*. Montreal, Quebec, Canada: The American Society of Mechanical Engineers (ASME). doi:10.1115/FEDSM2018-83199

14. **Abdo, P.**, & Huynh, B. P. (2018). Effect of passive green wall modules on air temperature and humidity. In *ASME International Mechanical Engineering Congress and Exposition, Proceedings (IMECE)* Vol. 7. Pittsburgh, Pennsylvania. doi:10.1115/IMECE2018-86963

15. **Abdo, P.**, Huynh, B. P., & Avakian, V. (2017). Distribution of Air Flow through a Green Wall Module. In *ASME 2017 Fluids Engineering Division Summer Meeting* Vol. 1B. Waikoloa, Hawaii, USA. doi:10.1115/FEDSM2017-69134

16. **Abdo, P.**, & Huynh, B. P. (2017). Effect of combining buoyancy driven and winddriven ventilation in a two dimensional room fitted with a windcatcher. In *ASME International Mechanical Engineering Congress and Exposition, Proceedings (IMECE)* Vol. 7 (pp. 1-7). USA: AMSE. doi:10.1115/IMECE2017-70212

17. **Abdo, P.**, Huynh, B. P., Avakian, V., Nguyen, T. T., Gammon, J., Torpy, F. R., & Irga, P. J. (2016). Measurement of air flow through a green-wall module. In *Proceedings of the 20th Australasian Fluid Mechanics Conference*. Perth: Australasian Fluid Mechanics Society.

Reports

18. Irga, P. J., Paull, N. J., **Abdo, P.**, Huynh, B. P., Avakian, V., Nguyen, T., & Torpy, F. (2017). *DEVELOPING THE JUNGLEFY BREATHING WALL FOR ENHANCED INDOOR AIR QUALITY REMEDIATION*. Sydney, Australia.

19. Pettit, T., Irga, P., **Abdo, P.**, Huynh, B., Stephen, J., & Torpy, F. R. (2017). *DEVELOPMENT AND AUGMENTATION THE JUNGLEFY BREATHING WALL*. Sydney, Australia: UTS.

Table of Contents

List of Tables

List of Figures

xv

Nomenclature

Symbols

C_l, C_2, σ_k, and σ_ε : Realisable K-ε model constants, dimensionless

C_p: Air specific heat [J/(kg K)]

K: Turbulent kinetic energy [m^2/s^2]

k: Air thermal conductivity [W/(m K)]

L: Characteristic length [m]

T: Temperature [K]

T_o: Reference Temperature [K]

Pr_t: Turbulent Prandtl number

κ: Von Karman constant [dimensionless]

ε: Dissipation rate of turbulent kinetic energy [m^2/s^3]

ρ: Air density [kg/m^3]

μ: Air dynamic viscosity [Pa s]

υ: Air kinematic viscosity [m^2/s]

β: Thermal expansion coefficient [1/K]

A: Area [m^2]

B: A constant

C: A constant

D: Diameter [m]

K: Loss coefficient

P: Gauge pressure reading [Pa]

Q: Air flow rate [L/s or m^3/s]

Subscripts

F-L: Funnels, large

F-S: Funnels, small

Free: No funnels used; the module is free

Dry: Dry condition

Wet: Wet (saturated) condition

S: Plant-growing medium (Soil replacement)

Acronyms

ADC: Analogue to Digital Convertor

CFD: Computational Fluid Dynamics

DNS: Direct Numerical Simulation

FVM: Finite Volume Method

GUI: Graphical User Interface

HVAC: Heating, Ventilation and Air Conditioning

IAQ: Indoor Air Quality

LES: Large Eddy Simulation

LWS: Living Wall Systems

MUX: Multiplexer

PCM: Phase Change Material

PM: Particulate Matter

RANS: Reynolds Averaged Navier-Stokes

RNG: Re-Normalisation Group

SBS: Sick Building Syndrome

VOCs: Volatile Organic Compounds

Abstract

Natural ventilation is the process of supplying and removing air through an indoor space by natural means. There are two types of natural ventilation occurring in buildings: wind-driven ventilation and buoyancy-driven ventilation. Efficient design for natural ventilation in buildings should implement both types of ventilation. Furthermore the architectural design of the windcatcher inlet affects its performance and influences the occupant's human comfort. Combining the wind-driven and the buoyancy-driven ventilation will be investigated in this study using a windcatcher natural ventilation system. The effect of the windcatcher's inlet design is also investigated to achieve better air flow and to increase the efficiency of windcatchers. Experimental studies of windcatcher systems are very costly and mostly impossible in practice. CFD (computational fluid dynamics) tools will be used in this research to simulate the air flow through a two sided windcatcher. Two dimensional and three dimensional simulations are performed using Ansys Fluent and CFD Ace + to obtain quantitative and qualitative analysis of velocity magnitude, flow patterns and ventilation flow rate.

Furthermore, the increased pollution levels in cities highlights the importance of innovative strategies that can help to improve the quality of air introduced into buildings.
Green walls have recently been used to help with this and even thermal comfort. Enhancing the flow distribution and air flow rate through active green wall modules will be studied in this research considering the different parameters involved such as module geometry, moisture content, growing-medium-plant-roots mix and plant type. The current work represents a detailed assessment of airflow through an active green wall module. Airflow distribution through the module, the effect of wetting the substrate, and the effect of introducing a cover to the module's open top face were investigated, with the aim to improve the module's design and achieve more appropriate and effective airflow. Four cases of both planted and unplanted modules under both dry and wet conditions are considered. This work's primary observation is that *more* air will pass through a typical green wall substrate, and hence become cleansed, when the substrate is saturated wet more than when it is dry. The increase was substantial at approximately 50% more with 14.9 L/s total air flow rate passing through the wet planted module versus 10 L/s when dry. Reducing the 15.5 % of airflow passing through the module's open top face was found to be essential to maximize the bio-filtration capacity. Adding a top

cover to the module having six 10 mm holes for irrigation decreased the airflow through the top by 6 %, and directed it through the filter increasing the percentage of air flow passing through the front openings from 79 % to 85 %.

The effect of green walls on thermal comfort (Temperature and humidity) is also experimentally investigated. For the active modules, lower temperatures in the range of 1 to 3 °C, along with increased humidity levels have been observed when modules are saturated wet, similarly passive modules provided lower temperatures in the range of 0.5 to 2 °C. None of the plant species studied showed any preference, indicating that the moisture content of the substrate plays the major role affecting the temperature and humidity variations.

The effect of using phase change material (PCM) as a passive cooling technique on the performance of a windcatcher to meet the demand for thermal comfort, hence energy conservation and savings purposes, is studied in this research. Incorporating PCM located in the floor, ceiling and walls of a room as well as in the windcatcher's inlet channel has shown the best performance. This set up provided a significant reduction of temperatures during the discharging process of about 3.61 ℃ (equivalent to 9.33%) and an increase in the average temperatures of 3.40 ℃ (equivalent to 15.70 %) during the charging process (solidification of PCM) compared with an empty room with no PCM. The effect of PCM on humidity was not significant as variations of maximum 3.88% is observed when PCM is used.

The ultimate aim of this research is to develop a natural ventilating system to enhance a healthy, comfortable and energy efficient indoor environment; PCMs and green wall modules are appropriately incorporated.

Chapter 1 Introduction

1.1 Global warming and building design

Global warming has recently become daily news in the media around the world. Summer temperature data indicates that many of the continent's capitals have warmed up by as much as 2 - 3 °C in the last 30 years. CO2 emissions have also increased by more than 200% from 1995 to 2011 [1]. New guidelines and regulations are being introduced in the building industry in order to reduce related energy consumption. In the last few decades HVAC (Heating Ventilating and Air Conditioning) systems have become widely used in buildings in order to control their internal conditions, as they provide adequate amounts of ventilation rates, heating and cooling loads. HVAC systems however significantly contribute in greenhouse gas emissions. Besides C02 emissions that have a great effect on global warming, emissions from refrigerants including CFC's (chlorofluorocarbon 11 and 12) play a major role in ozone depletion. In addition the energy consumption of HVAC systems is extremely high. It is obvious that air conditioning contributes dramatically to global warming and climate change. The energy used in ventilation, heating and cooling systems accounts for more than 60% of the total building energy consumption [1].

The approach to building design is essential in producing buildings that are energy efficient. Air flow patterns and ventilation rates are some of the most important aspects for controlling the environmental conditions within buildings as well as improving human comfort. Natural ventilation is increasingly explored as a feasible method for passive cooling and improved energy efficiency. It is especially important to treat the subject in conjunction with other aspects of architectural and engineering design and in the context of an overall environmental design strategy. [2]

1.2 Natural ventilation

Natural ventilation is the process of supplying and removing air through an indoor space naturally. It uses outside fresh and cool air to ventilate and cool down the inside of a building. The introduced air replaces the indoor contaminated air which exhausts from the building openings. The cooling capacity of natural ventilation is not very high and depends mainly on the temperature of the outside air. In many cases related to buildings in the urban areas, the outside temperatures are higher than in the rural areas and thus natural ventilation cannot cope with the internal heat gains [3]. There are several benefits for natural ventilation such as contamination removal and providing fresh oxygen, thereby enhancing indoor air quality [4].

1.2.1 Natural ventilation in an urban environment

Many challenges are associated with the use of natural ventilation in the urban environment. These challenges may include, and are not limited to, low wind speeds, high temperatures, and high pollution and noise levels. Santamouris et al [5] claim that the urban heat effect reduces significantly (about 25%) the efficiency of air conditioning systems. This can lead to a further increase in overall size and use of air conditioning systems and thus intensify peak electricity demand and energy consumption for cooling purposes [6]. The urban heat would also reduce the effectiveness of passive ventilation and in particular night ventilation [7]. The urban environment has some beneficial aspects such as over shading based on experimental data and empirical modelling by [8]. It is highly important to further investigate innovative strategies which contributes to controlling the source, rate and quality of air introduced in naturally ventilated buildings [3].

1.2.2 Winddriven and Buoyancy driven ventilation

There are two types of natural ventilation occurring in buildings: wind-driven ventilation and buoyancy-driven ventilation. Stack ventilation is temperature induced and is driven by buoyancy effect which makes it less dependent on wind and its direction. Heat emitted in the room causes a temperature difference between two adjoining volumes of air, the warmer air will have lower density and be more buoyant thus will rise above the cold air creating an

upward air stream. Figure 1 shows the operation of a typical windcatcher (wind-driven ventilation), and Figure 1-2 [9] shows the operation of a typical solar chimney (buoyancy-driven ventilation).
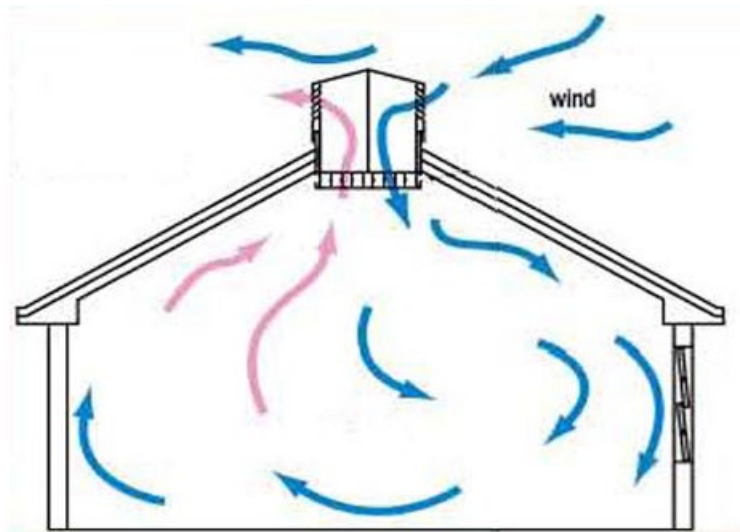
Figure 1-1. Operation of a typical windcatcher (wind-driven ventilation) [10]
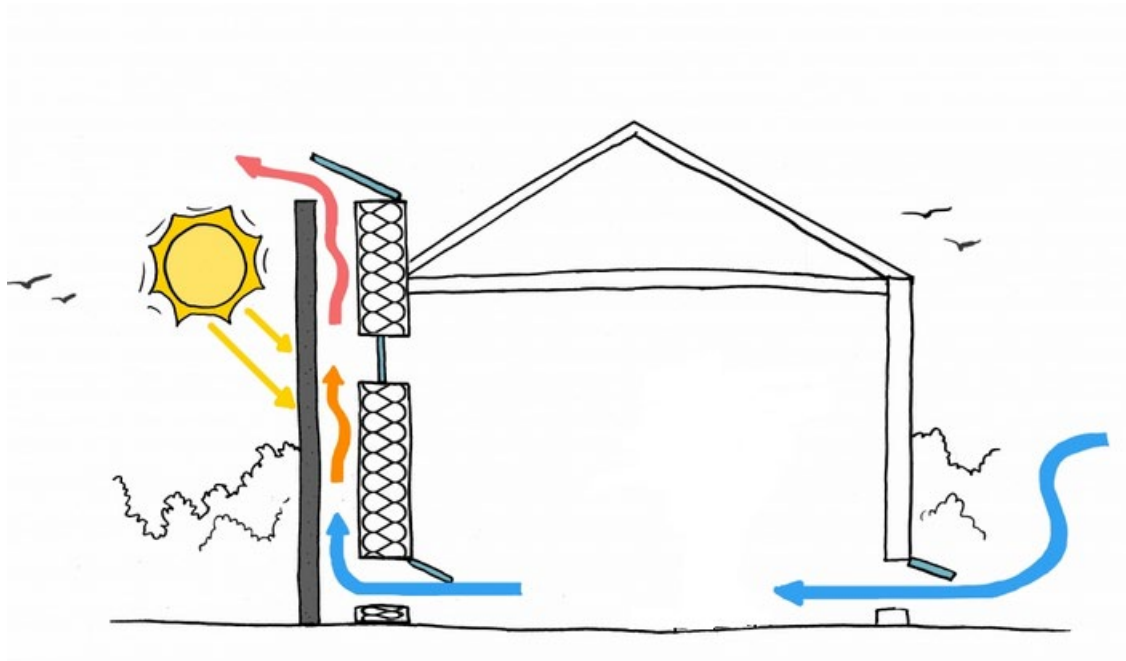
Figure 1-2. Operation of a typical solar chimney (buoyancy-driven ventilation) [9]

1.3 The windcatcher

Windcatcher is a green feature which provides natural ventilation using wind power. It has been employed over centuries in the Persian Gulf area called as Baud-Geer and in the Egyptian architecture called as Malqaf [11, 12]. It is a structure fitted on the roof of a building [13] to deliver fresh outside air to the interior replacing the inside stale air. Windcatcher's work by pressure difference between the outside and the inside of the building. The low cost of windcatcher system (operational and maintenance cost) in comparison with mechanical ventilation system, being noiseless, durability, requiring no fossil energy, supplying clean air and using sustainable energy of wind have led to the use of the windcatcher today as a passive and environmental friendly system [14]. The experimental studies of windcatcher systems for all different cases are obviously expensive or even impossible. Figure 1-3 shows various windcatcher shapes.
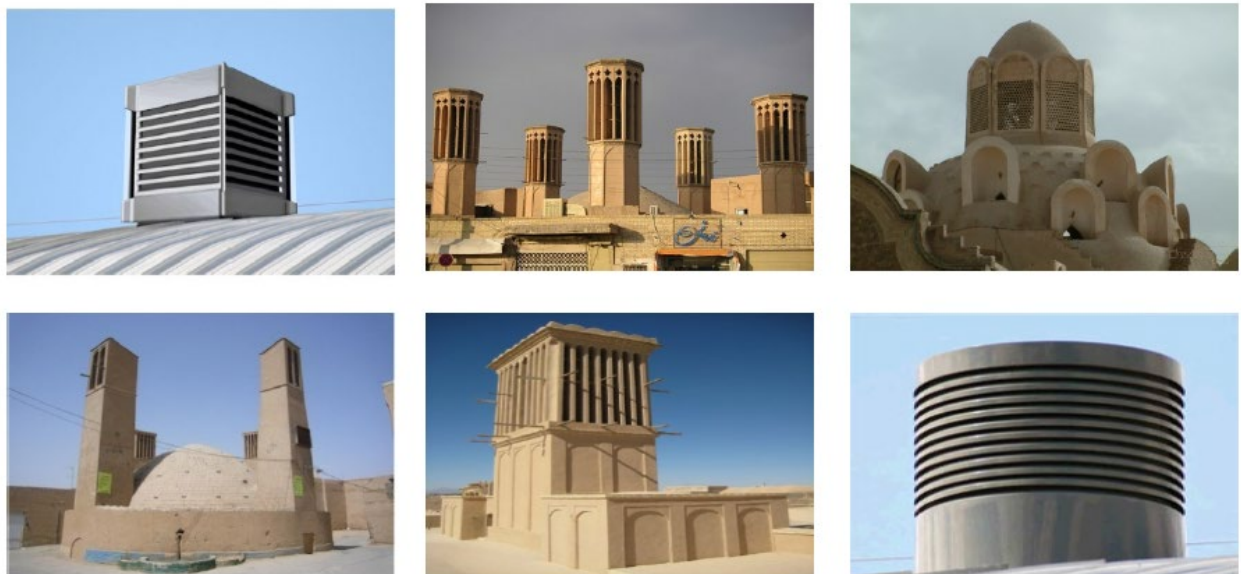
Figure 1-3. Various windcatcher shapes

1.3.1 Windcatcher's components

Windcatchers usually have rectangular or octagonal cross sectional plan with a chimney shaped tower which is subdivided into several shafts by brick partitions. This chimney shape device

has at least one opening at the top. The main components of a windcatcher are the tower, openings, and partitions.

The tower is the main part of the windcatcher which is usually located above the building to be ventilated and its height depends on the location and the surroundings. The tower is divided into two parts: the higher part is where the openings and the vents are placed and the lower part which is the stalk. The height of the stalk is affected by the overall windcatcher's height and they may be decorated for aesthetic reasons.

Vents or openings are located in the highest part of the windcatchers' column to catch fresh and clean air and channel it down into the building. The number of openings depends on the windcatcher's location and it's cross sectional area. Square, rectangular, hexagonal and octagonal windcatchers cross sectional plan are common. In the modern design of windcatchers, circular plan windcatchers are also reported. According to Saadatian et al. [1] the number of openings in a windcatcher affects its efficiency. The windcatcher's efficiency or its ability to capture air, decreases as the number of openings increase.

Figure 1-4 [15] shows traditional windcatchers with different number of openings:
   a) One sided
   b) Two sided
   c) Four sided
   d) Octahedral
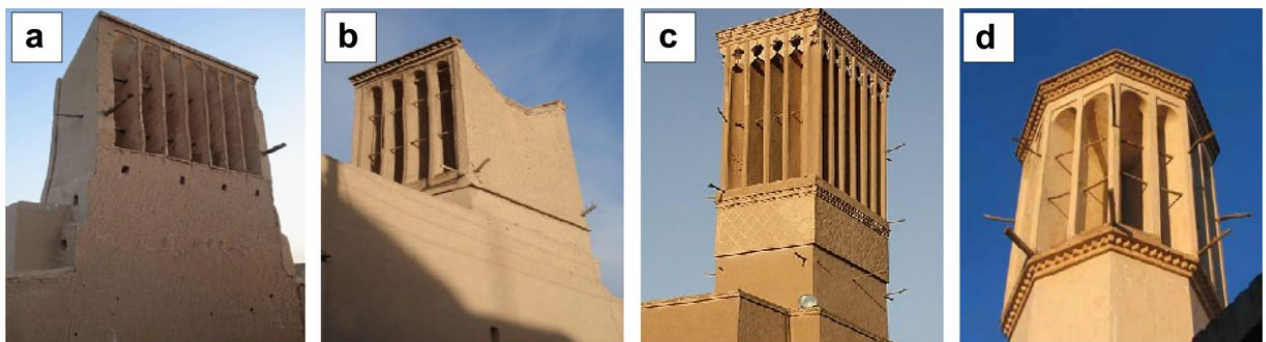
Figure 1-4. Traditional windcatchers with different number of openings [15]

The sustainable design of a windcatcher improves the building`s energy performance by utilizing natural resources providing oxygen to the indoor environment and increasing the human comfort level consequently. Previous research have revealed a gap regarding the effect of the architectural design of the windcatcher such as its width, height and openings sizes and

the influence of their performance on the airflow and human comfort [16]. Nowadays the advanced modelling and simulation tools are capable to test and evaluate the building performance effectively and help design a naturally ventilated building [17]. In this study the effect of the windcatcher's inlet design is investigated to achieve better air flow and to increase the efficiency of windcatchers [18-20].

1.3.2 Combined winddriven and buoyancy driven ventilation

Efficient design for a natural ventilation building should implement both types of natural ventilation, wind-driven ventilation and buoyancy or stack ventilation [21-23]. Figure 1-5 [24] shows a schematic representation of air movement in a combined windcatcher (wind-driven ventilation) and solar chimney (buoyancy-driven ventilation). The air enters through the wind tower and exits through windows, doors and through the solar chimney. Stack driven air rises as it leaves the windcatcher and it is replaced with fresh air from outside as it enters through the positively pressured windward side. When wind speed is low, the solar chimney creates natural air flow; the fresh air enters through the windtower as the warm air exits through the solar chimney. Combining the wind driven and the buoyancy driven ventilation will be investigated in this study through the use of a wind catcher natural ventilation system [21-23].
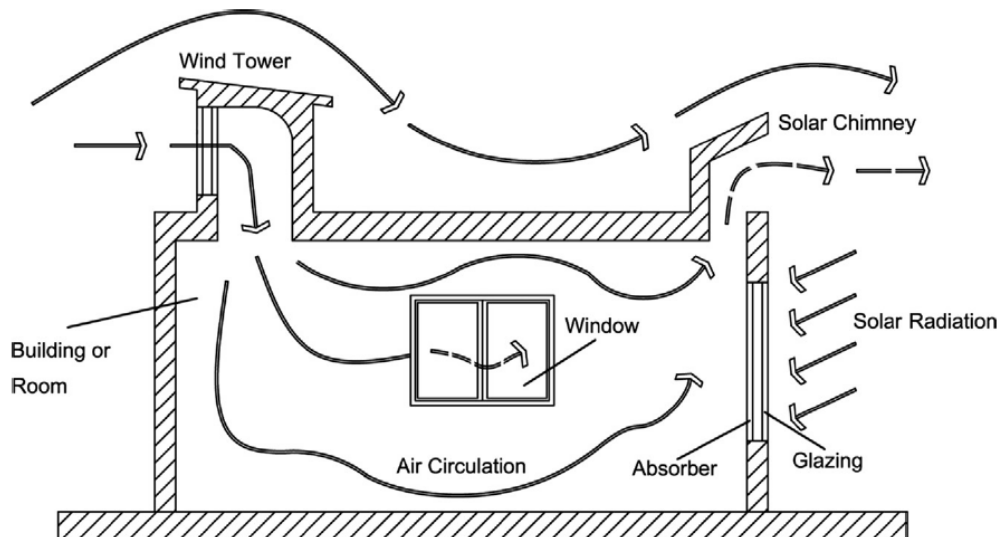
Figure 1-5. Schematic representation of air movement in a windcatcher combined with a solar chimney [24]

1.4 Green walls

The increased pollution levels in cities highlight the importance of further investigating innovative strategies that can control the quality of air introduced in naturally ventilated buildings. Green wall is the common term to refer to all forms of vegetated wall surfaces. Green walls can be subdivided in two main systems: green facades and living walls. Heat stress in cities can be addressed by increasing green spaces and using green walls and green roofs. This can contribute to decrease air pollution hazards, reduce energy demand in buildings (by 10–15%) and improve quality of life [25]. In fact the integration of vegetation in urban areas has several environmental benefits contributing to improve air quality, through the absorption of CO_2 and the retention of dust particles and heavy metals. There is also an international body of evidence that demonstrates direct beneficial effects of indoor plants on human health, psychological wellbeing, and work productivity [26-29]. Figure 1-6 shows a green wall module with *Schefflera amate* plants.

Figure 1-6. *Schefflera amate* green wall module

The green wall module (tested in this study) is normally a key component of a green wall system [30, 31] (the 'Breathing Wall' manufactured by Junglefy Pty Ltd, Sydney, Australia) has been the subject of previous research [32-34]. The modules, which normally can support a wide variety of plant species [35], are typically fixed in a vertical alignment (Figure 1-7) to a vertical wall or frame to form a green wall system. This system can produce changes in ambient temperature and humidity of the surrounding air [36, 37], thus creating an interesting insulation effect [38]. Like most systems designed to provide air quality remediation functions, the system is 'active', utilizing mechanical ventilators which force air through the substrate and plant roots where the air becomes purified and filtered [33, 39].

Pressurized air enters a port (100 mm dimeter) on the rear face of the modules, where it is distributed across the rear of the substrate in a plenum (20 mm depth), before passing through the substrate and returning to ambient through the foliage. Polluted air is passed from back to front to avoid humidification of the ducting, which would occur if the airflow passed from front to rear.

Figure 1-7. Green wall modules with *Schefflera arboricola* on the left and *Chlorophytum comosum* 'variegatum' on the right.

Improving the design of the green wall module is the aim to obtain more appropriate flow distribution [40, 41] and better flow rate throughout the module [42] considering the different parameters involved such as the moisture content, growing-medium-plant-roots mix and plant type. All this is in addition to the better understanding of air flow through complex moist porous media as well as investigating the effect of green walls on enhancing thermal comfort [36, 37].

1.5 Phase change material

Materials that change phase at room temperature are frequently referred to as Phase Change Materials (PCMs). Phase change materials use the latent heat properties of materials to store large amounts of energy, which is charged and discharged by passing air through a heat exchanger. PCM products have different types and come in different performance temperatures and densities. During the last years comprehensive and particular reviews of PCM latent heat systems and their applications have been made, and more than 20 extensive review articles about the potential of integrating PCMs in buildings were published, allowing concluding that interest in the subject is rising [43, 44]. The effect of using PCM (Figure 1-8) as a passive cooling technique on the performance of a windcatcher to meet the demand for thermal comfort, hence energy conservation and savings purposes, will be studied in this research.

Figure 1-8. BioPCM phase change material used in this study

1.6 Research significance

Harnessing wind power and using it as a natural resource for ventilation originated in the Middle East since more than 2000 years. Using Windcatchers widely have made the arid climate more bearable. Persian windcatchers of the 17th century functioned in many different ways depending on the type of home and the location of the structures. Windcatchers have always had the benefit of providing the air supply above the roof level which is often cleaner than that found at the ground level, especially when the building is near roads within the urban environment [45].

Natural ventilation has some disadvantages and may not be suitable for regions with cold climate or for regions with hot windless weather. When buildings are located in polluted areas, natural ventilation may cause some health risks to the occupants. The variation of wind speeds may as well lead to air quality problems [45].

Despite the draw backs natural ventilation strategy satisfies the needs of its occupants without excessive energy consumption. Natural ventilation can be considered as a sustainable technology which helps develop the social, environmental and economic aspects [46].

In this study a two sided windcatcher will be used to investigate the performance of windcatchers and mainly study the effect of its inlet design as well as the effect of combining buoyancy driven and wind driven ventilation. The two sided windcatcher is the simplest type of a windcatcher which is used in this study to concentrate on key parameters rather than complex architecture.

On the other hand, heat stress in cities can be addressed by increasing green spaces and using green walls and green roofs. These measures could reduce temperature by up to 10 °C in Mediterranean areas [47]. The integration of vegetation in urban areas has several environmental benefits, contributing to the improvement of air quality.

Green wall systems have the ability to function as a complementary acoustic protection [48] contributing to improve comfort of interior spaces. In fact, green walls can be integrated in buildings among several passive design solutions as a strategy of evaporative cooling [38]. Active green walls represent an emerging technology for the removal of pollutants present in air streams, with many conventional analyses yet to be applied to these systems [49]. Currently there is a gap in knowledge for this rapidly expanding technology, and it is clear that a uniform and standardized approach to characterizing key parameters is required for accurate performance evaluation. This, in practice, may be difficult to achieve, with the existing green wall systems having differing structures and thus differing air flow distributions, with air either flowing through the filtration media of the system and into ducting before return to the environment, or the reverse [50], and a vast diversity in designs, substrate types and thicknesses, moisture levels and pressure drop characteristics. The current work thus provides an initial study directed at optimizing the airflow characteristics through a green wall module and investigating the effect of these green walls on indoor thermal comfort (temperature and humidity).

Phase change material (PCM) has been recently regarded as a sustainable passive cooling method [51]. The review of the literature reveals the necessity of exploring new techniques to

enhance the performance of windcatchers (and natural ventilation). PCM shows promise when combined with windcatchers to be very effective at providing both cooling and ventilation in a sustainable system. Recently many articles studied the problem of integrating PCMs in buildings, to meet the demand for thermal comfort and energy conservation / savings purpose. the main draw back for using PCM is the solidification process which may not fully complete if the outside temperature were not lower than the melting temperatures. This research will study the effect of incorporating PCM inside a scaled two sided windcatcher. In some specific situations such as in the Middle East, windcatchers are thermally massive which should be taken into consideration when selecting the suitable PCM required for such high thermal mass applications.

As it has been discussed in the introduction section more than 40% of the total world energy consumption is allocated to the building sector, of which more than 60% [1] of the total building sector energy consumption is used for heating, ventilation and cooling. By using the techniques proposed in this study the electrical energy needed to operate any type of air-conditioning will be reduced, and thus reducing the overall energy consumption and providing an enhanced indoor environment with better air quality and ventilation rates. Implementing the three proposed techniques may be possible in practice, however some difficulties may arise due to the building constraints, special design requirements, cost of PCM and potential refurbishment of constructed buildings.

1.7 Research objectives and contribution to knowledge

The key questions related to this study are as follows:

1. How to enhance the performance of a two sided windcatcher and what are the effects of its inlet design and of combining the buoyancy driven ventilation with the winddriven ventilation on the air flow through the windcatcher and on the human thermal comfort?
2. What are the effects of green wall systems on indoor thermal comfort and what are the parameters affecting the evaluation and distribution of air flow through an active green wall module?

3.   What is the effect of using PCM (phase change material) on the performance of a two sided windcatcher and how to incorporate it effectively?

The ultimate aim of this research is to develop a natural ventilating system that enhances a healthy, comfortable and energy efficient indoor environment. To achieve this CFD (computational fluid dynamics) tools will be used for modelling airflow through a room, two dimensional and three dimensional simulations will be conducted. Experiments using green wall modules and phase change material will also be held in the UTS laboratories. Specific objectives are as follows:

1.   To investigate the windcatchers performance by studying the effect of its inlet design and the effect of combining wind-driven and buoyancy-driven ventilation like the use of a solar chimney to enhance the natural ventilation of buildings and improve human thermal comfort.

2.   To investigate the effect of green walls on thermal comfort and on ventilation including evaluating the air flow rate and the flow distribution through the modules.

3.   To investigate the effect of using phase change material PCM on the performance of a windcatcher in order to obtain better human thermal comfort.

1.8 Research methodology

To achieve the objectives of this research both numerical simulation and experimental techniques are used. Computational fluid dynamics tools (Ansys Fluent or CFD Ace+) are used for two dimensional and three dimensional numerical simulations related to objective 1. Experimental techniques with green wall modules and phase change materials are conducted in the UTS Metrology laboratory in relation to objective 2 (using green walls) and objective 3 (using PCM).

1.8.1 Objective 1 research methodology

In relation to the first objective that is investigating the windcatchers performance by studying the effect of its inlet design and the effect of combining buoyancy driven and winddriven ventilation, two dimensional and three dimensional simulations are performed using computational fluid dynamics tools (Ansys Fluent or CFD Ace+).

Wind is distributed uniformly at the computational domain inlet. In reality the wind profile is not uniform however it is not important in our study as the windcatcher captures air in a small region only located at its opening. In addition the distribution of wind at the windcatcher's inlet corresponding to a uniform wind distribution at the computational domain's inlet would be similar for a certain real profile (for example logarithmic profile).

The results of the three dimensional simulation with wind speed of 3 m/s are compared and validated against an available published study with similar conditions [14]. Additional details about this validation will be presented in section 3.3.

1.8.1.1 Effect of windcatcher's inlet shape on ventilation flow through a two dimensional room

A two dimensional real sized room with a width of 5 m and a height of 3 m fitted with a windcatcher is modeled in this study using Ansys Fluent. The height of the windcatcher is assumed to be 2 m from the roof of the room up to the top of the windcatcher. Figure 1-9 shows a representative model of the room studied.
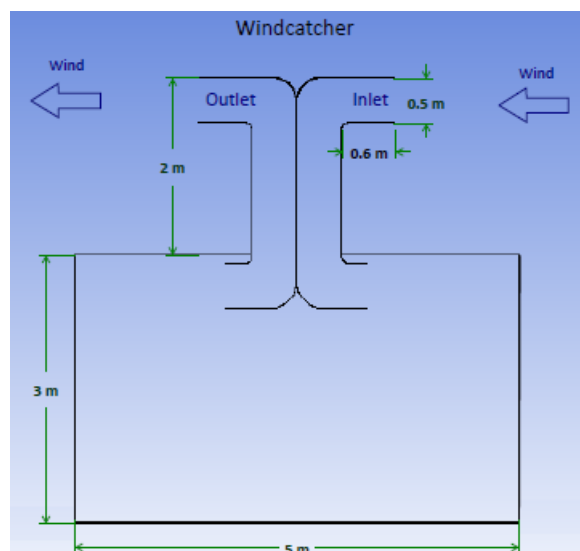
Figure 1-9. A two dimensional room fitted with a windcatcher

The effect of the windcatcher's inlet design on ventilation flow is investigated to achieve better air flow and to increase the efficiency of windcatchers. The common and simplest design is the uniform inlet which is the easiest for construction and has been implemented in many windcatchers. A divergent inlet and a bulging-convergent inlet are also investigated in this

study. A divergent inlet is expected to capture more air flow compared to the uniform inlet since its area is relatively larger, however the pressure distribution around it may affect its performance thus it is investigated. The bulging-convergent inlet, similar in design to a jet engine inlet, is also studied to investigate whether it would positively affect the windcatcher's performance. The different inlet designs considered are of three types as shown in Figure 1-10:

- Type A: Uniform inlet
- Type B: Divergent inlet
- Type C: Bulging-convergent inlet to mimic a jet engine inlet.

The windtunnel width is 0.5 m in all the cases however the projected area of the inlet type B and type C is 0.58 m in order to allow for the divergence and for the bulging.
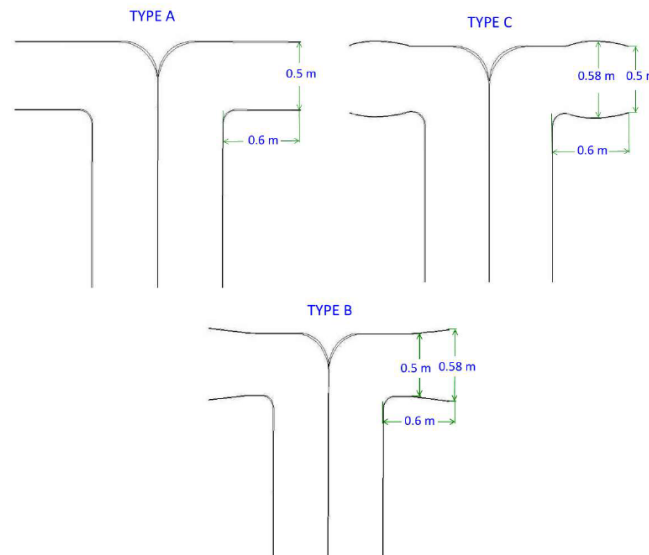
Figure 1-10. Types of inlet designs studied A, B and C

To simulate a more realistic air flow condition outside the building (free ventilation), the addition of a surrounding domain is used. Wind is blown from the right side to the left distributed uniformly over a height of 55 m; the air inlet is at a distance of 55 m away from the edge of the room as shown in figure 1-11. The total width of the surrounding domain is 105 m and the room is fitted at its center.

More details about the dimensions of the room and windcatcher tunnel, simulation boundary conditions, meshing and convergence criteria will be presented in section 3.1.1.
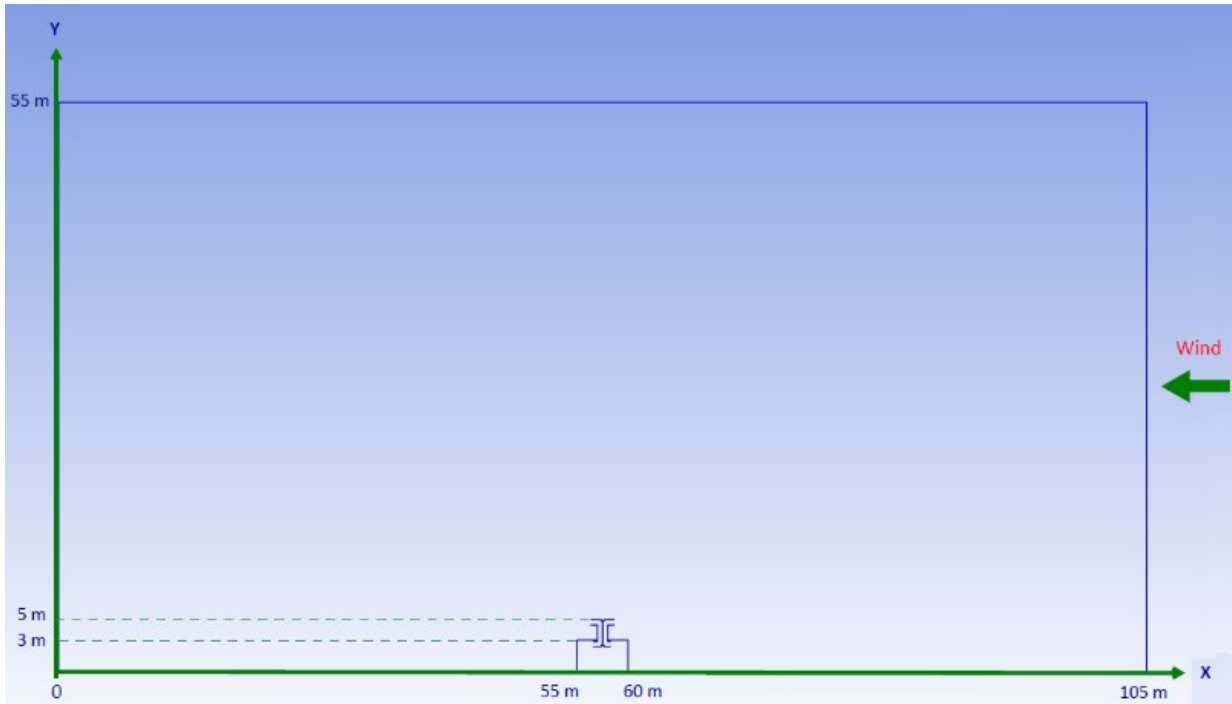
Figure 1-11. Schematic representation of the room, windcatcher and the surrounding showing the dimensions and the direction of the wind

1.8.1.2 Effect of combining buoyancy driven and winddriven ventilation in a two dimensional room fitted with a windcatcher

Combining the winddriven and the buoyancy driven ventilation will be investigated through the use of a two sided windcatcher natural ventilation system. Figure 1-12 shows a representative model of the two dimensional real sized room with a width of 5 m and a height of 3 m fitted with a windcatcher. The height of the windcatcher is assumed to be 3 m from the roof of the room up to the top of the windcatcher. It is modeled in this study using CFD-Ace+ [52], a CFD computational fluid dynamics software package from ESI group.

15
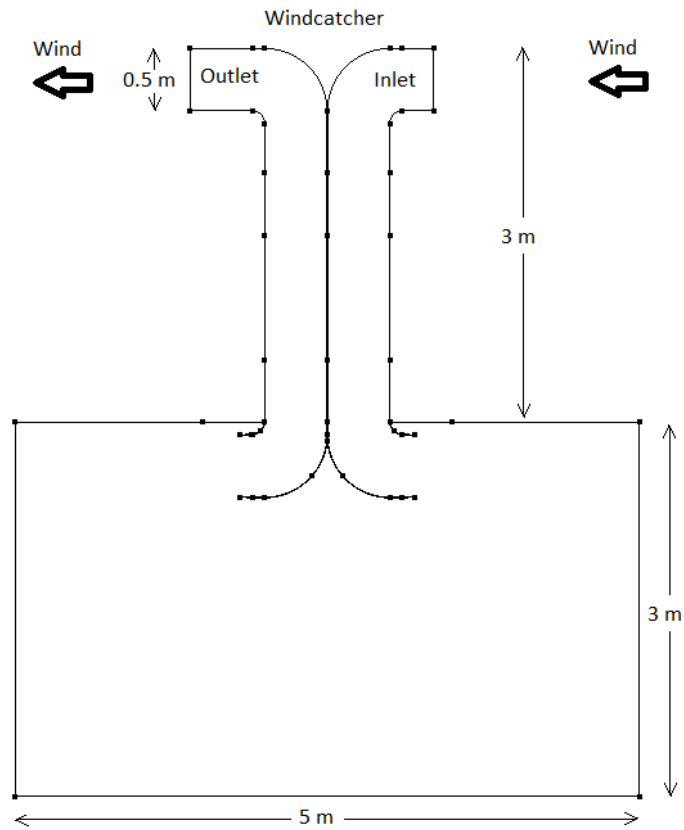
Figure 1-12. Two dimensional room fitted with a windcatcher

To simulate a free ventilation air flow the addition of a second domain that contains wind is considered. Wind is driven from the right side at a velocity of 3 m/s distributed uniformly over a height of 7 m; the air inlet is at a distance of 5 m away from the edge of the room as shown in figure 1-13. The total width of the surrounding domain is 15 m and the room is fitted in its center. Figure 1-13 shows a schematic representation of the room, windcatcher and the surrounding with the dimensions (measured along the x and y axis) and the direction of the air inlet and outlet.
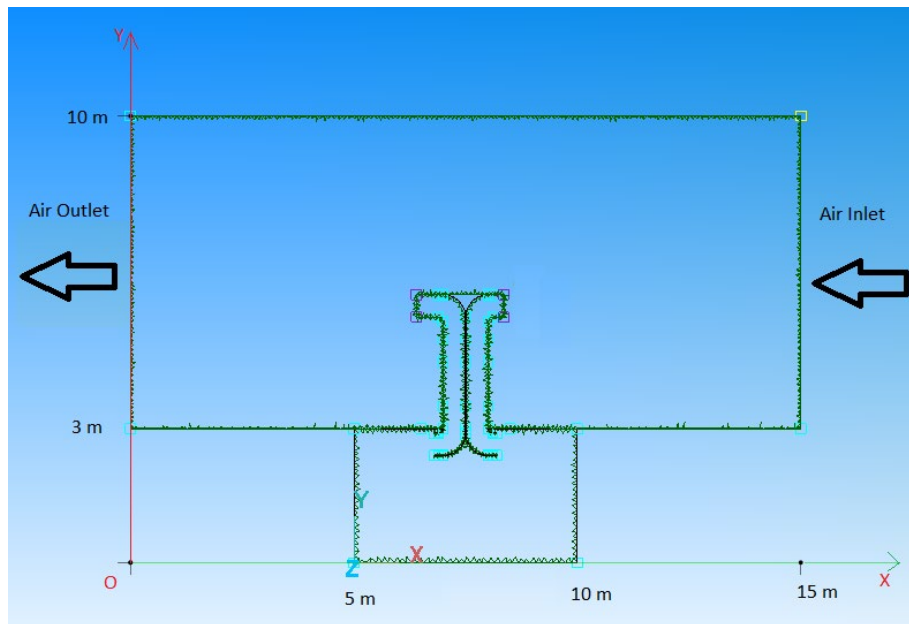
Figure 1-13. Schematic representation of the room, windcatcher and the surrounding.

To simulate the buoyancy driven effect, heat flux is applied to both sides of the windcatchers outlet. A fixed value of 400 W/m² is applied on the internal side of the chimney and the upper side of the opening while different values of heat flux (1000, 800 and 600) W/m² are applied to the external side of the outlet chimney and the lower side of the opening as shown in figure 1-14.
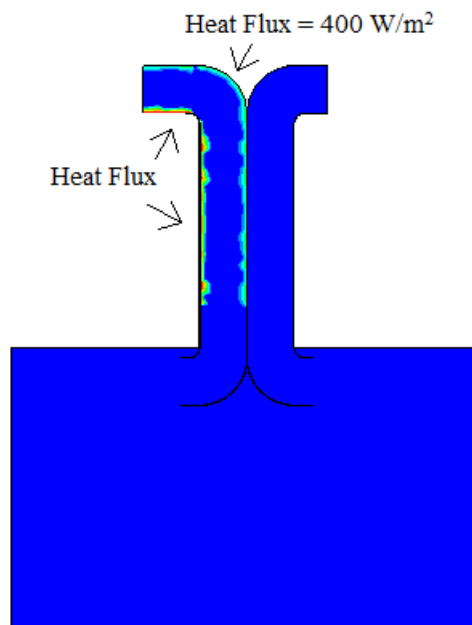
Figure 1-14. Heat Flux locations at the internal and external walls of the windcatcher outlet

The values of the heat flux considered are based on the solar radiation arriving to the atmosphere on a cloudless sky where the direct sun would be about 1050 W/m^2 [53] and the global radiation on a horizontal surface at ground level is about 1120 W/m^2. In fact the corresponding actual figures would vary based on sun's angle and atmospheric circumstances. The sun's rays are attenuated as they pass the atmosphere, leaving maximum normal surface irradiance at approximately 1000 W/m^2 at sea level on a clear day.

Additional details about the simulation conditions and convergence criteria will be presented in section 3.2.1.

1.8.1.3 Effect of windcatcher's inlet shape on ventilation flow through a three dimensional room

A three dimensional room fitted with a windcatcher is simulated in this study. The length of the room is 5m, its width is 4 m and its height is 3 m. The windcatcher's tunnel has a total height of 2 m from the room's roof. Figure 1-15 shows a representative model of the room studied.
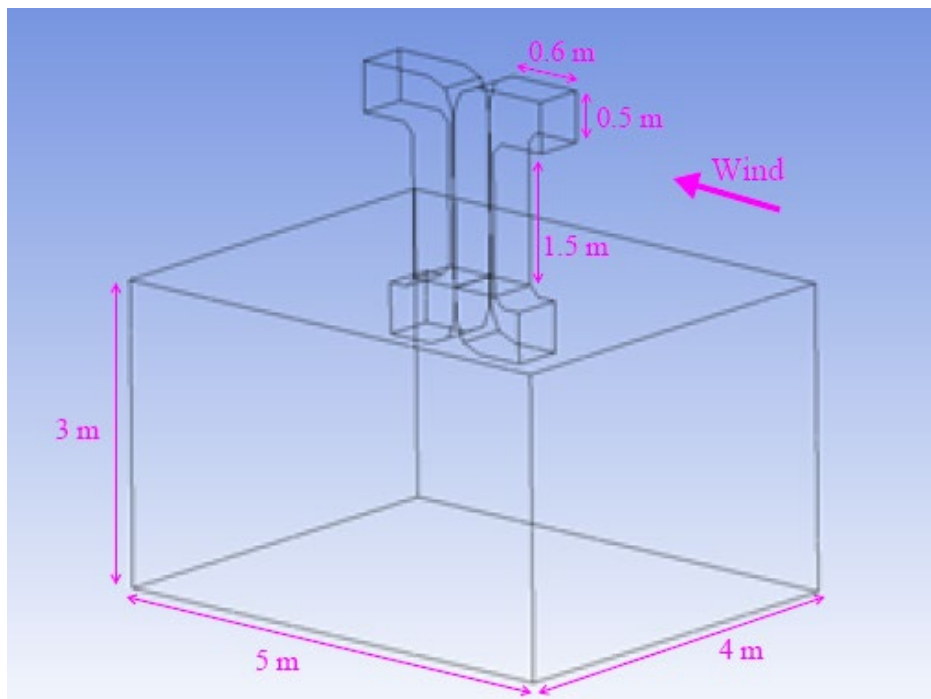
Figure 1-15. A three-dimensional room fitted with a windcatcher

Figures 1-16 shows the three dimensional schematic of the three inlet designs A, B and C studied. They are the same as shown in the two dimensional schematic figure 1-10.
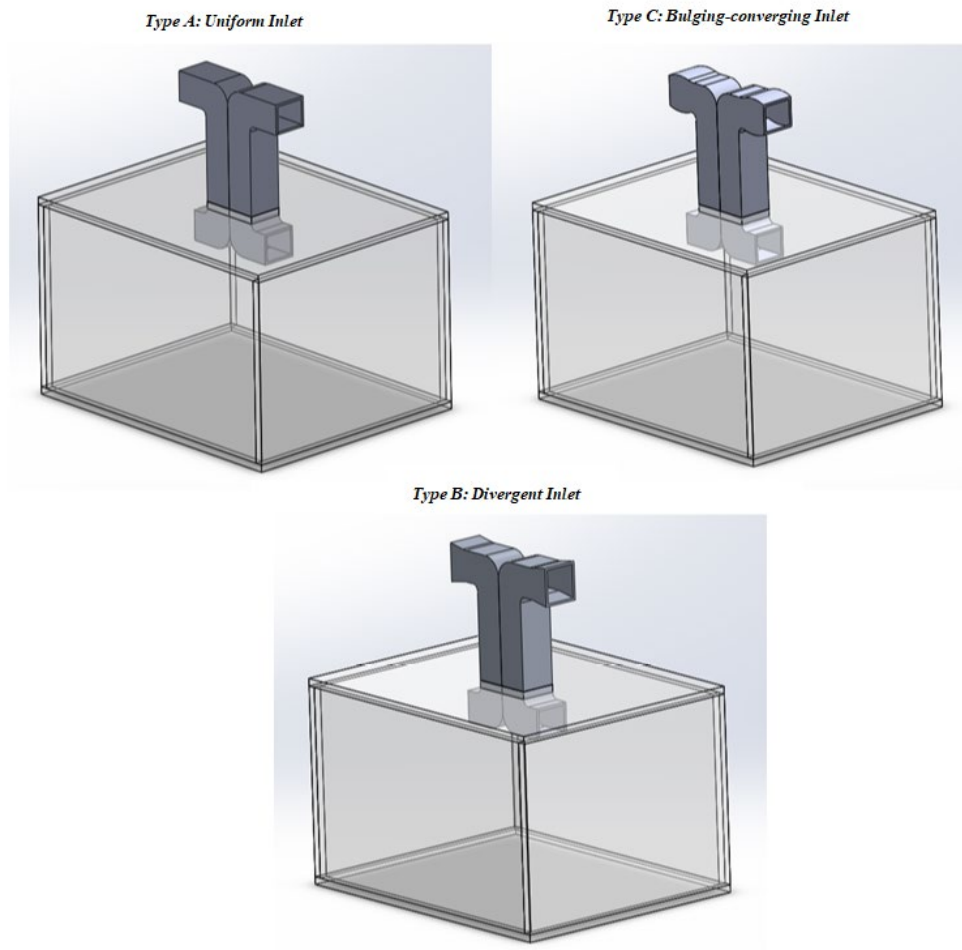
Figure 1-16. Three dimensional schematic of the three types of inlets studied

Free ventilation is simulated by the addition of a surrounding domain that contains wind. Wind, distributed uniformly with speeds of 1, 2, 3 and 6 m/s, is driven from the domain's inlet at the right side. The height of the inlet is 20 m and located at 15 m away from the right edge of the room. The dimensions of the surrounding domain are 35 m width, 28 m in depth and 20 m height. The room is fitted in its centre as shown in Figure 1-17. More details about the dimensions of the room and windcatcher tunnel, simulation boundary conditions, meshing and convergence criteria will be presented in section 3.1.2.
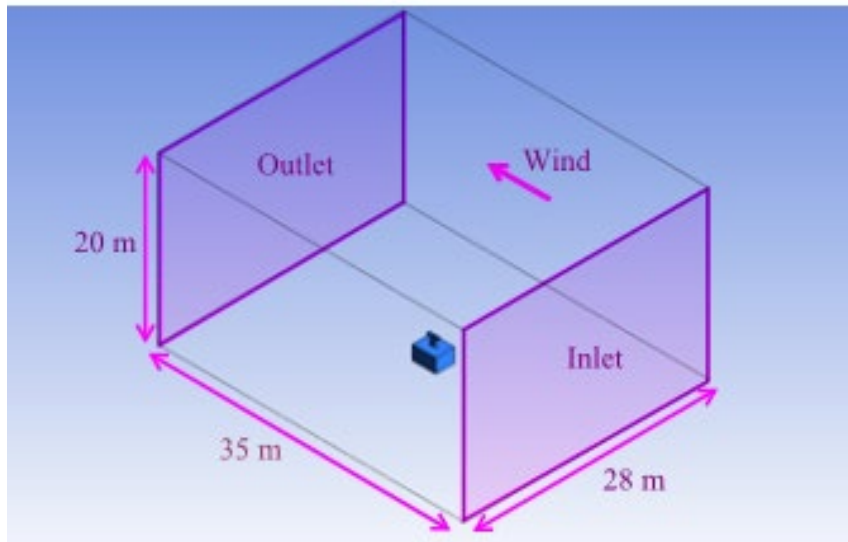
Figure 1-17. Schematic representation of the surrounding domain indicating the wind direction

For computational efficiency the surrounding boundary condition were set as walls however care was taken to see that the presence of the wall does not affect the flow. In addition pressure values near the wall boundaries were in the range of 0.2-0.3 Pa compared to the maximum pressure values near the room which were about 23.5 Pa.

1.8.1.4 Simulation of Buoyancy Driven and Winddriven Ventilation Flow in a Three Dimensional Room Fitted with a Windcatcher

A three dimensional real sized room shown in Figure 1-15 with a length of 5 m, a width of 4 m, and a height of 3 m fitted with a windcatcher is modeled in this study using Ansys Fluent [54]. The height of the windcatcher is assumed to be 2 m from the roof of the room up to the top of the windcatcher.

To simulate a free ventilation air flow the addition of a surrounding domain that contains wind is considered. Wind is driven from the right side at different velocities (0, 0.25, 0.5, 0.75, 1, 1.5, 2, 2.5 and 3) m/s distributed uniformly over a height of 20 m; the air inlet is at a distance of 15 m away from the right edge of the room. The total width of the surrounding domain is 35 m, its depth is 28 m and its height is 20 m. The room is fitted in its center as shown in Figure 1-17.

To simulate the buoyancy driven effect, Temperature of 350 K and of 400 K is applied at the windcatchers outlet in the part above the roof as shown in figure 1-18 on the front surface (A) and on the bottom of the outlet (B). The applied temperature is estimated to be due to solar heated elements with high heat storage capacity. The orientation of these surfaces A and B is assumed to be to the west where the sun is at its maximum during summer and especially low in the afternoon. The other walls of the windcatcher are assumed to be transparent (example glass cover) and thus the solar radiation would penetrate them and accordingly heat up the surfaces (A and B) where the temperatures are applied.
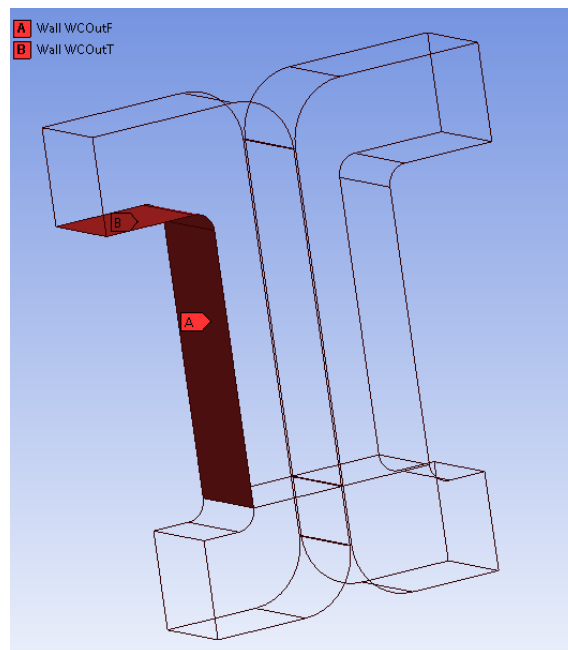
Figure 1-18. Temperature locations at the windcatchers outlet applied on the bottom and front surfaces.

Additional details about the simulation conditions and convergence criteria will be presented in section 3.2.2.

1.8.2 Objective 2 research methodology

To investigate and analyse the air flow through the green wall module and since the air velocity coming out of the module's openings (front, top and bottom) is very small, we had to find a suitable experimental set up.

To achieve our aim funnels were used to cover all the module's outlets and increase the flow velocity to measureable levels. The effect of different parameters such as the module geometry,

the moisture content and plant roots have been considered as well as the effect of the fan speed on the air flow and air distribution. Figure 1-19 shows the set up using small funnels covering all the modules opening. Complete details related to the materials used, methods and derivation procedure will be presented in Chapter 4.
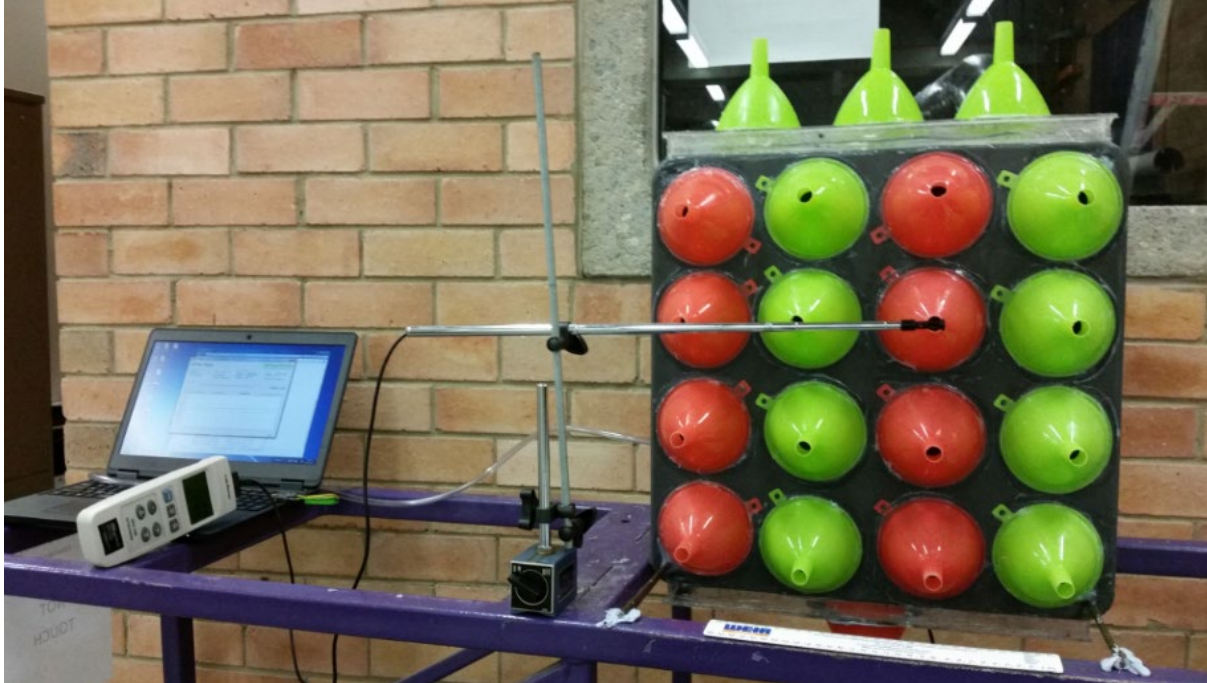
Figure 1-19. Green wall module with small funnels

To investigate the effect of green walls with different plant species on thermal comfort, a chamber made of acrylic sheets of dimensions 780mm x 960mm and of height 590 mm is used as shown in Figure 1-20. The green wall module is placed at the centre of the chamber. Both passive mode and active mode will be investigated. Temperature and humidity inside the chamber will be measured at different time intervals during operation and will be compared to the temperature and humidity outside of the chamber (Ambient conditions in the lab).

Figure 1-20. Set up to monitor effect of Green Wall module on Temperature and humidity

1.8.3 Objective 3 research methodology

To investigate the effect of incorporating phase change material on the temperature and humidity inside a room (1.25 m x 1 m x 0.75 m) fitted with a windcatcher, PCM is integrated respectively at the walls of the room, its floor and ceiling and within the windcatchers inlet tunnel. Five models are investigated and the results compared, one model when the room is empty (No PCM), another model when PCM is found on the walls only, a third model is with the PCM placed on the floor and walls of the room, a fourth model is with the room full with PCM (PCM on floor, walls and ceiling). The fifth model included the PCM located in the inlet of the windtunnel in addition to the floor, ceiling and walls of the room. Figure 1-21 shows the room fitted with the two sided windcatcher and PCM is incorporated in the floor, walls and ceiling. The phase change material used in this study is Bio PCM M51 Q24. Temperature and

humidity variations inside the chamber were monitored via BME sensors. Air velocity sensors were also used to monitor the velocity inside the chamber at different locations.

Figure 1-21. PCM placed on floor, walls and ceiling of the room fitted with a windcatcher

Both the discharging and the charging processes were investigated. During the discharging process a hot box fan with different heating elements is used to blow heated air at two different temperatures (corresponding to two stages) into the room fitted with a windcatcher. During the discharging process the room was also located in two positions to investigate the effect of different flow rate captured by the windcatcher on the performance of PCM.

During the charging process (solidification of PCM) an air conditioning unit was used to cool down the lab and a small fan was used to direct the cool air through the windcatcher inlet. All the five models have been used, and the results obtained and compared.

Chapter 5 will present complete details about the methods, material used, as well as the results obtained and conclusions.

1.9 Thesis structure

This thesis introduces the research studied and presents the methodology and results related to the above mentioned objectives in the following chapters:

Chapter 1 is mainly the introduction which presents some information about building design, natural ventilation types, windcatchers, green walls and phase change material (PCM). It also presents the research significance, research questions, objective and contribution to knowledge as well as an introduction related to the research methodology applied to achieve the objectives.

Chapter 2 briefs the background of the study by presenting the literature review related to natural ventilation, thermal comfort, indoor air quality, windcatchers function and components, solar chimney and its design elements as well as green walls and phase change material. It also reviews the CFD techniques and turbulence models.

Chapter 3 describes the methodology followed in relation to the first objective. It presents two dimensional and three dimensional simulations done by Ansys and CFD Ace plus along with the results obtained. It consists of four sections of which sections 3.1 and 3.3 investigate the effect of inlet shape of the ventilation flow through a windcatcher while sections 3.2 and 3.4

investigate the effect of combining buoyancy driven and winddrinven ventilation on the performance of a windcatcher.

Chapter 4 investigates experimentally the effect of green walls on ventilation and on thermal comfort. It describes the methods followed in detail and presents the results obtained and conclusions. A novel method for characterizing air flow through an active green wall module is presented taking into consideration the different parameters such as moisture content, plant roots, module geometric design and fan speeds. The effect of green wall modules on temperature and humidity is also investigated.

Chapter 5 presents an experimental set up used to investigate the effect of incorporating phase change material on the temperature and humidity in a room fitted with a two sided windcatcher. It describes the methods followed in detail and presents the results obtained and conclusions. Different parameters are considered such as the location of the PCM, the wind temperature and the wind speed during both discharging and charging processes.

Finally, Chapter 6 presents the summary and conclusions of this thesis based on the achieved results in the simulations of chapter 3 and experimental observations of chapters 4 and 5. Recommendations for future work are also presented in this chapter.

Chapter 2 Literature Review

2.1 The role of ventilation in buildings

Ventilation in buildings can be naturally or mechanically induced or even a combination of both (hybrid ventilation) and it fulfils a number of important functions related to health, thermal comfort and cooling.

2.1.1 Ventilation and Health

Ventilation is essential in providing oxygen (O2) for respiration. Fresh air requirements for humans will depend on the level of activity taking place indoors. Ventilation is also very important in displacing hazardous indoor pollutants such as products of normal human activity (CO2), or gasses and particles originating from construction materials, furnishings or building equipment [3]. Adequate fresh air can prevent and even eliminate the development of microorganisms such as dust mites [55]. Some of the building diseases such as sick building syndrome could be prevented or at least minimized by adequate ventilation.

Extensive urbanization and subsequently increased pollution and noise levels in cities pose a major design challenge in selecting an appropriate ventilation strategy for a building. This problem becomes more evident when considering natural ventilation techniques which require free movement of air uninhibited by filters and noise buffers. The orientation, size, location and degree of opening of any apertures as well the methods of ventilation become very important in minimizing pollution and noise [55].

2.1.2 Ventilation and thermal comfort

The human body temperature is maintained within a very narrow range through a variety of thermoregulatory structural and physiological devices. In any environmental condition that the human body is exposed, it must maintain a core temperature of approximately 37° C (±0.5).

Maintaining heat balance is the primary condition for achieving a neutral thermal sensation yet, even though the human thermoregulatory system can effectively create heat balance within relatively wide range of environmental conditions, comfort may not necessarily be achieved [3].

The main environmental factors that affect thermal comfort are the mean radiant temperature, air temperature, speed and relative humidity. Ventilation will have a direct influence on air temperature, air speed and humidity in a building. Air movement may increase psychologically the perception of cooling. Overall natural ventilation is often seen as a user friendly option and occupants tend to accept wider variations of indoor environmental conditions than they would with any mechanical methods [3]. Physical factors such as the metabolic rate and the clothing insulation may also affect thermal comfort. Psychological parameters such as the individual expectations also affect thermal comfort. There are many models of thermal comfort of which two are widely used according to the building type and operation. The predicted Mean Vote (PMV) model is the most recognized model, it is developed using principles of heat balance and experimental data collected under steady state conditions. The adaptive model, on the other hand, is developed based on hundreds of field studies while the occupants dynamically interact with their environment and control their thermal environment by means of clothing, operable windows, fans, heaters and sun shades. The PMV model can be applied to air-conditioned buildings, while the adaptive model can be generally applied only to buildings with no mechanical systems.

2.1.3 Ventilation and cooling

Ventilation can provide significant cooling to buildings and occupants [3]. This cooling takes place through convective heat transfer by the followings ways:

1. Introducing cool, fresh air while displacing internal warm air
2. Creating a comfort breeze which removes heat directly from occupants and equipment
3. Directly removing heat stored in buildings thermal mass

Heat transfer by convection depends upon the temperature difference between the surface and the air, the surface roughness, the air velocity and the direction of heat flow. Convective heat transfer where there is significant air movement is a more complex phenomenon. Night time ventilation takes advantage of diurnal temperature swings to improve cooling. Furthermore it may be used to cool the building fabric, effectively transforming the building mass into a "cool" storage and thus allowing it to absorb more internal heat gains during the day [3].

2.2. Natural ventilation

2.2.1 Types of natural ventilation

Natural ventilation is the process of supplying and removing air through an indoor space by natural means. Natural ventilation provides oxygen and removes contaminants, thereby promoting good indoor air quality [4]. There are two types of natural ventilation occurring in buildings: wind-driven ventilation and buoyancy-driven ventilation. The pressures generated by the stack effect mechanisms are quite low (typical values are 0.3 Pa to 3 Pa) while wind pressures are usually far greater (1 Pa to 35Pa). The majority of buildings will rely mostly on wind-driven ventilation yet stack ventilation can offer several benefits [3]. Efficient design for a natural ventilation building should implement both types of ventilation.

2.2.1.1 Wind driven ventilation

The impact of wind on a building affects the ventilation and infiltration rates through it and the associated heat losses or heat gains. Wind speed increases with height and is lower towards the ground due to frictional drag [3]. The impact of wind on the building form creates areas of positive pressure on the windward side of a building and negative pressure on the leeward side of the building. Figure 2-1 shows the impact of wind on the windward and leeward sides of a building. Thus building shape is crucial in creating the wind pressures that will drive air flow through its apertures. In practical terms wind pressure will vary considerably creating complex air flows and turbulence by its interaction with elements of the natural environment (trees, hills) and urban context (buildings, structures) [3].
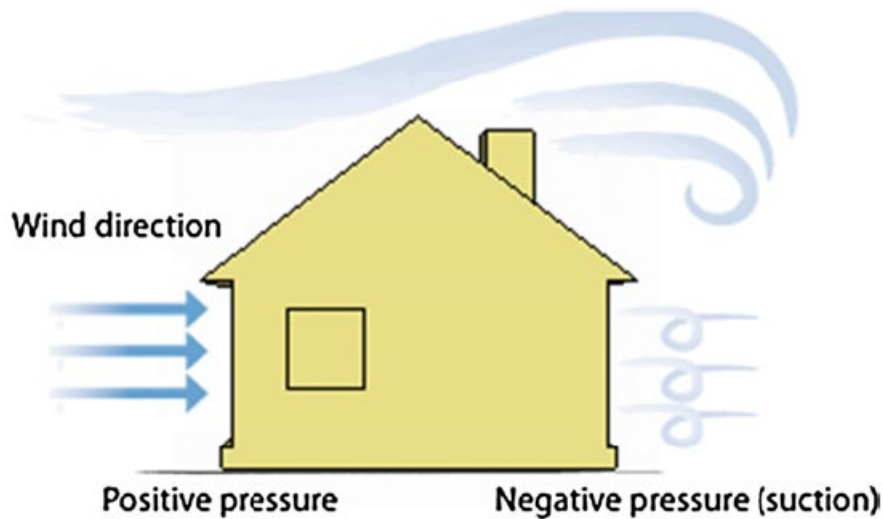
Figure 2-1. Impact of wind on the windward side and on the leeward side [15]

Typical building design relies on harnessing the power of wind for the purpose of natural ventilation. Design guidelines include a variety of recommendations on several subjects such as:

- Building location and orientation
- Building form and dimensions
- Construction methods
- External elements
- Urban planning conditions

2.2.1.1.1 Benefits and limitations of wind driven ventilation

Wind driven ventilation has several significant benefits as follows [3]:

- Great magnitude and effectiveness compared to other types of ventilation such as stack ventilation.
- Readily available (natural occurring force)
- Relatively economic implementation
- User friendly (when provisions for control are provided to occupants)

Some limitations of wind driven ventilation are as follows:

- • Unpredictable due to constant change and turbulence

- • Design restrictions due to variations in speed and direction

- • The quality of air it introduces in buildings may be polluted

- • May create draughts and discomfort.

Possible ways to overcome the limitations is by using a filter, a baffle system, or by redirecting the flow. Some limitations occur naturally and almost impossible to overcome such as turbulence and wind velocity changes.

2.2.1.2 Stack driven ventilation

Stack effect is temperature induced. When there is a temperature difference between two adjoining volumes of air the warmer air will have lower density and be more buoyant thus will rise above the cold air creating an upward air steam. Figure 2-2 shows the layout of stack ventilation. Forced stack effect in a building takes place in a traditional fire place. Passive stack ventilators are common in most bathrooms and other type of spaces without direct access to the outdoors [3].
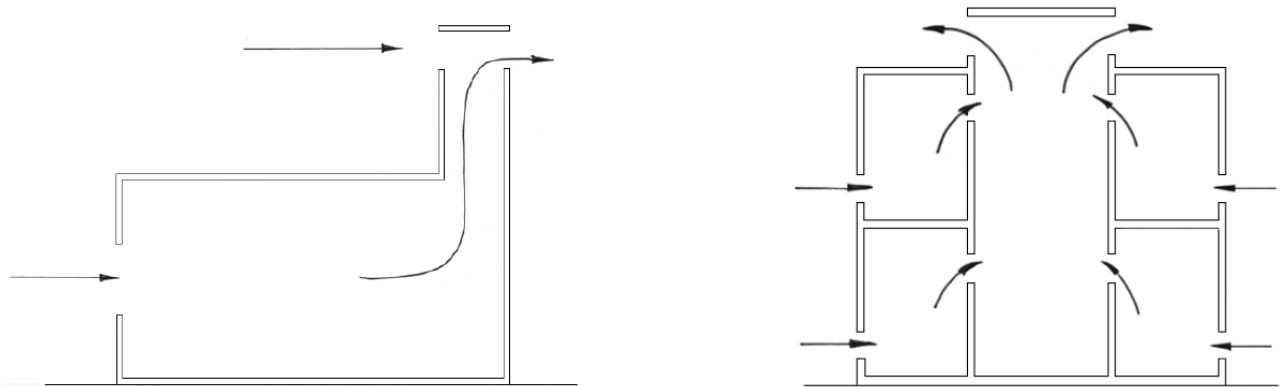
Figure 2-2. Stack ventilation layout [3]

In order for a building to be ventilated adequately via stack effect the inside and outside temperatures must be different so that warmer indoor air rises and escapes the building at higher apertures, while colder, denser air from the exterior enters the building through lower level openings. Stack effect increases with greater temperature difference and increased height between the higher warm pressure and lower apertures. The neutral plane in a building occurs

at the location between the high and low openings at which the internal pressure will be the same as the external pressure (in the absence of wind). Above the neutral plane, the air pressure will be positive and air will rise. Below the neutral plane the air pressure will be negative and external air will be drawn into the space. Figure 2-3 [3] shows the representation of airflow in stack effect and an example of stack driven ventilation.
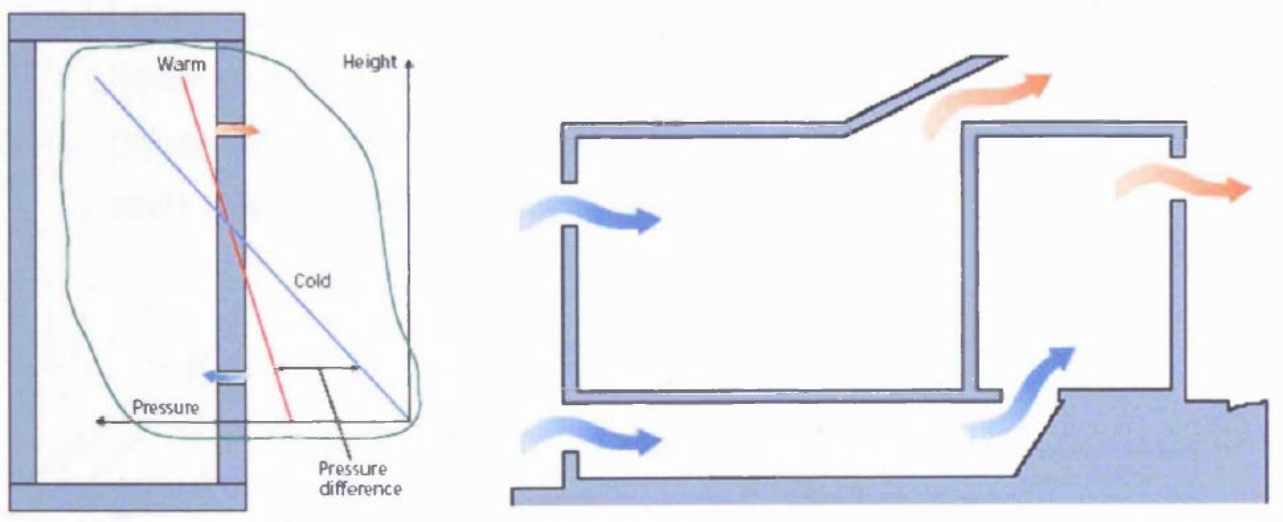
Figure 2-3 - Representation of airflow in stack effect [3]

2.2.1.2.1 Benefits and limitations of stack driven ventilation

Stack driven ventilation has a number of considerable benefits [3]:
1. Does not rely on wind: can take place on still, hot summer days when it is most needed.
2. Natural occurring force (hot air rises)
3. Relatively stable air flow (compared to wind); reduced amplitude
4. Greater control in choosing areas of air intake
5. Sustainable method

Limitations of stack driven ventilation [3]:
1. Lower magnitude compared to wind ventilation
2. Relies on temperature differences

Natural ventilation in buildings relies mostly on wind pressure differences but stack effect can augment this type of ventilation and partly restore air flow rates during hot, still days. With stack ventilation air inflow in a building does not solely rely on wind direction. Wind can augment the stack effect but also reduce its effect depending on its speed, direction and the design of air inlets and outlets. Therefore prevailing winds must be taken into account when designing for stack effect ventilation [3].

2.2.2 Natural Ventilation and indoor air quality

Australians spend up to 90 per cent of their time indoors [56], and thus indoor air quality has a major impact on their health [57]. Pollution levels in indoor air are generally two to five times higher [58] and sometimes are up to 100 times more concentrated than outside air [59].

Sick Building Syndrome (SBS) is known as the condition which is the result of continuous exposure to indoor air pollution [60]. The term 'SBS' is used to describe situations where building occupants experience health and discomfort effects that appear to be linked to the duration of time spent in a building [61, 62]. Typical SBS symptoms include headache; eye, nose and throat irritation; dry cough; dry or itchy skin; dizziness and nausea; difficulty concentrating and fatigue. The direct cause of the symptoms is not completely known, but symptoms are rapidly relieved after leaving the building, implicating poor indoor air quality [63].

Although natural ventilation provides numerous benefits, the concentration of indoor airborne pollutants can be higher in naturally ventilated buildings in some circumstances, due to outdoor particles and gases being transported indoors through openings in the building envelope [59]. Concentrations of indoor pollutants within naturally ventilated buildings are significantly influenced by the penetration of outdoor particles through the openings [64]. Urban air pollution is a worldwide health problem, some of its pollutants are biological in nature and are referred to as bioaerosols, while most of the other pollutants result from fossil fuel emissions and comprise a mixture of solid particulate matter (PM), and gases including Sulfur Oxides (SOx), Nitrogen Oxides (NOx), Carbon Monoxide (CO), Carbon Dioxide (CO2), Volatile Organic Compounds (VOCs), hydrocarbons, and ozone (O3) [60]. Gaseous pollutants are VOCs and inorganic gases.

2.2.2.1 Volatile Organic Compounds

Volatile organic compounds (VOCs) are gases or volatilized substances comprised of hydrocarbons, alcohols, aldehydes and chlorinated compounds with a vapour pressure greater than 2 mm Hg at 25 °C [59]. Indoors, these chemicals are emitted from furniture, carpets, construction materials, sprays, and cleaning products [65]. Outdoor concentrations are derived from industrial and transport-related activities (vehicle emissions, vehicle manufacturing, printing, equipment coating, electronics and furniture manufacturing). A mixture of hundreds of VOCs can be found in indoor air. These compounds exhibit very large variations in concentration as well as physical, chemical, and biological properties [66].

2.2.2.2 Inorganic gases

The most inorganic gaseous compounds of concern are CO, CO_2, NO_2 and sulfur dioxide (SO_2) [59]. These compounds are mainly generated from fossil fuel burnings, with most outdoor sources derived from road transport, power stations, and refineries [67] whereas residential sources include kerosene heaters, gas-fired appliances, wood stoves, gas-fired hot water heaters, and tobacco smoking [68].

CO_2 levels higher than the outdoor ambient concentration has been associated with adverse symptoms related to the mucous membranes (dry eyes, sore throat, nose congestion, sneezing) and to the lower respiratory tract (tight chest, short breath, cough and wheezing) [69]. This mainly occurs in closed spaces, indoors, where excess CO_2 is produced by human respiration [70]. The incomplete combustion of fossil fuels, can produce CO. Exposure to low concentrations of CO result in headache, drowsiness, and severe chest pains, while high concentrations leads to neurological damage and death [71].

Concentrations of NO and NO_2 in ambient air has declined since the early 1990s, however high concentrations can still be found near busy roads [59]. High concentrations of NO_x cause inflammation of the airways and other respiratory effects [72]. Similarly, SO_2 is also a respiratory irritant, causing adverse respiratory symptoms [73].

2.2.3 The windcatcher

A windcatcher is a fixed chimney shaped device which is able to act as an air inlet and outlet simultaneously. It is an environmentally friendly device that can benefit from both wind and stack effect at the same time. Windcatchers have vertical shafts with openings on two, four, six or eight sides at the top of the shaft to catch the breeze from any direction. Those vertical shafts subdivide to several shafts and allow air to enter from one or two sides and exit from the other sides [74].

2.2.3.1 Windcatcher's function

The function of windcatchers is based on the wind and on the stack effect which is the result of temperature differences. It is maximized by applying special forms of opening and exit. Generally it is hard for wind to change its direction, and enter a room through usual openings such as windows. A windcatcher is used to overcome such problems since they have vertical columns that help wind to change its direction and channel it down to the inside of a building [74].

2.2.3.1.1 Wind

Wind creates pressure differences around an obstacle. When wind hits any obstacle the air density in the windward area increases with respect to the leeward area. Therefore, positive pressure is made on the windward face of the building and the negative pressure forms on the other side of the obstacle (windcatcher) and wind enters from the area with the positive pressure and tends to move to the lower pressure zone. In the case of windcatcher, lower pressure zone is located at the bottom of the windcatcher's shaft, therefore fresh air enters to the building and indoor hot and polluted air exhausts to the opposite side of the inlet with higher negative pressure.

The cooling process in some types of windcatcher (such as the vernacular windcatchers) can also be accompanied by evaporation (as evaporation is a heat consuming process). In this type of windcatcher, moisture is located at the bottom of the shaft, and when wind pass over a

moister, it helps evaporation and absorb ambient heat which help cooling processes. Although the evaporating technique is very useful to improve the efficiency of windcatchers, it might not be very feasible once the issues of cost and benefit are considered [1].

2.2.3.1.2 Stack effect

The stack effect occurs in windcatchers due to density differences between indoor and outdoor air. Wherever a breeze passes through the top of a windcatcher, even if it is not felt at the bottom, a pressure gradient forms between top and bottom of the column which helps to introduce cooler denser air to the building and exhaust warmer, lighter air from the windcatcher's structure. Furthermore, as there are usually some openings in lower level of the building (where denser heavier cool air is located), fresh air enters the building from the openings and hotter lighter air exhausts from the top of the room [12].

During the night the temperature of outdoor area reduces, therefore denser cooler air enters to the windcatcher's structure. The cooler denser air that enters to the structure is mixed with the hot air that have been absorbed by the windcatcher's structure and building during the day, then mixed hotter air goes up from structure or other opening in the building and fresh, cooler air is introduced to the indoor area, this cycle continues until the temperature of the windcatcher's structure and outdoor temperature become equal. For that reason, windcatcher can benefit from this function during the night in the area where the cumulative effect over a 24 hour period is quite noticeable [75]. Figure 2-4 [15] shows the function of a wind catcher system during day time and night time.
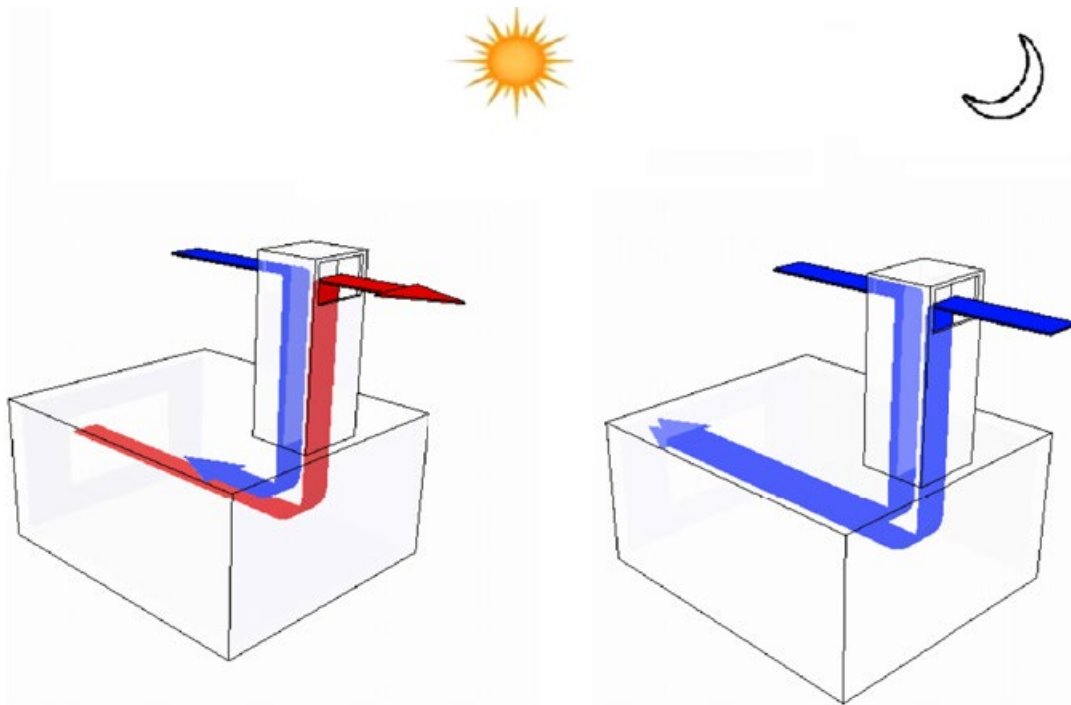
Figure 2-4. Function of a windtower system during day time and night time [15]

During the day when there is no or less wind, the windcatchers act as solar chimneys. And same as a solar chimney, windcatcher increases the air exhaust as a result of heating up the windcatcher's surface. Furthermore, as windcatchers create air movement inside the area and the air movement helps with the evaporation of sweat from body surfaces, windcatcher creates more pleasant environment in a very hot time of the year.

2.2.4 Solar chimney

A solar chimney is a vertical shaft utilizing solar energy to enhance the natural stack ventilation through a building. Solar chimneys rely primarily on the principles of thermal buoyancy. There are however many parameters that can affect the performance of a solar chimney. These can be based on weather conditions such as wind speed, wind direction, shading conditions and variations in external temperature [6]. Figure 2-5 shows various forms of solar chimneys.
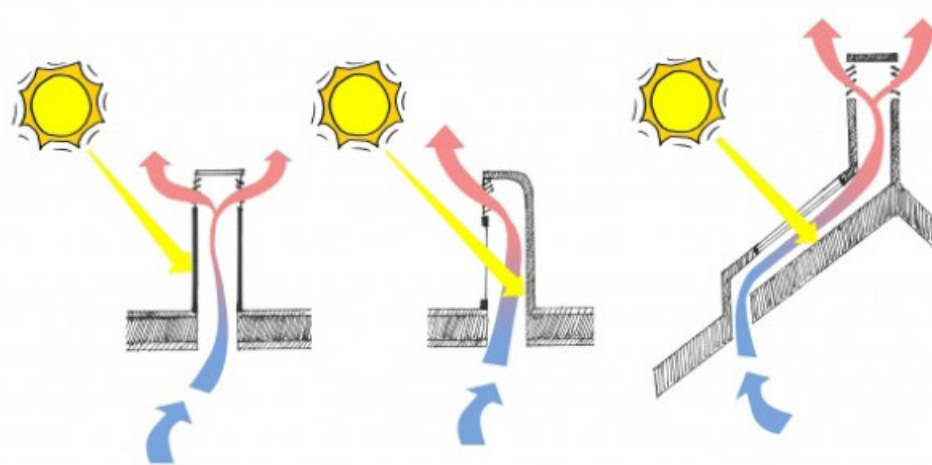
Figure 2-5. Various forms of solar chimneys [76]

Building design parameters such as internal heat gains, building fabric, chimney height, length and width, shape, dimensions, orientation, and inlet and outlet aperture size, glazing, and insulation will also play an important role in the performance of a solar chimney.

2.2.4.1 Design elements of solar chimney

The role of a solar chimney is to generate stack driven ventilation therefore, its primary design targets are to maximize and sustain the conditions that create stack effect which are temperature and pressure differences [3]. The basic design elements of a solar chimney are the solar collector, the ventilation shaft and the inlet and outlet openings. The solar collector area: mainly located at the top part of the chimney. It can include the entire shaft. The orientation, type of glazing, insulation and thermal properties of the solar collector are important to utilize solar gains.

Chimney height is an important parameter that will affect temperature and pressure differences and thus the potential force of the stack effect. According to Afonso and Oliveira [77] greater air flow rates and amplitude can be achieved through a solar chimney by increasing its length and cross section; this can be more effective than increasing the height.

Elmualim and Awbi [78] investigate the relationship between air flow and the cross section shape of a chimney. They found that air flow for a rectangular chimney extract is much higher than that for a cylindrical for the same wind speed. It is speculated that the sharp edges of the

38

square system create a larger region of flow separation and thus higher pressure difference across the device. The use of insulation reduces heat losses therefore it can increase day time as well as night time flow rates. It has been demonstrated that in certain climate and type of solar chimney the lack of insulation can reduce the efficiency of ventilation considerably [77].

Increasing the length of a solar chimney increases its exposure to solar gains. It also allows apertures to be elongated and placed at higher levels thus drawing air from a wide area closer to the ceiling where it is warmer. AboulNaga and Abdrabboh [79] demonstrate that combining a wall shaft with a solar chimney on the roof of a building, effectively increasing the overall height of chimney, increases the induced flow rate and cooling load of a building.

Ding, Hasemi [80] note that the height of a solar chimney connected to a double skin space influences the quantity of solar radiation absorbed by the thermal storage wall and stack effect occurring in the space, consequently increasing air change rate. The use of a solar chimney may benefit natural ventilation and passive cooling strategies of buildings thus help reduce energy use, C02 emissions and pollution in general.

2.2.5 Computational Fluid Dynamics (CFD)

CFD is particularly dedicated to fluids that are in motion, and the effects of the fluids flow behaviours on different processes [81]. This directly infers to the fluid dynamics description appearing in the terminology. Additionally, the physical characteristics of the fluid motion can usually be described through fundamental mathematical equations, usually in partial differential form, which govern a process of interest and are often called governing equations in CFD [82].

CFD is fundamentally based on the governing equations of fluid dynamics. They represent mathematical statements of the conservation laws of physics:
1. Mass conservation law
2. Newton's second law
3. First law of thermodynamics

CFD has become a powerful tool to be employed either for pure or applied research or industrial applications. Computational simulations and analyses are increasingly performed

in many fluid engineering applications [81]. However, CFD results and predictions does not provide 100% accuracy and they will need to be checked by experimental observations and empirical measurements. CFD can provide detailed airflow velocity distribution and thermal conditions; for most applications of ventilation and turbulence flow, the results have been approved to be useful and reasonably accurate [74].

There are many advantages in considering computational fluid dynamics. Firstly, CFD presents the perfect opportunity to study specific terms in the governing equations in a more detailed fashion. Secondly, CFD complements experimental and analytical approaches by providing an alternative cost-effective means of simulating real fluid flows. Particularly, CFD substantially reduces lead times and costs in designs and production compared to experimental-based approach and offers the ability to solve a range of complicated flow problems. Thirdly, CFD has the capacity of simulating flow conditions that are not reproducible in experimental tests found in geophysical and biological fluid dynamics, such as nuclear accident scenarios or scenarios that are too huge or too remote to be simulated experimentally. Fourthly, CFD can provide rather detailed, visualized, and comprehensive information when compared to analytical and experimental fluid dynamics [81].

A complete CFD analysis consists of pre-processor, solver, and post-processor. It simply encompasses the procedures of appropriately setting up the flow problem, solving and monitoring the solution, and analyzing the CFD results at the end of the simulation [83].

2.2.5.1 CFD Techniques for Turbulence Models

The most common CFD techniques for turbulence models are as the following:
- Direct Numerical Simulation (DNS)
- Large Eddy Simulation (LES)
- Reynolds Averaged Navier-Stokes (RANS)

Each method handles turbulence differently and among those models RANS is widely used by most of CFD software [84].

DNS offers the highest accuracy in flow simulation as the instantaneous continuity and the Navier-Stokes equations were computed without approximations. To certain extent, DNS

provides more information than experiments do. It requires a fine grid resolution to catch the smallest eddies in the flow. An eddy, a small element of swirling flow, is typically 0.1 to 1 mm in size in a room with turbulence flow. This often requires the total grid number for a three-dimensional indoor airflow exceeding 10^{10}. Current super computer capacity is still far too small to solve such a flow (current super computers can handle a grid resolution as fine as 10^8). In addition, the DNS method solves the time-dependent flow with very small time steps to account for eddy backup and reforming that occurs in a flow that on average is steady. This makes the calculation extremely time consuming [81].

Large eddy simulation (LES) is based on the approach of resolving large turbulent structures in space and time down to the grid limit everywhere in the flow. It refers to small elimination in the numerical simulation for turbulence flows [81]. It is done through a proper low pass filter applied to Navier-Stokes equations, and to equations for the energy and the other quantities transported by the fluid. It is somehow insufficient to describe eddies of all scales solely using the Reynolds-averaging approach as the properties of eddies change with their length scale. LES is a simulation that directly solves the large-scale motion but approximates the small-scale motion [85].

RANS is the fastest method but it may be the least accurate one. RANS solves the time-averaged Navier-Stokes equations by employing approximations to simplify the calculation of turbulent flow. Steady flow can be solved as time independent in RANS method. Therefore, the computing cost are the cheapest compared to those for LES and DNS [81].

2.2.5.2 Different RANS CFD methods

There are many RANS turbulence models including algebraic one, one-equation, two-equation, and Reynolds stress models. Two-equation models are the most popular turbulence models for scientific and engineering calculations. Some of the well-known two-equation turbulence models are:

- K- ε model
- K- ω model
- RNG K- ε model

2.2.5.2.1 K- Ɛ model

This turbulence model was proposed by Harlow and Nakayama in 1968 [86] and has been known as the most widely-used two-equation eddy-viscosity turbulence model; mainly due to its good convergence rate, relatively low memory requirements and reasonable predictions for many flows. The K- Ɛ model solves for two variables: K; the turbulent kinetic energy, and Ɛ the rate of dissipation of kinetic energy. It does not very accurately compute flow fields that exhibit adverse pressure gradients, strong curvature to the flow, or jet flow. It does perform well for external flow problems around complex geometries [81].

The standard K- Ɛ model turbulence model was introduced by Launder and Spalding in 1974 [87] based on the minimizing of unknown parameters and presenting a set of equations which can be applied to a large number of turbulent applications. Its accuracy is reasonable based on its computational efforts It is very applicable to many complex flows of engineering importance.

2.2.5.2.2 K-ω model

The K-ω model is similar to K- Ɛ however, it solves for ω which is the specific rate of dissipation of kinetic energy. The SI unit for ω is 1/s. It also uses wall functions and therefore has comparable memory requirements. It has more difficulty converging and is quite sensitive to the initial guess at the solution. The K-ω model is useful in many cases where the K- Ɛ model is not accurate, such as internal flows, flows that exhibit strong curvature, separated flows and jets. It is generally used for near wall problems [81].

2.2.5.2.3 RNG K- Ɛ model

The RNG model was developed using Re-Normalisation Group (RNG) methods by Yakhot et al [88] to renormalize the Navier-Stokes equations, to account for the effects of smaller scales of motion. In the standard K- Ɛ model the eddy viscosity is determined from a single turbulence length scale, so the calculated turbulent diffusion is that which occurs only at the specified scale, whereas in reality all scales of motion will contribute to the turbulent diffusion. The RNG approach, which is a mathematical technique that can be used to derive a turbulence model similar to the K- Ɛ model, results in a modified form of the epsilon equation which attempts to account for the different scales of motion through changes to the

production term. Although the technique for deriving the RNG equations was quite revolutionary at the time, its application has become less frequently used due to no improvements over the standard model for predicting vortex evolution [81].

2.2.5.3 CFD and Finite Volume Method

The finite volume method (FVM) is a discretization technique for partial differential equations, especially those that arise from physical conservation laws (governing equations). FVM uses a volume integral formulation of the problem with a finite partitioning set of volumes to discretize the equations. FVM is in common use for discretizing CFD equations. The finite-volume characteristic of CFD codes implies that an infinite reality has to be constrained in an internal volume of a domain. This domain is defined by physical boundaries and sub-divided into cells, which transmit the flow information calculated by equations through their nodes and faces. Conversely, the domain dimensions and the mesh type and size must not influence or change the characteristics of the resultant flow. Accurate results must be grid independent [81].

2.2.6 Review about windcatcher's in the literature

2.2.6.1 Windcatchers performance

Much research has been undertaken with regards to the ability of windcatchers to provide natural ventilation and cooling in hot and arid areas. Elmualim [75] investigated the post occupancy performance of a building ventilated by a windcatcher. The results show that there is a better ventilation rate in buildings with a windcatcher in comparison to a building ventilated with the same size of windows. Elmualim and Awbi [78] carried out wind tunnel tests and CFD modelling to compare the performance of a windcatcher with square and circular plans. This research revealed that the performance of a square plan windcatcher is considerably better than circular plan windcatcher due to a larger area of flow separation and higher pressure differences on the sharper edges of square windcatchers. Elmualim and Awbi [78] has also run a CFD model of a square windcatcher to examine the relationship between air flow rate and external wind velocity upon different wind angles. By comparing experimental and numerical results, they found that wind tunnel testing and CFD together are vital in terms of analysing the

performance of a windcatchers. In addition they have found that in the examined windcatcher of 500 mm square and 550 mm circular openings during the times when outdoor wind velocity is less than 3 m/s, windcatcher cannot provide sufficient fresh air for ventilation purposes. Estimating the performance of a natural ventilation system is found to be very important if one is to correctly size the system for a particular application. Jones and Kirby [89] have presented a semi empirical approach using experimental data published in the literature in order to provide a fast but accurate estimate of the windcatchers performance.

Hughes and Ghani [90] investigated the performance of windcatchers with different wind-directions and wind velocities in order to provide recommended amount of fresh air to the building. The results show that windcatchers can provide acceptable amount of fresh air to the building even if the outdoor wind velocity is low. However, this research did not investigate the ability of windcatcher to provide acceptable thermal comfort for occupants.

Niktash and Huynh [14] has investigated the effect of two sided windcatcher inlet / outlet on ventilation of a three dimensional room. This research has concluded that when the inlet / outlet cross section is perpendicular to the wind direction it satisfies the human comfort requirements for having proper indoor ventilation and it leads to enhance the performance of windcatchers. Li and Mak [74] made a three dimensional CFD model of a windcatcher to investigate its performance under different wind speed and wind direction. Both studies prove that windcatcher's performance depends on wind speed and as wind speed increases, the windcatcher's performances improve with the best direction of wind being face on windcatcher is 0 degrees.

Dehghani et al [24] proposed a new design for windcatchers where the windtower can rotate manually or electronically to face the direction of the maximum wind speed. A wind vane can be used to detect the direction of the wind. Hosseini et al [16] have investigated six configurations of four sides windcatchers and summarized that the general features of the streamline and air flow velocities predicted by the realizable k - ε model for turbulent flow were similar to those predicted by the standard k - ε and standard k – ω models [19].

Ahmed et al [91] has also studied the performance of windcatchers in 3D using two CFD solvers Ansys Fluent and Open Foam and has concluded that the geometry and location of the windcatcher has to be optimized to improve the thermal comfort inside the room [19]. Spentzou

et al evaluated retrofit strategies including individual night and day ventilation, a windcatcher and a dynamic façade, and concluded that the combined operation of the windcatcher and dynamic façade delivered operative temperature reductions of up to 7 °C below the base case strategy, and acceptable ventilation rates for up to 65% of the cooling period [92].

According to Bahadori [93] the disadvantage of applying windcatchers is that, it allows dust, insects, small birds and hail to enter buildings. In addition, the wind speed affects windcatcher's performance which becomes inefficient in areas with low wind speeds.

2.2.6.2 Windcatcher based on a combined winddriven and buoyancy driven ventilation

Jazayeri [94] has investigated the necessity of enhancing the traditional windcatcher and concluded that the solar windcatcher that uses both sun energy and wind energy helps lower CO_2 levels. Saadatian et al [1] have reviewed windcatcher technologies and concluded that the combination of different passive tools such as solar chimney and windcatcher is recommended for its efficiency where a combined solar chimney and windcatcher can serve to reduce the temperature up to 15°C and to double the internal air flow.

Bansal et al [95] studied a solar chimney-assisted wind tower for natural ventilation in buildings. The combination of wind tower and solar chimney enabled wind and buoyancy forces to be utilized to generate air flow in the building. The estimated effect of the solar chimney was shown to be substantial in promoting natural ventilation for low wind speeds. Hunt and Linden [96] described the fluid mechanics of natural ventilation by combined effects of buoyancy and wind. It was shown that there is a Pythagorean relationship between the combined buoyancy and wind driven velocity and the velocities produced independently.

Leng et al [97] observed that the performance of the absorber material of a solar chimney is based on its thermal conductivity. The findings show that metal absorber materials especially copper perform better compared to PVC, glass and concrete. Liu et al [98] analysed the natural cross ventilation in buildings driven by wind and buoyancy forces and indicated that the thermal buoyancy force has a significant impact on airflow structure and airflow rate of buildings. Dehghani et al [24] also proposed using a solar chimney or an air heater in another part of the building opposite to the windtower. Gan [99] has also carried out simulation for combined wind and buoyancy driven ventilation and the results showed that wind adversely

affects the air flow pattern in buildings designed with buoyancy driven natural ventilation. Wind can simultaneously assist and oppose buoyancy in the windward and leeward sides, respectively, while buoyancy can oppose winddriven flow in both sides.

Hughes & Cheuk-Ming [100] studied the wind and buoyancy driven flows through commercial windtowers and found that the wind is the primary driving force providing 76% more internal ventilation than buoyancy driven flow. This study determined that the addition of an external airflow passage such as a window in combination with buoyancy would increase the indoor ventilation by 47%.

The sustainable design of a windcatcher improves the building`s energy performance by utilizing natural resources to provide fresh air to the environment and increase the level of human comfort consequently. Previous research have revealed a gap regarding the effect of the architectural design of the windcatcher such as its width, height and openings sizes and the influence of their performance on the airflow and human comfort [16]. Nowadays the advanced modelling and simulation tools are capable to test and evaluate the building performance effectively and help design a naturally ventilated building [17].

2.3 Green Walls

2.3.1 Introduction

Green wall is the common term to refer to all forms of vegetated wall surfaces. Green walls can be subdivided in two main systems: green facades and living walls [47]. There is an evident distinction between green facades, where usually climbing plants grow along the wall covering it, and the most recent concepts of living walls, which include materials and technology to support a wider variety of plants, creating a uniform growth along the surface. Green facades can be classified as direct or indirect. Direct green facades are the ones in which plants are attached directly to the wall. Indirect green facades include a supporting structure for vegetation. Living wall systems (LWS) can be classified as continuous or modular, according to their application method. Continuous LWS are based on the application of lightweight and permeable screens in which plants are inserted individually. Modular LWS are elements with a specific dimension, which include the growing media where plants can grow [47]. Each element is supported by a complementary structure or fixed directly on the vertical surface

[25]. Figure 2-6 shows an indoor installation of a vertical green wall in the Faculty of Engineering and IT at UTS.

Figure 2-6. Indoor installation of a vertical green wall in the FEIT at UTS

Heat stress in cities can be addressed by increasing green spaces and using green walls and green roofs. These measures could reduce temperature by up to 10 °C in Mediterranean areas. This can also contribute to decrease flood risk and air pollution hazards, reduce energy demand in buildings (by 10–15%) and improve quality of life [47]. In fact the integration of vegetation in urban areas has several environmental benefits, contributing to the improvement of air quality, through the absorption of CO_2 and the retention of dust particles and heavy metals.

Green wall systems can also protect building envelope from local climate and surrounding environment. They have the ability to function as a complementary acoustic protection [48] contributing to improve comfort of interior spaces. In fact, green walls can be integrated in buildings among several passive design solutions as a strategy of evaporative cooling [38, 47].

2.3.2 The breathing wall

Consequently, in recent years, green wall technology has been proposed as a means of passively improving the capacity of botanical air cleaning methods [32]. Active green walls have the potential to accelerate the progress of horticultural means of air pollutant removal. They consist of patterns of relatively small (0.25 m^2) composite modules containing 16 plants, and includes an axial impeller to pass indoor air across the plant growth substrate. The addition of ventilation, plus the modular nature of the system may have the potential to both increase the systems' effectiveness at reducing some air contaminants, as well as increasing its installation flexibility as to allow increased light, through which the carbon dioxide removal potential can be increased. However ventilation also poses the potential risk of aspiration of dangerous microorganisms into indoor spaces [32]. Figure 2-7 shows a recent installation of the Junglefy breathing walls.

Figure 2-7. A recent installation of the Junglefy breathing wall

2.3.3 Green wall module design

The Junglefy Breathing wall modules are designed for use in vertical plant-walls. The module's material construction is composed of recycled plastic, supplied with a growth medium high in coconut fibre content, supplemented with a liquid fertilizer and periodic watering supplied via channels at the top of each module, connected to a receiving trough at the base. The dimensions of each module are 500 mm^2 and approximately 100 mm deep, which holds 16 plants horizontally in circular compartments. Each module includes a small electric axial impeller which, when activated, provides a uniform flow of air up through the growth medium and past the plants [32].

2.3.4 Plants as biofilters and botanical air cleaning

Research over the last three decades has demonstrated that passive biofiltration with indoor plants can significantly reduce concentrations of most types of urban air pollutants [101-103]. The primary advantages of passive biofilters are cost and flexibility of installation. There is an international body of evidence that demonstrates direct beneficial effects of indoor plants on human health, psychological wellbeing, and work productivity [26-28].

The biologically active component of botanical air filtration systems for hydrocarbon VOC biodegradation is the microorganisms associated with the roots of the plants or the growing substrate of the plants. The removal of several other contaminants, however, such as CO_2 [32, 104], SOx, NOx and ozone appear to be mostly or wholly plant mediated, and are taken up directly through the stomates (gas exchange pores) of the green shoots, which in most species are open only during daylight hours, and not in the dark [69].

Particulate matter [26] is effectively reduced by living plants by deposition through the extensive boundary layer area present around leafy tissue. To maximize the capacity of biofiltration systems, there is thus a need to process as large a volume of contaminated air as possible, whilst exposing the air to the biological material for the critical time period over which sufficient pollutant removal will occur to allow air contaminants to be reduced to habitable levels. These two variables: airflow and residence time are clearly the key attributes to maximise the efficiency of any system [69].

An active biofiltration system using a column containing inert substrates and compost, and supporting the growth of spider plant (Chlorophytum comosum), a species known to be capable of formaldehyde biodegradation, was tested by [105], and found to be very effective at removing high concentrations of formaldehyde. Active systems thus may have potential to substantially increase the effectiveness of botanical biofilters, although at the cost of some energy. Active biofiltration is now a widely used air pollution control technology for industrial waste gases and odours [69].

Systems are now becoming highly developed and due to low running costs, high removal efficiency for a range of organic and inorganic gaseous pollutants and lack of secondary pollutant production are now competitive. Whilst it is usually assumed that active biofilters will remove higher quantities of air pollutants than passive systems due to the increased rate of airflow over the biodegradative surfaces [67], there appears to be no literature comparing an active system to an otherwise identical passive arrangement, and thus there is no empirical evidence to show that actively increasing the airflow to a system increases biodegradation over simple diffusion. Also, the potential generation of CO_2 from substrate microorganism respiration, and the emission of microbial particles are other issues that have been inadequately addressed in the literature. Clearly, there is a need for greater research on the correlation between the rate of airflow and all types of air quality for active indoor air quality bioremediation systems [69].

2.3.5 Green walls and air quality

Extensive research has demonstrated that indoor plants can improve air quality. The combined biological activities of the plant and substrate have been shown to be capable of reducing many types of urban air pollutants including volatile organic compounds [103], carbon dioxide [106] and particulate matter [34, 107, 108]. VOCs are numerous and varied, they include both human made and naturally occurring compounds. Some examples of VOCs are Benzene, Methylene Chloride and Formaldehyde. There has been a small number of studies related to VOC removal by green wall systems. Darlington et al [109] and Wang et al [110] both detected VOC removal from their green wall systems. Darlington et al [109] documented the greatest reduction in green wall VOC concentrations under the slowest influent air flux tested (0.025 m/s); however, the maximum amount removed per unit time occurred under the

most rapid flux (0.2 m/s), roughly equivalent to 1.5 – 12.5 m^3 of air per m^2 of biofilter per minute. The removal capacity was between 1.3 and 2.4 $\mu molm^{-3}/s$.

Wang and Zhang [111] tested the capacity of an experimental active green wall to remove formaldehyde, detecting a high level of efficiency as did Lee et al [112] who also tested the particulate matter filtration efficiency of their system detecting 65 – 90% removal efficiency. Torpy et al [113] investigated the potential of green walls to reduce high CO_2 concentrations, and demonstrated that functional active green wall technology efficiently removes substantial CO_2 from the indoor air and thus reduce ventilation energy costs provided that sufficient light is supplied.

Active green walls also have the potential to be stand-alone air treatment systems [114], with their development specifically for air phytoremediation becoming a rapidly growing field of research interest [115]. Darlington et al [109] assessed the effect of air flow rate on the capacity of an active botanical biofiltration system to remove airborne toluene, ethylbenzene and o-xylene. Recent work by Irga et al [107] evaluated an active green wall's PM removal efficiency through the quantification of the system's single pass particulate filtration efficiency, finding that the maximum filtration efficiency for all particle fractions peaked an air flow rate of 11.25 L/s per 0.25 m^2 modular unit. The system at its maximum efficient air flow rate recorded single pass removal efficiencies of 53.35% for TSP, 53.51% for PM_{10} and 48.21% for $PM_{2.5}$.

Pettit el al [34] examined the influence of the botanical component of active green wall PM removal efficiency (SPRE) focusing on evaluating the air filtration features of different plant species in green wall modules, all tested botanical biofilters outperformed biofilters with only the substrate indicating that green wall plants play a role in PM filtration.

2.3.6 Green walls and acoustic comfort

Plants are able to absorb a valuable amount of acoustic energy, with this effect particularly associated with the soil substrate, which is able to absorb up to 80% of acoustic incident energy [116]. Green walls demonstrate equivalent or better acoustic absorption coefficients compared to other common building materials [117], with particular effects on low frequencies. Davis et al [118] tested the sound absorption properties of a vertical garden concluding that thicker substrates provide higher sound absorption coefficients in the lower frequencies. A thinner substrate can be used if lower frequencies are not important; in general they found that an 8 –

10 cm substrate thickness would result in a good sound absorption spectrum. Their study [118] also found that the weighted random incidence and absorption coefficient of modules densely planted with ferns equals 1.00 for mid and high frequencies, and 0.59 – 0.80 for low frequencies. This makes this type of substrate highly suitable for applications were sound attenuation is needed, paving the way for applying vertical garden systems for improving the acoustics indoor spaces or public areas.

2.3.7 Green walls and energy savings

Green walls also show promise in providing many additional benefits especially in regards to energy savings. The mechanisms by which green façades can be used as passive energy saving systems [38] are through the effects of the shadow produced by the vegetation, the insulation provided by both the vegetation and the substrate, the barrier effect to wind and the evaporative cooling by evapotranspiration. Coma et al [119] compared the performance of vertical green systems with green façades and have found that vertical green systems provide higher cooling performance, achieving savings in electrical energy consumption of 58.9% while green façades provided a reduction of 33.8%, with both systems compared to a reference with internal conditions at 24 °C.

Wong et al [120] simulated the effects of vertical greenery systems on temperature and energy consumption of buildings, specifically testing the influence of the shadow effect on energy consumption reductions for refrigeration. These authors concluded that the shadow effect was closely related to the density of the foliage, and that reductions between 10% and 31% in the cooling energy load were possible due to the effect of greenery. Perez et al [121] reviewed the literature on vertical greenery systems as a passive tool for energy savings in buildings, and concluded that there are four key aspects to be considered; the system classification, the influence of climate, the influence of plant species and the operational methods. It was concluded that vertical greenery systems are an effective tool for energy savings during the cooling period in warm temperature and arid climates, providing reductions between 5% and 50%, especially on the west façade influenced building surfaces.

De Gracia et al [122] investigated the impact of vegetation on the energy consumption in a real building by implementing an extensive green façade and an intensive green wall system. Experimental measurements showed that during the cooling period, the electrical energy

consumed by the HVAC system to achieve the desired temperature (24 °C) was reduced with both greening systems when compared to a reference system. The achieved energy savings were around 33.9% in case of extensive green façade and 59.9% in case of intensive green wall. Perini et al [123] performed an experimental investigation to evaluate the cooling potential of a well vegetated vertical greening system during summer in the Mediterranean climate of Italy and found out that the cooling capacity of vertical greening can be exploited to reduce energy demand for air conditioning, with a theoretical energy saving potential of 26% for summer season.

2.3.8 Gap in knowledge

Active green walls represent an emerging technology for the removal of pollutants present in air streams, with many conventional analyses yet to be applied to these systems [49]. Currently there is a gap in knowledge for this rapidly expanding technology, and it is clear that a uniform and standardized approach to characterizing key parameters is required for accurate performance evaluation. This, in practice, may be difficult to achieve, with the existing green wall systems having differing structures and thus differing air flow distributions, with air either flowing through the filtration media of the system and into ducting before return to the environment, or the reverse [50], and a vast diversity in designs, substrate types and thicknesses, moisture levels and pressure drop characteristics. Thus, we present a novel method for the characterization of air flow distribution and hence efficiency through a green wall module, to facilitate future Computational Fluid Dynamics (CFD) methods to be verified with empirical data. To obtain the correct parameters, which include the various resistances to flow, experimental work was conducted including measuring the air flow rate and pressure change across the module. To achieve this, it was essential to design an experimental set-up capable of measuring the very low airflow rate passing through the module, especially when such low through-flow is part of a much larger total flow that includes strong flow reversal occurring in the inlet air-duct and thus not passing through the filtration media. The current work thus provides an initial study directed at optimizing the airflow characteristics of our test system.

2.4 Phase Change Material

Phase change materials use the latent heat properties of materials to store large amounts of energy, which is charged and discharged by passing air through a heat exchanger. Materials that change phase at room temperature are frequently referred to as Phase Change Materials (PCMs). During the day as warm air is passed over the PCM it absorbs thermal energy from the air to turn from solid to a liquid thus cooling the air. Overnight as cooler air is passed across the PCM it releases the thermal energy it absorbed from the warm air during the day returning to its solid state.

2.4.1 Phase Change Material working principle

The working principle of PCM based free cooling for buildings consists of two modes of operation, the charging and the discharging process [124].

Charging process (solidification of PCM) is carried out during night time when ambient temperature is lower compared to room temperature. The cool ambient air flows through storage unit and takes away heat from liquid PCM which starts solidifying at certain constant temperature [125]. Charging process continues until the ambient temperature is lower enough than the melting/solidification temperature of PCM [126]. During the charging process the heat removed from the PCM is added to the air. Figure 2-8 [126] shows the working principle of PCMs.
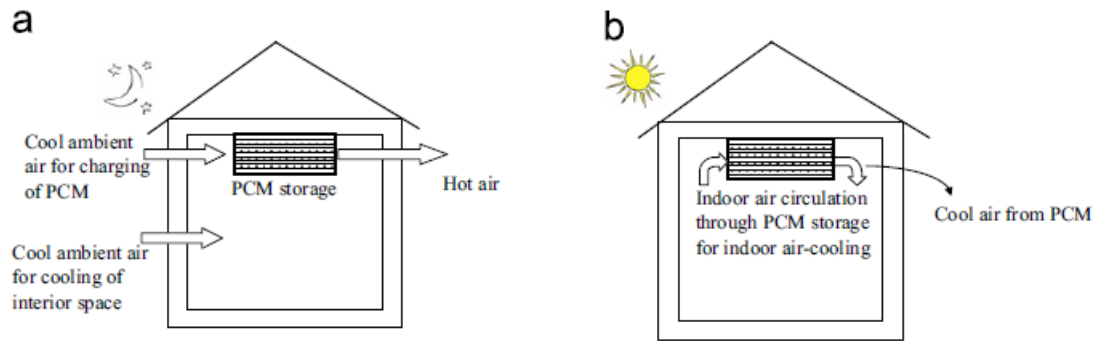
Figure 2-8. PCM working principle a) night time charging process, b) day time discharging process [126]

Discharging process (cooling of air) is carried out when the room temperature rises above the comfort limit and the cold stored in PCM is discharged. Hot air which is to be cooled passes through the PCM storage unit and PCM (which is in solid state after charging operation) absorbs heat from the air. The air thus cooled to comfort temperature from the storage is delivered to the living space. PCM absorbing heat from air, starts converting from solid to liquid phase at certain constant temperature. This process is called "discharging process [125]."

Melting point of PCM plays a key role in the designing of the PCM storage unit. For free cooling applications PCMs should be selected in such a way that the cooled air temperature out of the storage unit during discharging process be within the range of defined comfort levels which is between 23 °C and 27 °C for summer season. Therefore for free cooling systems the melting temperature of the PCM should be between 19 °C and 24 °C [127].

2.4.2 Types of Phase Change Material

Materials to be used for phase-change should have melting freezing temperature in the practical range of application and they must have a high latent heat of fusion and a high thermal conductivity [124]. Moreover, PCMs should have desirable thermophysical, kinetic, chemical and economic properties as suggested. PCMs should also have desirable environmental properties to decrease the environmental impact of the systems during their lifecycle.
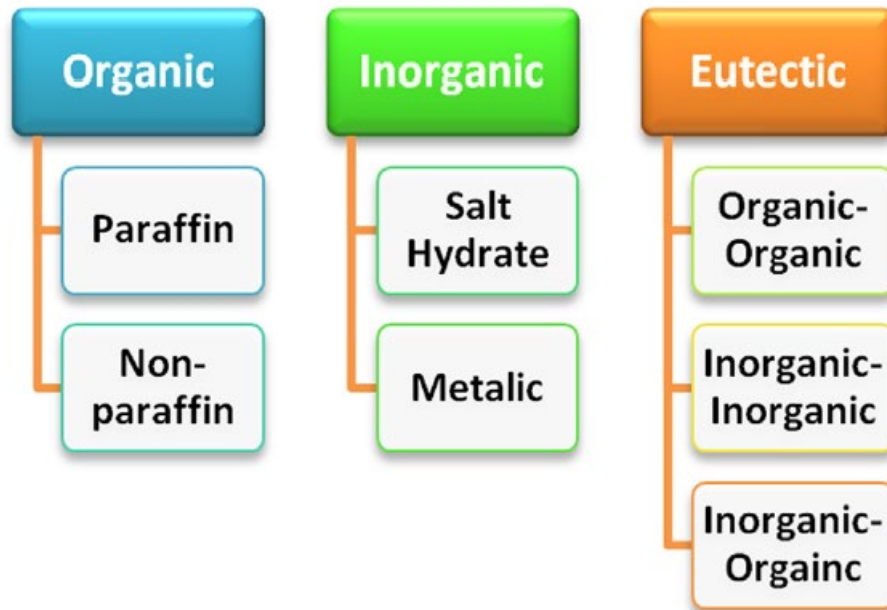
Figure 2-9. Types of Phase Change Materials [51]

PCMs are classified as organic, inorganic and eutectic. Organic PCMs are further described as paraffins and non-paraffins [124]. The non-paraffins include a wide selection of organic materials such as fatty acids, esters, alcohols and glycols [128]. Of most interest in this group are the fatty acids which are subdivided in 6 groups: caprylic, capric, lauric, myristic, palmitic and stearic [128]. Inorganic PCMs are further described as hydrated salts and metallic (metals have high melting temperatures for passive building applications). An eutectic is a minimum-melting composition of two or more components, each of which melts and freeze congruently forming a mixture of the component crystals during crystallization [129]. Eutectics PCMs are subdivided in organic–organic, organic–inorganic and inorganic–inorganic [44]. Figure 2-9 [51] shows the different types of phase change materials.

Figure 2-10. Different PCM products [126]

PCM products come in different performance temperatures and densities based on the manufacturer and the application conditions [124]. They are not a replacement for insulation. The best place to install the product is above you. Figure 2-10 shows different PCM products. To determine quantities used, the general rule is 1 to 2kg of PCM per m^3 of interior space. The actual amount is dependent on the quality of the build (insulation, tightness, quality, size, and orientation of windows), building design & orientation, but basically the more the better. Modelling of the quantities and of the position where to install the material can be done as required.

2.4.3 Phase Change Material research trend

According to the published literature [130, 131], the regions around the world where PCM based free cooling is either implemented or studied are conducted in Europe (73%) with very few in Asia like Japan and China. Most of the studies are conducted for the developed countries especially Europe where energy efficiency, energy conservation and climate change are much discussed topics.

The number of articles concerning the integration of PCMs in buildings to improve their energy efficiency has been increasing during the last decade. Before 2003 only 2 review articles on

this subject are found in the literature. During the last years more comprehensive and particular reviews of PCM latent heat systems and their applications have been made, and more than 20 extensive review articles about the potential of integrating PCMs in buildings were published, allowing to conclude that interest in the subject is rising [43, 44]. Most reviews deal with the general problem of using PCMs, focusing on the PCMs characterization classification and on the building active and passive applications. Figure 2-11 [51] indicates the number of published articles including all topics related to PCMs from 2000 to 2014 in the web of science database.
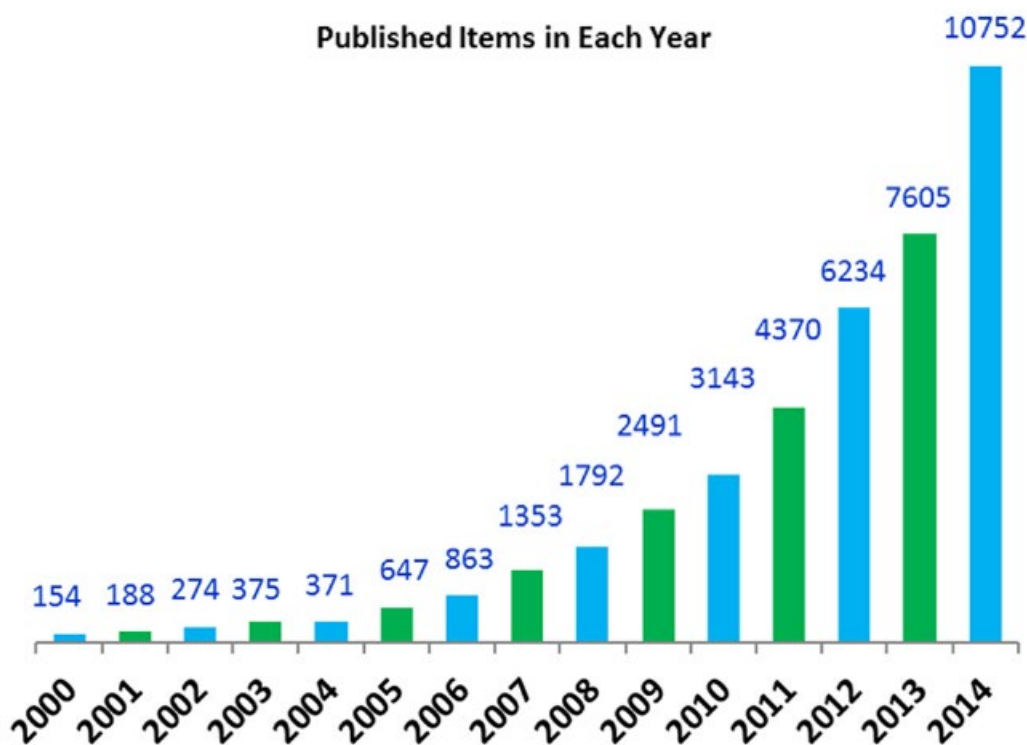
Figure 2-11. Papers published related to PCMs from 2000 to 2014 in the web of science database [51]

However, during the last years more specific issues were reviewed and it is foreseeable that the article reviews concerning the problem of integrating PCMs in buildings, to meet the demand for thermal comfort and energy conservation / savings purpose, will gradually be more specialized on certain subjects, as a consequence of the large amount of work that is being developed worldwide [124].

2.4.4 Review about PCM and buildings

Akeiber et al [51] reviewed PCM for sustainable passive cooling in buildings and concluded that the organic type particularly the paraffin is the most appropriate due to its price, stability and high heat of fusion however it has low thermal conductivity [126]. The study proposed that integrating PCM with natural ventilation must be explored, such as the combination of PCM with windcatchers could be very effective at providing both cooling and ventilation in a sustainable system. Ramakrishnan et al [132] analysed the performance enhancement of phase change material in naturally ventilated buildings and concluded that optimising the PCM based on its efficiency is the most appropriate approach to obtain maximum indoor thermal comfort. For Melbourne, Sydney, Perth and Brisbane the optimal phase change temperature to achieve the highest indoor thermal comfort was found to be 3-5 °C higher than the average outdoor temperature. The study also found that increasing the thickness of PCM results in enhanced thermal comfort but reduces the cooling efficiency.

Alvarez et al [133] has studied the integration of PCM for natural cooling of buildings and concluded that there are drawbacks in the way things have been done in PCM. Mosaffa et al [134] developed a computer model for the evaluation of a multiple PCM unit where its performance is studied numerically. Waqas and Ud din [126] has reviewed the phase change material storage for free cooling of buildings.

Soares et al [124] provided a comprehensive review in relation to how and where PCMs are used in passive cooling systems and how they are related to building energy efficiency. It was concluded that PCMs contribute to increase the indoor thermal comfort and in the reduction of CO2 emissions associated with heating and cooling.

2.5 Summary

This chapter has presented some of the literature related to natural ventilation, green walls and phase change materials.
The literature have revealed a gap regarding the effect of the architectural design of windcatchers such as its width, height and openings sizes and the influence of their performance on airflow. It is also concluded that efficient design for a natural ventilation

building should implement both types of natural ventilation, wind-driven ventilation and buoyancy or stack ventilation.

Green wall can produce changes in the ambient temperature and humidity of the surrounding air and they create an interesting insulation effect. The integration of vegetation in urban areas has several environmental benefits, contributing to the improvement of air quality. Green walls serve as a botanical filtration device which can decrease the percentages of VOCs and PMs and they contribute to a healthier indoor environment.

The review of the literature has also revealed that phase change materials are a passive cooling technique which enhance thermal comfort. They show promise when combined with windcatchers to be very effective at providing both cooling and ventilation in a sustainable system.

Chapter 3 Simulation of ventilation flow through a room fitted with a windcatcher

Two dimensional and three dimensional simulations have been conducted to investigate the windcatchers performance by studying the effect of its inlet design and the effect of combining buoyancy driven and wind driven ventilation. Computational fluid dynamics tools (Ansys Fluent or CFD Ace+) are used for simulations. Most of the simulations (sections 3.1, 3.3 and 3.4) were conducted using Ansys Fluent while CFD Ace + was used in section 3.2.

In all the models studied in the following sections, a rectangular shaped room with a length of 5 m and height of 3 m has been considered for the two dimensional simulations. The width of the room was considered as 4 m in the three dimensional simulations. A two sided windcatcher has been fitted on the roof of the room. More details about the dimensions of the models will be presented in the following sections for each of the 2D and 3D simulations. To fully concentrate on the effects of the windcatcher, no doors, windows or any room accessories have been included.

The governing equations are those of Reynolds-averaged conservation of mass (eq. 1) and momentum (eq. 2), and balance of energy (eq. 3), for turbulent incompressible flow, plus the two transport equations (eq. 4 and 5) for K and ε [135]. Following are the governing equations and turbulence-model constants:

$$\frac{\partial U_j}{\partial x_j} = 0 \tag{1}$$

$$\frac{\partial U_i}{\partial t} + U_j \frac{\partial U_i}{\partial x_j} = -\frac{1}{\rho}\frac{\partial P}{\partial x_i} + \frac{\partial}{\partial x_j}[\nu(\frac{\partial U_i}{\partial x_j} + \frac{\partial U_j}{\partial x_i}) - \overline{u_i u_j}] - \beta(T - T_{ref})g_i \tag{2}$$

$$-\overline{u_i u_j} = \nu_t (\frac{\partial U_i}{\partial x_j} + \frac{\partial U_j}{\partial x_i}) - \frac{2}{3}K\delta_{ij}$$

$$\rho c(\frac{\partial T}{\partial t}+U_j\frac{\partial T}{\partial x_j})=k\frac{\partial^2 T}{\partial x_j \partial x_j}-\rho c\frac{\partial}{\partial x_j}(\overline{u_j T'})+\Phi+\phi \qquad (3)$$

$$\overline{u_j T'}=\frac{v_t}{\sigma_t}(\frac{\partial T}{\partial x_j})$$

$$\Phi=\mu(\frac{\partial U_i}{\partial x_j}+\frac{\partial U_j}{\partial x_i})\frac{\partial U_i}{\partial x_j}$$

$$\phi=\mu\left(\overline{(\frac{\partial u_i}{\partial x_j})(\frac{\partial u_i}{\partial x_j})}+\overline{(\frac{\partial u_i}{\partial x_j})(\frac{\partial u_j}{\partial x_i})}\right)$$

$$\frac{\partial K}{\partial t}+U_j\frac{\partial K}{\partial x_j}=\frac{\partial}{\partial x_j}[(v+\frac{v_t}{\sigma_K})\frac{\partial K}{\partial x_j}]+v_t[(\frac{\partial U_i}{\partial x_j}+\frac{\partial U_j}{\partial x_i})\frac{\partial U_i}{\partial x_j}+\frac{\beta}{\sigma_t}g_j\frac{\partial T}{\partial x_j}]-\varepsilon \qquad (4)$$

$$K=\frac{1}{2}\overline{u_i u_i}$$

$$\varepsilon=v\overline{(\frac{\partial u_i}{\partial x_j})(\frac{\partial u_i}{\partial x_j})}$$

$$\frac{\partial\varepsilon}{\partial t}+U_j\frac{\partial\varepsilon}{\partial x_j}=\frac{\partial}{\partial x_j}[(v+\frac{v_t}{\sigma_\varepsilon})\frac{\partial\varepsilon}{\partial x_j}]+C_1\frac{\varepsilon}{K}v_t[(\frac{\partial U_i}{\partial x_j}+\frac{\partial U_j}{\partial x_i})\frac{\partial U_i}{\partial x_j}+\frac{\beta}{\sigma_t}g_j\frac{\partial T}{\partial x_j}]-C_2\frac{\varepsilon^2}{K} \qquad (5)$$

The subscript t refers to turbulence where: $\mu_t=\rho C_\mu K^2/\varepsilon$; $v_t=\mu_t/\rho$; $C_\mu=0.09$;

$C_1=1.44$; $C_2=1.92$; $\sigma_K=1.0$; $\sigma_\varepsilon=1.2$; and the turbulent Prandtl number $\sigma_t=0.9$

In the above equations (1) to (5), the reference temperature $T_{ref}=300$ K; U_i, u_i, T and T' are the mean and fluctuating parts of velocity components and temperature, respectively [135]. P is the mean pressure, t is the time, and x_i is the coordinate in the i-direction.

In sections 3.1 and 3.3, which will investigate the effect of the windcatchers inlet shape, the process has been assumed as an isothermal process minimizing the influence of thermal changes on ventilation quality. In these sections, temperature change due to the air flowing through the room (as a result of viscous heating) is expected to be negligible.

In sections 3.2 and 3.4, which will investigate the effect of combining buoyancy driven and wind driven ventilation, the Boussinesq model is used. For many natural convection flows, faster convergence is obtained with the Boussinesq model compared to setting up the problem with fluid density as a function of temperature. The Boussinesq model treats density as a constant value in all solved equations, except for the buoyancy term in the momentum equation:

$$(\rho - \rho_0)g \approx -\rho_0\beta(T - T_0)g$$

where

- ρ_0: is the constant reference density of the flow.
- T_o: is the operating temperature
- β: is the thermal expansion coefficient.

The Boussinesq approximation $\rho = \rho_0(1 - \beta\Delta T)$ is used to eliminate ρ from the buoyancy term. This approximation is accurate as long as $\beta(T - T_0) << 1$. More details about the specifications used for the Boussinesq approximation will be presented in sections 3.2 and 3.4.

In this study, the orientation of the inlet/outlet of the windcatcher is assumed based on the prevailing wind direction. It is supposed that the wind blows from the right side of the computational domain to its left in all simulations and models. Wind is distributed uniformly at the computational domain inlet. In reality the wind profile is not uniform however it is not important in our study as the windcatcher captures air in a small region only located at its opening. In addition the distribution of wind at the windcatcher's inlet corresponding to a uniform wind distribution at the computational domain's inlet would be similar for a certain profile distribution which reflects the reality.

All of the simulations conducted using either Ansys or CFD-ACE+ are based on the finite-volume method (FVM) to solve the Navier-Stokes equations and the energy equations for temperature. Specific details of the boundary conditions, mesh, grid convergence and other parameters will be presented in the following sections. The convergence criteria is the minimum reduction in residuals for each variable and it is specified as 0.0001 (four orders of magnitude) for all models. In this study, to obtain accurate results, the second order scheme

is used for all simulations via the RANS method. The precision for all of the simulations is 64 bits.

3.1 Effect of windcatcher's inlet shape on ventilation flow through a two dimensional room

3.1.1 Introduction

In this study the effect of the windcatcher's inlet design is investigated to achieve better air flow and to increase the efficiency of windcatchers. To achieve this, CFD (computational fluid dynamics) tool is used to simulate the air flow in a two dimensional room fitted with a windcatcher (Figure 3-1) based on different inlet designs. The common and simplest design is the uniform inlet which is the easiest for construction and has been implemented in many windcatchers. A divergent inlet and a bulging-convergent inlet are also investigated in this study. A divergent inlet is expected to capture more air flow compared to the uniform inlet since its area is relatively larger, however the pressure distribution around it may affect its performance thus it is investigated. The bulging-convergent inlet, similar in design to a jet engine inlet, is also studied to investigate whether it would positively affect the windcatcher's performance. The different inlet designs considered are of three types as shown in Figure 3-2:

- Type A: Uniform inlet
- Type B: Divergent inlet
- Type C: Bulging-convergent inlet to mimic a jet engine inlet.
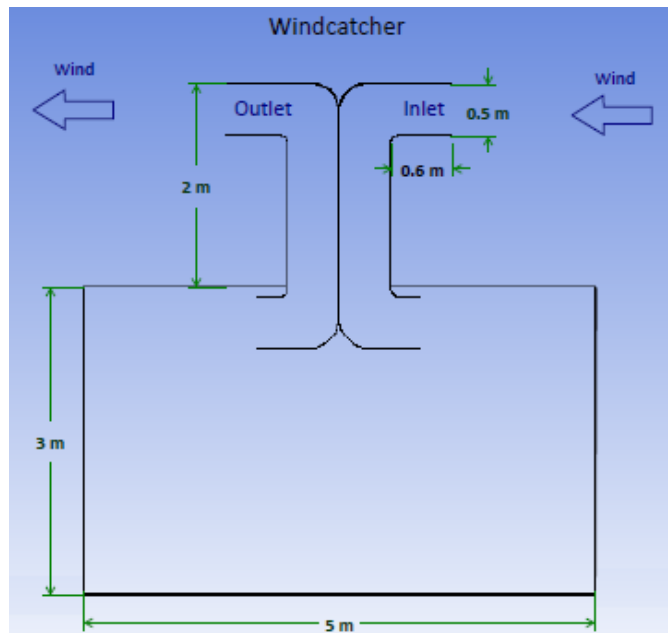
Figure 3-1. A two dimensional room fitted with a windcatcher

The windtunnel width is 0.5 m in all the cases however the projected area of the inlet type B and type C is 0.58 m in order to allow for the divergence and for the bulging. All entrances have been rounded.
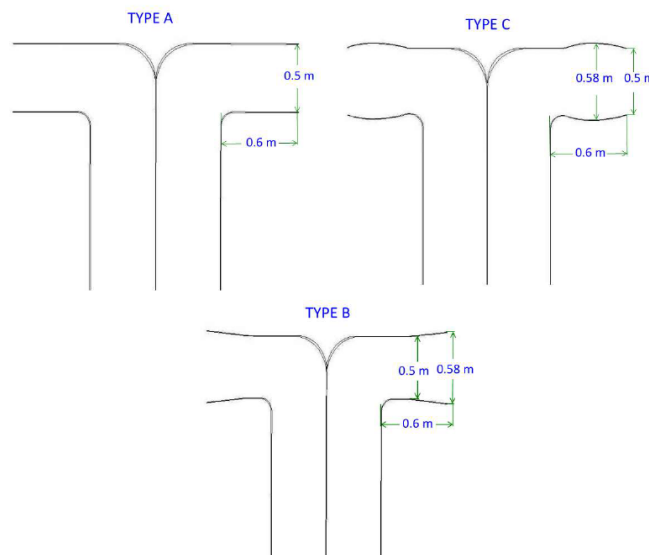
Figure 3-2. Types of inlet design studied A, B and C

3.1.2 Modelling and Computation

A two dimensional real sized room with a width of 5 m and a height of 3 m fitted with a windcatcher is modeled in this study using Ansys Fluent. The height of the windcatcher is assumed to be 2 m from the roof of the room up to the top of the windcatcher as shown in Figure 3-1.

The height of the inlet and outlet openings of the windcatcher is taken to be 0.5 m and they are perpendicular to the flow direction. Niktash and Huynh [14] has investigated the effect of windcatcher inlet / outlet on ventilation of a three dimensional room. This research has concluded that when the inlet / outlet cross section is perpendicular to the wind direction it satisfies the human comfort requirements for having proper indoor ventilation and it leads to enhancing the performance of windcatchers.

The windcatcher length inside the room is taken to be 0.1 m and the inside opening height is also 0.5 m. Niktash and Huynh [136] has studied the ventilation flow through a two dimensional room fitted with a windcatcher and concluded that the shape of the windcatchers bottom and its length strongly affects the flow pattern and flow velocity and that a good combination is achieved by a shorter bottom length which also does not obstruct the access through the room. It has been also found that when the windcatcher is located in the middle of the roof there is more uniform circulation in the lower parts of the room.

3.1.2.1 Wind driven ventilation

To simulate a more realistic air flow condition outside the building, the addition of a surrounding domain is used. Wind is blown from the right side to the left at a velocity of 3 m/s distributed uniformly over a height of 55 m; the air inlet is at a distance of 55 m away from the edge of the room as shown in figure 3-3. The total width of the surrounding domain is 105 m and the room is fitted at its center.

In addition, before the surrounding dimensions were selected, simulations using a height of 65 m and a width of 125 m were conducted. The pressure and velocity at a point close to the windcatchers inlet, located at 4.75 m high and 3.75 m from the room's left wall, differed by less than 1%.
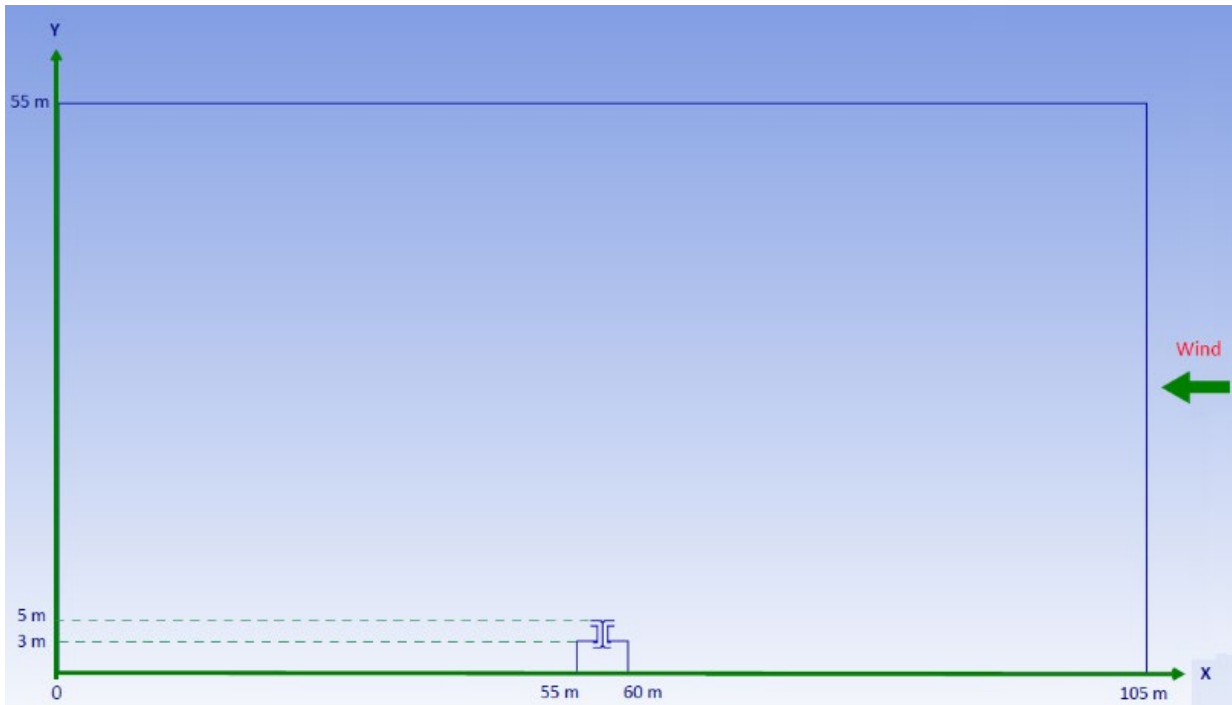
Figure 3-3. Schematic representation of the room, windcatcher and the surrounding showing the dimensions and the direction of the wind

3.1.2.2 Meshing of the two dimensional model and grid convergence

For meshing the geometry, quadrilaterals have been used with an edge sizing of the room and windcatcher of 0.005 m and a growth rate of 1.1, the global growth rate was set to 1.2 with a maximum face size of 0.75 m since a fine mesh is not necessary for the far field in the surrounding domain. Figure 3-4 shows the meshed room and the windcatcher with a uniform inlet. The maximum aspect ratio is 9.31 and the maximum orthogonal skewness is 0.59.
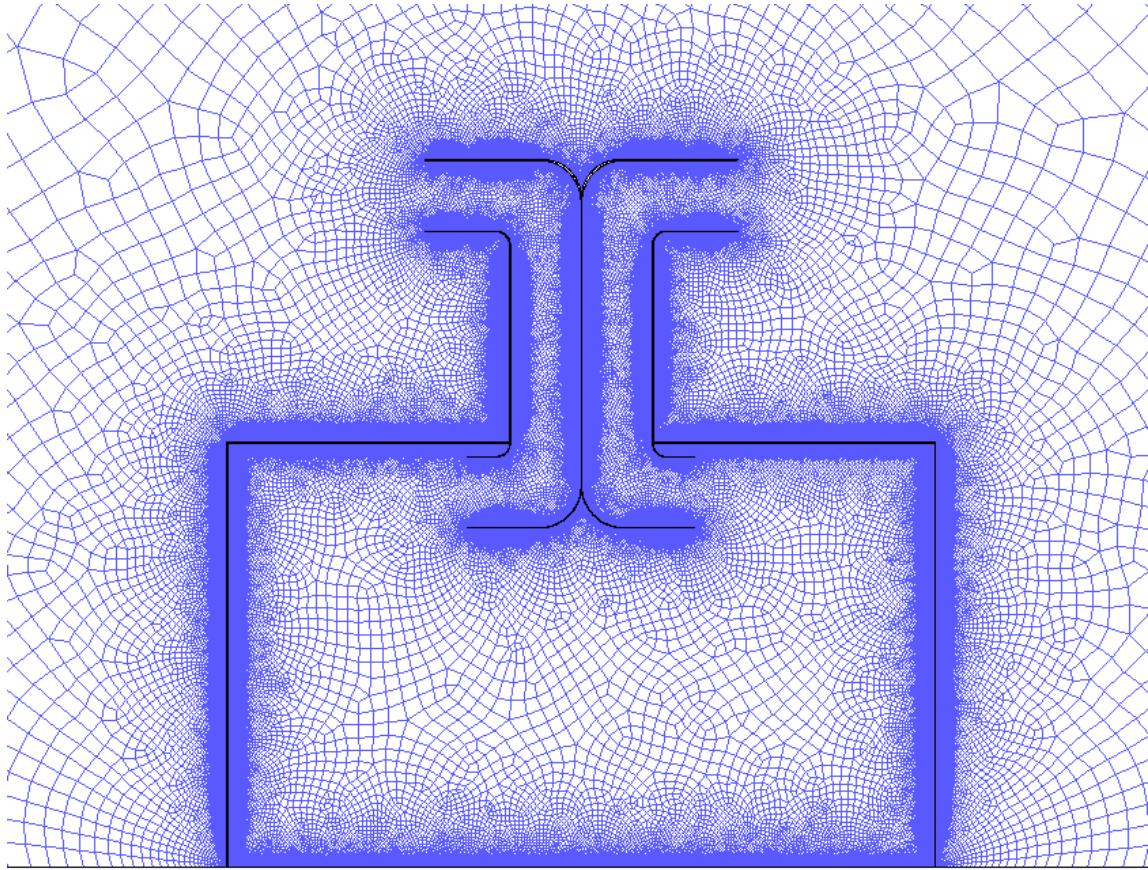
Figure 3-4. Quadrilaterals mesh of the model with a uniform inlet

To make sure that the grid pattern used is adequate, a grid convergence test was performed. The velocity magnitude and the pressure were compared at two points, one within the room at 1 m high and located at 3 m from the room's left wall. The second point was in the surrounding at 6 m high and located at 5 m from the room's left wall. As the number of elements increased from 126902 to 214110 to 304997 by decreasing the maximum mesh sizes from 1.25 m^2 to 0.75 m^2 to 0.5 m^2, the pressure and velocity at the first point changed by less than 1.5% as shown in table 3-1. Similar results were observed at both points. All simulations performed for the windcatcher's inlet designs used 0.75 m^2 maximum mesh sizing and an edge sizing of the room and windcatcher of 0.005 m.

No. of Elements	Max Mesh Size (m2)	Velocity (m/s)	Velocity Change %	Pressure (Pa)	Pressure Change %
126902	1.25	0.669	1.21%	0.686	1.48%
214110	0.75	0.661	--	0.676	--
304997	0.5	0.654	-1.06%	0.669	-1.04%

Table 3-1. Mesh convergence study at a point 1 m high and located at 3 m from the room's left wall

3.1.2.3 Simulation properties and boundary conditions

The simulation in this study is performed assuming the air properties to be constant, corresponding to air temperature at 288 K and air standard pressure at sea level at 101 kPa. The values for the air density and the dynamic viscosity are assumed as follows:

$$\rho = 1.225 \text{ kg/m}^3; \quad \mu = 1.789 \text{ x } 10^{-5} \text{ Pa s};$$

For defining turbulent flow the realizable k - ε model is used. The k – ε model is robust and stable and it is considered the default modeling option for handling turbulent flow in many commercial codes. The flow is turbulent as Reynolds number Re estimated at the chimney`s exit for one condition is approximately 108000. The turbulence intensity at the flow domain's inlet has been assumed as 1%, and the turbulent viscosity ratio as 1. As the turbulence intensity changed from 5% to 2% and 1% the results of the average velocity only differed by less than 1% which indicates that turbulence intensity did not have a significant effect. All simulations have been done using the steady flow mode.

The boundary conditions selected are as shown in Figure 3-5 and annotated by A, B, C and D. The right side of the surrounding (B) is a velocity inlet, where the speed of air is set to 3 m/s. The left (C) and the upper side (D) of the surrounding are both outlets with pressure set to zero gauge. The room, the windcatcher's boundaries and the bottom side of the surrounding are all set to be a stationary walls (A) with no slip shear condition.
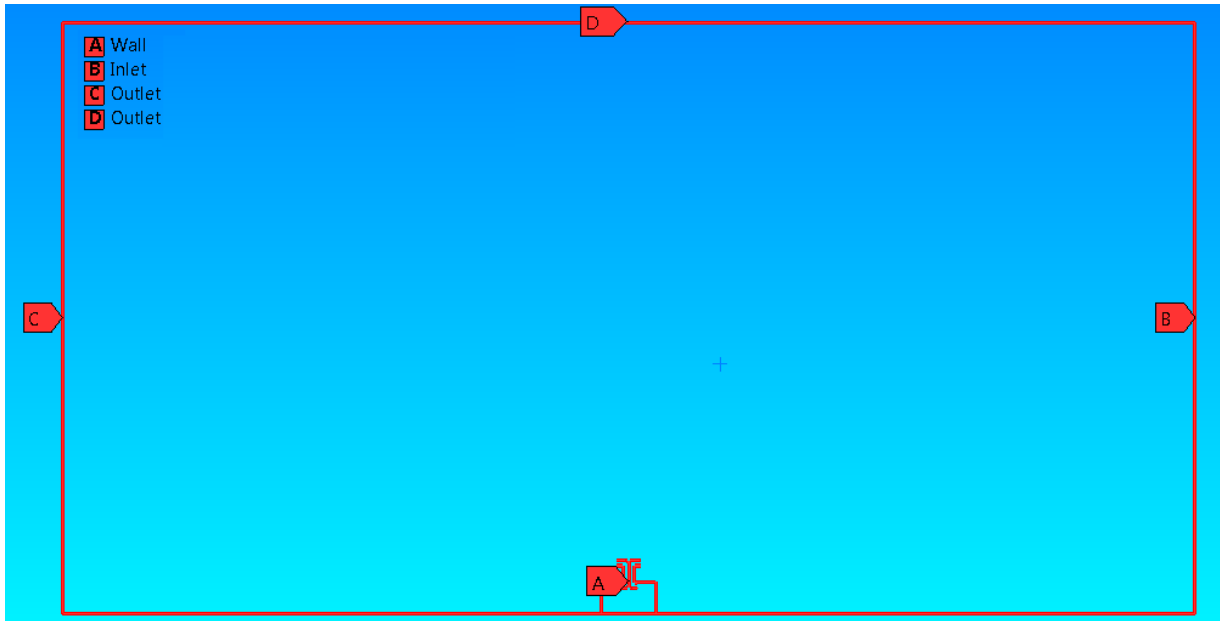
Figure 3-5. Boundary conditions of the model

In all the simulations the simple pressure-velocity coupling scheme and the second order spatial discretization have been used. The convergence criteria is 0.0001.

For each of the cases studied the average velocity of the air inside the room at a height of 1.2 m from the floor and the total flow rate through the chimney (hence also through the room) are investigated. To obtain the total flow rate a cut has been used at a height of 4.1 m in the inlet tunnel of the windcatcher to record the average velocity flowing into the room. The two cuts used are shown in Figure 3-6.
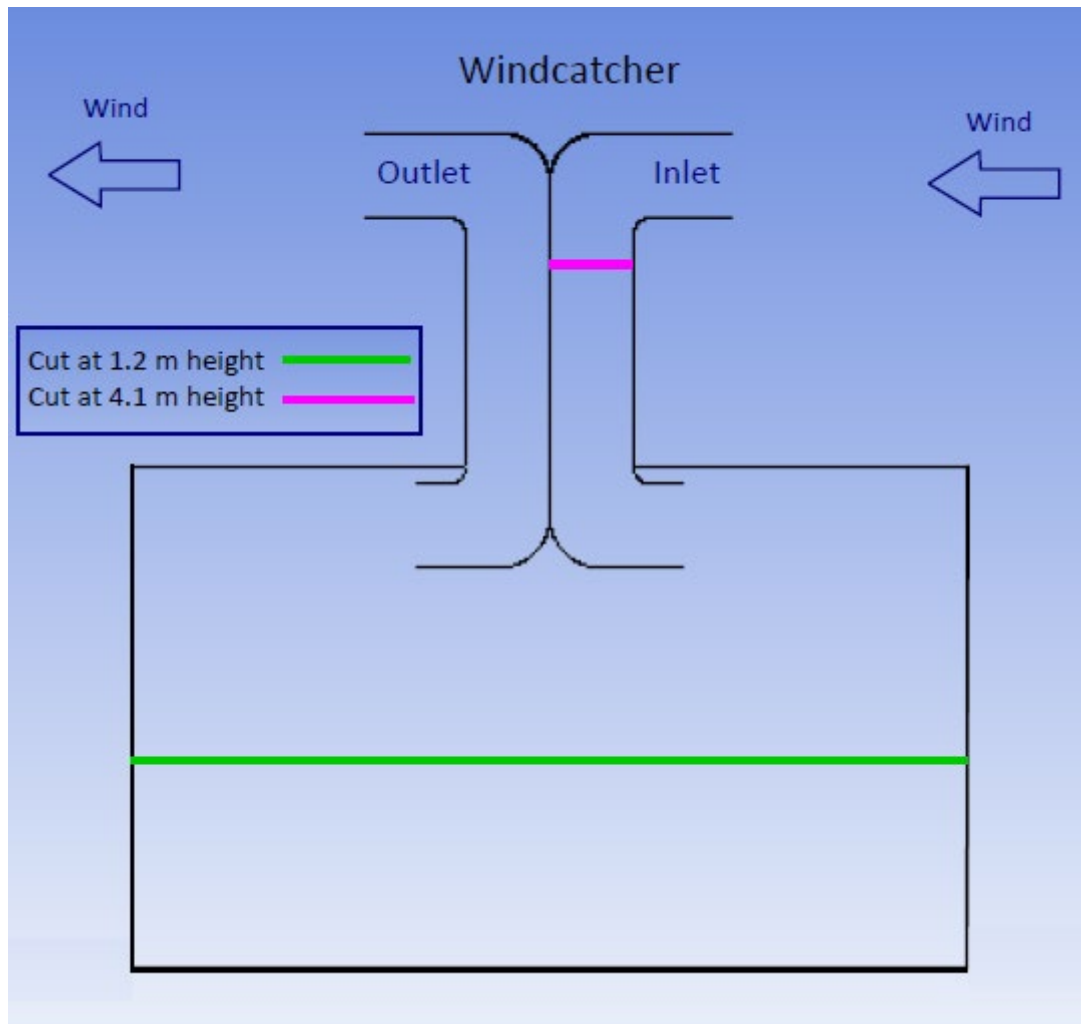
Figure 3-6. Cuts used to investigate average velocity magnitude

3.1.3 Results and discussion

The average velocity of the air inside the room at the height of 1.2 m from the floor and the total flow rate are investigated, and compared for the three types of inlets simulated.

3.1.3.1 Results for inlet type A – uniform inlet

For the inlet type A which is the uniform inlet the velocity magnitude throughout the room and its surrounding is shown in figure 3-7.

The results are viewed using Ansys CFD-Post after simulation is run by Ansys Fluent. The maximum number of iterations is set to 50000 and the convergence criteria to 0.0001. The problem converged in 2464 iterations.

Figure 3-7 shows the variation in the velocity as well as the pattern of the air flow inside the room. The average velocity at 1.2 m height inside the room is 0.72 m/s. The distribution of the air velocity at 1.2 m high is shown in figure 3-8 along with the distribution of the velocity at the cut 4.1 m high in the wind tunnel to monitor the total flow rate through the chimney (hence also through the room). The average velocity at the 4.1 m high cut is 1.50 m/s giving a total flow rate of 0.75 m²/s. It is evident that the higher velocities are located close to the walls of the room. The minimum speeds are in the middle of the room where the majority of human occupancy occurs. Refer to figure 3-6 for the location of the horizontal cuts.
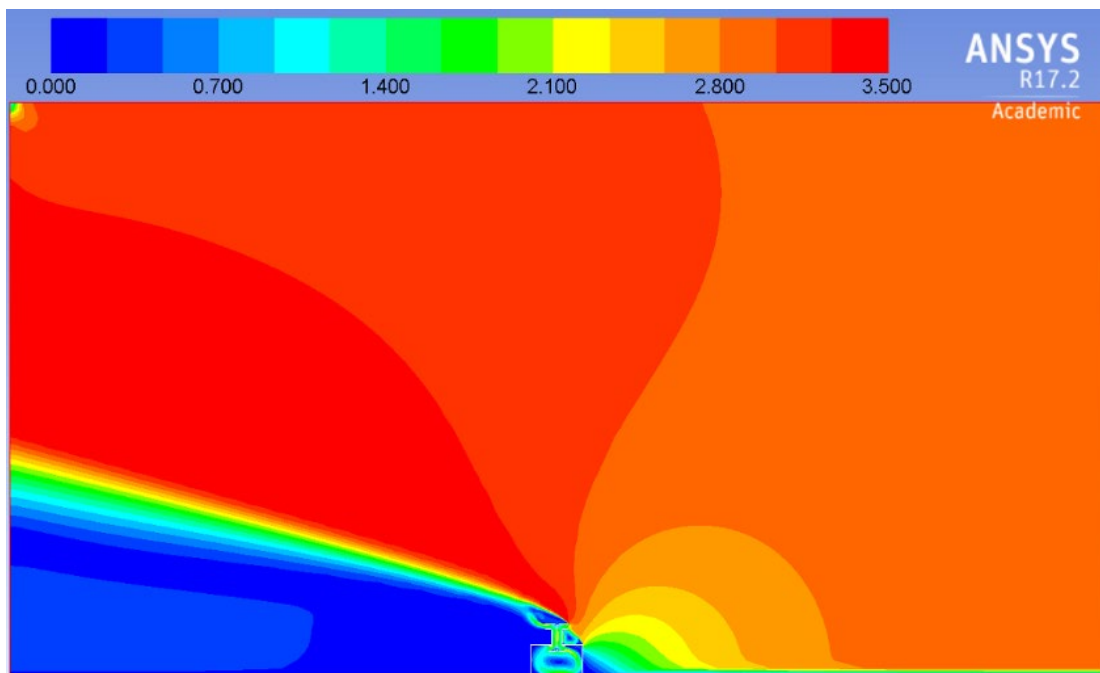
Figure 3-7. Velocity magnitude (m/s) of the model with the uniform inlet type A
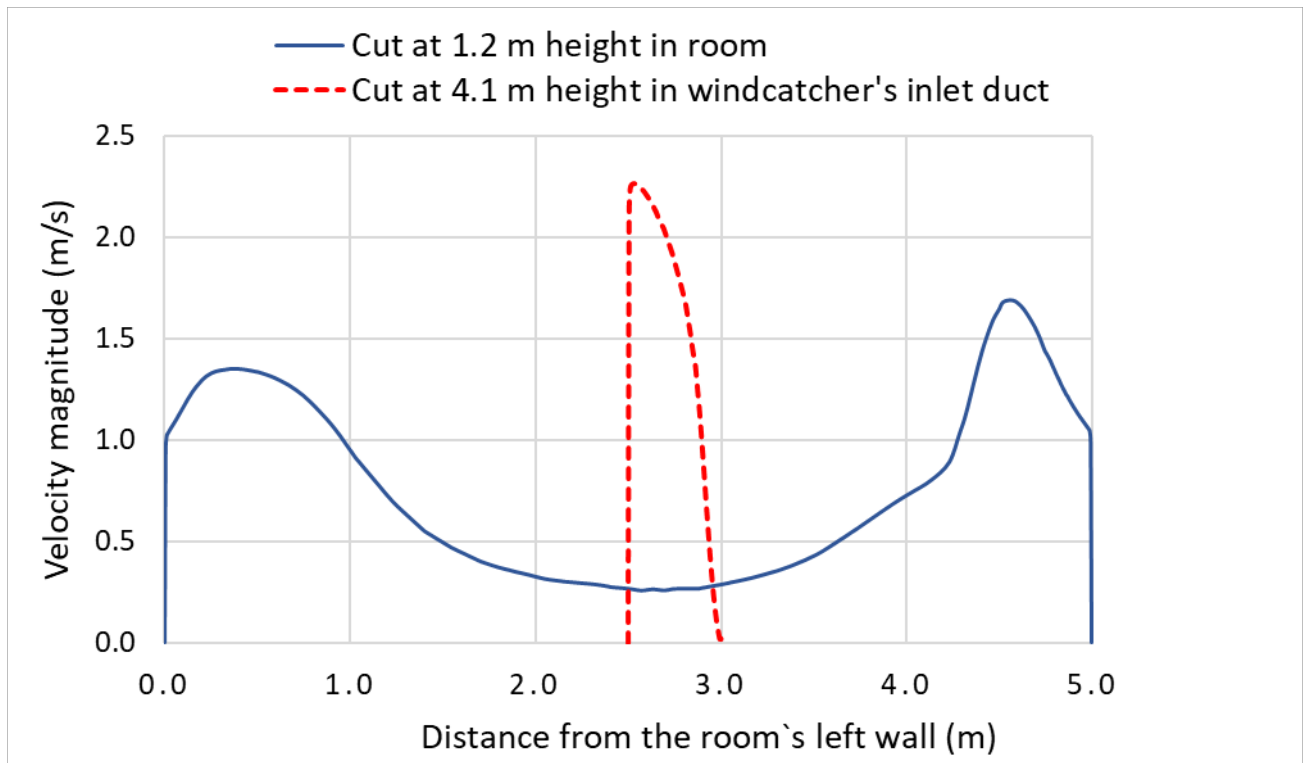
Figure 3-8. Velocity magnitude across the room for the uniform inlet type A at 1.2 m, and at 4.1 m height inside the windcatcher.

3.1.3.2 Results for inlet type B – divergent inlet

For the inlet type B which is the divergent inlet, the velocity magnitude through the room and part of its surrounding is shown in figure 3-9. The problem converged in 2860 iterations. Figure 3-9, zoomed close to the room for better representation, shows the variation in the velocity as well as the pattern of the air flow inside the room. The air flow pattern is similar to that for the uniform inlet type A, shown in figure 3-7.
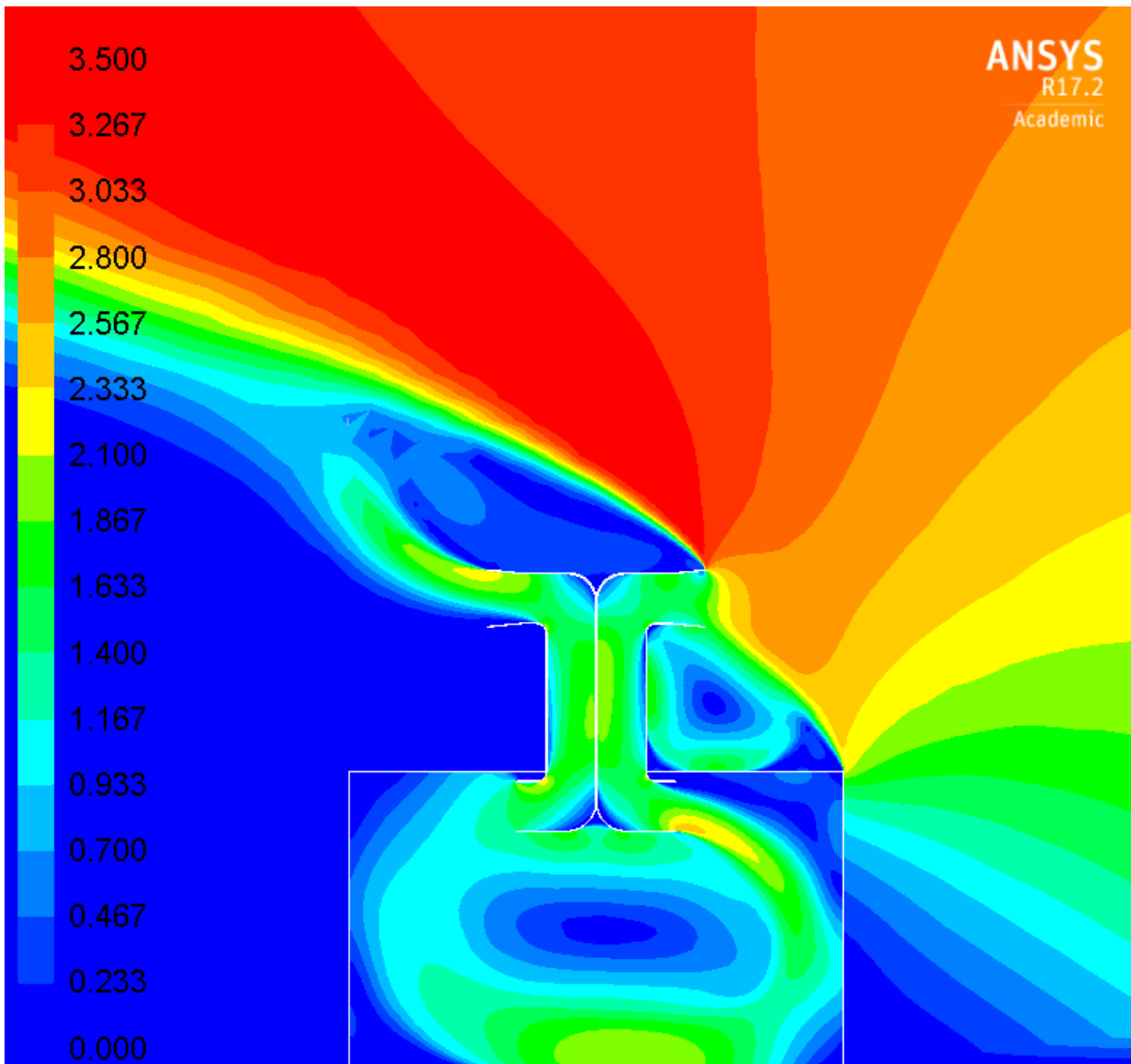
Figure 3-9. Velocity magnitude (m/s) of the room and windcatcher with the divergent inlet Type B

The average velocity at 1.2 m height inside the room is 0.75 m/s. The distribution of the air velocity at 1.2 m high is shown in Figure 3-10 along with the distribution of the velocity at the cut 4.1 m high in the wind tunnel. The average velocity at the 4.1 m high cut is 1.54 m/s giving a total flow rate through the windcatcher of 0.77 m^2/s. The higher velocities are located close to the walls of the room and the minimum speeds are in the middle of the room where the majority of human occupancy occurs. Refer to figure 3-6 for the location of the horizontal cuts.
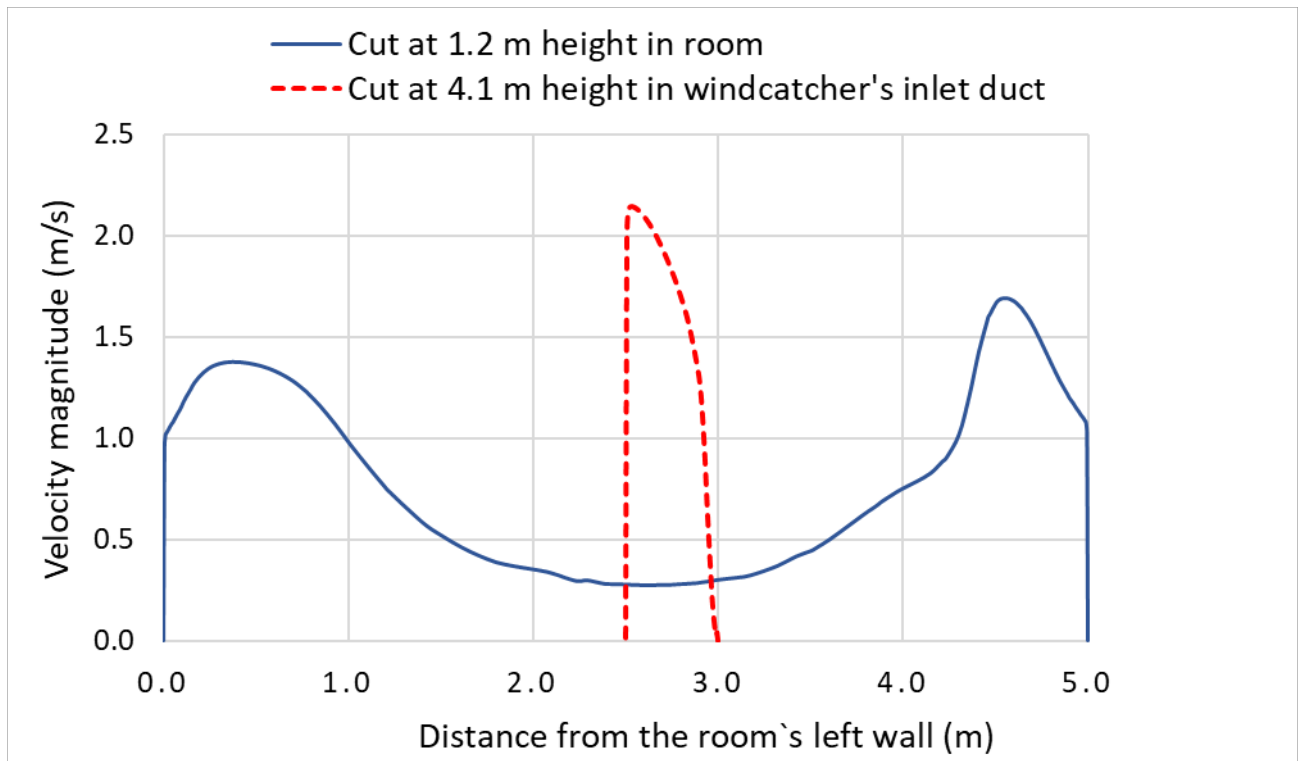
Figure 3-10. Velocity magnitude across the room for the divergent inlet type B at 1.2 m and at 4.1 m height.

3.1.3.3 Results for inlet type C – bulging convergent inlet

For the inlet type C which is the bulging convergent inlet, the velocity magnitude through the room and part of its surrounding is shown in figure 3-11. The problem converged in 2551 iterations. The average velocity at 1.2 m height inside the room is 0.67 m/s. The distribution of the air velocity magnitude at 1.2 m high is shown in Figure 3-12 along with the distribution of the velocity magnitude at the cut 4.1 m high in the wind tunnel. The average velocity at the 4.1 m high cut is 1.43 m/s giving a total flow rate of 0.72 m²/s. Refer to figure 3-6 for the location of the horizontal cuts.
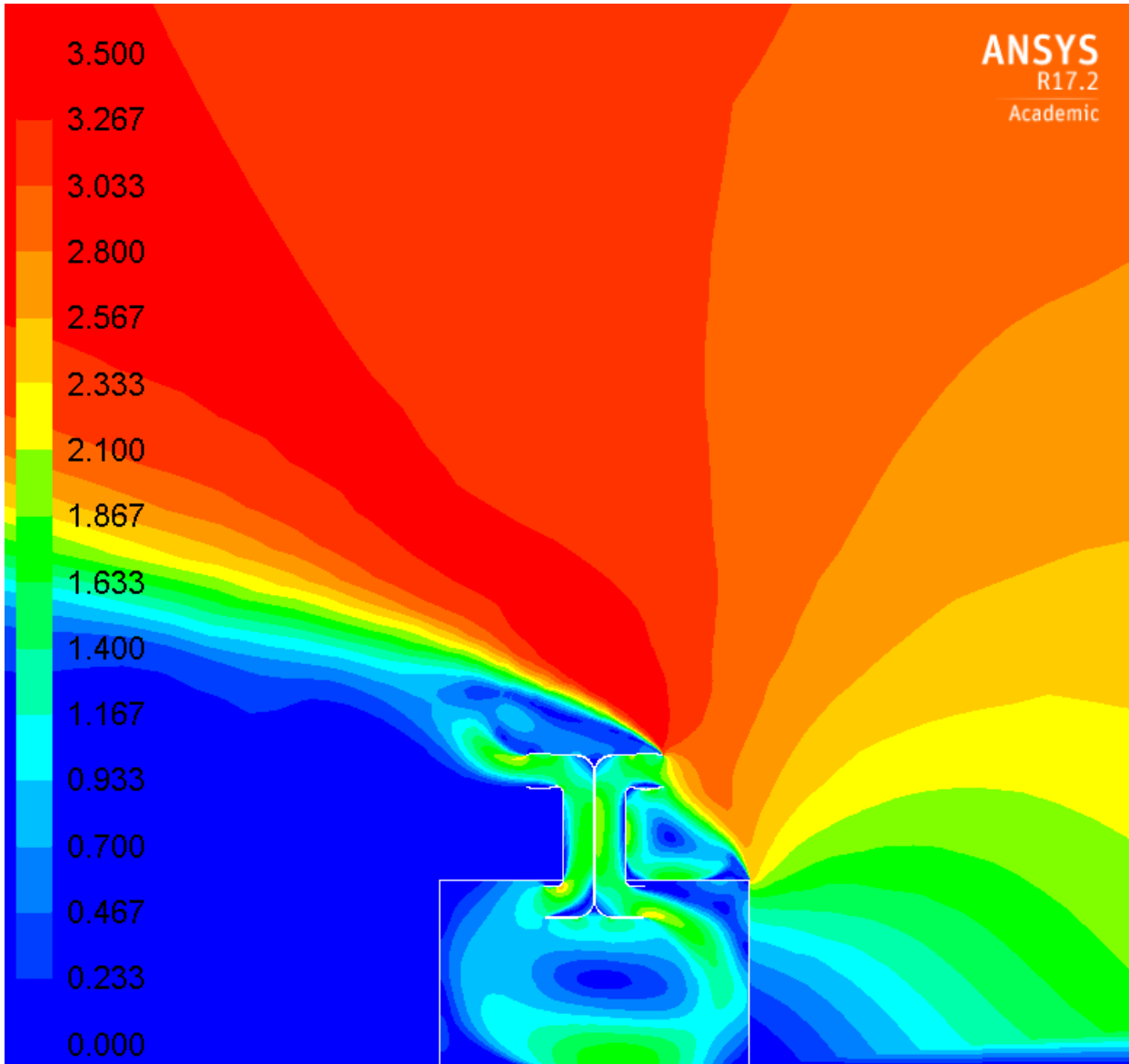
Figure 3-11. Velocity magnitude (m/s) of the room and windcatcher with the bulging-convergent inlet Type C
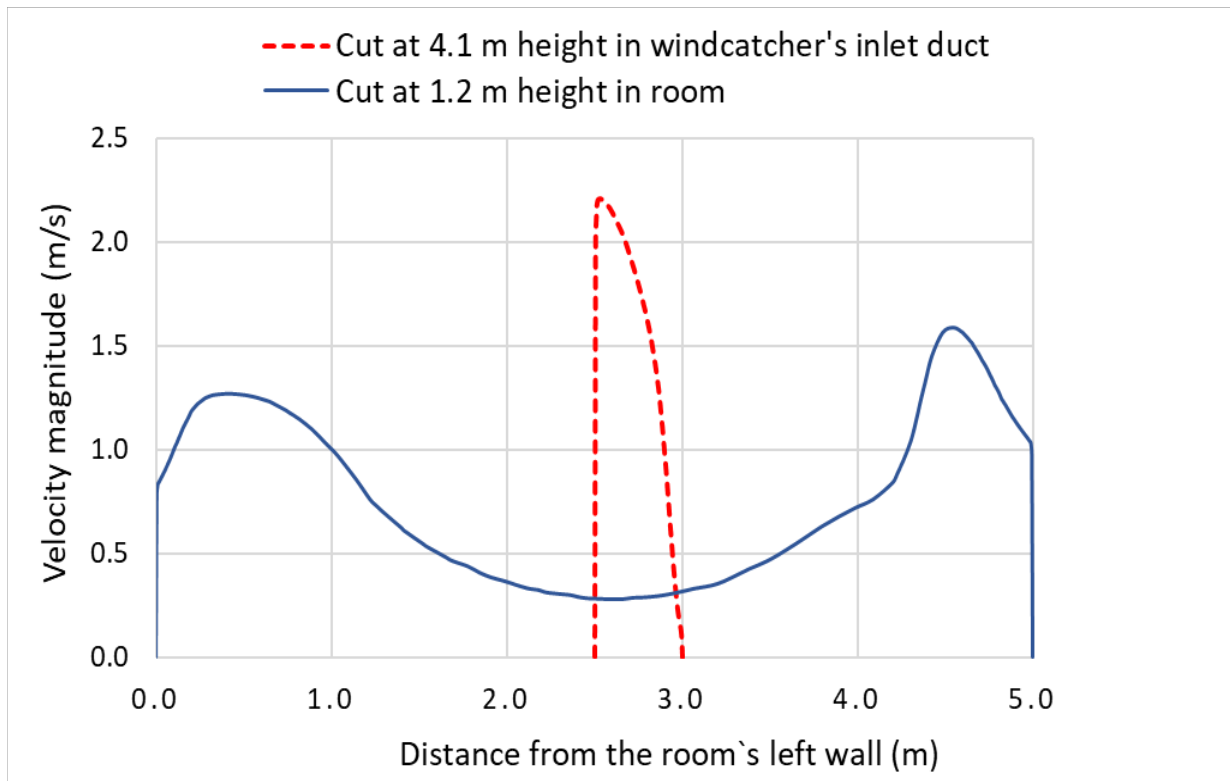
Figure 3-12. Velocity magnitude across the room for the bulging-convergent inlet type C at 1.2 m and at 4.1 m height

3.1.3.4 Summary and discussion

Summarized results of the three types of inlets are shown in table 3-2 and table 3-3. The divergent inlet, type B, has captured the highest air flow with a difference of approximately 3 % compared to the uniform inlet and a difference of approximately 8% compared to the bulging-convergent inlet. For all types of inlets studied, the pattern of the flow has provided full ventilation inside the room and especially in the living area.

In addition the contour of velocity magnitude shown in figures 3-7, 3-9 and 3-11 show that all the inlet designs have provided air flow velocities over 0.8 m/s at some locations in the room especially close to the walls, which does not satisfy the human thermal comfort conditions in hot climates as described in the ASHRAE standard [137]. This aspect is to be investigated since the two dimensional analysis does not fully represent the physical behavior of the air flow.

Average Velocity (m/s)			
Inlet type	A - Uniform	B - Divergent	C - Bulging-convergent
1.2 m cut	0.72	0.75	0.67
4.1 m cut	1.50	1.54	1.43

Table 3-2. Average velocity for the three types of inlets

Total flow rate at 4.1 m high (m2/s)			
Inlet type	A - Uniform	B - Divergent	C - Bulging-convergent
Flow rate (m2/s)	0.75	0.77	0.72
Increase (%)	3%		8%

Table 3-3. Total flow rate at 4.1 m cut for the three inlet shapes and the percentage increase of the divergent inlet compared to uniform and bulging-convergent

3.1.4 Conclusion

Computation of average air velocity through a two dimensional room fitted with a windcatcher have been conducted. Cases for three inlet shapes, uniform, divergent and bulging-convergent have been simulated using Ansys Fluent.

The pattern of the flow for the three inlets has provided full ventilation inside the room especially in the living area.

The divergent inlet has captured the highest air flow with a difference of approximately 3 % compared to the uniform inlet and 8% difference compared to the bulging-convergent inlet.

3.2 Effect of combining buoyancy driven and winddriven ventilation in a two dimensional room fitted with a windcatcher

3.2.1 Introduction

Combining the winddriven and the buoyancy driven ventilation will be investigated in this study through the use of a windcatcher natural ventilation system. Figure 3-13 shows a representative model of the two dimensional room studied.
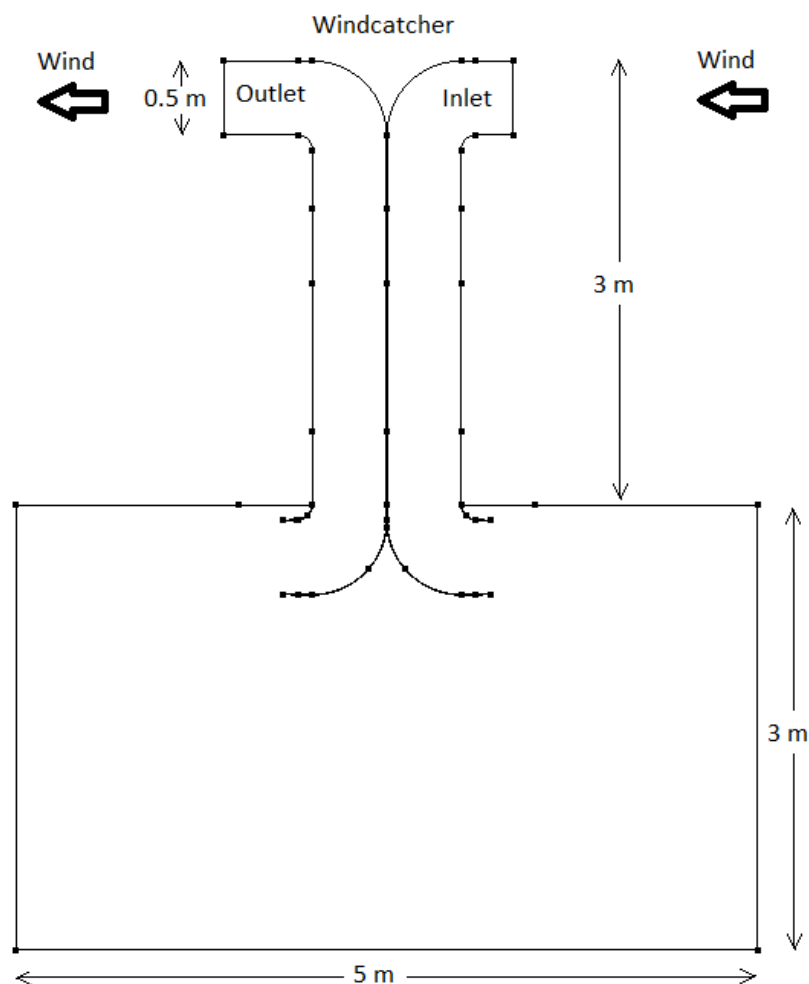
Figure 3-13. Two dimensional room fitted with a windcatcher

3.2.2 Modelling and Computation

A two dimensional real sized room with a width of 5 m and a height of 3 m fitted with a windcatcher is modeled in this study using CFD-Ace+, a CFD computational fluid dynamics software package from ESI group. The height of the windcatcher is assumed to be 3 m from the roof of the room up to the top of the windcatcher.

The height of the inlet and outlet openings of the windcatcher is taken to be 0.5 m and they are perpendicular to the flow direction. The windcatcher length inside the room is taken to be 0.1 m and the inside opening height is also 0.5 m. Figure 3-13 shows a representative model of the room studied.

3.2.2.1 Surrounding domain

To simulate a free ventilation air flow the addition of a surrounding domain that contains wind is considered. Wind is driven from the right side at a velocity of 3 m/s distributed uniformly over a height of 7 m; the air inlet is at a distance of 5 m away from the edge of the room as shown in figure 3-14. The total width of the surrounding domain is 15 m and the room is fitted in its center. Figure 3-14 [21] shows a schematic representation of the room, windcatcher and the surrounding with the dimensions (measured along the x and y axis) and the direction of the air inlet and outlet.
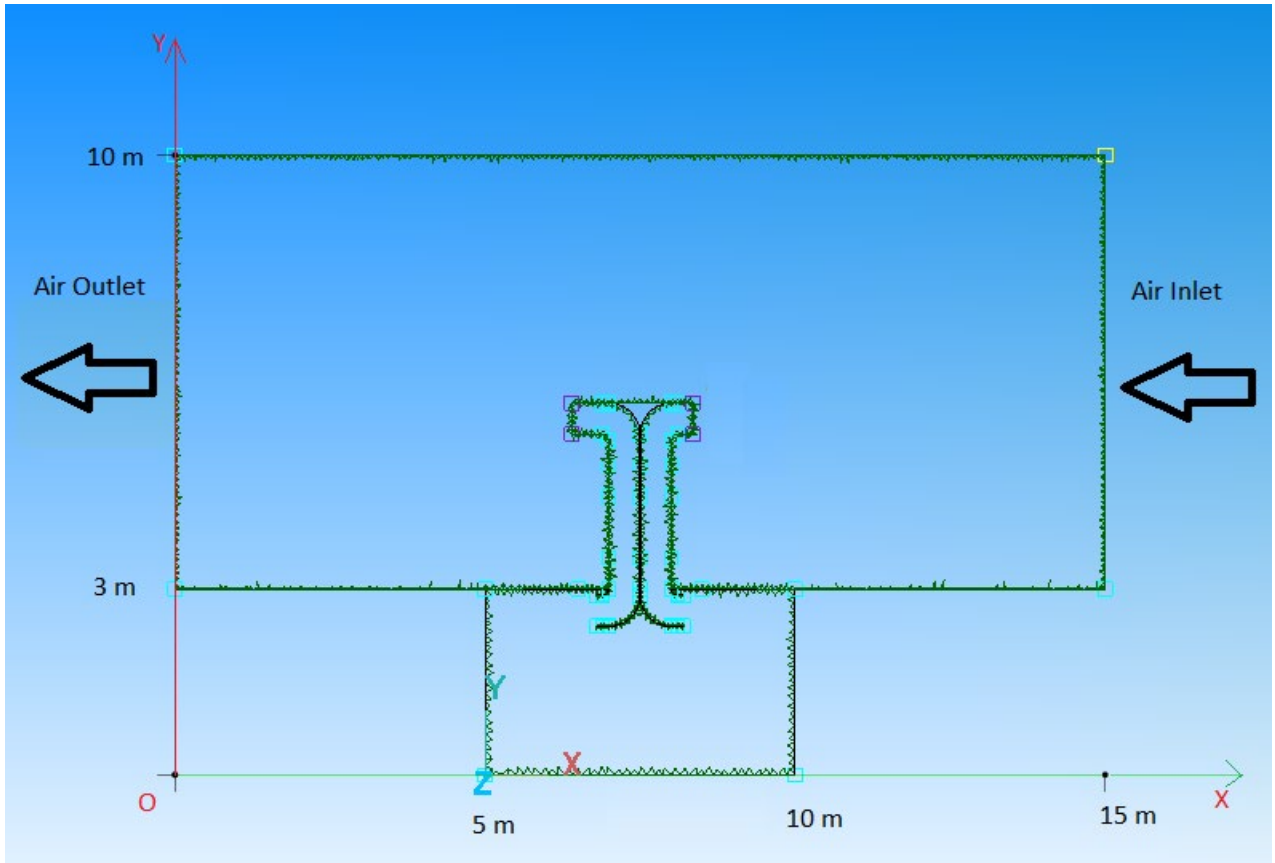
Figure 3-14. Schematic representation of the room, windcatcher and the surrounding

3.2.2.2 Meshing the model and grid convergence

Unstructured triangular meshes, shown in figure 3-15, were used in both domains with an automatic global cell size distribution. Consequently, a grid pattern with a total of 21998 cells is used in all cases. 3470 cells for the room and 18528 cells for the surrounding domain.

To make sure that the grid pattern used is adequate a grid convergence test was performed. The velocity magnitude and the pressure were compared at a point 1.2 m high and located at 4 m from the room's left wall. As the number of grid cells increased from 7324 to 21998 (by 200%) the velocity magnitude at the selected point changed by only 1.4% from 0.73 m/s to 0.74 m/s and the pressure changed by only 1.5% from 2.55 Pa to 2.59 Pa.
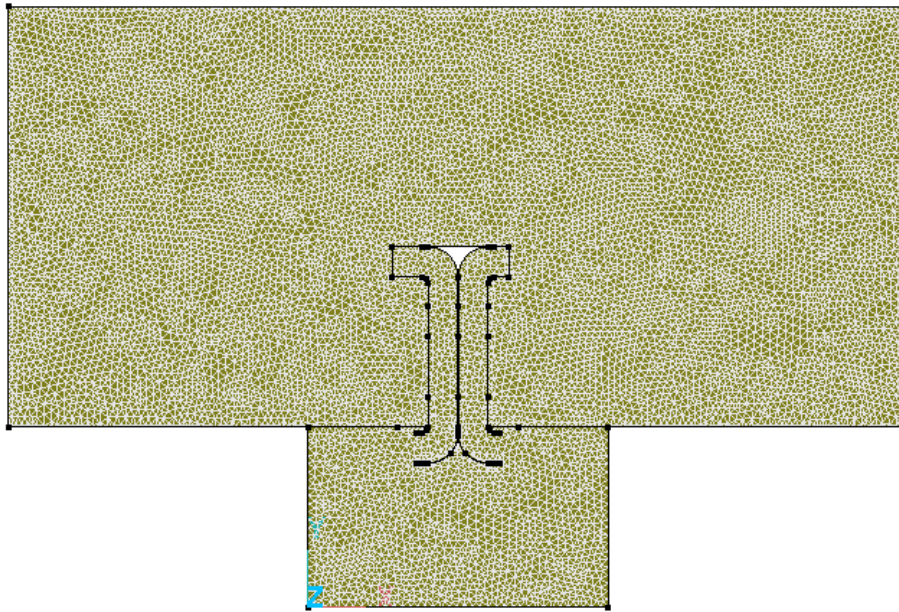
Figure 3-15. Unstructured triangular mesh of the model

3.2.2.3 Simulation properties and boundary conditions

The simulation in this study is performed assuming the air properties to be constant and corresponding to air temperature at 300 K and air standard pressure at sea level at 101 kPa. Generally, the values for the other air properties are assumed as follows:

$\rho = 1.161$ kg/m^3;

$\mu = 1.846$ x 10^{-5} Pa s;

$\upsilon = 1.585$ x 10^{-5} m^2/s;

$Pr_t = 0.9$

For defining turbulent flow the realizable k - ε model is used. The k – ε model is robust and stable and it is considered the default modeling option for handling turbulent flow in many commercial codes. Reynolds number Re estimated at the chimney exit for one condition is approximately 45000. All of the models are simulated in the steady flow mode.

The turbulent kinetic energy K and the dissipation rate ε are calculated using the following equations where V is the wind velocity [52]:

$$K = 3(0.02\ V)^2/2$$

$$\varepsilon = (C\mu^{0.75}\ K^{1.5})/\kappa L$$

The turbulence intensity has been assumed as 2%, the value of Cμ assumed to be 0.09 and the value of Von Karman constant κ is 0.4. The characteristic length L is assumed to be equal to the inlet width of the windcatcher which is 0.5 m.

For the inlet velocity of 3 m/s which is considered in this study, the values of K and ε are:

$$K = 0.0054\ m^2/s^2$$
$$\varepsilon = 0.0003255\ m^2/s^3$$

To simulate the buoyancy driven effect, heat flux is applied to both sides of the windcatchers outlet. A fixed value of 400 W/m^2 is applied on the internal side of the chimney and the upper side of the opening while different values of heat flux (1000, 800 and 600) W/m^2 are applied to the external side of the outlet chimney and the lower side of the opening as shown in figure 3-16. The values of the heat flux considered are based on the solar radiation arriving to the atmosphere on a cloudless sky where the direct sun would be about 1050 W/m^2 [53] and the global radiation on a horizontal surface at ground level is about 1120 W/m^2. In fact the corresponding actual figures would vary based on sun's angle and atmospheric circumstances. The sun's rays are attenuated as they pass the atmosphere, leaving maximum normal surface irradiance at approximately 1000 W/m^2 at sea level on a clear day.
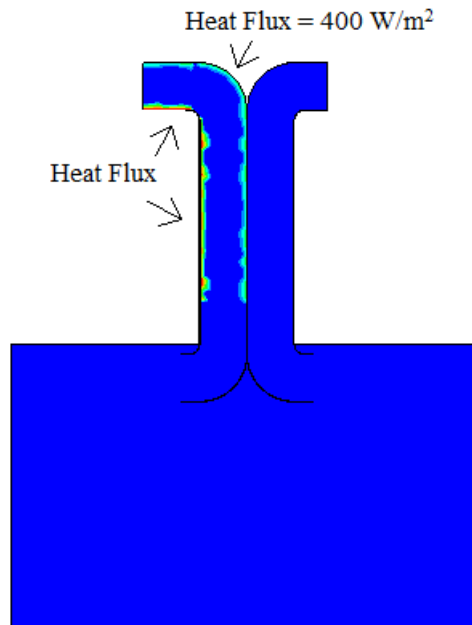
Figure 3-16. Heat Flux locations at the internal and external walls of the windcatcher outlet

Gravity is selected for the body forces in the y direction only, the Boussinesq approximation is applied with a reference temperature of 300 K and the volumetric coefficient of thermal expansion $\alpha_v = 0.003333$ 1/K [52].

The thermal parameters used are the specific heat C_p and the thermal conductivity k as follows:

$C_p = 1007$ J/(kg K)
$k = 0.0263$ W/(m K)

3.2.3 Results and discussion

The average velocity of air inside the room at a height of 1.2 m from the floor and the total flow rate are investigated in each of the following cases:

1. Winddriven ventilation alone
2. Combined winddriven and buoyancy driven ventilation with different values of heat flux applied to the windcatchers external outlet wall and 400 W/m² applied to the internal side of the chimney and top side of the openings:

- 2a - Heat flux = 1000 W/m^2
- 2b - Heat Flux = 800 W/m^2
- 2c - Heat Flux = 600 W/m^2

3.2.3.1 Results for winddriven ventilation alone

For the first case of air flow through a windcatcher using winddriven ventilation alone without the buoyancy effect, the velocity magnitude throughout the room and its surrounding is shown in figure 3-17 [21]. The results are viewed using CFD-View after simulation is run by CFD-ACE-GUI where two modules are selected, the flow and the turbulence module and then all related boundary and initial conditions are set along with the necessary output parameters. The maximum number of iterations is set to 1000 and the convergence criteria to 0.0001. The problem converged in 840 iterations [52].
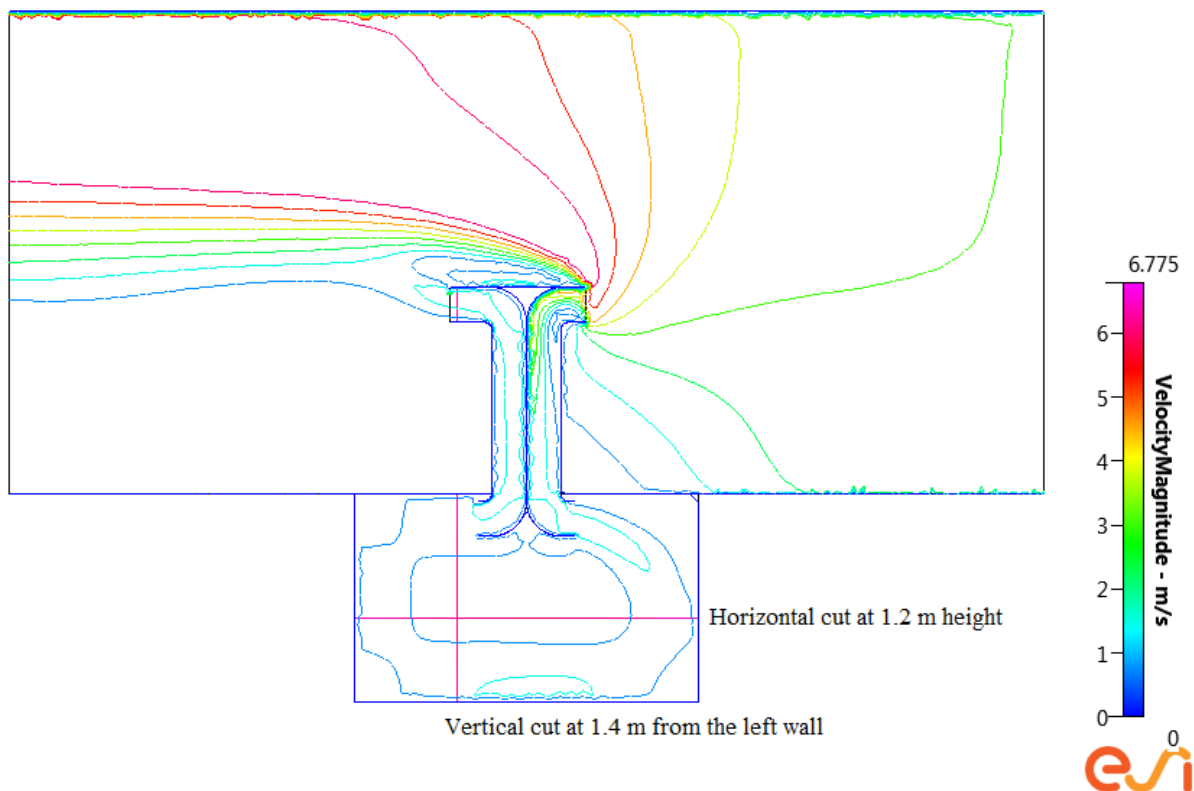
Figure 3-17. Velocity magnitude representation showing the horizontal and vertical cuts locations

Figure 3-17 shows the variation in the velocity as well as the pattern of the air flow inside the room, it also shows a horizontal line in red at a height of 1.2 m where a cut is taken to investigate

the velocity magnitude. A vertical line in red is shown at 1.4 m from the left edge of the room where a cut is taken to investigate the average velocity of the total air flow leaving the room through the windcatcher opening. The average velocity at 1.2 m height inside the room is 0.59 m/s which satisfies the human thermal comfort conditions as described in the ASHRAE standard [137].
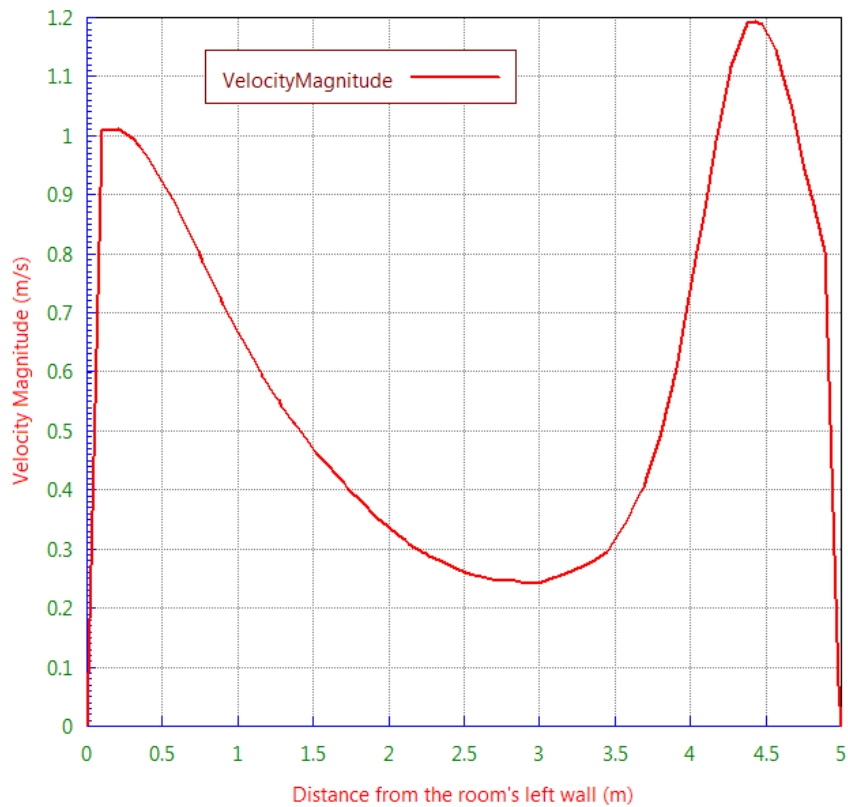
Figure 3-18. Velocity magnitude across the room at 1.2 m height for the winddriven ventilation.
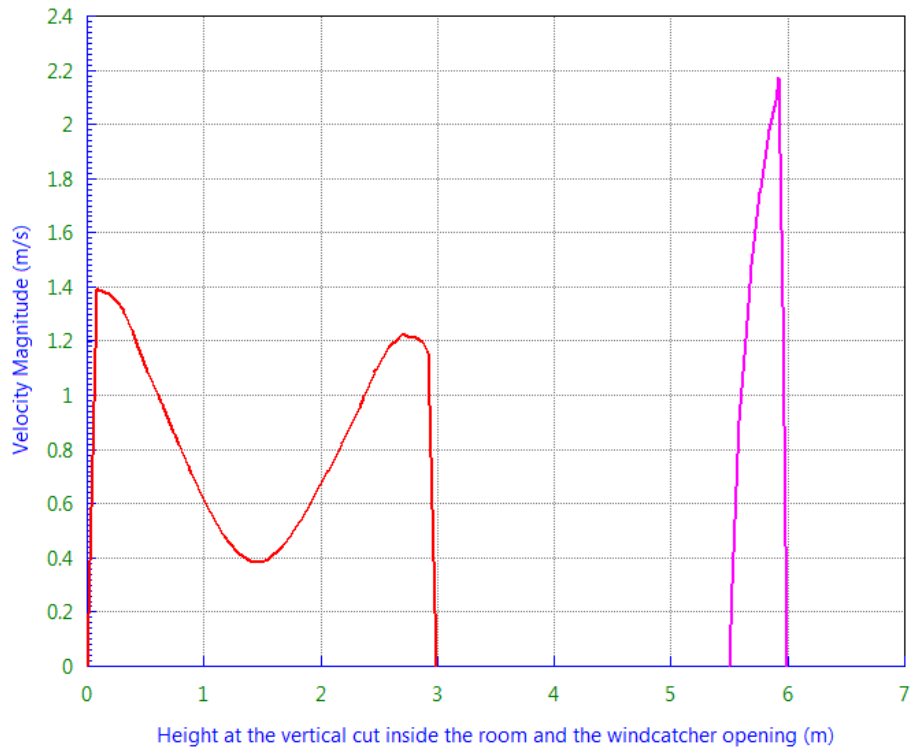
Figure 3-19. Velocity magnitude with respect to the height of the vertical cut for the winddriven ventilation. Red curve is in the room while the pink is inside the windcatcher.

Figure 3-18 shows the distribution of the air velocity magnitude at the height of 1.2 m from the room's floor with respect to the distance from the room's left wall. It is evident that the higher velocities are located close to the windcatcher's inlet, and close to the walls. Refer to figure 3-17 for the location of the horizontal cut. The minimum speeds are in the middle of the room where the majority of human occupancy occurs and the corresponding velocity is approximately 0.5 m/s which also satisfies the human thermal comfort conditions [137].

Figure 3-19 shows the distribution of the air velocity magnitude at the distance of 1.4 m from the room's left edge. This cut passes through the windcatcher outlet and allows investigating the average velocity leaving the room, which is 1.24 m/s between the height of 5.5 m and 6 m. The average velocity magnitude between 0 and 3 m is recorded as 0.84 m/s. Refer to figure 3-17 for the location of the vertical cut at 1.4 m from the room's left edge.

3.2.3.2 Results for combined buoyancy driven and winddriven ventilation

For the second case of air flow through windcatcher using combined buoyancy driven and winddriven ventilation, three modules are selected in CFD-ACE-GUI including the Heat Transfer module. The Heat flux is defined in the boundary conditions along with the related outputs. Different simulations were submitted with different values for the heat flux applied and the problem converged after more than 770 iterations for each of the three simulations. The results are viewed using CFD-View after simulation is run by CFD-ACE-GUI [52].
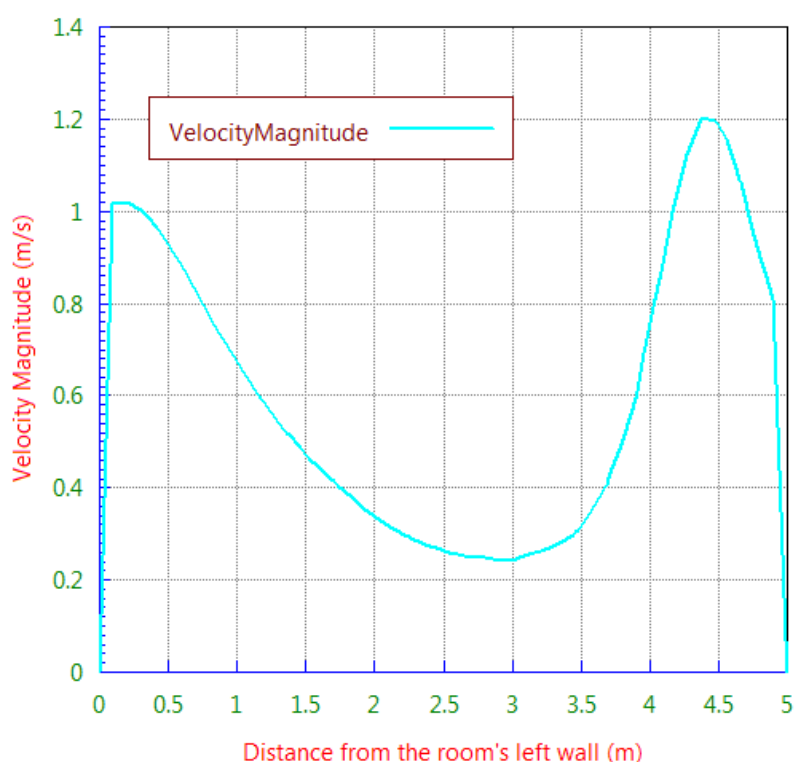
Figure 3-20. Velocity magnitude across the room at 1.2 m height for the combined buoyancy and winddriven ventilation.

Similar to the first case, the average of the velocity magnitude at the outlet of the windcatcher is investigated through a cut at 1.4 m from the left edge of the room. The average of the velocity magnitude is also shown at the height of 1.2 m above the floor. Temperature at the external wall of the windcatcher outlet is also investigated and compared for the three values of the heat flux taken.

The average velocity at 1.2 m height inside the room is 0.6 m/s when heat flux of 1000 W/m^2 is applied. Figure 3-20 shows the distribution of the air velocity magnitude at the height of 1.2 m from the room's floor with respect to the room's width. Refer to figure 3-17 for the location of the horizontal cut

Figure 3-21 shows the distribution of the air velocity magnitude horizontally at the width of 1.4 m from the room's left edge. Refer to figure 3-17 for the location of the vertical cut at 1.4 m from the room's left edge. When heat flux of 1000 W/m^2 is applied the average velocity leaving the room is 1.395 m/s with an addition of 0.155 m/s compared to that with the winddriven ventilation only. This addition represents an overall increase of 11.6% on the total air flow leaving the windcatcher. The average velocity magnitude between 0 and 3 m is 0.82 m/s.
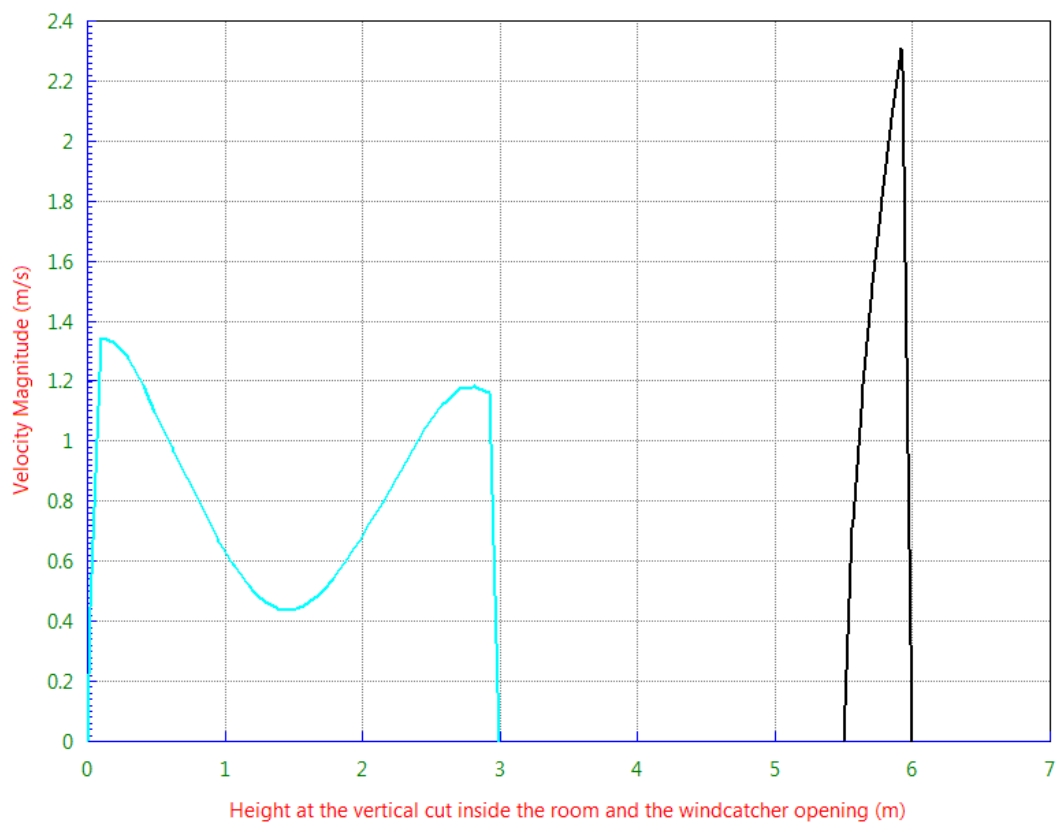
Figure 3-21. Velocity magnitude with respect to the height of the vertical cut for the combined buoyancy and winddriven ventilation. Blue curve is in the room while the black is inside the windcatcher

Similarly simulation with heat flux of 800 W/m^2 and 600 W/m^2 is done and the results are all summarized in table 3-4 which shows the increase in percentage of the total air flow rate leaving the windcatcher when the heat flux is applied.

It is obvious that the average velocity magnitude at the outlet of the windcatcher has increased as the heat flux increased from 600 W/m^2 to 1000 W/m^2 however this increase is not significant. The average velocity has remained approximately constant at 1.2 m above the floor.

Average velocity magnitude m/s	Winddriven only	Combined winddriven and buoyancy with Heat Flux (W/m^2)		
		600	800	1000
at 1.2 m height inside room	0.59	0.6	0.6	0.6
at 1.4 m width (inside room)	0.84	0.82	0.82	0.82
at 1.4 m width (windcatcher's outlet)	1.25	1.38	1.385	1.395
Increase in % of the total air flow rate leaving the windcatcher		**10.4**	**10.8**	**11.6**

Table 3-4. Average velocity magnitude for winddriven only and for combined buoyancy and winddriven ventilation with the increase in total air flow.

3.2.3.3 Temperature at the windcatcher outlet due to heat flux applied

With the addition of the heat flux, the temperature along the walls of the windcatcher outlet is increased. Figure 3-22 shows the distribution of the temperatures with a maximum of 500.5 K at the external wall once 1000 W/m^2 heat flux is applied [21].
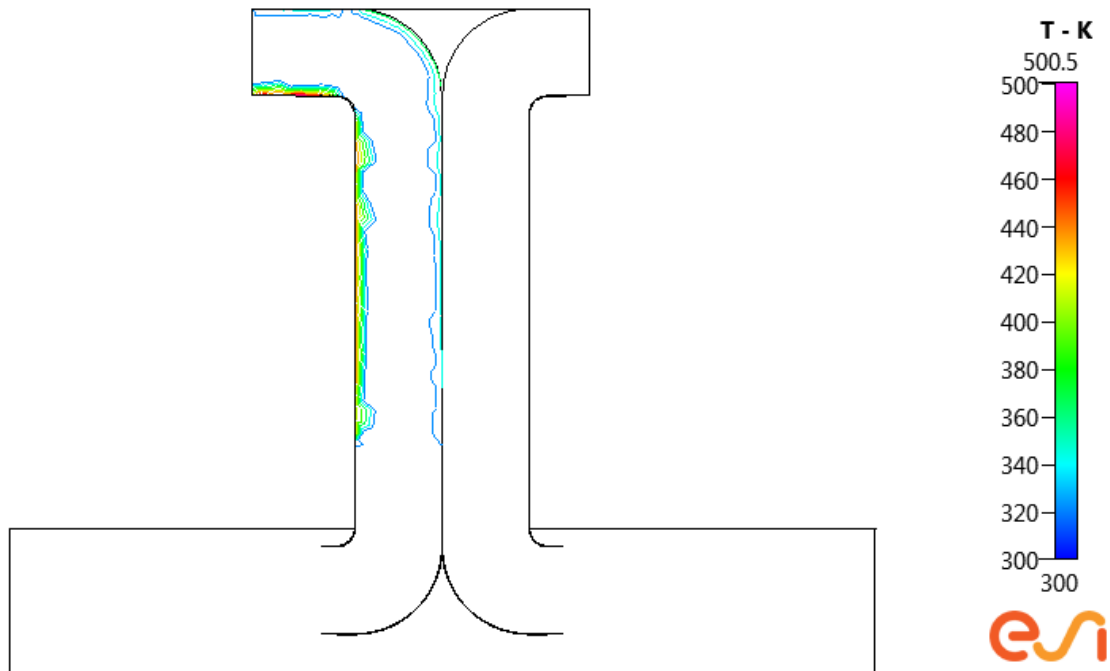
Figure 3-22. Distribution of the temperatures at the windcatcher's external wall

Table 3-5 shows the variation of the maximum temperature at the windcatcher external wall with respect to the change of the heat flux applied. As the heat flux increases by 200 W/m^2 the temperature increases by approximately 40 K and the corresponding increase in the average velocity is only 0.01 m/s.

Heat Flux (W/m^2)	Maximum Temp (K)
1000	500.5
800	461.2
600	421.6

Table 3-5. Temperature differences with respect to heat flux

3.2.4 Conclusion

Computation of average air velocity magnitude through a two dimensional room fitted with a windcatcher have been conducted. Cases for winddriven ventilation and combined winddriven and buoyancy driven ventilation has been simulated using CFD-Ace+ with different heat flux values applied at the windcatcher's outlet wall.

The average velocity at 1.2 m height inside the room in all the cases studied satisfied the human thermal comfort conditions as described in the ASHRAE standard.

The combined, buoyancy driven and winddriven ventilation, has provided at least 10% increase in the total air flow rate, when heat flux of 600 W/m^2 is applied compared to the winddriven ventilation only. Increasing the heat flux up to 1000 W/m^2 did not result in a significant increase in the total air flow, indicating that the flow is wind dominated.

3.3 Effect of windcatcher's inlet shape on ventilation flow through a three dimensional room

3.3.1 Introduction

In this study CFD (computational fluid dynamics) modelling is implemented to investigate and analyse the airflow entering a three dimensional room through a windcatcher tunnel fitted on its roof. Three dimensional simulations reflect real life situations and is much more realistic than two dimensional simulations. An efficient windcatcher would capture higher quantity of fresh air which results in providing a healthier and more comfortable occupant environment. To achieve this, the airflow simulation of a windcatcher with different inlet designs is studied. The dimensions and schematic of the inlet designs are the same as those studied in the two dimensional analysis [18, 19]. Figure 3-23 shows the three inlet design studied as follows [18, 19]:

1.   Type A which is a uniform inlet
2.   Type B which is a divergent inlet
3.   Type C which is a bulging-convergent inlet (similar to the design of a jet engine inlet).
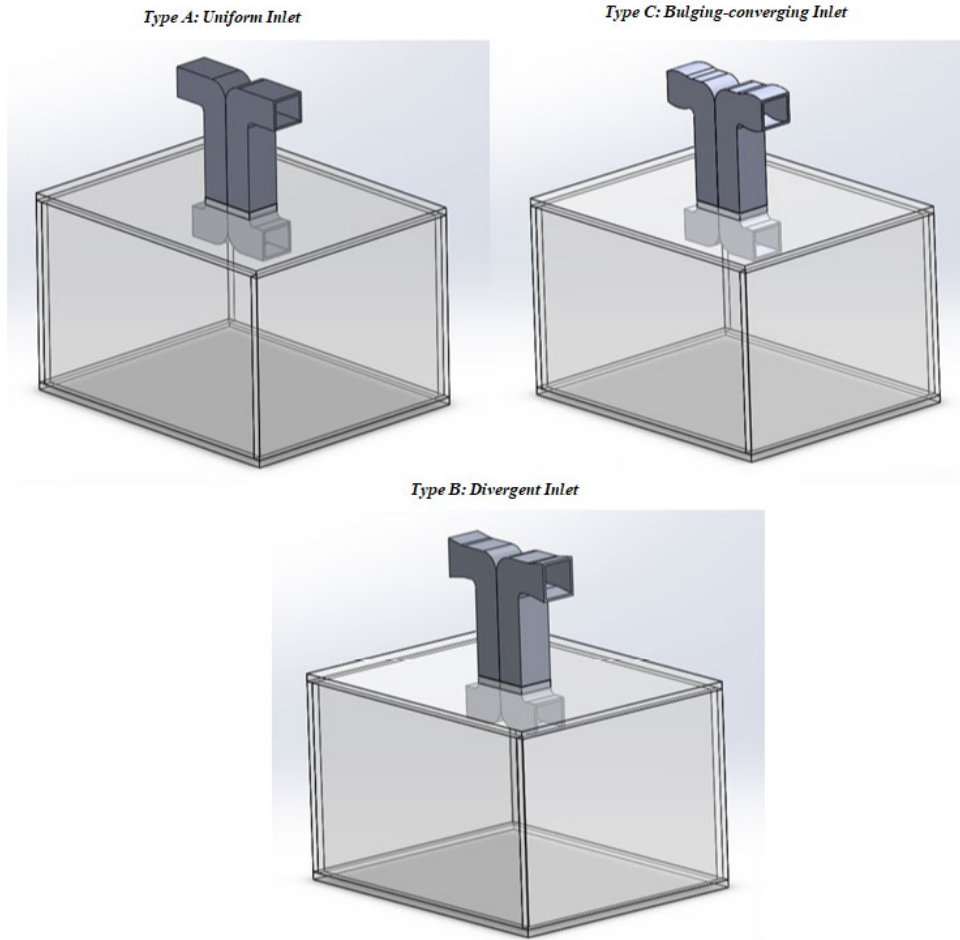
Figure 3-23. Three dimensional schematic of the three types of inlets studied. See Figure 3-2 for detailed dimensions

The room dimensions are shown in Figure 3-24 [22]. The length of the room is 5m, its width is 4 m and its height is 3 m. The windcatcher's tunnel has a total height of 2 m from the room's roof [20].
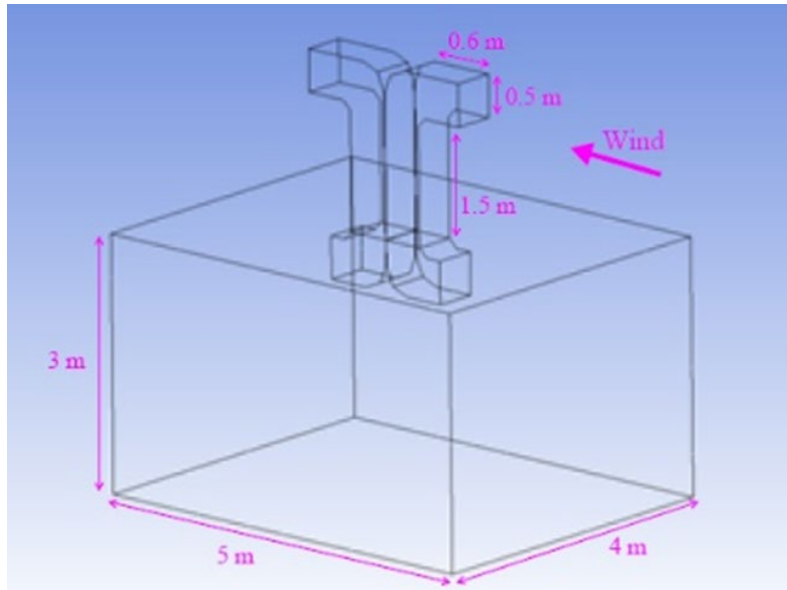
Figure 3-24. A three-dimensional room fitted with a windcatcher

Ansys Fluent [54] which is a computational fluid dynamics powerful tool is used to simulate the air flow.

3.3.2 Computational domain and boundary conditions

Wind driven ventilation is simulated by the addition of a surrounding domain that contains wind. Wind, distributed uniformly, is driven from the computational domain's inlet (upstream the room which is shown in blue in figure 3-25). The height of the inlet is 20 m and located at 15 m away from the right edge of the room. The dimensions of the surrounding domain are 35 m width, 28 m in depth and 20 m height. The room is fitted in its centre as shown in Figure 3-25. To make sure that the surrounding domain does not affect the simulation results and that the flow is developed completely, simulations using a larger surrounding (65 m length, 35 m height, and 52 m width) were conducted and the pressure and velocity at a point close to the windcatchers inlet were compared [19]. The results differed by less than 1%, indicating that the surrounding domain dimensions are suitable.
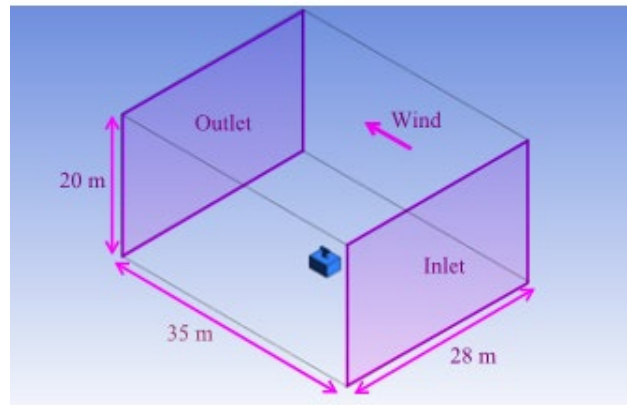
Figure 3-25. Schematic representation of the surrounding domain indicating the wind direction

The velocity inlet is defined normal to the inlet surface shown in Figure 3-25, whereas the outlet surface is defined as a zero gauge pressure outlet. The walls of the windcatcher and the room as well as the remaining sides of the surrounding are defined as stationary walls.

For computational efficiency the surrounding boundary condition were set as walls however care was taken to see that the presence of the wall does not affect the flow. In addition pressure values near the wall boundaries were in the range of 0.2-0.3 Pa compared to the maximum pressure values near the room which were about 23.5 Pa.

3.3.3 Meshing the 3D model and grid convergence

Tetrahedrals are used for meshing. Face sizing of 0.05 m and a growth rate of 1.2 are defined at the room walls and at the windcatchers walls.

Before the face sizing was chosen, a grid convergence test is performed. The velocity magnitude and the pressure were compared at two points [18, 19]. The first point was located inside the room at 1 m high, 1 m deep and at 3 m from the room's left wall. The second point was in the surrounding located at 6 m high, 1 m deep and at 5 m from the room's left wall [18, 19]. Three different mesh face sizing are used: 0.075 m, 0.06 m and 0.05 m, as the mesh size decreased the number of elements increased from 2045711 to 3506739 to 5614393. The variation in the pressure and velocity at the first point was less than 1.5% as shown in table 3-6. The grid convergence test for the second point provided similar results.

No. of Elements	Mesh Size (m)	Velocity (m/s)	Velocity Change %	Pressure (Pa)	Pressure Change %
2045711	0.075	0.2557	-1.25%	2.6573	-1.49%
3506739	0.060	0.2616	1.03%	2.6736	-0.87%
5614393	0.050	0.2589	--	2.6969	--

Table 3-6. Mesh convergence study at a point 1 m high and located at 3 m from the room's left wall

3.3.4 Simulation properties

The air properties are considered constant corresponding to sea level condition (air temperature of 288 K and air standard pressure of 101 kPa). The air density and the dynamic viscosity are assumed as follows:

$$\rho = 1.225 \text{ kg/m}^3; \qquad \mu = 1.789 \text{ x } 10^{-5} \text{ Pa s};$$

The realizable turbulent k - ε model is used. The k – ε model is robust and stable and it is considered the default modelling option for handling turbulent flow in many commercial codes [19]. The SIMPLE (Semi-Implicit Method for Pressure-Linked Equations) pressure-velocity coupling scheme is used in all the simulations along with the second order spatial discretization. The steady flow mode is used and the convergence criteria is set to 10^{-4}.

The majority of the human occupancy and activities occur at 1.2 m high, hence the average velocity of the air inside the room at a height of 1.2 m from the floor is investigated. Also to obtain the total flow rate through the room a cut at a height of 4.1 m in the inlet tunnel is used to obtain the average velocity in the windtunnel [18]. Figure 3-26 shows the two cuts used in green (at 1.2 m high) and in pink (at 4.1 m).
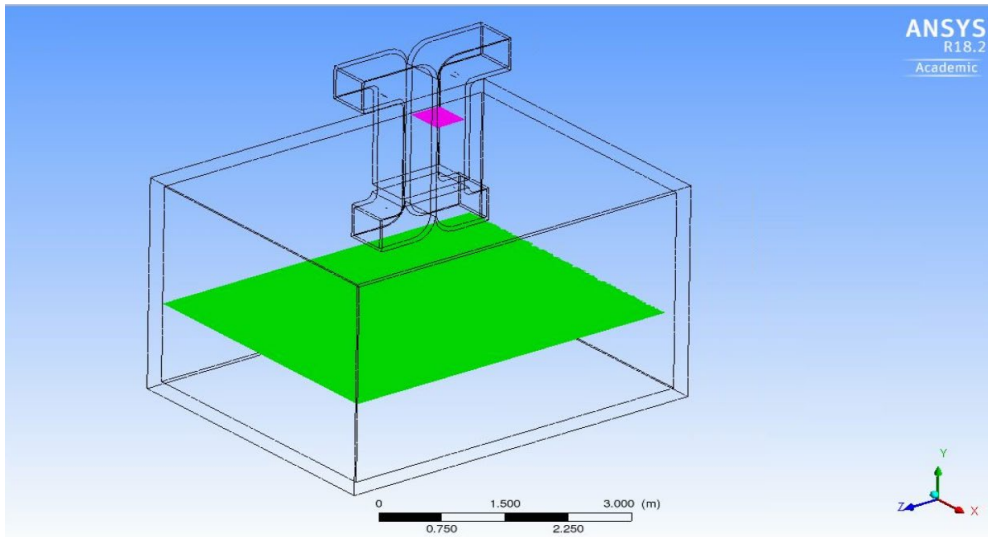
Figure 3-26. Surfaces used to obtain average velocity magnitude - green (at 1.2 m high) and pink (at 4.1 m high)

3.3.5 Results and discussion

Three dimensional simulations are conducted for the three inlet types at different velocities of 1, 2, 3 and 6 m/s respectively. Ansys CFD-Post is used to view results of simulations done by Ansys Fluent [54].

3.3.5.1 Inlet wind velocity at 3 m/s and inlet type A (uniform Inlet)

For inlet type A, the problem converged in 6716 iterations. The velocity magnitude contour through the room and the surrounding is shown in figure 3-27 at a surface located at the center of the domain passing through the windtunnel and parallel to the length of the domain. Figure 3-28 is zoomed closer to the room and windcatcher for better presentation.
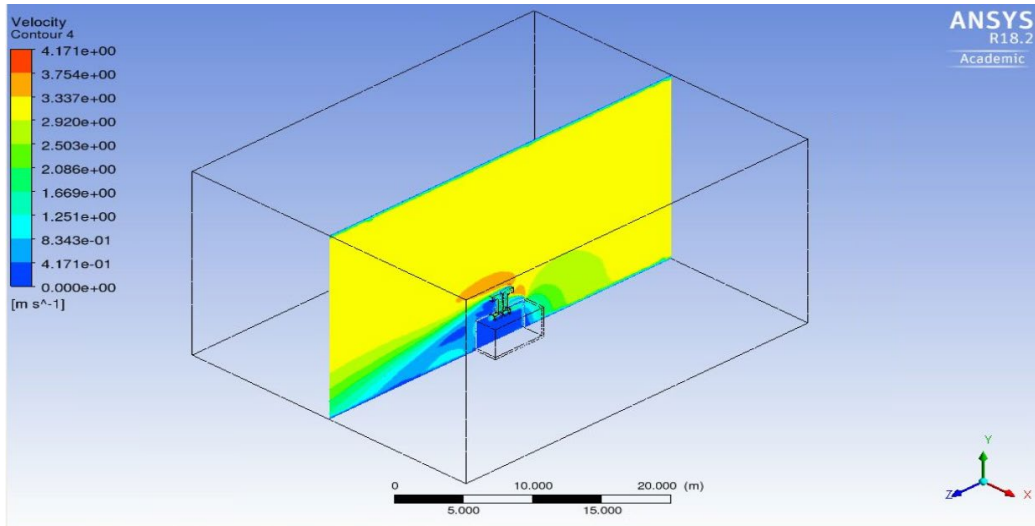
Figure 3-27. Velocity magnitude contour through the room, windcatcher and surrounding for the inlet Type A with 3 m/s inlet velocity
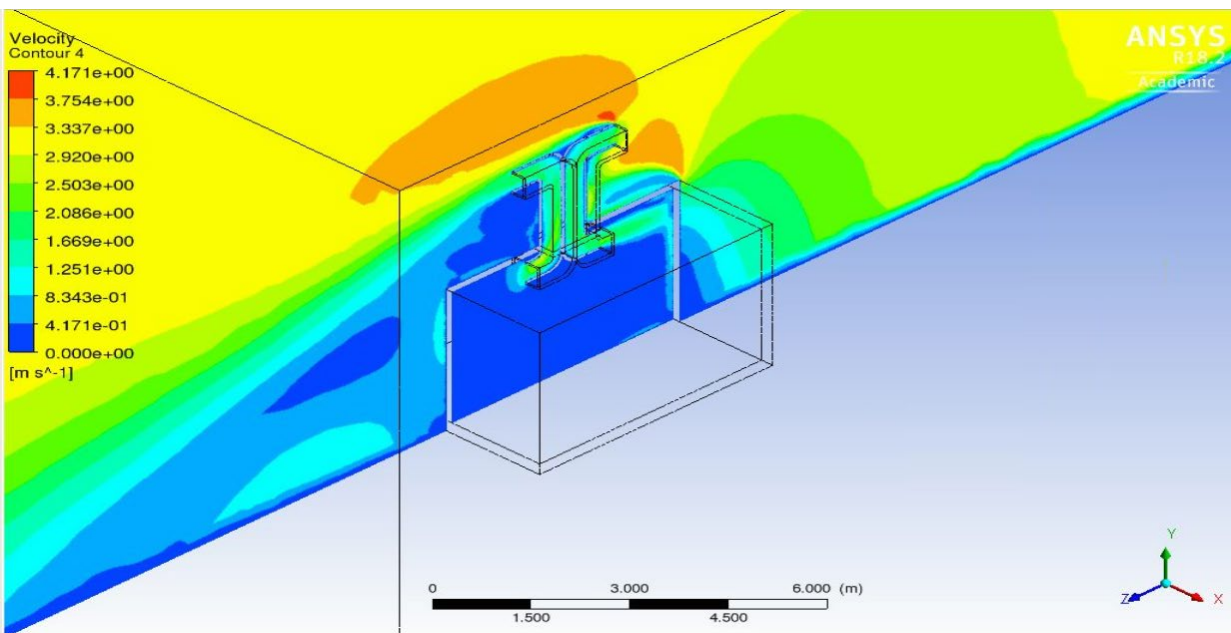
Figure 3-28. Velocity magnitude contour through the room and windcatcher for the inlet Type A with 3 m/s inlet velocity

Figures 3-29 and 3-30 show the air velocity contours at the surfaces located at 1.2 m high inside the room and at the 4.1 m high in the wind tunnel, with a uniform inlet type A and for the wind velocity of 3m/s.
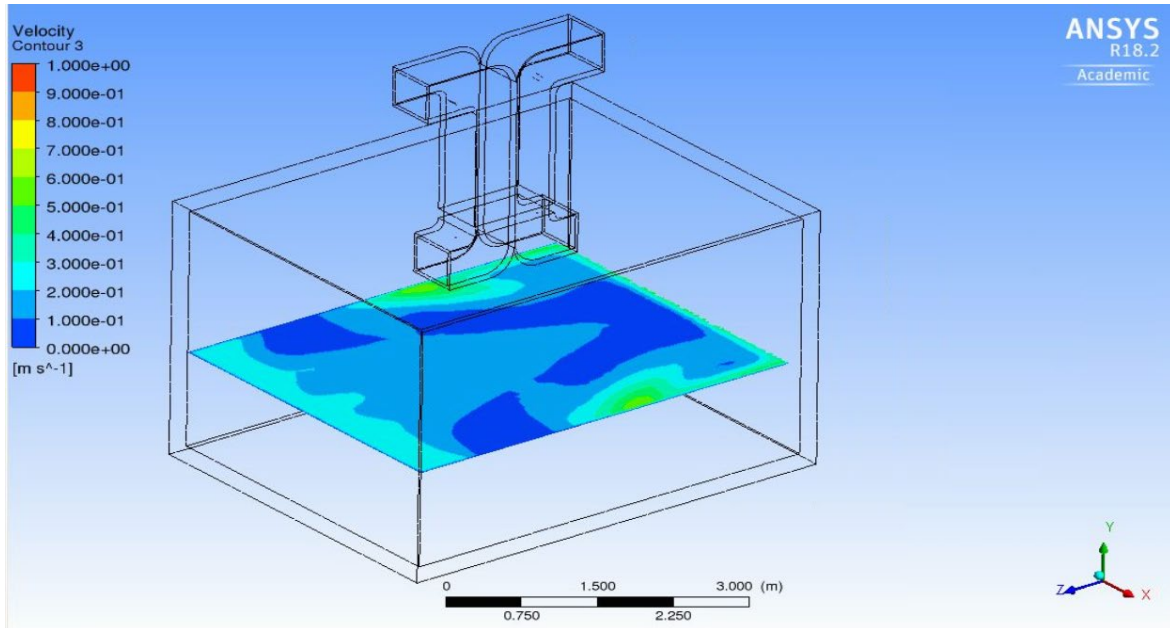
Figure 3-29. Velocity magnitude contour at a surface at 1.2 m height for the inlet Type A with 3 m/s inlet velocity
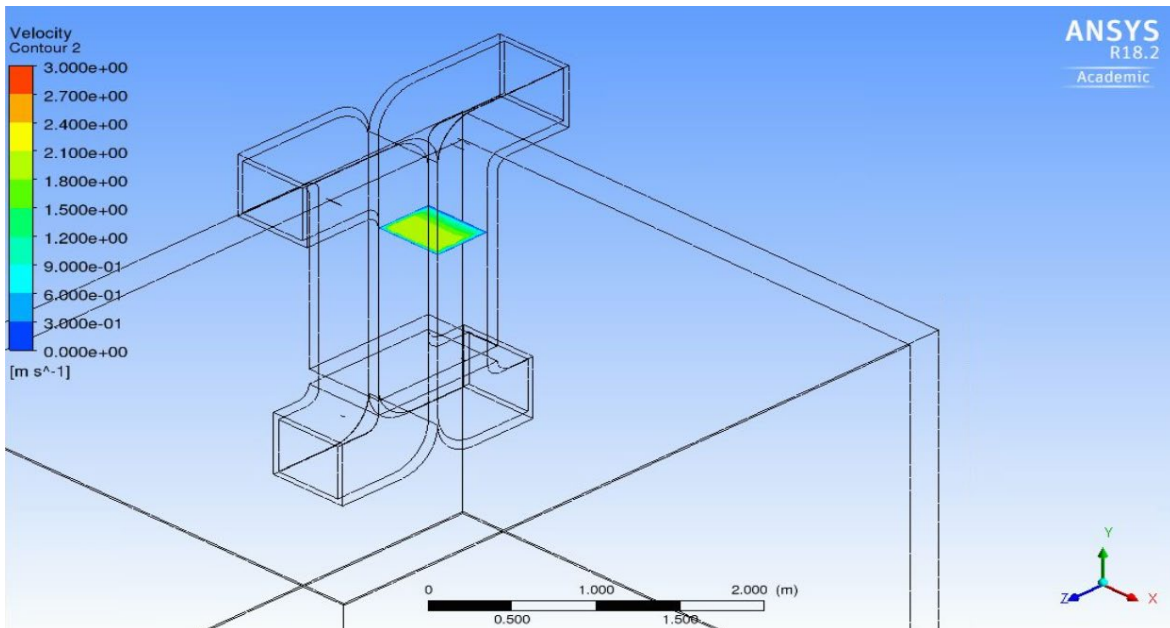
Figure 3-30. Velocity magnitude contour at a surface at 4.1 m height for the inlet Type A with 3 m/s inlet velocity

The average magnitude of air velocity at 1.2 m height inside the room is 0.179 m/s. Figure 3-31 shows the distribution of the air velocity, it shows that the higher velocities are closer to the walls of the room. The lower speeds are where the majority of human occupancy occurs.

Figure 3-32 shows the distribution of the air velocity magnitude at the cut 4.1 m high located in the wind tunnel. The average air velocity through the windtunnel (at the 4.1 m high cut) is 1.765 m/s.
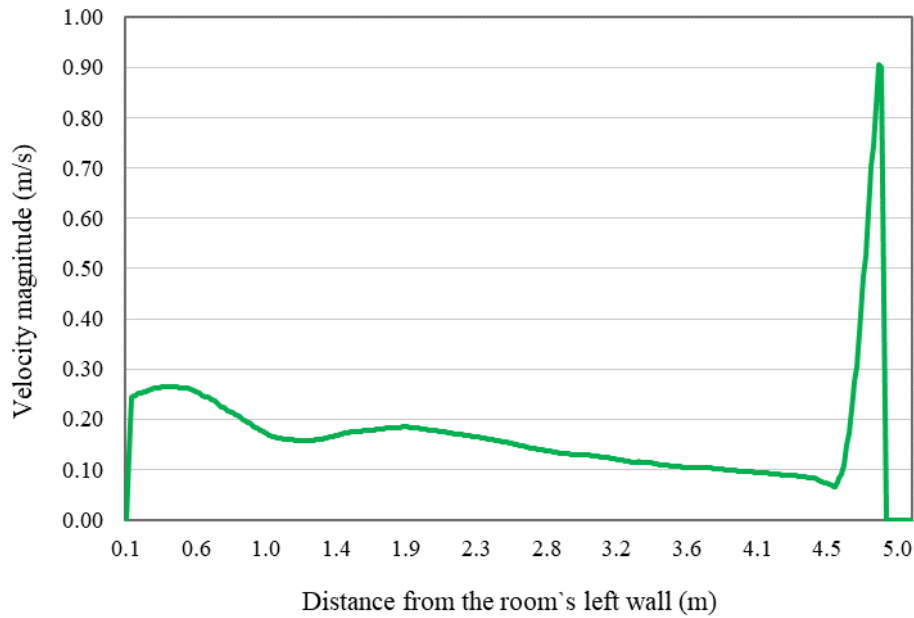
Figure 3-31. Air velocity magnitude through the room for the inlet Type A and at 1.2 m height with 3 m/s inlet velocity
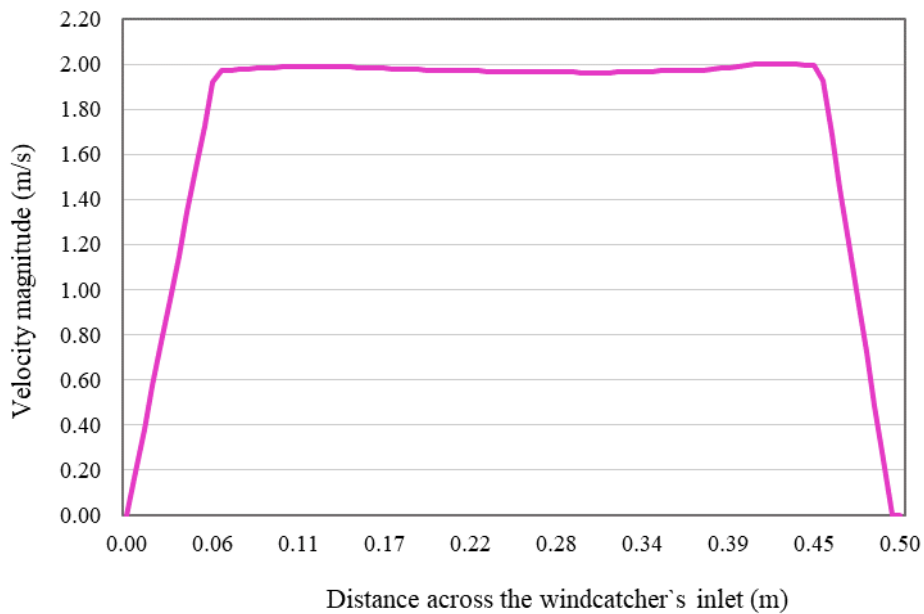
Figure 3-32. Air velocity magnitude through the windcatcher`s windtunnel for the inlet Type A and at 4.1 m height with 3 m/s inlet velocity

3.3.5.2 Inlet wind velocity at 3 m/s and Inlet type B (Divergent Inlet)

The problem converged in 5057 iterations for the inlet type B (divergent inlet). Figure 3-33 shows the variation in the air velocity contour and the pattern of the air flow inside the room and some of its surrounding.
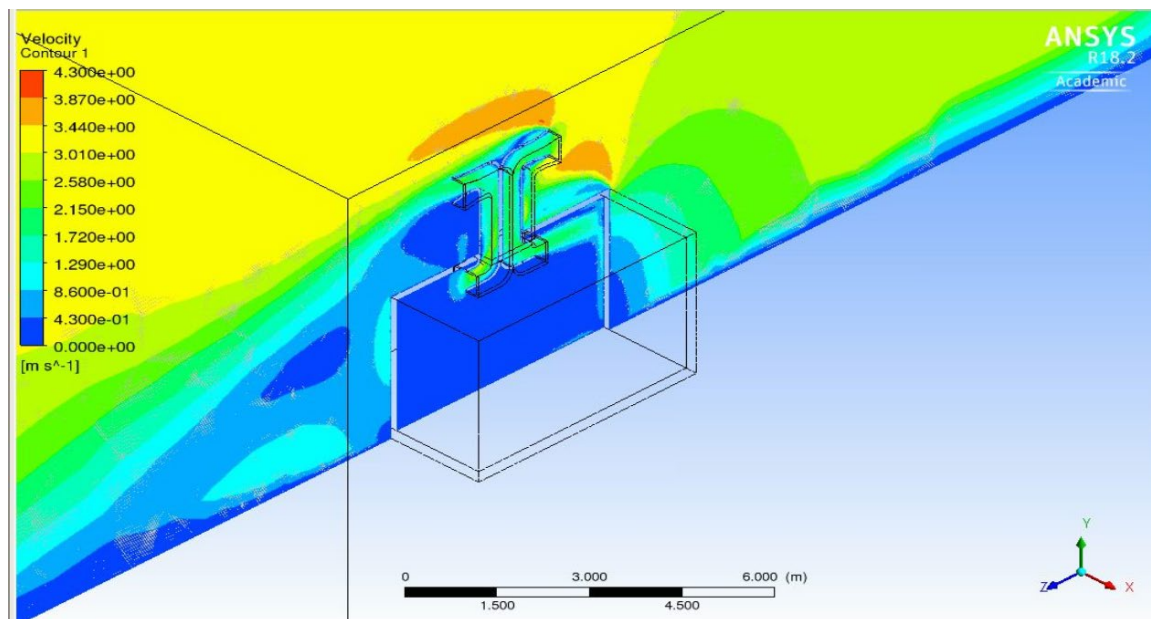
Figure 3-33. Air velocity magnitude contour of the room and windcatcher for inlet Type B with 3 m/s inlet velocity

Figure 3-34 shows the air flow pattern circulating through the room in three dimensions. It indicates the velocity of the air flowing inside the room with different colors. The velocity in the windtunnels inlet and outlet is much higher than inside the room. For better presentation the isometric view of one stream line of air is also shown in Figure 3-35.
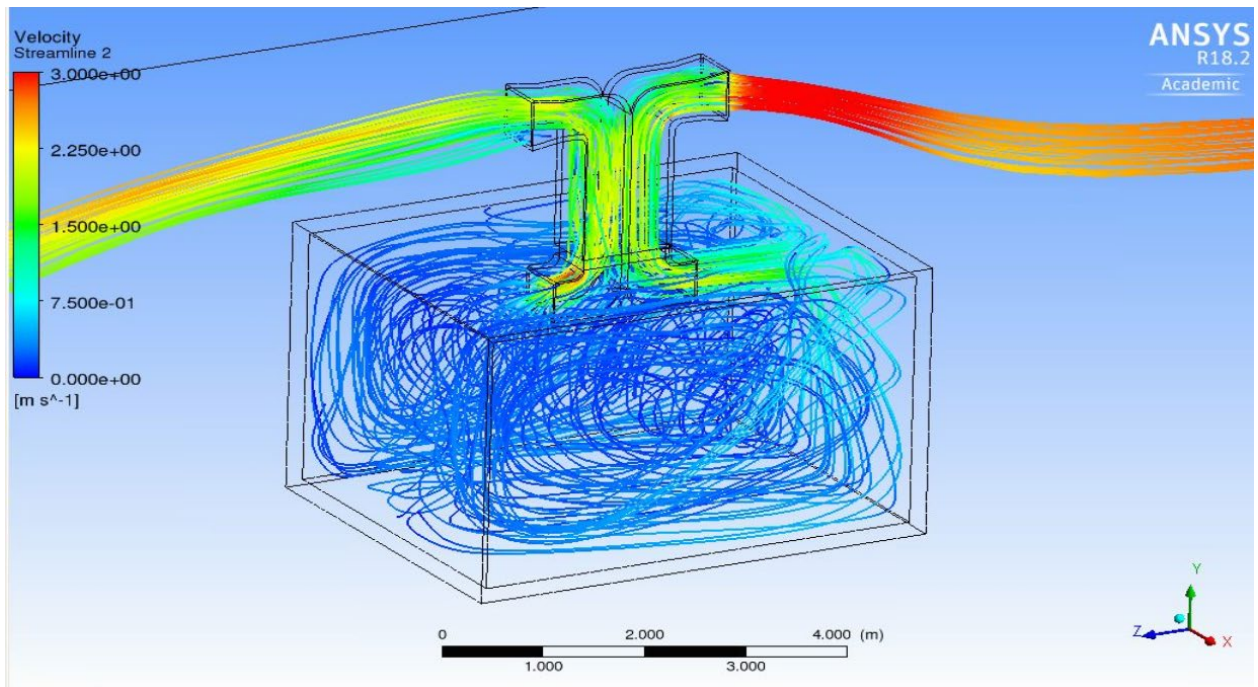
Figure 3-34. Air velocity magnitude streamline of the room and windcatcher for the inlet Type B with 3 m/s inlet velocity
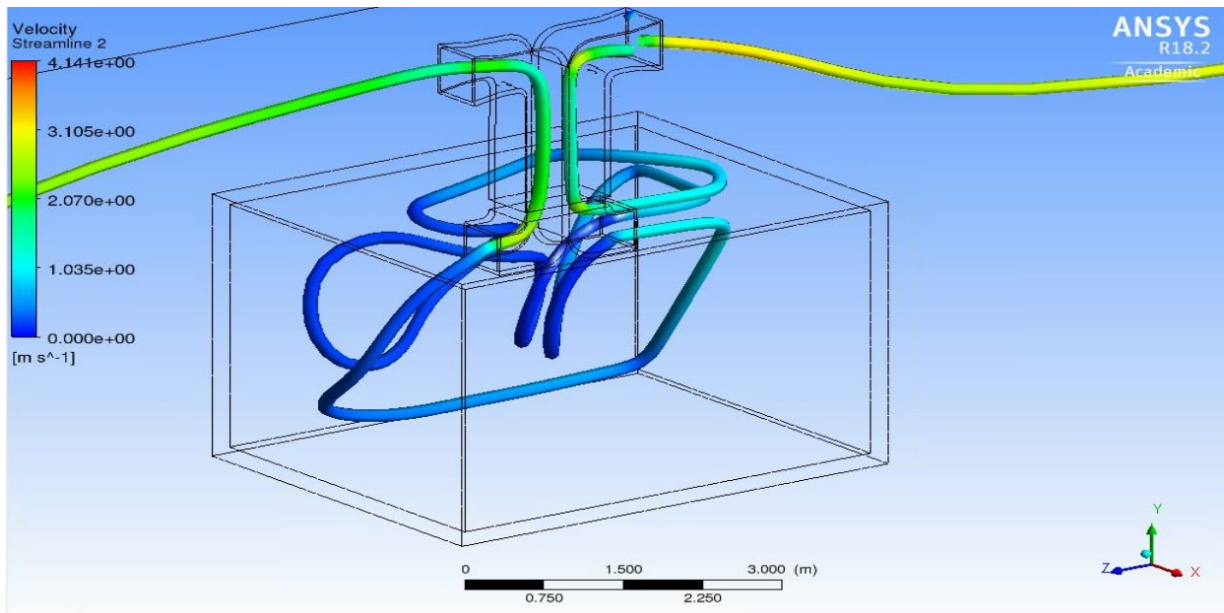
Figure 3-35. Air Velocity magnitude streamline through the three dimensional room with 3 m/s inlet velocity - Isometric View

Figures 3-36 and 3-37 show the contours of the air velocity magnitude at a surface 1.2 m high inside the room and at a surface at 4.1 m high in the wind tunnel, both are for the divergent inlet type B and for a velocity of 3 m/s.
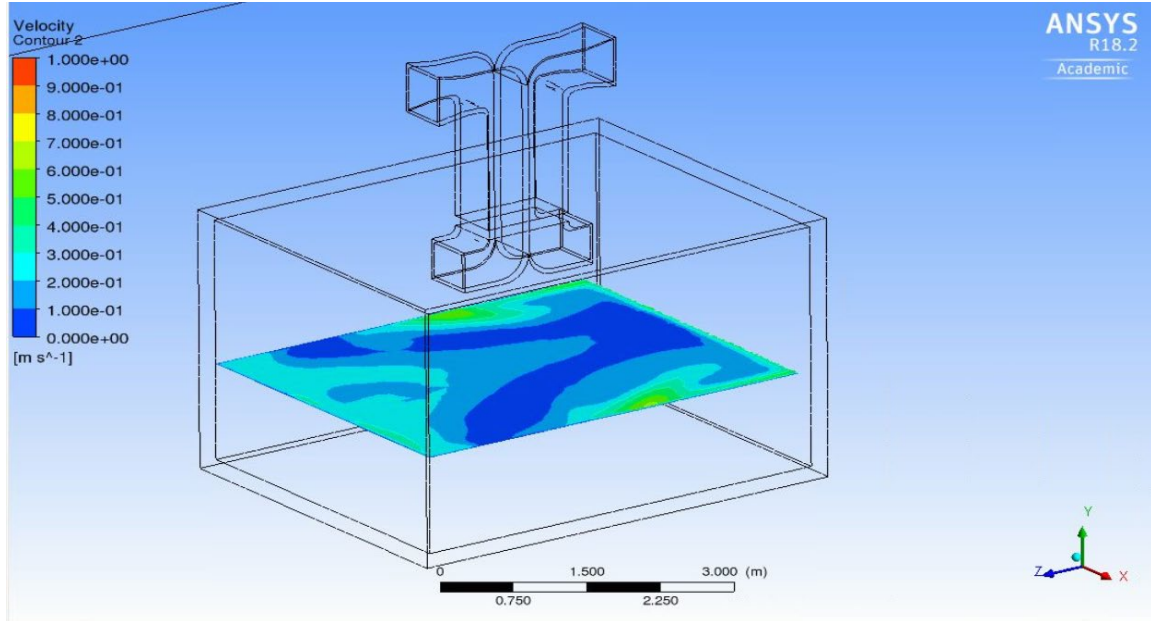
Figure 3-36. Air velocity magnitude at a surface 1.2 m height for the inlet Type B with 3 m/s inlet velocity
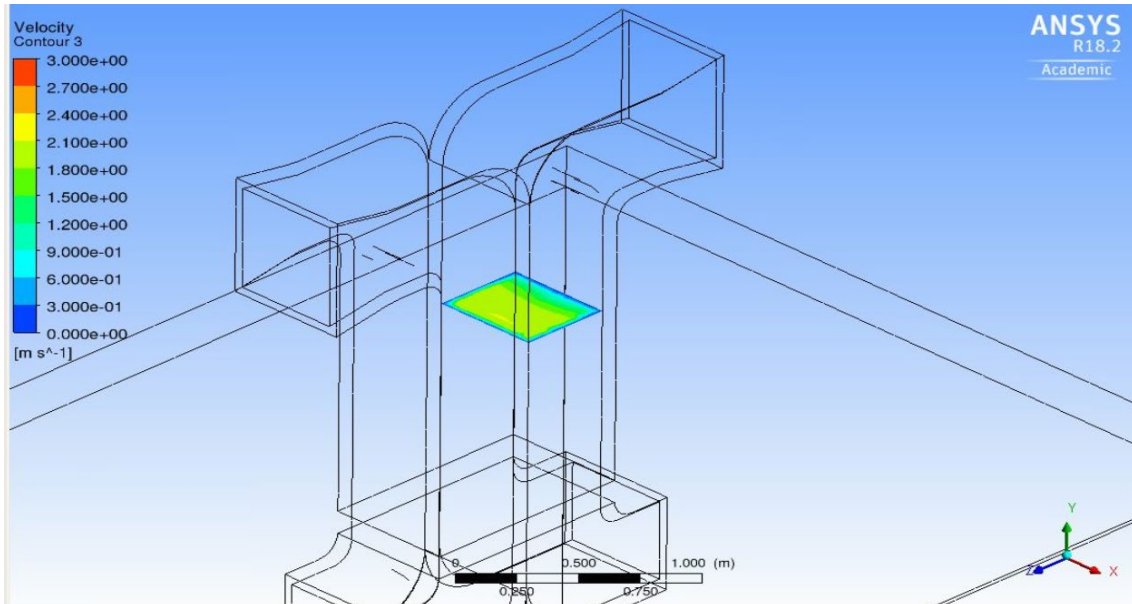
Figure 3-37. Velocity magnitude at a surface at 4.1 m high in the wind tunnel for the inlet Type B with 3 m/s inlet velocity

For the inlet type B, the average velocity at 1.2 m height inside the room is 0.188 m/s. The distribution of the air velocity at 1.2 m high is shown in Figure 3-38, the higher velocities are located close to the walls of the room and the lower speeds are in the middle of the room where the majority of human occupancy occurs. The distribution of the velocity at the cut 4.1 m high in the wind tunnel is shown in Figure 3-39. The average velocity at the 4.1 m high cut is 1.790 m/s.
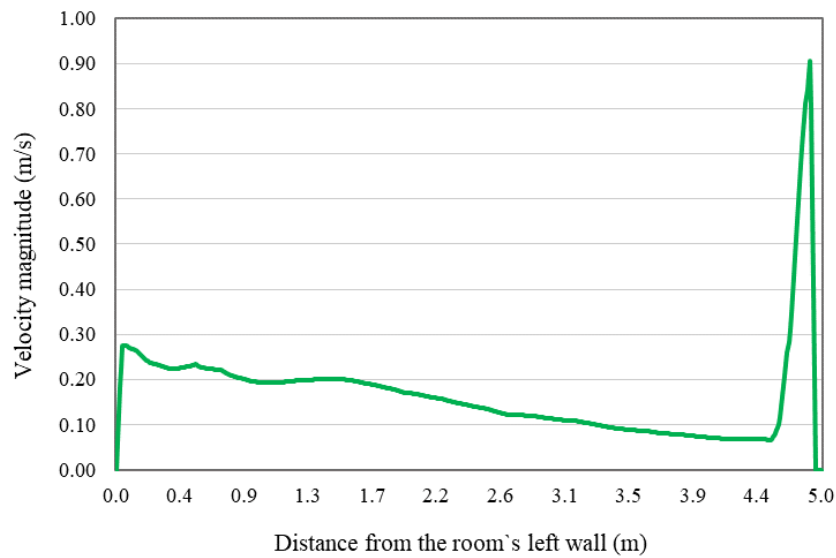
Figure 3-38. Velocity magnitude through the room for the inlet type B at 1.2 m high and with 3 m/s inlet velocity
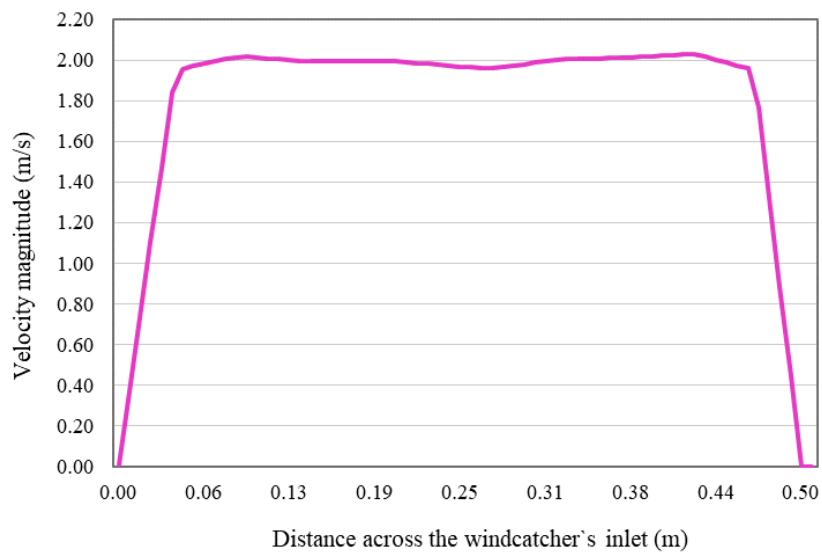
Figure 3-39. Velocity magnitude through the windcatcher`s inlet for the inlet type B at 4.1 m high and with 3 m/s inlet velocity

105

3.3.5.3 Inlet wind velocity at 3 m/s and Inlet type C (Bulging-convergent Inlet)

The problem converged in 4451 iterations, Figure 3-40 shows the three dimensional air flow pattern (streamlines) circulating through the room in three dimensions. The pattern of the air flow is similar to both inlet types A and B.
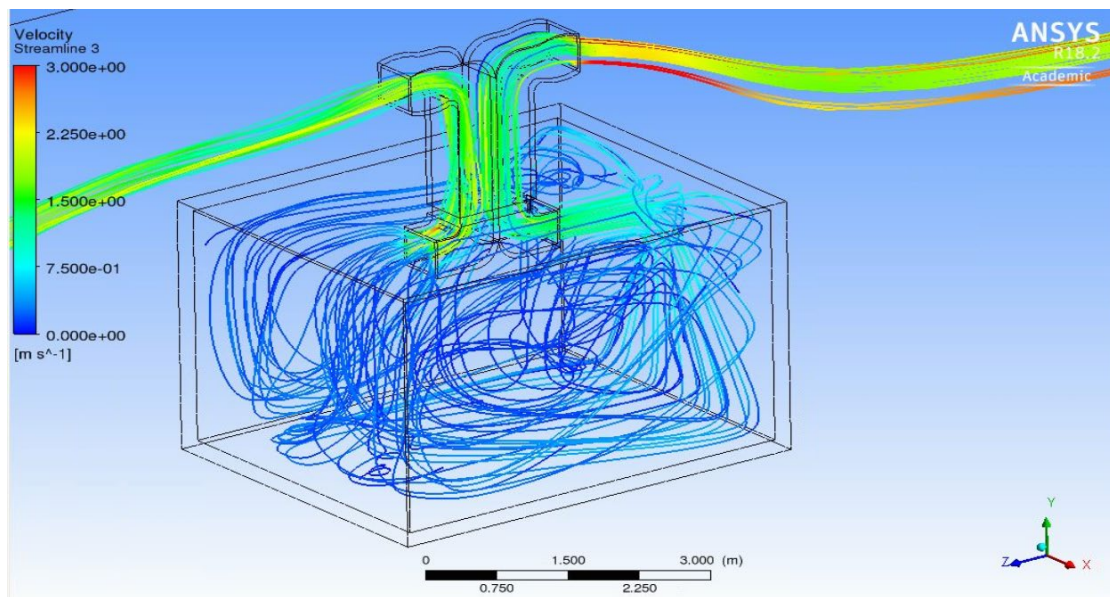
Figure 3-40. Air velocity magnitude streamlines through the room and windcatcher with the inlet Type C and 3 m/s inlet velocity

The air average velocity at the surface 1.2 m high in the room is 0.180 m/s. Figure 3-41 shows the distribution of the air velocity inside the room at 1.2 m height and Figure 3-42 shows the air velocity distribution at the cut 4.1 m high in the wind tunnel. The average air velocity at the 4.1 m high surface is 1.726 m/s. The distribution of air velocity is similar to both inlet types A and B shown in Figures 3-29, 3-30, 3-36 and 3-37.
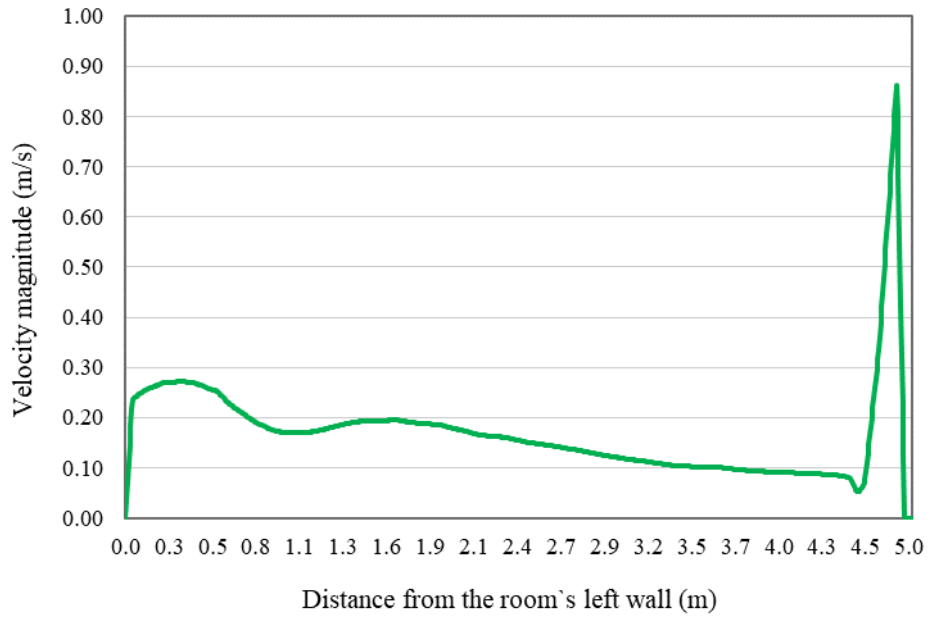
Figure 3-41. Air velocity magnitude through the room for the inlet type C at 1.2 m high and with 3 m/s inlet velocity
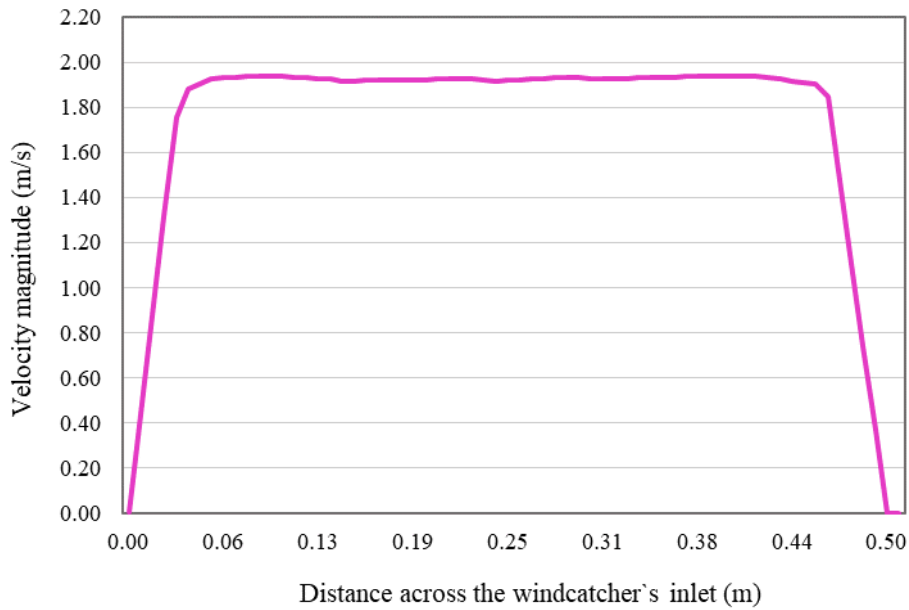
Figure 3-42. Air velocity magnitude through the windcatcher`s inlet for the inlet type C at 4.1 m high with 3 m/s inlet velocity

3.3.5.4 Summary of Results with inlet wind velocity at 3 m/s

The results of the three types of inlets are summarized in table 3-7 and table 3-8. The divergent inlet (type B) has captured the highest air flow (0.4475 m^3/s) with an approximate difference of 1.40 % compared to the uniform inlet (0.4413 m^3/s) and a difference of approximately 3.58% compared to the bulging-convergent inlet (0.4315 m^3/s). For the three types of inlets studied, the air flow pattern has provided full ventilation across the room and especially where the human occupancy occurs. The divergent inlet has also provided a higher average velocity (0.188 m/s) at the 1.2 m high cut with an increase of 4.79% compared to that provided by the uniform inlet (0.179 m/s) and an increase of 4.25% compared to the bulging convergent inlet (0.18 m/s). The three different inlet shapes have provided appropriate air speed throughout the living area which is an important factor for the human comfort as the ASHRAE standard recommends 0.2m/s to be the maximum air velocity [137].

Average Velocity (m/s)			
Inlet Type	Uniform (Type A)	Divergent (Type B)	Bulging-Convergent (Type C)
1.2 m cut	0.179	0.188	0.180
Increase %	4.79%		4.25%
4.1 m cut	1.765	1.790	1.726
Increase %	1.40%		3.58%

Table 3-7. Average air velocity for the three inlet types at 3 m/s

Total Flowrate at 4.1 m high (m^3/s)			
Inlet Type	Uniform (Type A)	Divergent (Type B)	Bulging-Convergent (Type C)
4.1 m cut	0.4413	0.4475	0.4315
Increase %	1.40%		3.58%

Table 3-8. Total air flow rate at 4.1 m surface for the three inlet types and the corresponding percentage increase of the divergent inlet

3.3.5.5 Results with various inlet wind velocities

In addition to the inlet velocity of 3 m/s, simulations with different velocities are conducted and the effect of the different speeds is investigated. Two lower inlet velocities of 1 and 2 m/s and a higher velocity of 6 m/s were applied. As the contours of velocities and the velocity magnitude distribution are all similar to those presented for 3 m/s the following would summarise the results avoiding repetition of multiple similar figures. Figure 3-43 shows the air velocity distribution at 1.2 m high for all of the various velocities studied for the divergent inlet type B, and Figure 3-44 shows the air velocity distribution at the cut 4.1 m high in the wind tunnel.
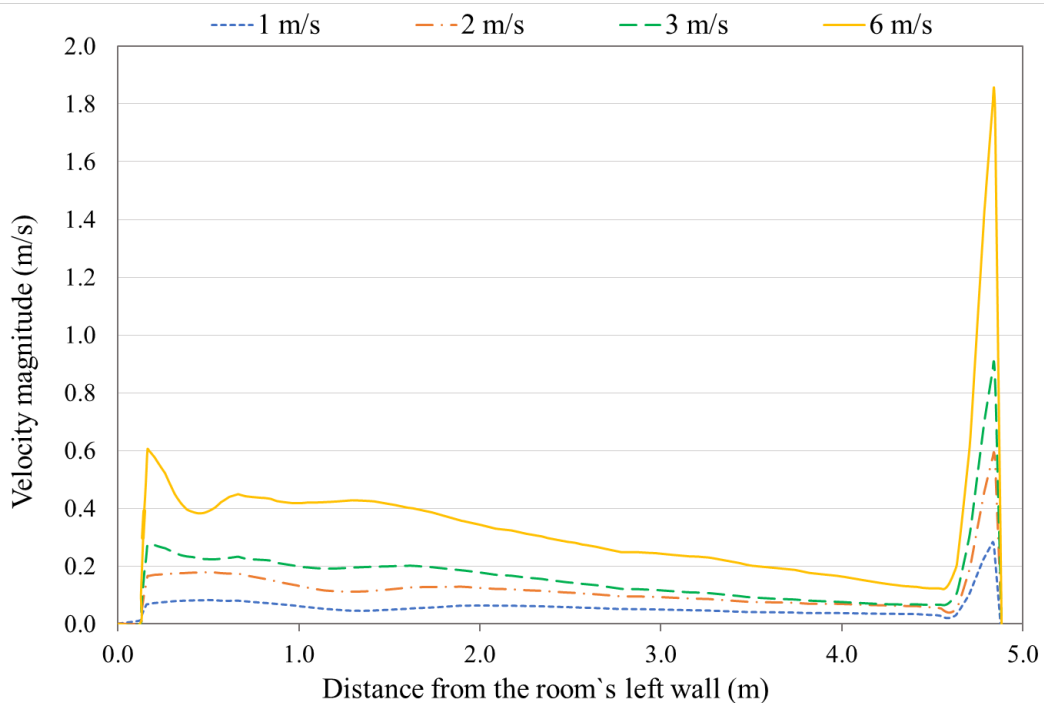
Figure 3-43. Air velocity magnitude through the room for the inlet Type B at 1.2 m high and with different inlet velocities.
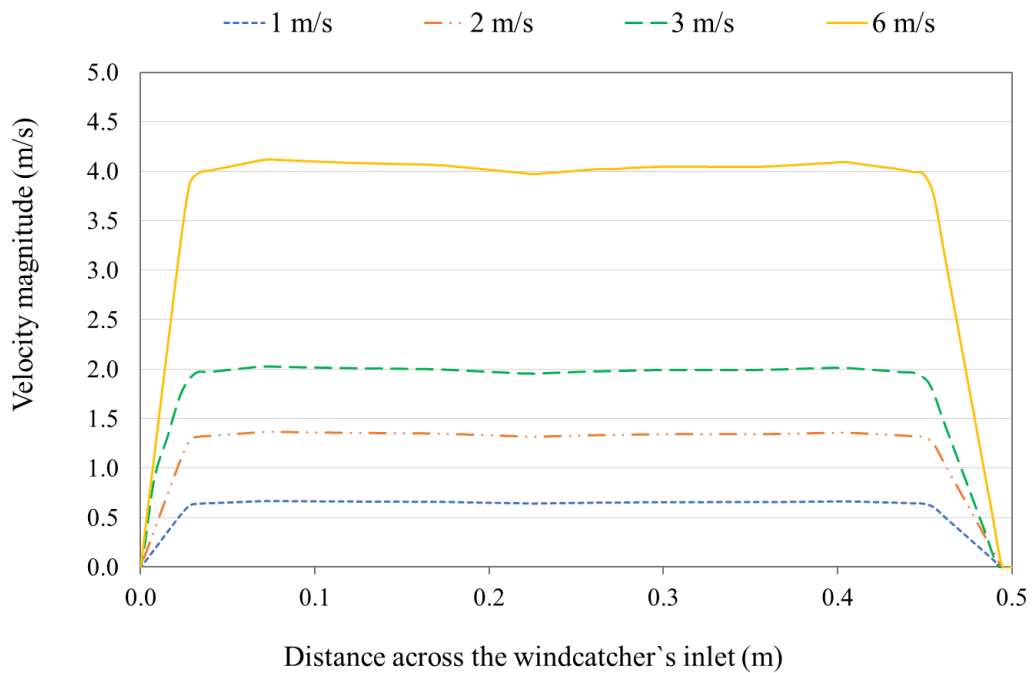
Figure 3-44. Air velocity magnitude through the windcatcher`s inlet for the inlet Type B at 4.1 m high and with different inlet velocities

3.3.5.6 Results with inlet velocity at 6 m/s

For inlet type A, the average velocity at the 1.2 m high surface inside the room is 0.363 m/s [20]. The average velocity at the 4.1 m high surface is 3.551 m/s. For inlet type B, the air average velocity at 1.2 m high surface inside the room is 0.391 m/s and the average velocity at the 4.1 m high is 3.644 m/s. For inlet type C the average air velocity at 1.2 m high surface inside the room is 0.358 m/s and the average velocity at the 4.1 m high surface is 3.473 m/s. in all cases the higher air velocities are closer to the walls of the room. It is noted that with inlet velocity of 6 m/s the average air speed throughout the living area is over 0.2 m/s which does not necessarily satisfy thermal comfort requirements as per the ASHRAE standard [137]. The divergent inlet (type B) captured the highest air flow. The difference is approximately 2.55% more than that provided by the uniform inlet and approximately 4.70% more than the bulging-convergent inlet. The distribution of velocity magnitude and the contours of velocity are similar to those presented for wind speed at 3 m/s.

Figures 3-45 and 3-46 show the contour of static pressure with an inlet velocity of 6 m/s. Figure 3-45 shows a larger area of high pressure (in red and orange) around the divergent inlet type B than that shown in figure 3-46 around the uniform inlet type A and the bulging-convergent inlet type C.
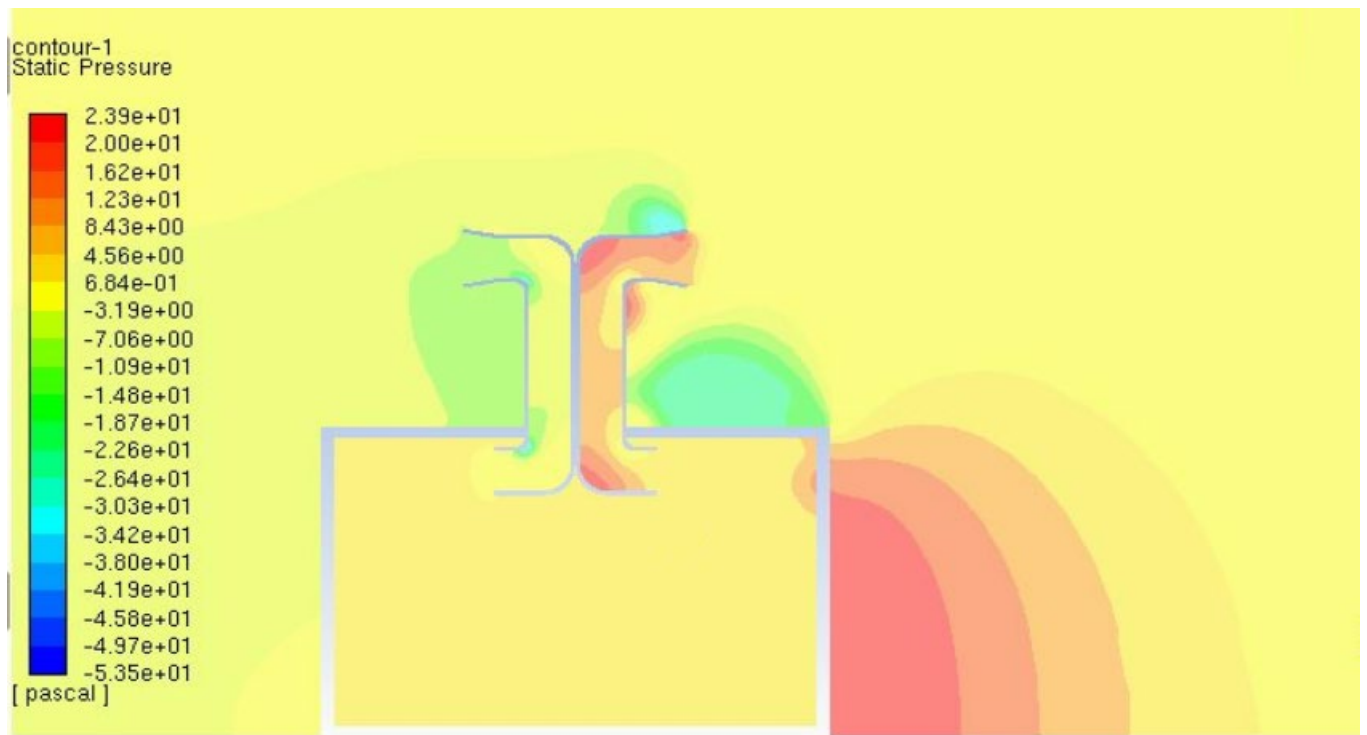
Figure 3-45. Contours of Static Pressure for the inlet Type B with 6 m/s inlet velocity
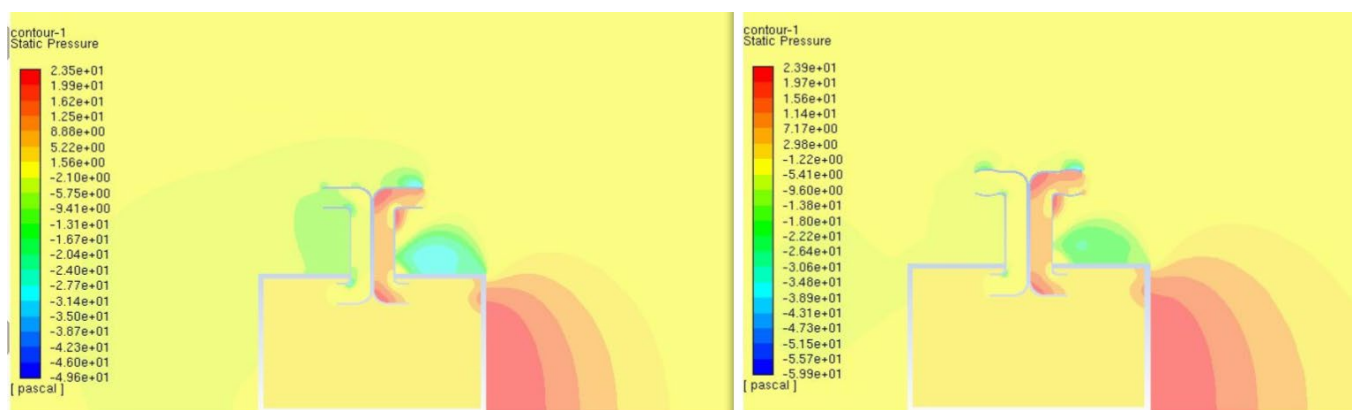
Figure 3-46. Contours of Static Pressure for the inlet Type A (left) and for the inlet type C (right) with 6 m/s inlet velocity

Both figures 3-45 and 3-46 show the typical function of windcatchers. When wind hits an obstacle (such as the windcatcher inlet and wind tunnel), it creates pressure differences around it and the air density in the windward area increases with respect to the leeward area. Therefore, positive pressure is made on the windward face and the negative pressure forms on the other side and wind enters from the area with the positive pressure and tends to move to the lower pressure zone [138]. In the case of windcatcher, lower pressure zone is located at the bottom of the windcatcher's shaft, therefore fresh air enters to the building and indoor hot and polluted air exhausts to the opposite side with higher negative pressure.

3.3.5.7 Summary of results with inlet velocity at 1, 2 and 6 m/s

Tables 3-9 and 3-10 show the summarized results related to the three inlet types at velocities of 1, 2, and 6 m/s. At all applied velocities the divergent inlet, type B provided the highest air flow.

At the low velocity of 1 m/s the divergent inlet provided only about 1.4% increase in air flow more than the uniform inlet and 3.2% increase with respect to the bulging convergent. However, and similar to inlet velocity of 3 m/s, the divergent inlet has provided an increase in the average velocity at the 1.2 m cut where the most of the human occupancy takes place. This increase is about 3.5% more than the uniform inlet and 5.5% more than the bulging convergent inlet.

Inlet Velocity	Inlet Type	Average Velocity (m/s)		
		Uniform (Type A)	Divergent (Type B)	Bulging-Convergent (Type C)
1 m/s	1.2 m cut	0.0602	0.0624	0.0590
	Increase %	3.50%		5.49%
	4.1 m cut	0.5796	0.5879	0.5691
	Increase %	1.40%		3.19%
2 m/s	1.2 m cut	0.1214	0.1273	0.1211
	Increase %	4.58%		4.87%
	4.1 m cut	1.1716	1.2035	1.1484
	Increase %	2.65%		4.58%

6 m/s	1.2 m cut	0.3630	0.3910	0.3580
	Increase %	7.16%		8.44%
	4.1 m cut	3.5510	3.6440	3.4730
	Increase %	2.55%		4.70%

Table 3-9. Average air velocity for the three inlet types at 6 m/s

| Inlet Velocity | Inlet Type | Total Flowrate at 4.1 m high (m³/s) | | |
		Uniform (Type A)	Divergent (Type B)	Bulging-Convergent (Type C)
1 m/s	4.1 m cut	0.1449	0.14697	0.1422
	Increase %	1.39%		3.19%
2 m/s	4.1 m cut	0.2929	0.300	0.2871
	Increase %	2.37%		4.30%
6 m/s	4.1 m cut	0.8878	0.9110	0.8683
	Increase %	2.55%		4.69%

Table 3-10. Total air flow rate at 4.1 m cut for the three inlet shapes and the corresponding percentage increase of the divergent inlet

With an inlet velocity of 2 m/s the divergent inlet has also provided the highest air flow rate with an increase of 2.37% and 4.3% compared to the uniform and bulging convergent inlets as shown in table 5. The average velocity at 1.2 m high has also been consistently increasing with the divergent inlet by approximately 4.58 % and 4.87% providing thermal comfort as per the ASHRAE standard [137]. Figure 3-47 shows that the higher air flow captured by the divergent inlet has been consistently observed as the inlet velocity varied.
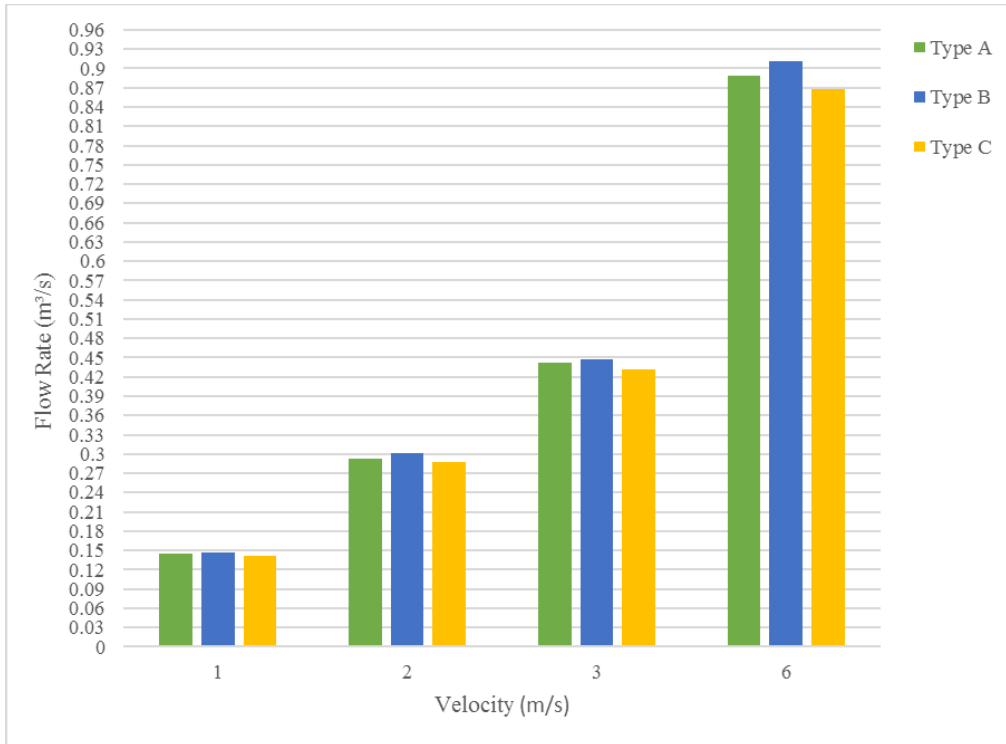
Figure 3-47. Total flow rate at 4.1 m cut for the three inlet shapes

3.3.6 Validation of simulations with 3 m/s inlet velocity

Ansys Fluent is a powerful simulation tool and is well known for its reliability and accuracy, it has been applied to various research works and found to be very useful [74]. Additionally, the results of our three dimensional simulation for the room with a uniform inlet are compared with available and published computational results by Niktash and Huynh [14] who had investigated the effect of windcatcher inlet angle with respect to wind direction on ventilation of a three dimensional room. Their room is similar in size and shape to the room simulated in this study (3m x 4m x 5m) and also fitted with a two sided windcatcher of total height 2m with an applied uniform inlet velocity of 3 m/s. The only difference between the two studies is that the opening of the windcatcher in Niktash and Huynh was 80cm x 80cm while the opening of our windcatcher is 50cm x 50cm, thus a scaling factor of 2.56 [(80*80)/(50*50)] applies.

The total flow rate obtained by Niktash and Huynh [14] is 1.119 m³/s as shown in table 3-11 while the total flow rate captured by our study is 0.441 m³/s. After using the scaling factor the difference is 0.95 % only. Both studies have used the RANS method with the K- ε turbulent model.

Total flow rate Q (m³/s)			Difference (%)
Current study	Scaled	Niktash and Huynh, 2014	
Uniform inlet 50cmx50cm	current x 2.56	Uniform inlet 80cmx80cm	
0.441	**1.130**	**1.119**	0.95%

Table 3-11. Comparison of our simulation results with Niktash and Huynh, 2014.

Niktash and Huynh [139] have also used the LES method (Smagorisky SGS model) and compared their LES results with their RANS result [14]. The LES and RANS results were in good agreement. Niktash [81] has also conducted an experimental validation for his simulations using a scaled model. The experimental results obtained using the scaled model approved the simulation's results for the same size model and with the similar inlet velocity.

All the above confirms the reliability of our simulations and gives extra confidence in our results.

3.3.7 Conclusion

CFD (computational fluid dynamics) modelling is implemented using Ansys Fluent to investigate the airflow entering a three dimensional room through a windcatcher with different inlet designs. Three designs are studied which are a uniform inlet, a divergent inlet and a bulging convergent inlet. The results of our simulations using a uniform inlet and with wind velocity of 3 m/s has showed a very good agreement with a published study using similar conditions.

Three dimensional simulations which reflect real life situation have been conducted and wind velocities of 1, 2, 3 and 6 m/s have been applied. The pattern of the air flow related to the different inlets provided adequate ventilation at a surface 1.2 m high inside the room. The divergent inlet design has captured the highest air flow through the room and provided higher average velocity at 1.2 m high enhancing the thermal comfort where most of the human occupancy occurs.

Using windcatchers would decrease the consumption of non-renewable energies by buildings. It would be an efficient sustainable method to preserve the environment and a major help in managing the limited available non-renewable energy resources. Applying a divergent inlet would provide additional flow captured by the windcatcher and contribute to enhancing the thermal comfort of the occupants and increase the efficiency of windcatchers.

3.4 Effect of combining buoyancy driven and winddriven ventilation in a three dimensional room fitted with a windcatcher

3.4.1 Introduction

Combining the winddriven and the buoyancy driven ventilation will be investigated in this study through the use of a windcatcher natural ventilation system.

To achieve this, CFD (computational fluid dynamics) tool is used to simulate the air flow in a three dimensional room fitted with a windcatcher based on the winddriven ventilation alone, buoyancy driven ventilation alone, and combined buoyancy and winddriven ventilation. Different wind speeds between 0 up to 3 m/s are applied and the total air flow rate through the windcatcher is investigated with applied temperatures of 350 K and 400 K applied at the windcatcher's outlet wall. Winddriven ventilation alone without any temperature applied is also investigated. Figure 3-48 shows a representative model of the three dimensional room studied.
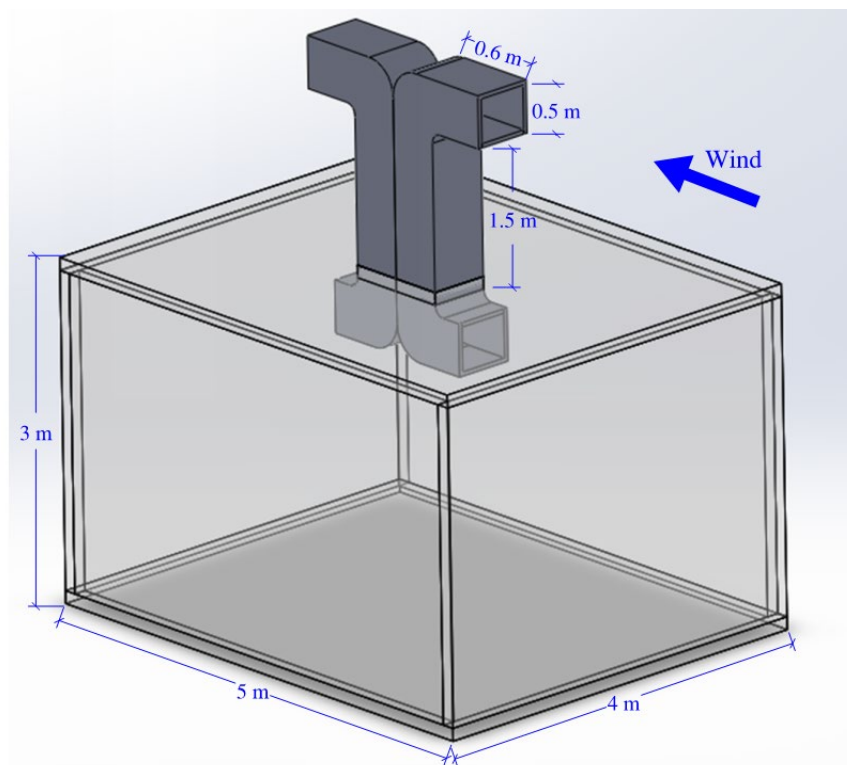
Figure 3-48. Three dimensional room fitted with a windcatcher

A three dimensional real sized room shown in Figure 3-48 with a length of 5 m, a width of 4 m, and a height of 3 m fitted with a windcatcher is modeled in this study using Ansys Fluent [54]. The height of the windcatcher is assumed to be 2 m from the roof of the room up to the top of the windcatcher [23].

The size of the inlet and outlet openings of the windcatcher is taken to be 0.5x0.5 m^2. They are perpendicular to the flow direction. The windcatcher length inside the room is taken to be 0.1 m and the inside opening size is also 0.5x0.5 m^2.

3.4.2 Computational domain and boundary conditions

To simulate a free ventilation air flow the addition of a surrounding domain that contains wind is considered. Wind is driven from the Inlet shown in Figure 3-49 at a velocity of 3 m/s distributed uniformly over a height of 20 m; the air inlet is at a distance of 15 m away from the right edge of the room. The total width of the surrounding domain is 35 m, its depth is 28 m and its height is 20 m. The room is fitted in its center as shown in Figure 3-49.
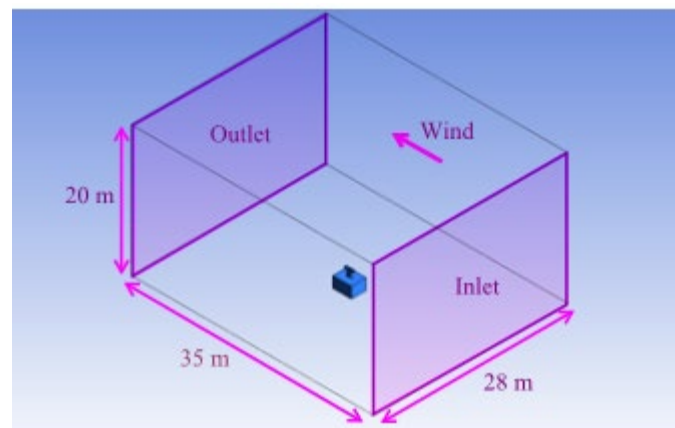
Figure 3-49. Schematic representation of the surrounding domain showing its dimensions and the direction of the wind. The room with the windcatcher is shown in blue at its center.

The right side of the computational domain (upstream) is a velocity inlet, where the speed of air is defined normal to the inlet surface. The left side (downstream) is an outlet with pressure set to zero gauge. The room, the windcatcher's walls and the remaining sides of the surrounding are all set to be a stationary wall with no slip shear condition.

Before the surrounding dimensions were selected, simulations using a surrounding with larger dimensions of length 65 m, a height of 35 m and a width of 52 m were conducted. The pressure and velocity at a point close to the windcatchers inlet, differed by less than 1%.

3.4.3 Meshing the 3D model and grid convergence

For meshing the geometry, tetrahedral have been used with a face sizing of the room and windcatcher of 0.04 m and a growth rate of 1.2, the global growth rate was set to 1.2 with a maximum face size of 0.5 m since a fine mesh is not necessary for the far field in the surrounding domain.

To make sure that the grid pattern used is adequate, a grid convergence test was performed. The velocity magnitude and the pressure were compared at two points, one within the room at 1 m high, 1 m deep and located at 3 m from the room's left wall. The second point was in the surrounding at 6 m high, 1 m deep and located at 5 m from the room's left wall. As the number of elements increased from 2768497 to 3737095 to 4498724 and to 5565752 by decreasing the face mesh sizing of the room and windcatcher from 0.06 m to 0.05 m to 0.045 m and to 0.04 m, the pressure and velocity at the first point changed by less than 2% as shown in table 3-12 and in table 3-13.

No. of Elements	Mesh Size (m)	Velocity (m/s)	Velocity Change %	Pressure (Pa)	Pressure Change %
2768497	0.06	0.684×10^{-2}	1.61%	-2.120×10^{-2}	-1.48%
3737095	0.05	0.684×10^{-2}	1.65%	-2.131×10^{-2}	-0.92%
4498724	0.045	0.662×10^{-2}	-1.53%	-2.179×10^{-2}	1.28%
5565752	0.04	0.673×10^{-2}	--	-2.151×10^{-2}	--

Table 3-12. Mesh convergence study at a point 1 m high and located at 3 m from the room's left wall

No. of Elements	Mesh Size (m)	Velocity (m/s)	Velocity Change %	Pressure (Pa)	Pressure Change %
2768497	0.06	0.502×10^{-2}	-1.89%	-1.627×10^{-5}	-0.36%
3737095	0.05	0.516×10^{-2}	0.83%	-1.612×10^{-5}	-1.33%
4498724	0.045	0.507×10^{-2}	-0.86%	-1.653×10^{-5}	1.22%
5565752	0.04	0.511×10^{-2}	--	-1.633×10^{-5}	--

Table 3-13. Mesh convergence study at a point 6 m high and located at 5 m from the room's left wall

3.4.4 Simulation properties

The simulation in this study is performed assuming the air properties to be constant, corresponding to air temperature at 288 K and air standard pressure at sea level at 101 kPa. The values for the air density and the dynamic viscosity are assumed as follows:

$$\rho = 1.225 \text{ kg/m}^3; \qquad \mu = 1.789 \times 10^{-5} \text{ Pa s};$$

To simulate the buoyancy driven effect, temperature is applied at the windcatchers outlet in the part above the roof. A fixed value of 350 K has been applied as shown in figure 3 on the front surface (A) and on the bottom of the outlet (B). The applied temperature is estimated to be due to solar heated elements with high heat storage capacity.

Gravity is selected for the body forces in the y direction only, the boussinesq approximation is applied with a reference temperature of 300 K and the volumetric coefficient of thermal expansion $\alpha_v = 0.003$ 1/K [54]. The thermal parameters used are the specific heat C_p and the thermal conductivity K_t as follows:

$$C_p = 1006 \text{ J/(kg K)}; \qquad K_t = 0.0242 \text{ W/(m K)}$$

For defining turbulent flow the realizable k - ε model is used. The k – ε model is robust and stable and it is considered the default modeling option for handling turbulent flow in many commercial codes. The flow is turbulent as Reynolds number Re estimated at the chimney`s exit for one condition corresponding for an inlet velocity of 3 m/s is approximately 80000. The turbulence intensity at the flow domain's inlet has been assumed as 5%, and the turbulent viscosity ratio as 10. As the turbulence intensity changed from 5% to 2% and 1% the results of the average velocity only differed by less than 1% which indicates that turbulence intensity imposed at the flow domain's inlet did not have a significant effect. The applied temperatures are estimated to be due to solar heated elements with high heat storage capacity [23]. The orientation of these surfaces A and B is assumed to be to the west where the sun is at its maximum during summer and especially low in the afternoon. The other walls of the windcatcher are assumed to be transparent (example glass cover) and thus the solar radiation would penetrate them and accordingly heat up the surfaces (A and B) where the temperatures are applied.
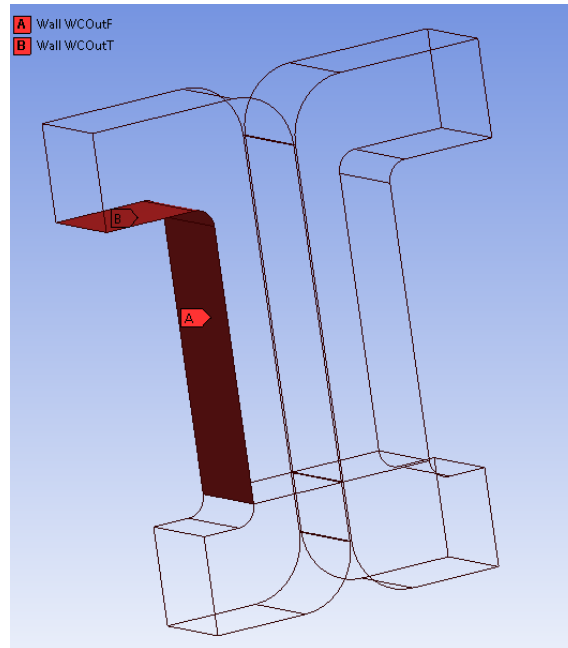
Figure 3-50 Temperature locations at the windcatchers outlet applied on the bottom and front surfaces.

In all the simulations the SIMPLE scheme and the second order spatial discretization have been used. The convergence criteria is 0.0001.

The total flow rate inside the room is investigated in each of the following cases:

1. Winddriven ventilation alone
2. Combined winddriven and buoyancy driven ventilation with a temperature of 350 K and 400 K applied respectively to the windcatchers outlet wall in the locations shown in figure 3-50.

The total air volumetric flow rate (m^3/s) is obtained for the above two cases at different wind speeds applied at the domains inlet which varied from 0 m/s up to 3 m/s, refer to figure 3-49 for the location of the domain's inlet.

Eight different wind speeds have been applied respectively as follows: 0, 0.25 m/s, 0.5 m/s, 0.75 m/s, 1 m/s, 1.5 m/s, 2 m/s, 2.5 m/s and 3 m/s and the results compared.

3.4.5 Results and discussion

The results are viewed using Ansys CFD-Post [54] after simulation is run by Ansys Fluent. The maximum number of iterations is set to 50000 and the convergence criteria to 0.0001. The results are compared based on the total air flow rate obtained from different wind speeds.

3.4.5.1 Results with zero wind speed applied at the domains inlet

With zero velocity applied at the surrounding domain's inlet and a temperature of 350 K at the windcatchers outlet wall, 0.02513 m^3/s of air has entered the room. Figure 3-51 shows the contours of velocity magnitude for this case, it shows the effect of the buoyancy driven ventilation caused by the applied temperature. Winddriven ventilation only with zero velocity inlet speed has provided zero flow rate. With 400 K applied at the windcatchers outlet 0.02776 m^3/s of air entered the room.
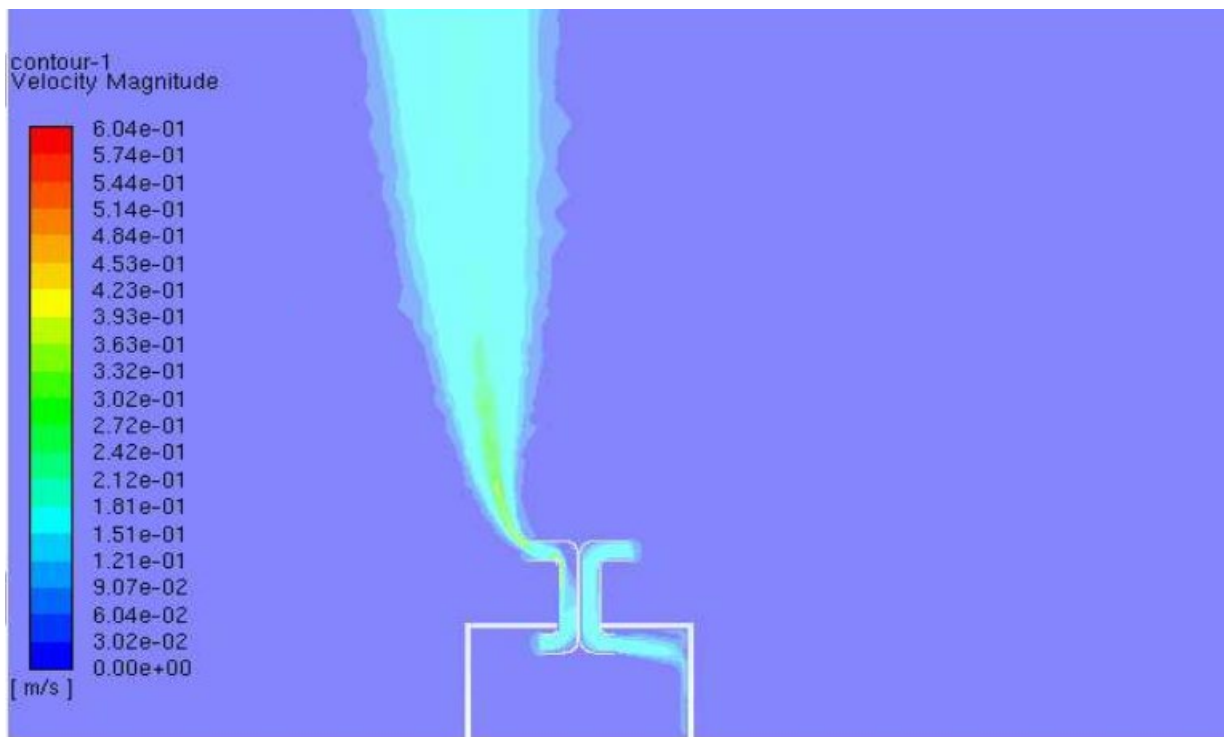
Figure 3-51. Velocity magnitude representation of the room, windcatcher and surrounding with zero wind speed at the domain's inlet

3.4.5.2 Results with 0.25 m/s wind speed applied at the domains inlet

With a wind speed of 0.25 m/s applied at the surrounding inlet the wind driven ventilation has provided 0.02772 m³/s of air into the room through the windcatcher while the combined wind driven and buoyancy driven ventilation with a temperature of 350 K applied at the windcatchers outlet has provided 0.03414 m³/s. The combined solar windcatcher has provided an increase of 23.16 % of total air flow rate. Figure 3-52 shows the contours of velocity magnitude with an inlet wind speed of 0.25 m/s. It is zoomed close to the room and windcatcher for better presentation. With 400 K applied at the windcatchers outlet 0.03864 m³/s of air entered the room which provides an increase of 39.39% compared the winddriven alone.
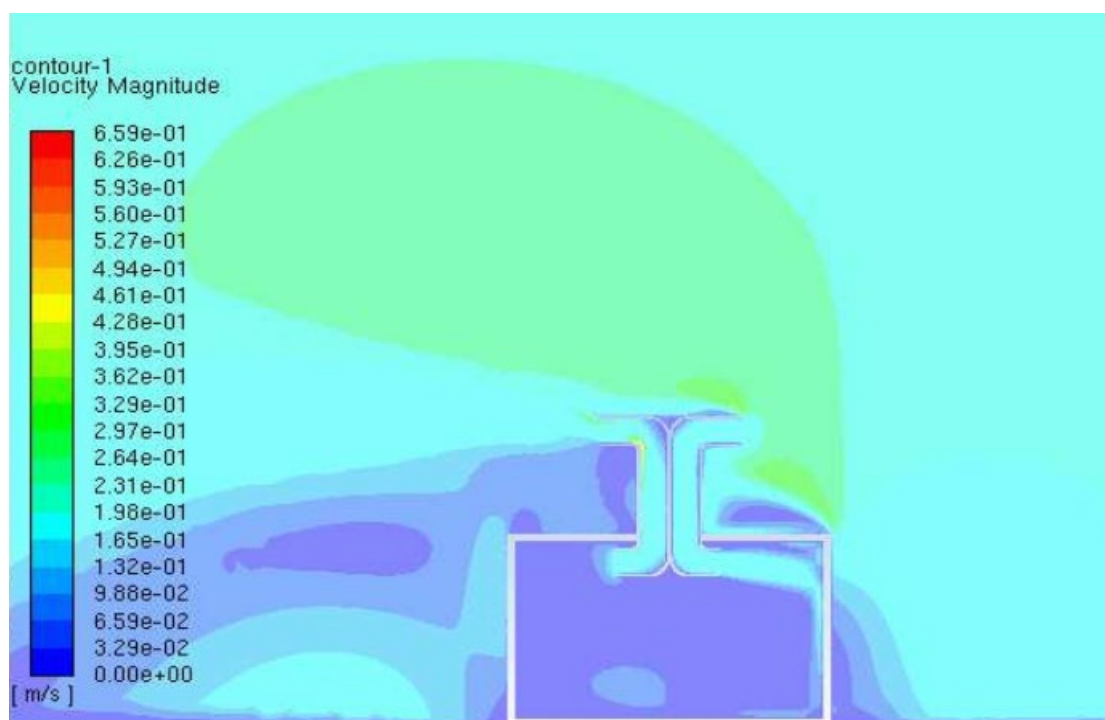
Figure 3-52. Velocity magnitude representation of the room and windcatcher with 0.25 m/s wind speed at the domain's inlet

3.4.5.3 Results with 0.5 m/s wind speed applied at the domains inlet

With a wind speed of 0.5 m/s applied at the surrounding inlet the wind driven ventilation has provided 0.059695 m³/s of air into the room through the windcatcher while the combined wind driven and buoyancy driven ventilation with a temperature of 350 K applied at the windcatchers outlet has provided 0.06427 m³/s. The combined solar windcatcher has provided an increase of 7.66 % of total air flow rate. Figure 3-53 shows the contours of velocity magnitude with an inlet wind speed of 0.5 m/s. it is zoomed closer to the room and windcatcher for better

presentation and it shows higher velocities in the windcatcher as air flow enters and leaves the room. With 400 K applied at the windcatchers outlet 0.06646 m³/s of air entered the room which provides 11.33% increase compared to the winddriven alone.

Figure 3-53. Velocity magnitude representation of the room and windcatcher with 0.5 m/s wind speed at the domain's inlet

3.4.5.4 Results with 0.75 m/s wind speed applied at the domains inlet

With a wind speed of 0.75 m/s applied at the surrounding inlet the wind driven ventilation has provided 0.091411 m³/s of air into the room through the windcatcher while the combined wind driven and buoyancy driven ventilation with a temperature of 350 K applied at the windcatchers outlet has provided 0.09484 m³/s. The combined solar windcatcher has provided an increase of 3.75 % of total air flow rate. With 400 K applied at the windcatchers outlet 0.09829 m³/s of air entered the room.

It is noted that as the inlet wind speed increased the effect of the combined solar windcatcher with applied temperature of both 350 K and 400 K decreased. As the inlet velocity increased from 0.25 m/s to 0.5 m/s and to 0.75 m/s the percentage increase dropped from 23.16% to 7.66% and to 3.75% with T = 350 K, and the percentage increase dropped from 39.39% to 11.33% and to 7.53% with T = 400 K.

3.4.5.5 Results with 2 m/s wind speed applied at the domains inlet

With a wind speed of 2 m/s applied at the surrounding inlet the wind driven ventilation has provided 0.24731 m^3/s of air into the room through the windcatcher while the combined wind driven and buoyancy driven ventilation with a temperature of 350 K applied at the windcatchers outlet has provided 0.2486 m^3/s. The combined solar windcatcher has provided an increase of only 0.4% of total air flow rate. Figure 3-54 shows the contours of velocity magnitude with an inlet wind speed of 2 m/s. With a temperature of 400 K and wind speed of 2 m/s, 0.24916 m^3/s of air entered the room and provided an increase of 0.75 % compared to wind driven alone.
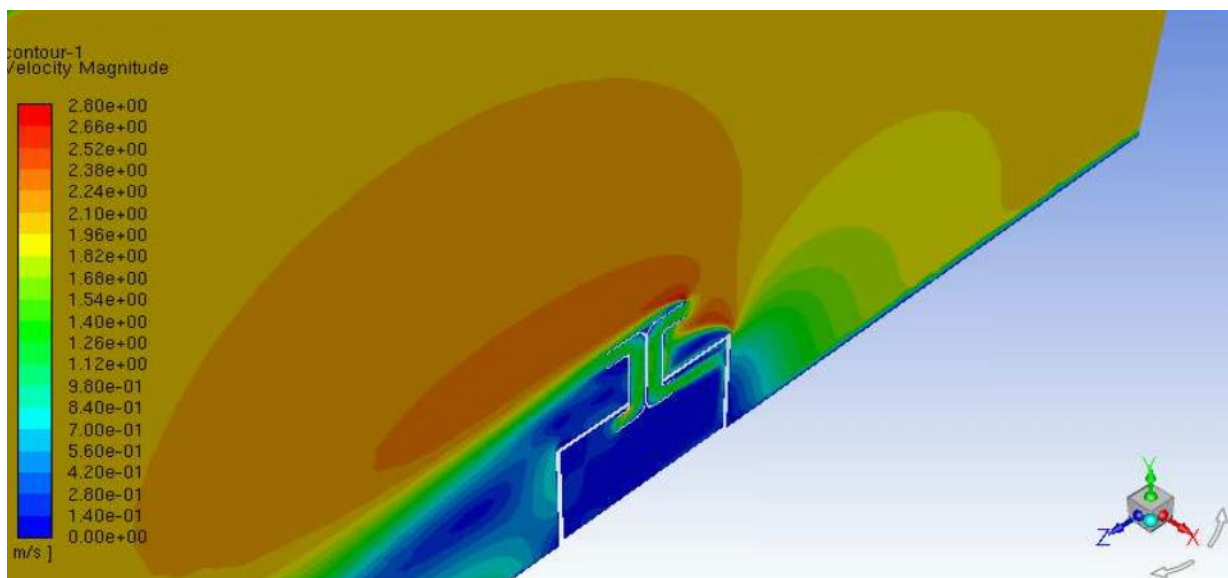
Figure 3-54. Velocity magnitude representation of the room and windcatcher with 2 m/s wind speed at the domain's inlet

3.4.5.6 Summarized results with the applied wind speed at the domains inlet

Table 3-14 shows the summarized results with the different inlet velocities ranging from 0 up to 3 m/s. As the wind speed increases the percentage increase between the combined solar windcatcher and the winddriven windcatcher has dropped significantly.

With a wind speed of 2.5 m/s applied at the surrounding inlet the wind driven ventilation has provided 0.30978 m^3/s of air into the room through the windcatcher while the combined wind driven and buoyancy driven ventilation with a temperature of 350 K applied at the windcatchers

outlet has provided 0.31079 m^3/s. The combined solar windcatcher has provided an increase of only 0.33% of total air flow rate only. With a temperature of 400 K at the windcatchers outlet the percentage increase was 0.52% which is also insignificant.

Similar results were observed when the wind speed is 3 m/s which provided 0.37287 m^3/s air into the room while 0.37348 m^3/s entered when 350 K is applied at the windcatcher's outlet providing an increase of only 0.16 %. With a temperature of 400 K, 0.37402 m^3/s air entered the room providing an increase of only 0.31% increase compared with the winddriven ventilation alone [23].

Inlet Velocity m/s	Air Flow Rate (m^3/s)			% increase	
	wind driven	combined with T = 350 K	combined with T = 400 K	T = 350 K w.r.t winddriven	T = 400 K w.r.t winddriven
0	0	0.0215	0.0277	100.00%	100.00%
0.25	0.0277	0.0341	0.0386	18.80%	39.39%
0.5	0.0596	0.0642	0.0664	7.12%	11.33%
0.75	0.0914	0.0948	0.0982	3.62%	7.53%
1	0.1239	0.1250	0.1271	0.95%	2.62%
1.5	0.1845	0.1857	0.1867	0.63%	1.15%
2	0.2473	0.248	0.2491	0.40%	0.75%
2.5	0.3097	0.3107	0.3114	0.32%	0.52%
3	0.3728	0.3734	0.3740	0.16%	0.31%

Table 3-14. Air flow rate and % increase through the windcatcher for winddriven only and for combined solar windcatcher at different wind speeds

Different wind speeds between 0 up to 3 m/s are applied and the total air flow rate through the windcatcher is investigated with and without temperatures of 350 K and 400 K applied at the windcatcher's outlet wall. As the wind speed increased the efficiency of the solar windcatcher decreased. The combined solar windcatcher provides the highest increase in flow rate of 18.18 % when wind speed is 0.25m/s, this percentage drops till about 1% when the wind speed is 1m/s and drops to about 0.33% as the wind speed increases to 2.5 m/s. Figure 3-55 shows the differences in the air flow rate as the wind speeds increase.

This seems to indicate that as the wind speed increases the winddriven ventilation dominates the flow and reduces the effect of the buoyancy forces. The combined solar windcatcher is useful however when the wind speeds are lower than 1 m/s.
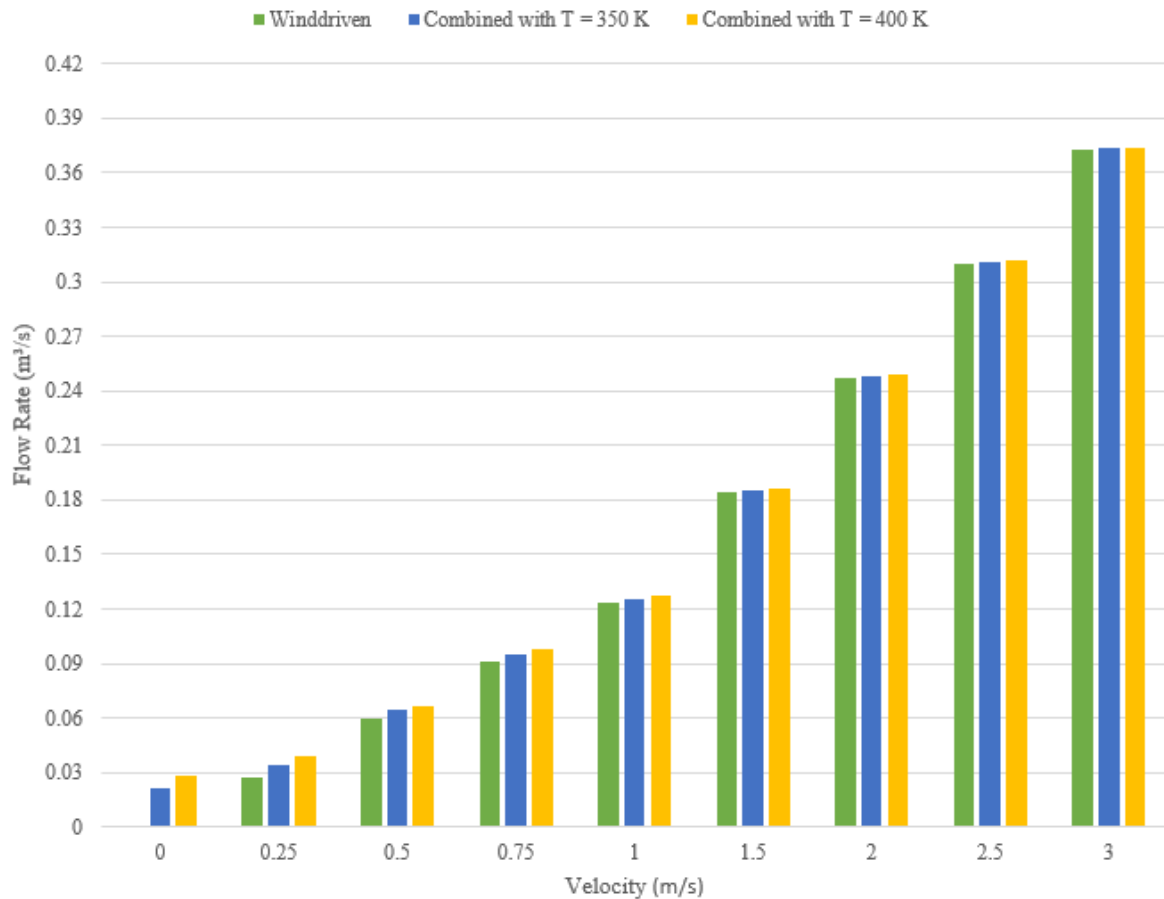
Figure 3-55. Air flow rate through the windcatcher for winddriven only and for combined solar windcatcher with temperature of 350 K and 400 K at different wind speeds

3.4.6 Conclusions

Computation of average air flow rate through a three dimensional room fitted with a windcatcher have been conducted. Cases for winddriven ventilation and for a combined winddriven and buoyancy driven ventilation have been simulated using Ansys Fluent. Temperature of 350 K and 400 K are applied at the windcatchers outlet to simulate the buoyant effect, and different wind speeds between 0 up to 3 m/s are applied.

The combined solar windcatcher provided the highest increase in flow rate of 18.80 % when wind speed is 0.25m/s, this percentage drops till about 1% when the wind speed is 1m/s and to about 0.33% as the wind speed increases to 2.5 m/s. At 3 m/s wind speed the differences are almost negligible.

This indicates that as the wind speed increases the winddriven ventilation dominates the flow and reduces the effect of the buoyancy forces. The combined solar windcatcher is useful however when the wind speeds are lower than 1 m/s.

Chapter 4 The effect of green walls on ventilation and on thermal comfort

4.1 Evaluation of air flow through an active green wall biofilter

4.1.1 Introduction

Active green walls represent an emerging technology for the removal of pollutants present in air streams, with many conventional analyses yet to be applied to these systems [49]. Currently there is a gap in knowledge for this rapidly expanding technology, and it is clear that a uniform and standardized approach to characterizing key parameters is required for accurate performance evaluation. This, in practice, may be difficult to achieve, with the existing green wall systems having differing structures and thus differing air flow distributions, with air either flowing through the filtration media of the system and into ducting before return to the environment, or the reverse [50], and a vast diversity in designs, substrate types and thicknesses, moisture levels and pressure drop characteristics. Thus, we present a novel method for the characterization of air flow distribution and hence the filtration efficiency through a green wall module. Experimental work was conducted including measuring the air flow rate and pressure change across the module [40, 42, 140]. To achieve this, it was essential to design an experimental set-up capable of measuring the very low airflow rate passing through the module, especially when such low through-flow is part of a much larger total flow that includes strong flow reversal occurring in the inlet air-duct and thus not passing through the filtration media. The current work thus provides an initial study directed at optimizing the airflow characteristics of our test system [42].

4.1.2 Active green wall biofilter design

The green wall modules tested (Figure 1) were composed of a rectangular plastic box (500 mm x 500 mm x 130 mm) holding a permeable polyethylene bag containing a plant-growing medium composed of coarse (~25 mm particle size) coconut husks and fibre. The front face of the module has 16 openings for plants, which protrude out from the bag inside. Plant roots are imbedded within the medium. The plant used in this work was *Chlorophytum comosum* 'variegatum' shown in Figure 4-1. Green walls containing this species have previously performed well for PM, VOC and CO_2 removal [33, 107]. A mechanical fan shown in figure 4-2 (constant-speed FANTECH TEF-100 16-W in-line axial fan) positioned at a central opening on the module's back-face, drives air through the medium and root system and then outward through the plants' canopy; all of which have functional value in removing both gaseous and particulate pollutants from the air. Drip-irrigation water was dispensed from a tube running along the open top-face of the module, with the excess drained through multiple small drainage holes on its bottom face. All front and rear ventilation openings are circular with diameter 100 mm. Figure 4-1 shows a test green wall module.

Figure 4-1. Green wall modules with plant species, *Schefflera arboricola* on the left and *Chlorophytum comosum* 'variegatum', used in this study, on the right.

Figure 4-2. A constant-speed FANTECH TEF-100 16-W in-line axial fan

4.1.3 Performance characterization and experimental design

Because of the very high resistance to air flow produced by the bag and its contents, including both substrate and plant roots, the air velocity exiting from the module's outlets (front, top and bottom) is very small. On the other hand, there was significant flow reversal in the inlet fan-and-duct assembly connected to the back opening; this makes any flow measurement through the back opening not feasible. Similarly, because of strong flow reversal, it was not feasible to simply read off the flow rate against pressure from a manufacturer fan-performance-curve. Thus, so as to increase the air-flow velocity to measurable levels, funnels were used to reduce the diameter of all of the module's outlets.

Acrylic sheets were used to form rectangular-box chambers of 20 mm height at the top and bottom faces of the module; see Figure 4-3. Circular holes of size similar to the front-face

openings' were cut out on the chambers' outer face and funnels also fitted to these holes for air-velocity measurement. Three holes were cut in the top-face chamber and one hole at the bottom-face. Thus air exited from the module via 20 openings, and identical funnels were fitted to all openings for airflow measurement. The module with its funnels in place is shown in Figure 4-3. Two sets of funnels with exit-opening (smaller) diameters of 17.8 mm and 14.5 mm were used separately. The funnels' larger openings are slightly larger than 100 mm in diameter, thus totally covering the modules' 100 mm-diameter openings. The velocity of the air was thus increased by 32 and 48 times respectively, as it moved from the modules' outlet openings to the funnels' exit.

A Cole Parmer hot-wire thermo-anemometer was used to measure the air velocity and temperature. This device had a telescopic probe with a maximum length of 95 cm including its sensing head. The measurement of air velocity was in the range of 0.01 to 20 m/s with an accuracy of ±1% at full scale. During measurements, the probe was securely placed normal to the air-flow direction, approximately 2 cm from the funnel exit (see Figure 4-3), after verification that readings fluctuated by less than 6% as the distance between the probe and the funnel exit was varied from 0.5 – 3 cm, and over a period of several minutes. The hot-wire velocity probe can be seen in Figure 4-3 at the black right end of the silver horizontal shaft; the handle itself is mounted on a vertical post seen at the left of the module. The thermo-anemometer's accuracy was verified for low speeds using a rotating circular disk driven by a motor with variable speeds. The probe was placed on the rim of the disk and the speed recorded by the anemometer was compared to the disk's rotational speed. The difference between the readings was less than 5% [42]. Figure 4-4 [40] shows the assembled hotwire anemometer, and its general specifications are listed in table 4-1.

Figure 4-3. Green wall module with funnels attached (16 covering the front openings, 3 on top and 1 at bottom).

Figure 4-4. Hot wire anemometer used to measure air velocity.

Circuit	Custom one-chip of microprocessor LSI circuit	
Display	LCD size: 58mm×34mm	
Sampling Time of Data Logger	2 sec to 8 hour 59 min. 59 sec@ Auto data logger	
Sensor Structure	Air velocity and Air flow: Tiny glass bead thermistor	
Data Output	RS 232 PC serial interface	
Dimension	Main instrument: 203×76×38 mm Telescope Probe: Round, 12mm Dia×280 mm (min Length) Round, 12mm Dia×940 mm (min Length)	
Measurement unit	Air Velocity	Range:0.01 to 20 m/s Resolution: 0.01 m/s Accuracy:±(5%+0.01) reading or ±(1%+0.01) full scale
	Air Flow	Range: 0 to 36,000 m^3/min Resolution: 0.001-1 Area: 0.001-30 m^3/min

Table 4-1. General specifications of hot wire anemometer

Pressure difference was measured using a Sensirion digital-sensor SDP610 – 125 Pa, shown in figure 4-5 [40]. This instrument is 0.1 Pa accurate for low air-pressure difference up to 125 Pa. Values were recorded every second and the average value was calculated from a data logger. All pressure (gauge) readings were taken at the module's back-opening. Figure 4-3 shows the inline fan used and the location of the sensor connected to the computer as well as to a probe between the fan and the module.
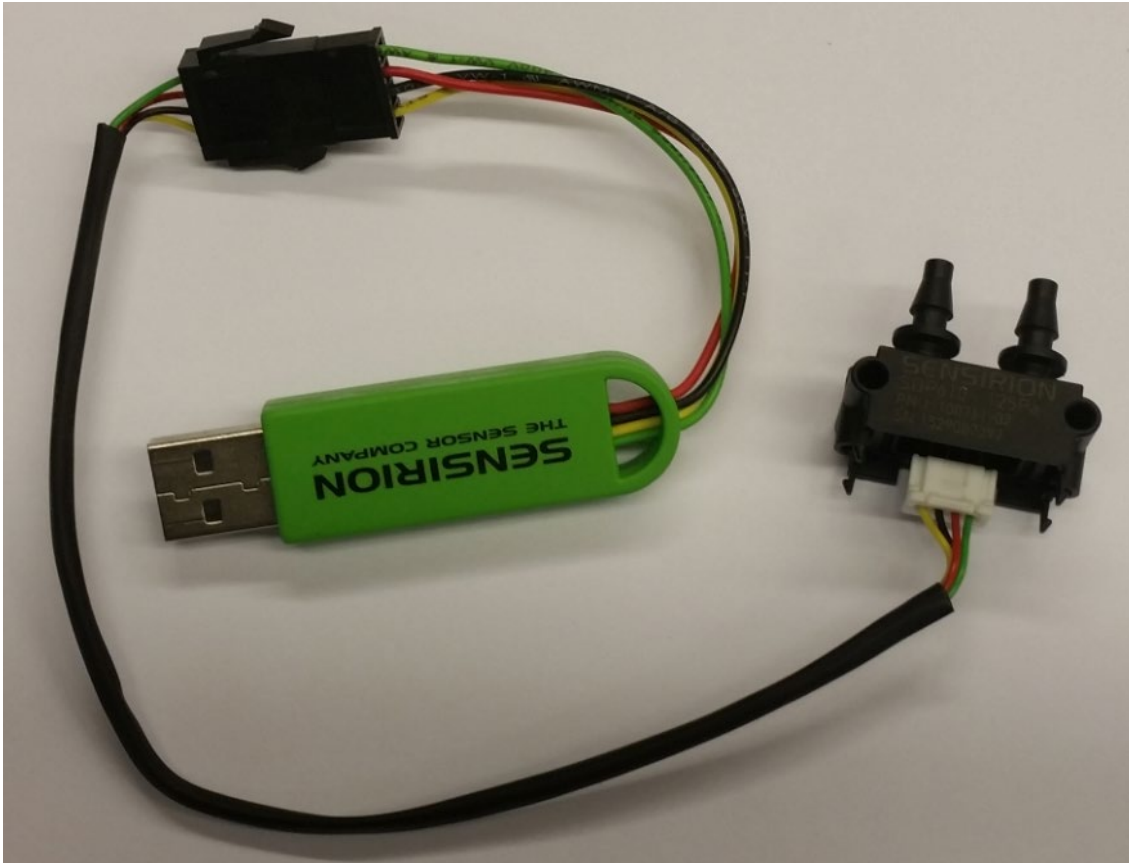
Figure 4-5. Sensirion digital-sensor SDP610 – 125Pa

A closed-loop wind-tunnel was used for verifying the readings of the pressure-differential sensor. The sensor was connected in parallel with an inclined manometer which gives the pressure difference from a Pitot-static tube placed in a wind tunnel. Measurements were recorded at 9 different speeds of the wind-tunnel motor. An excellent linear relationship was obtained between readings from the digital pressure-sensor and the inclined manometer (Figure 4-6).
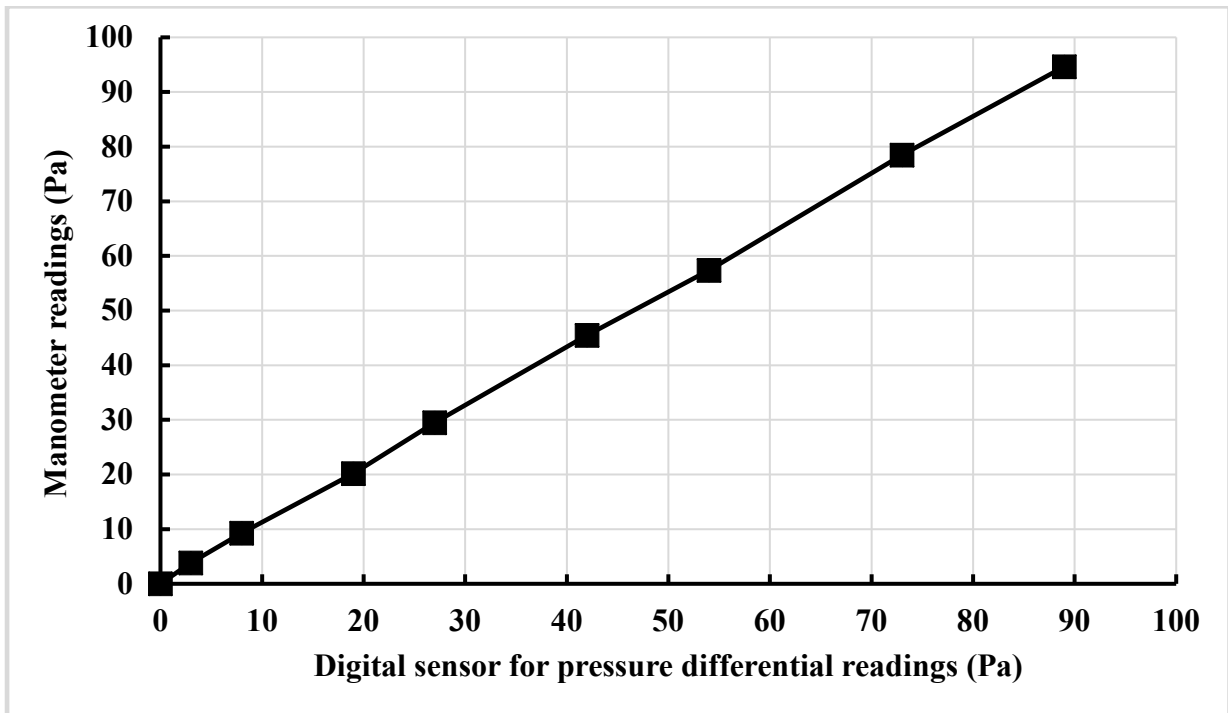
Figure 4-6. Digital-Pressure-Sensor Verification.

To identify the different openings, they were numbered as shown in Figure 4-7, with the letter T denoting top, B for bottom, F for front and A, B, C, D for the 4 rows. Thus, for example, FC2 indicates the 2nd opening on row C (3rd row) on the front face.
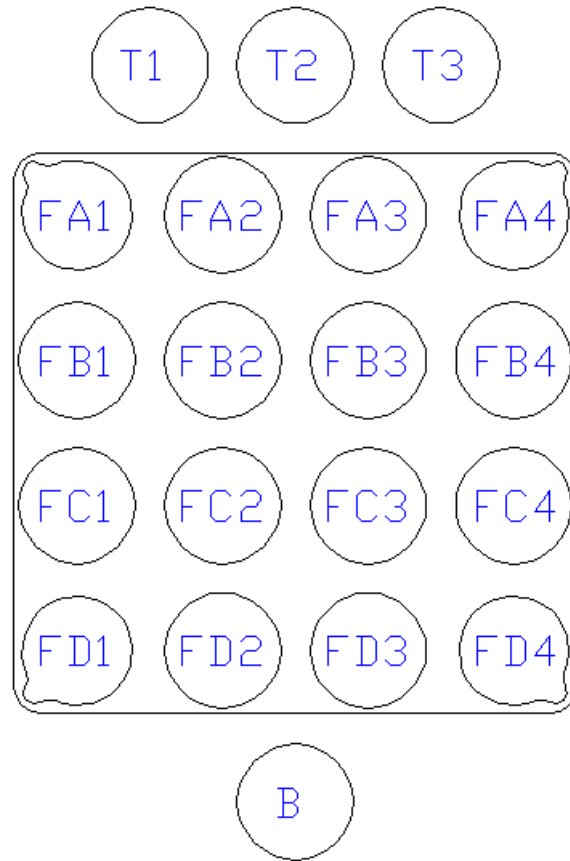
Figure 4-7. Nomenclature used to identify the different module openings.

In order to further understand the relationship between pressure and total air-flow rate through the module, some exit openings were blocked, thereby increasing flow resistance. Thus Table 4-2 shows 6 patterns of blocking, involving 6, 10, 12, and 14 openings. The different patterns of blocking some openings while leaving others open also facilitates identification of the airflow distribution among the openings.

Patterns	Blocked Funnels	Number of Blocked Openings
1	T2, FA2, FB4, FC3, FD(1,4)	6
2	T2, FA(2,4), FB(1,4), FC(1,3), FD(1,4), B	10
3	T2, FA(1,2,4), FB(1,4), FC(1,3), FD(1,2,4), B	12
4	T(1,2,3), FA(2,4), FB(1,4), FC(1,3), FD(1,4), B	12
5	T(1,2,3), FA(1,2,4), FB(1,4), FC(1,3), FD(1,2,4),	14
6	T(1,2,3), FA(1,3,4), FB(2,4), FC(1,3,4), FD(1,4),	14

Table 4-2. Blocked funnel patterns.

VOC and PM are both reduced by processes associated with the plant-growing medium [105, 111] while the removal of other inorganic contaminants appear to be mostly plant mediated [141], taken up directly through the plant's stomates or leaf surfaces [69]. To maximize the capacity of VOC and PM bio-filtration , there is thus a need to pass as large a volume of contaminated air as possible through the plant-growing medium, by reducing the percentage of air that exits through the module's open top face (a feature common to most green wall systems to allow for irrigation and fertilization), thus going only partially through the substrate and not at all through the plant canopy. Therefore, attaching a cover to the top face of the module achieved a more effective flow rate and distribution. The top cover used included 10 mm diameter holes to allow for irrigation. The top cover design and dimensions are shown in Figure 4-8 [40, 42].

Different numbers of holes in different patterns were tested (Figure 4-8). The top covers were made from laser-cut 10 mm acrylic sheets bent at their center to produce a V-shape to help drain irrigation water.
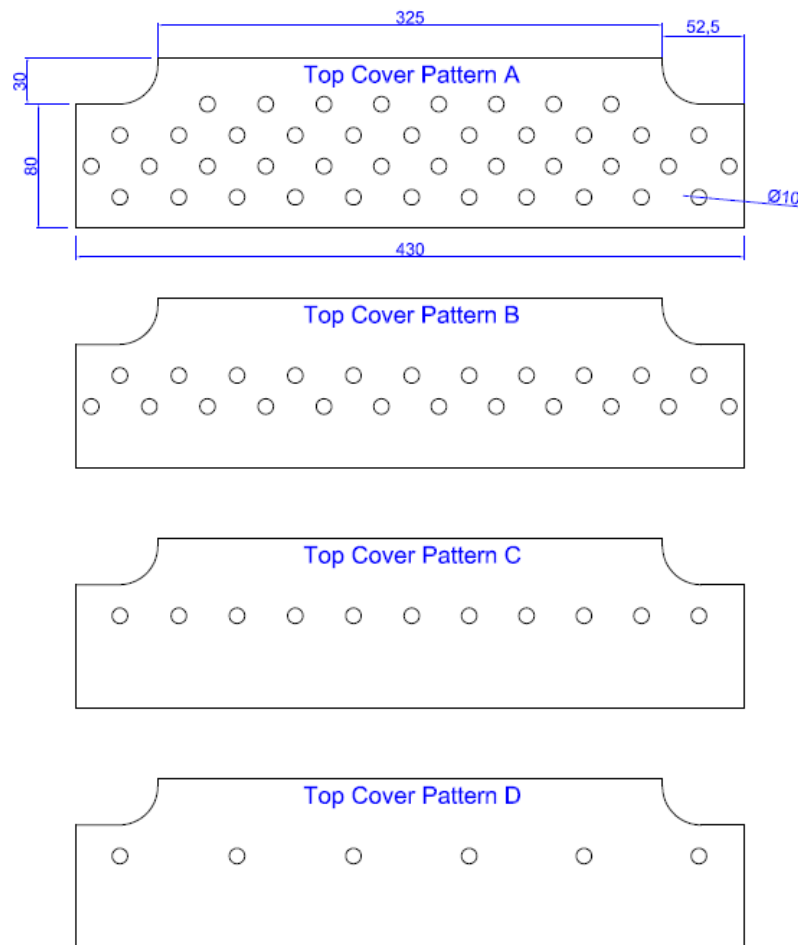
Figure 4-8. Top cover patterns. Dimensions are in mm

4.1.4 Data analysis and calculation hypothesis

When air exits the module, whether funnels were used or not, it returns directly to ambient. Thus pressure readings at the module's rear opening (air inlet) are equal to the pressure difference across the module. Recordings of pressure drop were recorded over several minutes, until a stable value was obtained whereby readings were within a 10% range.

In the following, all pressure (gauge) readings were taken at the module's back-opening. To determine the total air-flow rate Q_{Free} across the module the following measurements were taken: P_{Free}, P_{F-L} , P_{F-S} , Q_{F-L}, and Q_{F-S} (refer to nomenclature for the parameters definition and units). The Q_{Free} was thus obtained as follows [42, 140]:

When measurements were taken with the large funnels covering the green wall outlet openings, the following approximate energy relation is used [142]:

$$P_{F-L} = C \ (\ K_S + K_{F-L} \ )(\ Q_{F-L} \ )^2 \qquad\qquad \text{Eq. (4-1)}$$

Similarly, with small funnels covering the module's openings:

$$P_{F-S} = C \ (\ K_S + K_{F-S} \ )(\ Q_{F-S} \ )^2 \qquad\qquad \text{Eq. (4-2)}$$

Thus for free openings, when no funnels were used on the module outlet openings:

$$P_{Free} = C \ (\ K_S \ )(\ Q_{Free} \ )^2 \qquad\qquad \text{Eq. (4-3)}$$

However, when airflow is restricted through a narrow orifice, the loss coefficient (K) decreases with the outlet area ratio (A_{Small} / A_{Large}) or the square of the outlet diameter ratio (D_{Small} / D_{Large})^2 [82]. Here D_{Large} is the module-opening diameter (100 mm) and D_{Small} the funnel's exit diameter [142].

Assuming the decreasing relationship between K and $(D_{Small})^2$ to be $K = B / (D_{Small})^2$, then

$$K_{F-L} = B / (D_{F-L})^2 \text{ and similarly, } K_{F-S} = B / (D_{F-S})^2 \quad \text{Eq. (4-4)}$$

Substituting Eq. (4-4) into Eq. (4-1) and Eq. (4-2), the product of constants C×B can be obtained from measured values of P, Q, and D associated with large funnels and small funnels. Eq. (4-1) or Eq. (4-2) then gives C.K_S. Substituting C.K_S into Eq. (4-3) thus allows Q_{Free} to be calculated from the measured value of P_{Free} [142].

The total air-flow rate through the module and the corresponding pressure difference across it were obtained for the following 4 cases of the content of the module's internal bag:

A) Dry, unplanted: Dry plant-growing medium only, with no plants

B) Wet, unplanted: Plant-growing medium with no plants; watered to saturation (substrate watered to field capacity and allowed to drain for 1 hour)

C) Dry, planted: Dry growing medium, planted with "16 *C. comosum*", grown in a glasshouse for 4 months prior to testing.

D) Wet, planted: Growing medium watered to saturation (as above), planted with "16 *C. comosum*".

Note that the presence of the plants would have precluded the use of the funnels, and therefore the plant canopy was trimmed to substrate level directly before testing; however it was clear that the canopy offered very little resistance to flow, as pressure readings taken at the module's back-opening differed by less than 1% between with-canopy and without-canopy cases.

4.1.5 Measurement of air flow through the active green wall module

Using the calculation procedure above (equations 1 to 4), the total air-flow rate Q_{Free} through the module corresponding to its free openings (without any funnels used) has been obtained, and is shown in Table 4-3. Measured values of P_{Free}, P_{F-L}, P_{F-S}, Q_{F-L} and, Q_{F-S} are also shown in Table 4-3. Figure 4-9 shows the air-flow rate versus pressure difference for the four cases considered.

2 Sets of 20 Funnels	Dry Unplanted		Wet Unplanted		Dry Planted Module		Wet Planted Module	
	Press. Diff. (Pa)	Total Air flow (L/s)	Press. Diff. (Pa)	Total Air flow (L/s)	Press. Diff. (Pa)	Total Air flow (L/s)	Press. Diff. (Pa)	Total Air flow (L/s)
Free	**20.1**	**9.10**	**24.5**	**15.79**	**16.4**	**10.00**	**18.4**	**14.90**
Large	22.2	8.72	26.1	8.60	18.8	9.29	21.3	9.55
Small	23.5	8.61	29.6	7.84	20.3	9.10	25.3	9.02

Table 4-3. Pressure difference and airflow rate for dry and wet planted and unplanted modules.
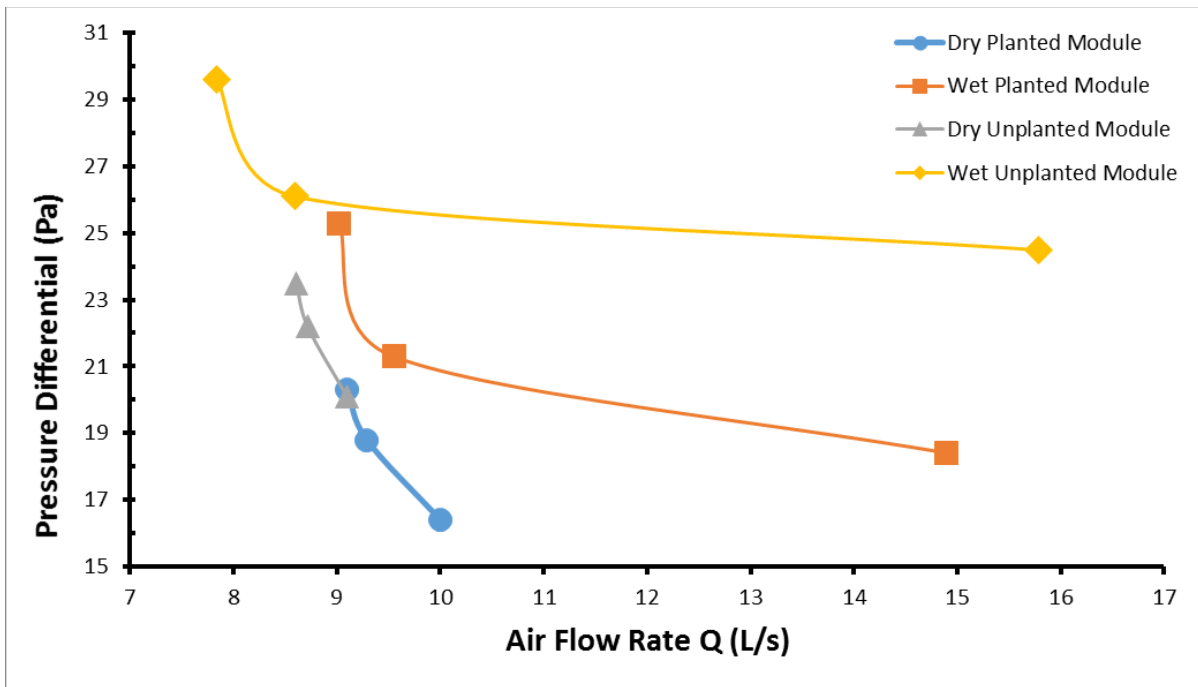
Figure 4-9. Air-flow rate (Q) versus pressure for the four tested cases.

The flow-rate findings are of practical interest. It was observed that a wet module allowed more air flow through than a dry one, both with and without plant roots; and the increase was substantial, at ~ 50% (Table 4-3). This seems to indicate that water may have coalesced the plant-growing medium particles, making them larger but also less numerous, thus resulting in larger pores for air to pass through. Since higher volume of air would pass through the wet substrate and become filtered as compared to a dry substrate, it is noted that wet modules potentially would clean air more effectively than dry ones.

4.1.5.1 Effect of plant roots on air flow through the module

The difference in air-flow rate between unplanted and planted cases was much smaller (5 and 10 % for dry and wet modules respectively), indicating that plant roots probably play minor roles in creating resistance to the air flow through active green walls. This would agree with expectation, since in terms of individual objects that have a boundary-layer region that tends to inhibit air flow, the roots would offer only a small such region due to their much smaller number in comparison with substrate particles [142]. It was also clearly noticed that the canopy of the planted module (trimmed before testing) offered very little resistance to flow, as pressure readings taken at the module's back-opening differed by less than 1% between with-canopy and without-canopy cases [140].

Measurement of back-opening pressure (which essentially is the pressure difference across the module, as discussed above) versus plant type was also taken with the plant-growing medium ("soil") being saturated wet, and the plants fully grown; see Figure 4-10. The first set of data (hollow symbols) corresponding to "raw" readings shows very large variations in the pressure [140]. However, "soil" bags of two different sizes were used; and the higher pressures were associated with bags weighting about 9.5 kg, whereas the lower pressures with bags weighting about 6 kg. In addition, different baffles were used; these are essentially plastic plates (reinforced with ribs on one side for strength) having multiple holes (circular or triangular) of characteristic dimension $1-2$ cm for air to go through; these baffles are used to help with keeping the "soil" bags in place, and to even out the air flow. Because the holes are numerous and large (about 90 for circular holes of diameter about 2 cm, and about 780 for triangular holes of side about 1 cm), resistance to air flow by the baffles can safely be taken to be negligible compared to that of the "soil" bag next to them.

On the other hand, Figure 4-10 also shows the second set of data (filled symbols) of pressure normalized with the weight of the "soil" bag [Pressure / ("Soil"-Bag Weight)] versus plant type. This second data-set indicates very small variations of the normalized pressure among different plant types, here varying only within the narrow range of $3.1-3.3$ Pa/kg . All this thus corroborates well the conjecture above about the small influence of plant roots and plant canopy on the flow resistance; rather, resistance to air flow is essentially due to the plant-growing medium [142].

In figure 4-10 [140, 142], note that Hollow symbols correspond to "raw" Pressure Difference [Pa], whereas filled symbols correspond to Pressure normalized with the weight of the "soil" bag, i.e. [Pressure Difference / ("Soil"-Bag Weight)] in Pa/kg. Pla*nt types are: 1 Epipremnum aureum; 2 Schefflera amate; 3 Chlorophytum Orchidastrum; 4 Schefflera Arboricola; 5 Ficus lyrata; and 6 Chlorophytum comosum variegatum.*
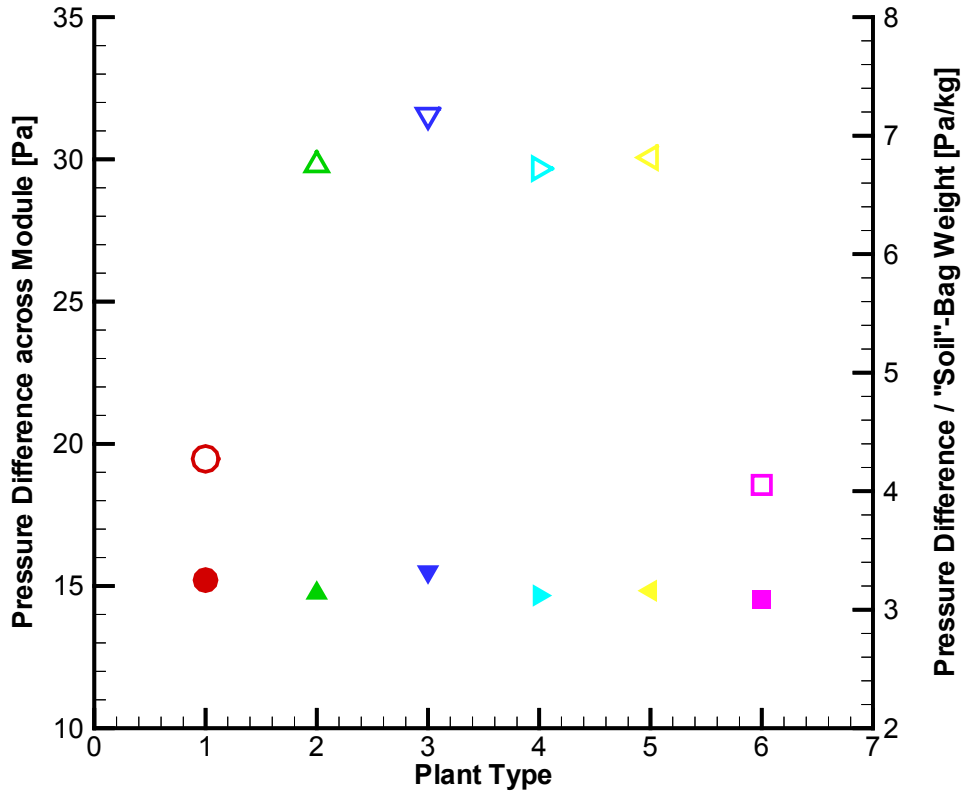
Figure 4-10. Pressure difference across module for different types of plant. Hollow symbols correspond to "raw" Pressure Difference [Pa], whereas filled symbols correspond to Pressure normalized with the weight of the "soil" bag [Pa/kg].

4.1.5.2 Effect of boundary layer on the air flow through the wet versus dry module

A boundary layer region of slow velocity in fact surrounds any solid or liquid particle [82]. Due to this boundary layer surrounding each separate dry plant-growing medium particle, the free area for air flow (porosity) is reduced due to the large number of separate particles [143]. The addition of water would coalesce the large number of separate dry particles into a much smaller number of admittedly larger particles, these larger particles along with their boundary layers could result in a larger net free area for air flow (Figure 4-11) [42, 143].
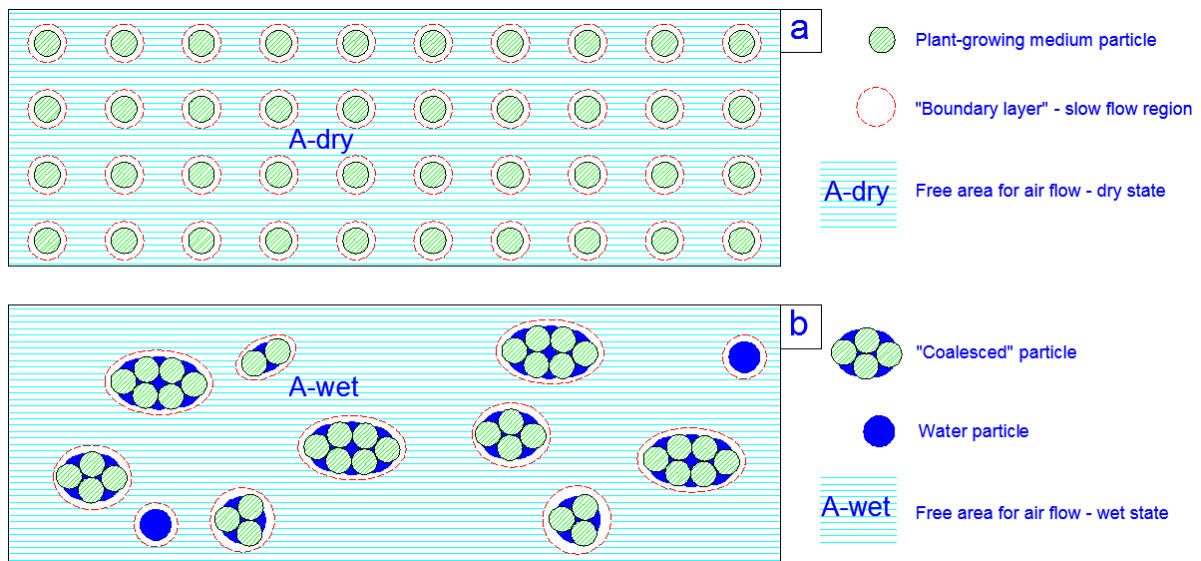
Figure 4-11. Schematic of a) plant-growing medium particles in dry state, b) coalesced particles in wet state

4.1.6 Air flow distribution through the module

Air flow and pressure changes resulting from the different air-distribution (blocked funnel) patterns are shown in Tables 4-4 and 4-5 using large and small funnels respectively. Figure 4-12 shows the air flow rate versus pressure difference for the dry and wet unplanted modules with large and small funnel patterns [40].

Patterns with Large Funnels	DRY Unplanted		WET Unplanted		DRY Planted Module		WET Planted Module	
	Press. Diff. (Pa)	Total Air flow (L/s)	Press. Diff. (Pa)	Total Air flow (L/s)	Press. Diff. (Pa)	Total Air flow (L/s)	Press. Diff. (Pa)	Total Air flow (L/s)
1	24.2	7.92	27.8	8.09	21.8	8.54	23.6	8.73
2	26.3	7.18	29.5	7.42	24.8	8.02	26.0	8.04
3	27.6	6.60	31.0	6.78	27.0	7.23	30.0	7.42
4	28.3	6.53	31.3	6.61	27.2	7.23	30.0	7.37
5	30.3	5.67	33.6	5.89	31.9	6.38	33.9	6.29
6	31.1	5.47	34.2	5.59	31.4	6.38	33.7	6.19

Table 4-4. Air flow versus pressure for dry and wet planted and unplanted module for patterns with blocked large funnels.

Patterns with Small Funnels	DRY Unplanted		WET Unplanted		DRY Planted Module		WET Planted Module	
	Press. Diff. (Pa)	Total Air flow (L/s)	Press. Diff. (Pa)	Total Air flow (L/s)	Press. Diff. (Pa)	Total Air flow (L/s)	Press. Diff. (Pa)	Total Air flow (L/s)
1	27.1	7.99	31.7	7.38	22.8	8.04	28.2	7.99
2	30.4	7.08	34.3	6.34	27.7	6.95	33.3	6.92
3	32.6	6.20	35.5	5.66	30.4	5.94	35.3	5.98
4	33.0	6.27	36.2	5.49	30.4	5.96	36.1	5.98
5	36.0	5.20	38.2	4.64	34.1	4.87	38.7	4.97
6	36.5	5.17	38.8	4.54	33.9	4.88	39.1	4.98

Table 4-5. Air flow versus pressure for dry and wet planted and unplanted module for patterns with blocked small funnels.
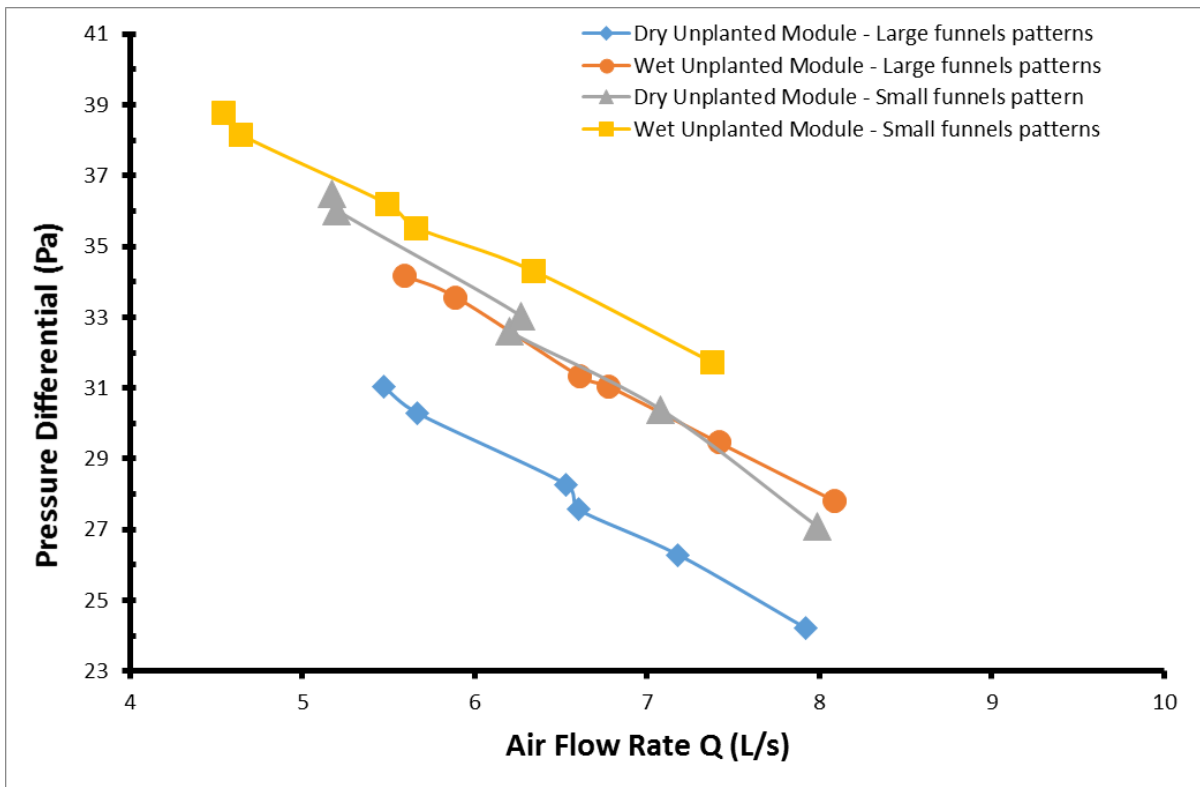
Figure 4-12. Air-flow rate Q versus pressure for dry and wet unplanted modules with large and small funnels

The flow-rate versus pressure (Q-P) relationship (Figures 4-9 and 4-12) in all cases displayed trends agreeing with typical fan performance curves, namely as Q increases, P decreases. It should also be noted that considerable back flow was observed in all cases. Given that the substrates used in the green wall modules were designed primarily for plant health rather than filtration performance, this is not surprising, although it is encouraging that considerable PM filtration could also be obtained [34, 107]. It is clear from the current work that dealing with back flow from biofilter matrices, and the associated energy wastage, would be a valuable area of development for botanical biofilter design.

Changing the locations of blocked openings did not have a major effect on the pressure difference across the module, and hence the total air-flow rate (Tables 4-4 and 4-5). This applied for both planted and unplanted modules and both dry and wet substrates. For both planted and unplanted modules under both dry and wet conditions, 79 % of the total air flow (i.e. the sum of all percentage values shown for the front openings in Figure 8) passed through the front openings, leaving 21% (i.e. the sum of percentage values shown for top and bottom openings in Figure 8) of the air passed through the top and bottom irrigation holes. The second front-face row (FB) recorded the highest percentage at 22.5 % of the total flow, while FA (1st row) and FC (3rd row) recorded approximately 21 % each. The lower front-face row FD recorded 14.5 % of the total flow. The middle front openings FB2, FB3, FC2 and FC3 recorded only slightly higher flow compared to the side front-openings, despite being located just in front of the axial fan. 15.5 % of the total flow passed through the top side of the module, while 5.5 % passed through the bottom opening. These top and bottom flows passed only partly through the substrate, while not passing through the plant canopy at all, and hence received little filtration, thus reducing the overall air cleaning capability of the system. Approximately the same amount of air passed through each of the top openings. Figure 4-13 shows the distribution in percentage of the air-flow rate throughout the different openings of the module.
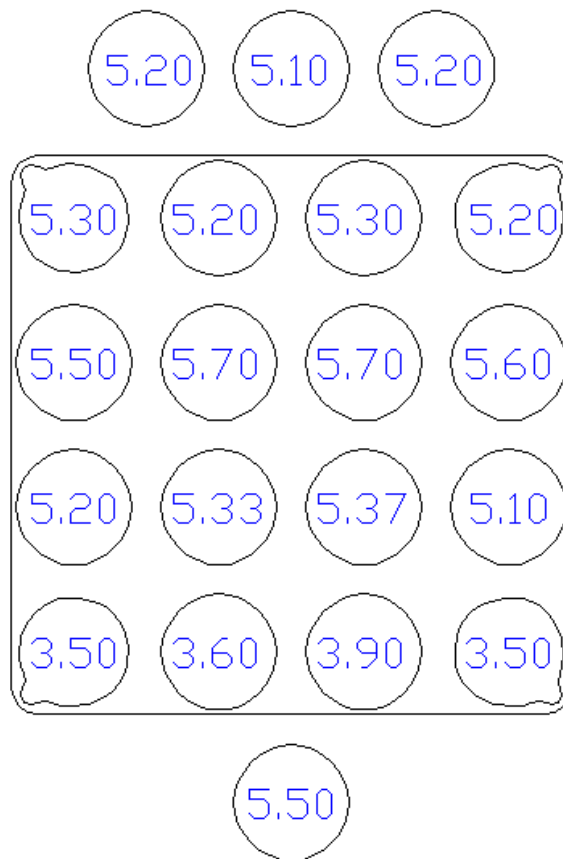
Figure 4-13. Distributions in % of total air-flow rate through the module (without a top cover).

It should be noted that no substantive preferential airflow through the center holes was observed, despite the fact that the fan was located centrally within the rear of the case. This was however not totally unexpected, as the substrate's very high resistance would have dissipated much of the flow momentum and hence removed flow-direction preferences. The medium itself was thus sufficient to distribute air flow relatively evenly across the active component of the filter, negating the requirements for complex baffle systems.

4.1.7 Effect of introducing a top cover to the module

The effect of introducing a top cover to the module was tested on the unplanted module when dry. With the top cover installed, patterns A and B (Figure 4-8) did not show any major change in the percentage of air flow passing through the front face's top row, with an air-flow reduction of only 0.5% recorded with both patterns. Both patterns A and B provided very similar results in terms of pressure differences and flow rate using both large and small funnels. This is

probably due to the large number of holes used in both patterns, thus creating a very low flow resistance relative to the substrate matrix.

Top-cover pattern C provided a reduction in air-flow through the top opening of 2.5%, while pattern D reduced the top flow by 6%, of which 4.5% was added to the top row FA and 0.5% added to each of rows FB, FC and FD.

With pattern D installed, 9.5% of the total flow passed through the top side, distributed evenly among the three openings T1, T2 and T3. 85% of the flow passed through the front side with the highest percentage (25.5%) through FA, 23% through FB, 21.5% through FC and 15% through FD. Only 5.5 % of the flow passed through the bottom opening B. Figure 4-14 shows the air flow distribution with pattern D installed. The higher percentage of air flow through the upper front rows FA and FB compared to the lower front rows FC and FD was due to the gravitational effect which makes the substrate more compact at its lower half, resulting in additional restriction of air flow.
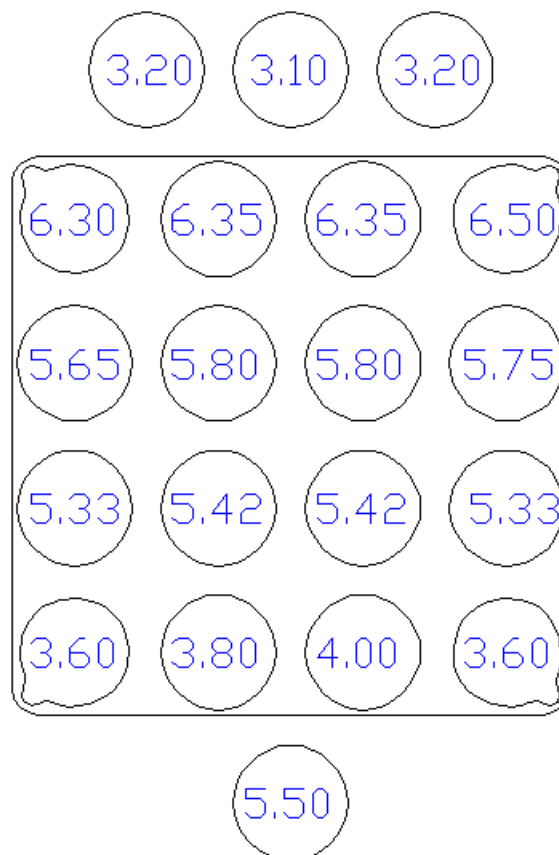
Figure 4-14. Percentage distributions of total air-flow rate through the module with top cover pattern D.

For the module with top cover pattern D installed, the total calculated air-flow rate (Q_{Free}) through the module corresponding to its free openings (i.e. with no funnels used), based on values with large, and small funnels in dry conditions is shown in Table 4-6. The total flow rate with free openings was very close to that for the module without the top cover, indicating that the addition of the cover did not contribute substantial resistance to flow, and thus did not affect the overall total flow rate through the module [42].

Unplanted Module 2 Sets of 20 Funnels	Dry Unplanted Module with Top Cover Pattern D	
	Press. Diff. (Pa)	Total Air flow (L/s)
Free Openings	20.9	9.26
Large Funnels	22.8	7.80
Small Funnels	23.7	7.20

Table 4-6. Summary for Dry Unplanted Module Values with top cover pattern D installed.

4.1.8 Energy consideration

HVAC usage constitutes the greatest energy load in buildings, and between 10 and 20% of the total energy consumption in developed countries [38]. Thus reducing HVAC energy draw is one of the most effective means of improving building sustainability. Whilst the primary function of HVAC is to provide thermal comfort, ventilation requirements (i.e. the mechanical removal of accumulated CO_2) also play a substantial role, which interacts with temperature modulation as incoming air for ventilation will require heating or cooling depending on the indoor–outdoor temperature difference. HVAC systems in large buildings generally also have an air humidification role [38], which will not be considered here. Estimating building HVAC energy use is difficult, and suffers from an uncertainty of ± 25–40% due to the variability in occupant behavior and resulting ventilation requirements [144]. The calculations we have done here account only for ventilation effects: green wall systems are known to provide cooling and humidification of the air passing through them [26, 120], which will contribute further to the performance of the system over the presented findings [143].

In this work, a 16-W inline fan was used for each module with face area of 0.25 m^2 (0.5m × 0.5m). From Table 4-3, an average of approximately 12.5 L/s of air can be forced to flow through the planted module. Thus 1 m^2 of green wall or 4 modules would deliver 50 L/s of

treated air using 64 W of fan power. Assuming 8 hours for a working day, 5 working days per week, and 48 working weeks per year, the energy usage for 1 m^2 of green wall would be 123 kWh per year [143].

The US regulation for minimum ventilation rates in office space occupied at a density of 10 m^2 per person is 5.5 L/s per person fresh air as described in the ASHRAE 2010 standard [137]. Thus 1 m^2 of the tested green wall modules could deliver air to approximately 9 persons, who would require 90 m^2 of office floor area. Lam et al. (2004) [145] estimate building electrical usage for office buildings in Hong Kong at 270 kWh/m^2 per year, with 47.5% or 128 kWh/m^2 used for HVAC. At this energy usage, 11520 kWh per year would be required from a centralized HVAC system for a 90 m^2 office occupied by 9 persons, while only 123 kWh per year is required by 1 m^2 of green wall to treat the air and thus improve the indoor air quality (IAQ) [143].

On the other hand, plant efficiency at ameliorating respiratory CO_2 emissions has been modelled previously [103, 106]. Irga et al. (2013) [103] estimated that an average human exhales 34.5 g CO_2.h^{-1}. Based on this estimate, a 1 m^2 green wall containing *Chlorophytum* at 250 μmol.m^{-2}.s^{-1} (light intensity) with the fans running would be capable of removing ~16% (5.5 g/h) of the respiratory CO_2 from a single occupant. If an office is occupied for only 8 working hours per day, the total CO_2 exhaled daily by one person is 276 g, and if the green wall module fans run for 24 hours per day 1 m^2 of green wall would remove 132 g of CO_2. Therefore to remove 100% of a person's daily CO_2 emission, 2.1 m^2 of green wall is needed which would require 9 of our tested modules consuming a total of 144 W fan power. The energy usage for 9 modules operating 24 hours per day, for 5 days per week and 48 weeks per year would be 829 kWh per year, while the HVAC energy requirement for a 10m^2 of office area for one person would be about 1280 kWh per year based on the estimate of Lam et al [145]. It is noted that above calculations take only the CO_2 removal into account, however the same air flow passing through the green wall modules would also contribute to the removal of pollutants such as VOCs and PMs.

While it is recognized that in addition to maintaining adequate IAQ through ventilation with filtration, a major role for HVAC is to provide thermal comfort, whereas this work concerns mainly with IAQ only, nevertheless the two figures 829 kWh per year for green walls and 1280 kWh per year for HVAC point to a potential for significant energy saving when green walls are used for providing good IAQ for office buildings [143]. Figure 4-15 shows a section of a green

wall made up of the same modules tested, installed in the Faculty of Engineering and Information Technology at The University of Technology Sydney.

Figure 4-15. In situ vertical green wall comprised of modules tested in the current study

4.1.9 Conclusion

If active green walls are to be used as air cleaning devices, the airflow through these systems must be maximized so as to provide maximized air cleaning efficiency, with minimal energy wastage. The primary observations of the current work are that more air will pass through a typical green wall substrate [42], and hence become cleansed, when the substrate is saturated with water than when it is dry. The increase was substantial at approximately 50% more with 14.9 L/s total air flow rate passing through the wet planted module versus 10 L/s when dry. Thus effective irrigation and maintenance will become a key part of botanical biofilter usage. Plant roots themselves, on the other hand, play minor roles in creating resistance to the air flow [42], indicating that root morphology may not be of prime importance in plant selection, allowing other criteria to be used, such as pollution tolerance, low maintenance or longevity, low watering needs for eco-efficiency, or pollutant removal effects. Airflow distribution within the system tested was reasonably even, despite the absence of a complex

baffle system in the green wall air intake plenum, indicating that plenum design can be simplified, potentially reducing system cost both through cheaper design and back pressure reduction [42].

Reducing the 15.5 % of polluted air that bypasses the substrate and plant canopy in green walls will clearly improve their filtration performance. Adding a top cover to the module having six 10 mm diameter holes for irrigation decreased the air flow through the top (and thus returning to atmosphere with much less filtration) by 6 %, and directed it instead through the filter improving the system's capacity for VOC and PM biofiltration by increasing the percentage of air flow passing through the front openings from 79% to 85 %. The top cover's presence had little effect on the total air-flow rate through the module, and the pressure drop across it.

4.2 Effect of fan speeds on air flow through an active green wall biofilter

4.2.1 Introduction

Breathing walls may play a role in cleaning up polluted cities, as the filtered air will effectively contain lower concentrations of pollutants and particulate matter than the ambient, untreated outdoor air [146]. However, before these systems can be widely distributed in cities, it is necessary to determine the optimal operating conditions of the mechanical component of the systems, to ensure that the energy used does not subsume the predicted benefits gained.

The aim of this study is to evaluate the air flow through a plant-based active green wall module, and to investigate the effect of fan speeds [41] on the total air flow rate through the green wall module and on its distribution, in order to optimize the energy consumption of the fans whilst maintaining the modules' biofiltration efficiency. Pressure drop and air flow rate through green wall modules have been obtained previously in section 4.1 [42, 140], and the air-flow distribution has also been preliminarily investigated in section 4.1 [40, 42]. The current experimental work aimed to improve the design of the module and achieve more appropriate flow rate and flow distribution. To achieve this it was essential to design a novel set up to measure the air flow rate exiting the module. Due to the very low velocity of the air flow passing through the green wall module, funnels were used to help measure the velocity of the air and correspondingly calculate the total flow rate [41, 42].

4.2.2 Materials and methods

The module is essentially a rectangular plastic box (dimensions about 500 mm x 500 mm x 130 mm) that holds a permeable bag containing a plant-growing medium based on coconut husks. The front face of the module has 16 openings for plants to protrude out from the bag inside (Figure 4-16). Plant roots grow and ramify within the medium. A fan positioned at a central opening on the module's back-face drives polluted air through the medium-plant-roots, and then onward through the plants' canopy before return to atmosphere. The module

has an opening at its top and bottom faces for water irrigation and drainage respectively. The front openings are circular with a diameter of 75 mm.

Figure 4-16. Green-wall modules with plants, Schefflera amate.

Acrylic sheets were used to form rectangular-box chambers of 20-mm height at the top and bottom faces of the module. Circular holes of size similar to the front-face openings were cut out on the chambers' outer face and funnels were fitted to these holes for air-velocity measurement. Three holes were cut out at the top-face chamber and one hole at the bottom-face one. Thus air exits from the module via 20 openings (16 at front, 3 on top and 1 at bottom) and funnels were fitted to all these circular openings for increasing air velocity to measurable levels. The module with its funnels in place is shown in Figure 4-17 [41], (16 covering the front openings, 3 on top and 1 at bottom)
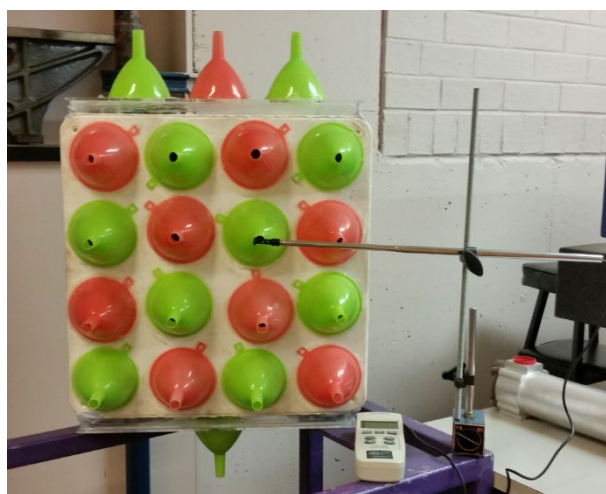
Figure 4-17. Green-wall module with funnels attached.

The fan used in this work is a constant-speed FANTECH TEF-100 which is a 16-W in-line axial fan, fitted to 100mm diameter duct connected to a central opening on the module's back face. To operate the fan at different speeds a Variac Autotransformer (figure 4-18) was used to supply different voltages to the fan. A Digitech digital Tachometer (figure 4-19) was then used to measure the fan speed in revolutions per minute, corresponding to the supplied voltages. In the following, all reported readings (pressure and air velocity) are averages; and all pressures are gauge pressure readings taken at the module's back opening.

Figure 4-18. Variac Autotransformer used in this work

Figure 4-19. Digitech digital Tachometer QM1448

4.2.3 Results and discussion

Total air-flow rate through the module and the corresponding pressure difference across it were obtained for dry modules without plants. The fan was operated at 4 different speeds corresponding to the supplied regulated voltage. The voltages varied from 240–180 V in 200 V increments. Table 4-7 shows the different voltages and their corresponding fan speeds in RPM (revolutions per minute) as well as the corresponding pressure differential across the module [41].

Voltage	240	220 V	200 V	180 V
Press. Diff. (Pa)	18.9	18.4	16.1	14.9
Fan speed (RPM)	2550	2470	2380	2220

Table 4-7. Fan speeds and pressure differential corresponding to different voltages applied

The following measurements of P_{Free} , P_{F-L} , P_{F-S} , Q_{F-L} and , Q_{F-S} were obtained (Table 4-8). Using the calculation procedure presented in section 4.1.2.3 [40, 42, 140], the total air-flow rate Q_{Free} through the module corresponding to its free openings (without any funnels used) was also calculated (Table 4-8). Figure 4-20 shows the curve of the air flow rate versus pressure for the four fan speeds considered. As the fan speeds increased, the pressure difference across the module increased, as well as the corresponding air flow rate, as expected.

Fan Speed (RPM)	Dry Module	Free Openings	Large Funnels	Small Funnels
2550	Press. Diff. (Pa)	18.9	23.6	25.1
2550	Total flow (L/s)	**9.14**	8.87	8.62
2470	Press. Diff. (Pa)	18.4	22.5	23.8
2470	Total flow (L/s)	**8.73**	8.45	8.22
2380	Press. Diff. (Pa)	16.1	21.2	21.7
2380	Total flow (L/s)	**8.54**	8.17	7.71
2220	Press. Diff. (Pa)	14.9	18.8	18.9
2220	Total flow (L/s)	**8.18**	7.69	7.18

Table 4-8. Values for pressure differential and total flow rate corresponding to different fan speeds

The Q-P relationship in all cases showed trends agreeing with typical fan performance curves, namely as Q increases, P decreases [40, 140]. But it should also be noted that there was much back flow in all cases.
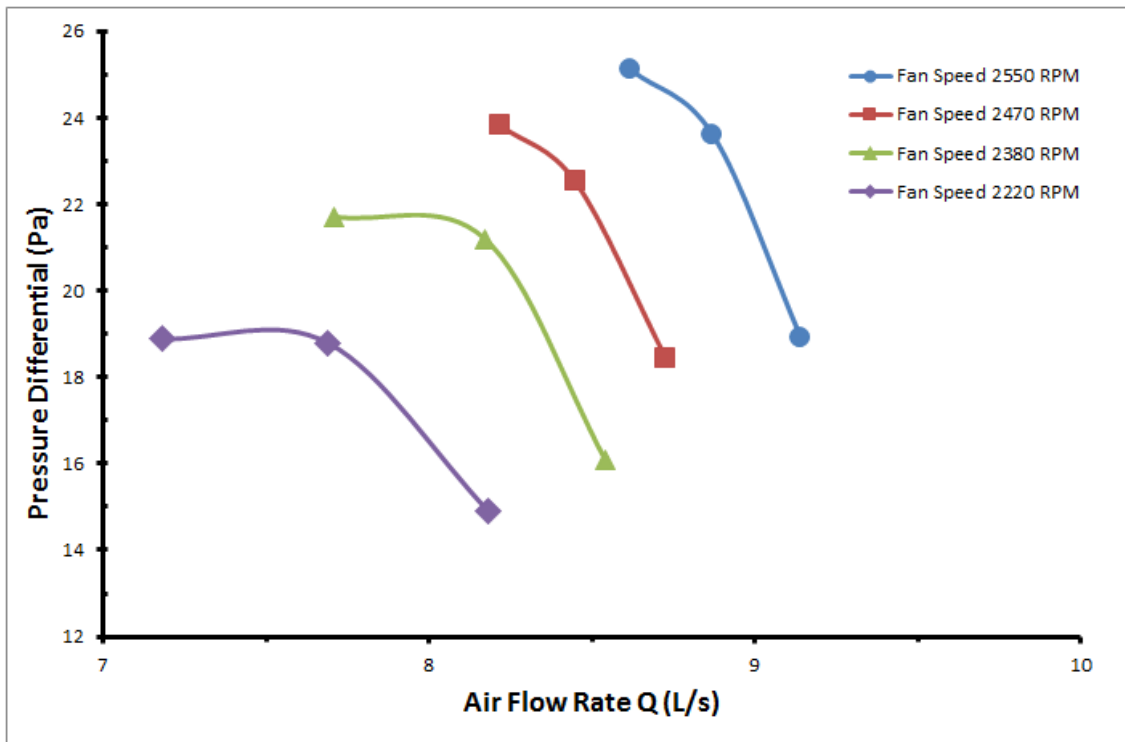
Figure 4-20. Plot of air flow rate Q versus pressure for the four fan speeds considered

For all fan speeds, the air flow distribution was very similar, as shown in Figures 4-21 to 4-24. We recorded 79 % of the total air flow passing through the front openings, and thus passing through the filtration media. The top row (FA) recorded the highest percentage of 22%, while FB recorded ~ 20%, and FC recorded ~ 18%. Row FD recorded the lowest proportional air flow of ~ 16.5 % of the total flow. Approximately 18% of the total flow passed through the top side of the module with an equal distribution among the three top openings, T1, T2 and T3. Only 6 % of the flow passed through the bottom opening B. Air flow passing through the top and bottom of the module did not pass through the full thickness of the filter media, and as such would not be cleaned to the same degree as air passing through the front face of the module.

It should be noted that no substantive preferential airflow through the centre holes was observed, despite the fact that the fan was located centrally within the rear of the module. This is because of the substrate's very high flow resistance, which would have dissipated much of the flow momentum and hence removed flow-direction preferences. The higher percentage of air flow through the upper front rows FA and FB compared to the lower front rows FC and FD is due to the gravitational effect which makes the substrate more compact at its lower half, resulting in additional restriction of air flow. This is likely to be a major concern for larger-scale biofiltration systems similar to the one tested.

157
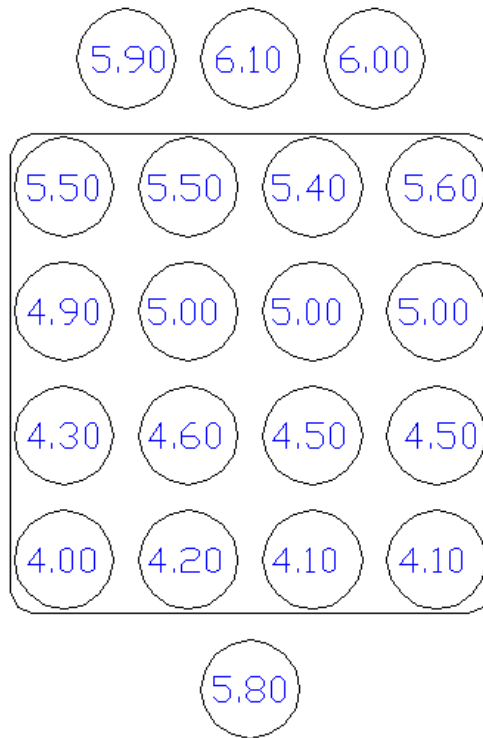
Figure 4-21. Distribution in % of total air flow rate through the module at 2550 RPM fan speed
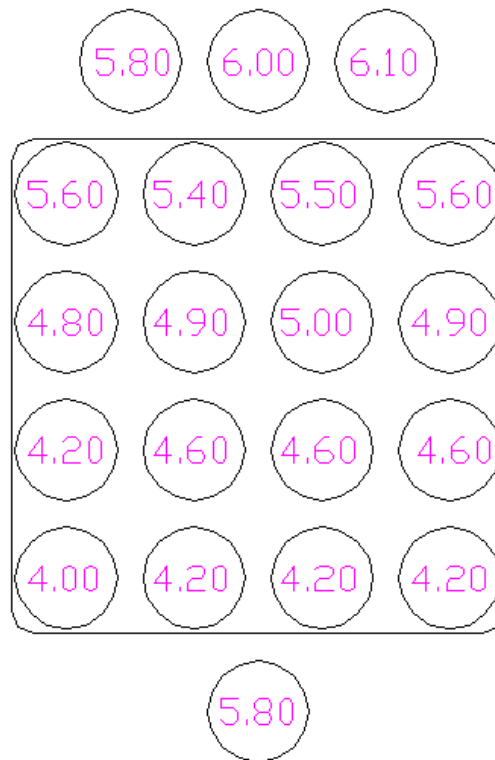
Figure 4-22. Distribution in % of total air flow rate through the module at 2470 RPM fan speed

Figure 4-23. Distribution in % of total air flow rate through the module at 2380 RPM fan speed

Figure 4-24. Distribution in % of total air flow rate through the module at 2220 RMP fan speed

Previous section 4.1 has observed that the airflow distribution within the system tested was reasonably even, similar to the results found in this study for the different fan speeds, indicating that the plenum design can be simplified, potentially reducing system cost both through cheaper design and back pressure reduction. Although the fan was located centrally within the rear of the module, there was no preference for air flow distribution through the centre holes, indicating that the medium has dissipated much of the flow momentum and removed flow direction preference due to its high resistance.

Reducing the amount of polluted air that bypasses only partially through the substrate and not at all through the plant canopy in green walls will clearly improve their filtration performance, thus improving the system's capacity for VOCs and PM biofiltration.

Irga et al [107] demonstrated that an enhanced removal of particulates from air can be achieved by ventilation of the polluted airstream through the tested biofilter. As expected, with increasing air flow rates an increase in filtration efficiency was observed. With each step wise increase in air flow through the system, particle removal from the experimented chamber air was increased in most cases. On the other hand Pettit el al [34] found out that pressure drop through root-induced substrates led to an increased filtration capacity. With higher pressure drop, air passing through the biofilter experienced increased resistance to flow resulting in increased residence time within the substrate and thus increased PM removal efficiency.

4.2.4 Conclusion

Measurements of air flow through a green wall module that holds a permeable bag containing a plant-growing medium have been conducted. Cases of different fan speeds were considered, and the corresponding air-flow rates and pressure difference compared. As the fan speeds increased between 2220 RPM and 2550 RPM, the pressure difference across the module increased from 14.9 Pa to 18.9 Pa, and the corresponding air flow rate increased from 8.18 L/s to 9.14 L/s.

The distribution of airflow through the module openings under the same plant-growing medium was approximately the same for different fan speeds. With all the cases investigated, the Q-P relationship (curve of flow-rate versus pressure) agreed with the typical fan performance curves, namely as Q increased, P decreased.

4.3 Effect of Green Walls on Air Temperature and Humidity

4.3.1 Introduction

Experimental work has been conducted in this work to investigate the effect of green wall modules on the air temperature and on humidity. A closed chamber made of acrylic sheets is used to monitor the temperature and humidity variation caused by a green wall module placed at its center. The effect of both passive green walls and active (breathing) wall modules on temperature and humidity is investigated for different plant species and under varied ambient conditions.

4.3.2 Experimental design for active green walls (Breathing Wall)

A chamber made of 10 mm acrylic sheets is used to monitor the temperature and humidity variation caused by the green wall modules placed at its center. The dimensions of the chamber are 960 x 780 x 590 mm^3. Figure 4-25 [37] shows the chamber with a green wall module (*Nephrolepis cordifolia).*

Figure 4-25. Acrylic-sheets chamber with a green wall module (*Nephrolepis cordifolia*)

To monitor temperature and humidity variations six BME280 (Pressure, Temperature and Humidity) sensors shown in figure 4-26 were distributed in the chamber, two inserted from the front sheet through 10 mm holes, another two sensors were inserted form the top sheet and placed in front of the module. The last set of BME280 was placed behind the module at the lower right and left corners. A seventh BME280 sensor was used to monitor the ambient conditions in the lab room's air, outside the acrylic chamber.

Figure 4-26 Adafruit BME280 Pressue Temperature and humidity sensor

All the BME280 sensors were connected to a multiplexer and then to the computer (Raspberry Pi 2). The software was set to record readings every 15 seconds and the data was exported to excel. Graphs showing the temperature and humidity measurement for the seven sensors are downloaded from the software as well. During a course of recording, temperature and humidity fluctuating temporal readings varied by less than 3% about an average value. Figure 4-27 shows a two dimensional schematic of the BME sensors locations and their connection with the Raspberry Pi (Figure 4-28) through the multiplexer.
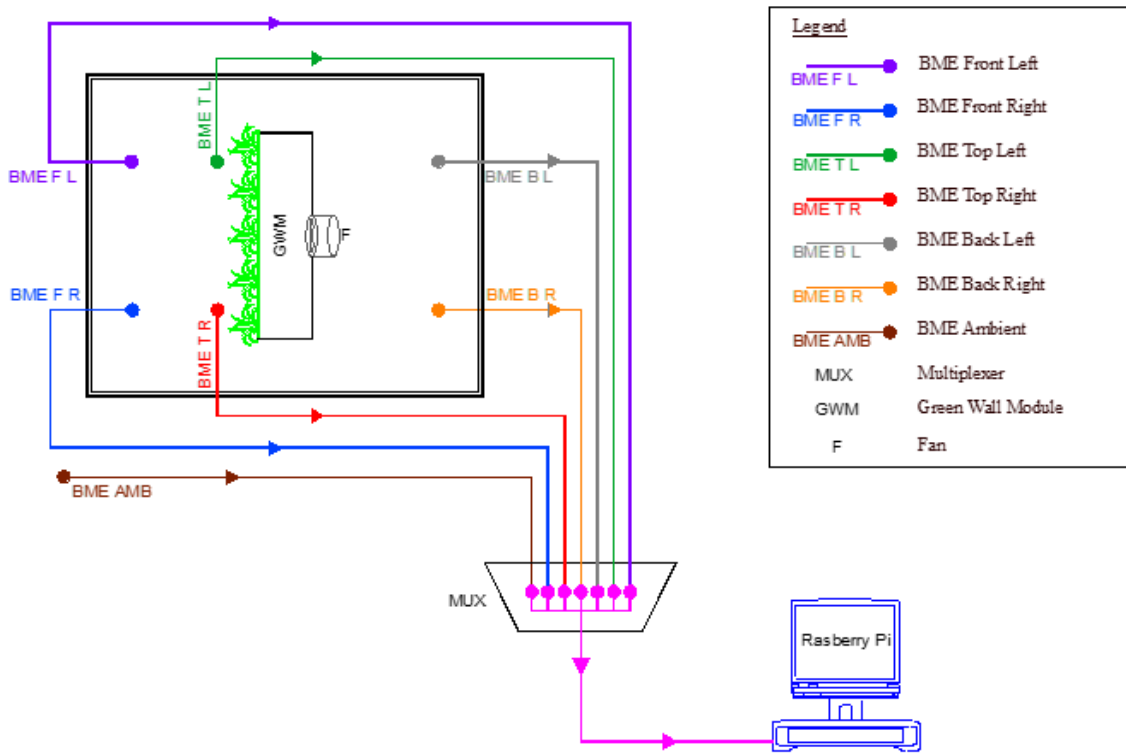
Figure 4-27. Two dimensional schematic of the BME sensors location and their connection with the Raspberry Pi through the Multiplexer.
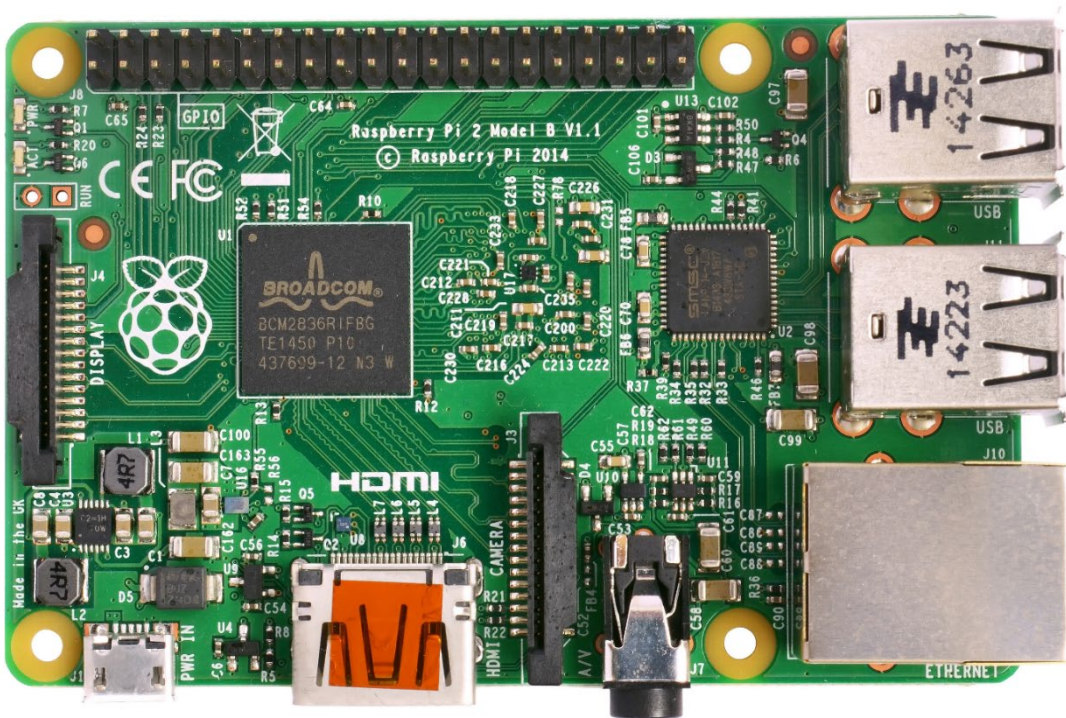
Figure 4-28. Raspberry Pi 2

In addition, four Vaisala (Humidity and Temperature) sensors shown in figure 4-29 have been used to digitally record measurements of both temperature and humidity. Two of these sensors are inserted into the chamber from the front sheet through 10 mm holes and the other two are placed on the top cover sheet and are at a closer proximity to the module as shown in Figure 4-25. Readings of the Vaisala sensors were recorded manually and compared to the reading recorded by the BME280 sensors; the difference between the two kinds of sensors varied by less than 2 %.

Figure 4-29. Vaisala HUMICAP Humidity and Temperature Transmitters HMD60

All experiments lasted at least 24 hours to cover day and night time conditions, since the ambient conditions changed during night time. The lights were on at all times in the lab however the air conditioning was off during the night. The air flow due to the air conditioning outside of the chamber was insignificant throughout the lab.

All modules were tested under the active mode with the fan pushing air at ambient conditions through a 100 mm duct into the module. During operation the lid of the chamber remained

slightly open to insure no buildup of humidity and to provide proper circulation of air. This small opening can be seen in Figure 3 on the chamber's top.

Figure 4-30 shows the setup, but without the module in place in order to provide a clear representation of the locations of sensors. The inside BME sensors are indicated by BME-T, BME-F and BME-B for the sensors inserted from top, front and bottom respectively. During the active mode the BME sensor to monitor ambient conditions was placed outside of the acrylic chamber at the inlet of the duct connected to the fan; its location is indicated by BME-H at the top right corner of Figure 4-30. The Vaisala sensors are indicated by V-F and V-T on their grey case which holds a stainless steel probe, connected to an electronic box with a screen for digital recordings. An opening can be seen on the chamber's top to allow for air circulation and insure no build-up of humidity [37].
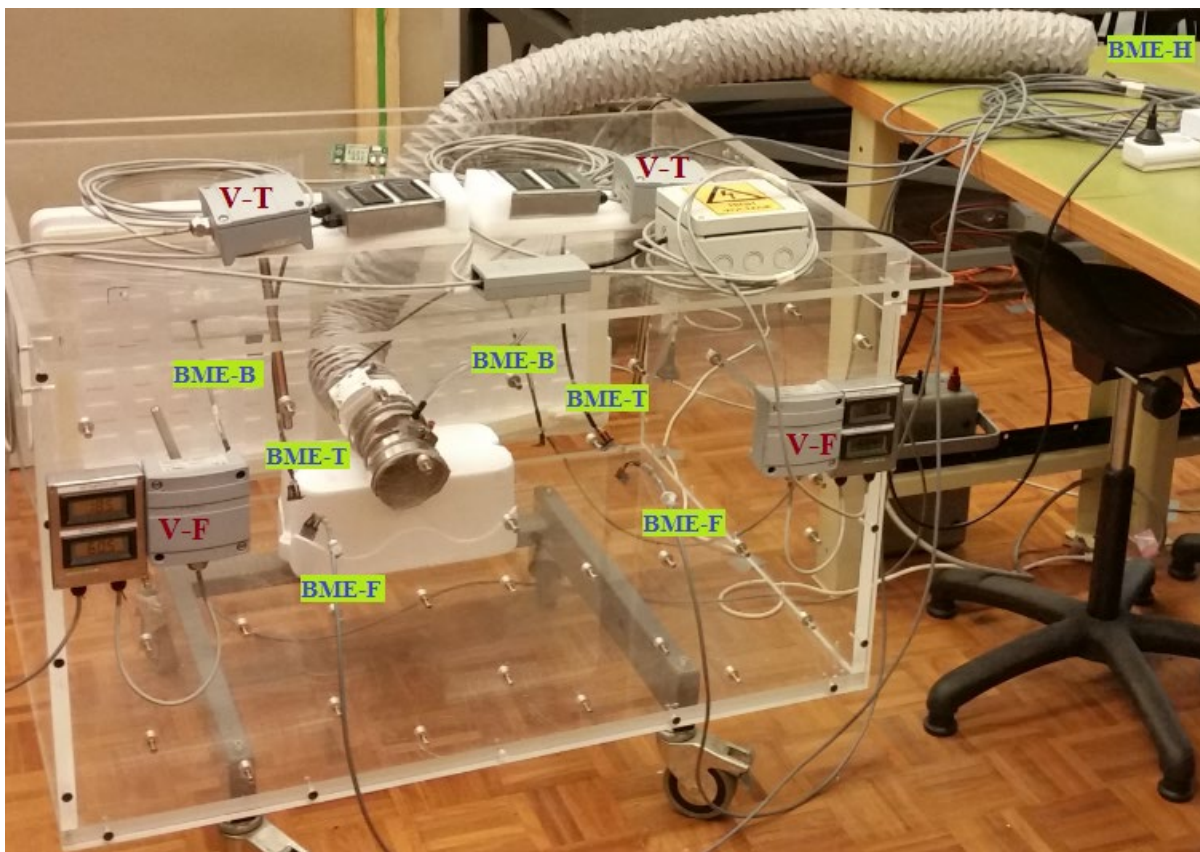
Figure 4-30. Set up of the chamber indicating the locations of the sensors used.

The study has assessed four plant species shown in Table 4-9, these species grow well in the vertical alignment which the present biofilter module uses and they are widely used by the vertical gardening industry. These plants have been grown in a glass house for more than a year. The modules were irrigated with sufficient water to saturate them 24 hours before the experiments were conducted.

In addition one unplanted module with growing medium only was tested. This unplanted module was experimented dry first in its initial condition, and then experimented saturated wet after irrigation before 24 hours from experiment. The chamber was also tested empty without a green wall, and there were no variations noted in the temperature and humidity between the inside of the chamber and the outside (lab).

Species name	Common name	Image
Nematanthus glabra	Goldfish plant	
Schefflera arboricola	Dwarf umbrella tree	
Nephropelis exaltata bostoniensis	Boston fern	
Nephrolepis cordifolia	Lemon button fern	

Table 4-9. Plant species used in this experiment

Pressure difference across the module has been measured using a Sensirion digital-sensor SDP610 – 125Pa. It is 0.1-Pa accurate for low differential air-pressure up to 125 Pa. Values have been recorded every second and the average value was then calculated from a data logger. When air exits from the module, it exits to the ambient. Thus readings from the digital sensor for (gauge) pressure at the module's back-opening are also the pressure difference across the module. During a course of recording which typically lasts several minutes, pressure readings varied by less than 10% about an average value [140].

4.3.3 Experimental design for passive green walls

The setup of the experiment using the passive modules was very similar to the setup used for the active ones. As the passive green walls modules do not utilize a fan for operation, during the time of the experiment the lid of the chamber remained closed. To ensure no excessive buildup of humidity some openings of 10mm diameter were kept open.

Figure 4-31 shows the setup, with a tested green wall module (*Nematanthus glabra*) inside the chamber. The locations of the inside BME sensors are indicated by BME-T, BME-F and BME-B. The BME sensor to monitor ambient conditions was placed outside of the acrylic chamber, on a nearby table at the top right corner of Figure 4-31 [36]. The Vaisala sensors are indicated by V-F and V-T on their grey case.
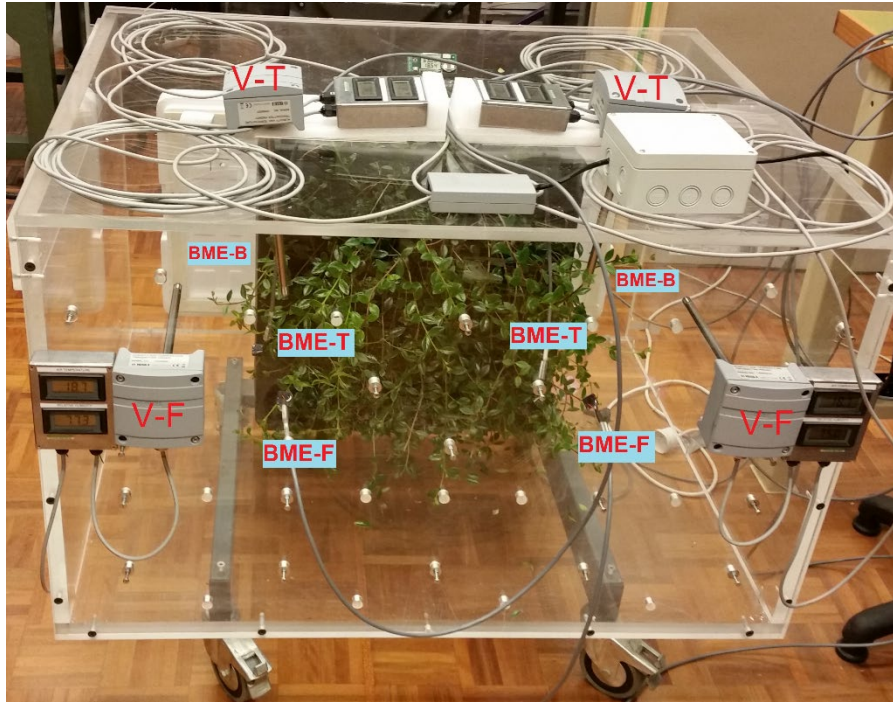
Figure 4-31. Set up of the chamber during passive mode indicating the locations of the sensors used

Under the passive mode the study has assessed three plant species shown in Table 4-9 (*Nematanthus glabra, Schefflera arboricola,* and *Nephrolepis cordifolia*). The modules were irrigated with sufficient water to saturate them 24 hours before the experiments were conducted.

4.3.4 Results for active green walls (Breathing Wall)

For the plant species studied, time-dependent temperature and humidity inside the acrylic chamber have been monitored and recorded. Similarly, the ambient conditions (temperature and humidity) were also recorded. Experiments were held during day time and during night time. Various averages have also been obtained such as the averages from all sensors inside the acrylic chamber at any particular time and the average from a particular sensor over a time period (day or night). Comparisons have been made especially between averages of the ambient and inside the chamber. The ambient temperature during day time was approximately 18-18.5 °C while at night it was approximately 21.5-22.5 °C. The ambient humidity during the day was approximately 62-65 % while during the night it was 65-70%.

Table 2 shows the average temperature values recorded by the BME sensors during the day and night time; refer to Figure 4-30 for the location of the sensors inside the chamber. The average of the six sensors was also obtained and shown in Table 4-10 to indicate the temperature of the chamber. All of the sensors recorded lower temperatures than the ambient temperature and the average difference was in the range of 1 – 1.5 °C during the day and in the range of 2.5 – 3 °C during the night.

Plant type	Time	Temperature (°C)							
		BME-F (Right)	BME-F (Left)	BME-T (Right)	BME-T (Left)	BME-B (Right)	BME-B (Left)	Ambient	Average Chamber
Nematanthus glabra	Day	17.8	17.5	16.7	16.7	17.1	17.0	18.2	17.2
	Night	21.4	21.1	20.0	20.2	20.3	20.3	22.8	20.5
Schefflera arboricola	Day	16.9	16.4	16.8	16.1	16.6	16.5	18.3	16.5
	Night	20.3	20.2	20.1	19.7	20.0	19.9	22.3	20.0
Nephropelis exaltata bostoniensis	Day	17.0	16.4	16.8	16.8	17.2	17.1	18.2	16.9
	Night	19.8	19.3	19.6	19.6	19.8	19.7	22.6	19.6
Nephrolepis cordifolia	Day	17.7	15.8	17.4	17.1	17.3	16.7	18.6	17.0
	Night	20.5	18.4	20.1	19.7	19.7	19.3	22.2	19.6

Table 4-10. Average temperature values recorded by BME sensors for different plant species

Table 4-11 shows the average humidity values recorded by the BME sensors during the day and night time. The average of the six sensors was also obtained and shown in Table 3 to indicate the average humidity inside the chamber.

Plant type	Time	Humidity (%)							
		BME-F (Right)	BME-F (Left)	BME-T (Right)	BME-T (Left)	BME-B (Right)	BME-B (Left)	Ambient	Average Chamber
Nematanthus glabra	Day	76.1	71.6	82.9	87.4	85.2	80.8	62.3	80.7
	Night	82.9	80.3	91.5	97.8	92.6	89.4	65.7	89.1
Schefflera arboricola	Day	83.6	82.3	82.1	95.9	89.7	88.5	62.9	87.0
	Night	94.3	90.2	93.4	99.0	96.5	96.6	72.0	95.0
Nephropelis exaltata bostoniensis	Day	92.6	88.8	91.9	94.9	90.7	90.4	63.4	91.5
	Night	97.4	95.3	97.0	99.0	96.1	96.5	68.7	96.9
Nephrolepis cordifolia	Day	81.2	93.1	81.5	92.3	87.7	90.1	64.4	87.7
	Night	85.9	96.1	86.4	99.2	92.6	95.0	67.6	92.5

Table 4-11. Average humidity values recorded by BME sensors for different plant species

All of the sensors has recorded higher humidity readings compared to the ambient and the average difference was approximately 25% during both day and night times. Higher humidity level has been expected due to the moisture content of the substrate which has been saturated 24 hours before the experiments.

Readings of the Vaisala sensors were recorded manually and compared to the readings recorded by the BME280 sensors for both temperature and humidity, the values varied by less than 2 %. It is noted that none of the plant species had any preference except for some slight differences in the temperature and humidity which is probably due to the different moisture content of the substrate. In most of the cases, the sensors closest to the module (BME-T), has recorded higher humidity levels compared to other sensors. Figure 4-32 shows the graph of the time-dependent temperatures for *Nephropelis exaltata bostoniensis* between 6:30 pm till 11:00 am next day. As mentioned the difference is approximately 3 °C during night time between the ambient temperature (higher) and the temperature inside the chamber while this difference is about 1°C during the day. The highest trace is the ambient temperature; the other lower traces are from sensors inside the acrylic chamber.
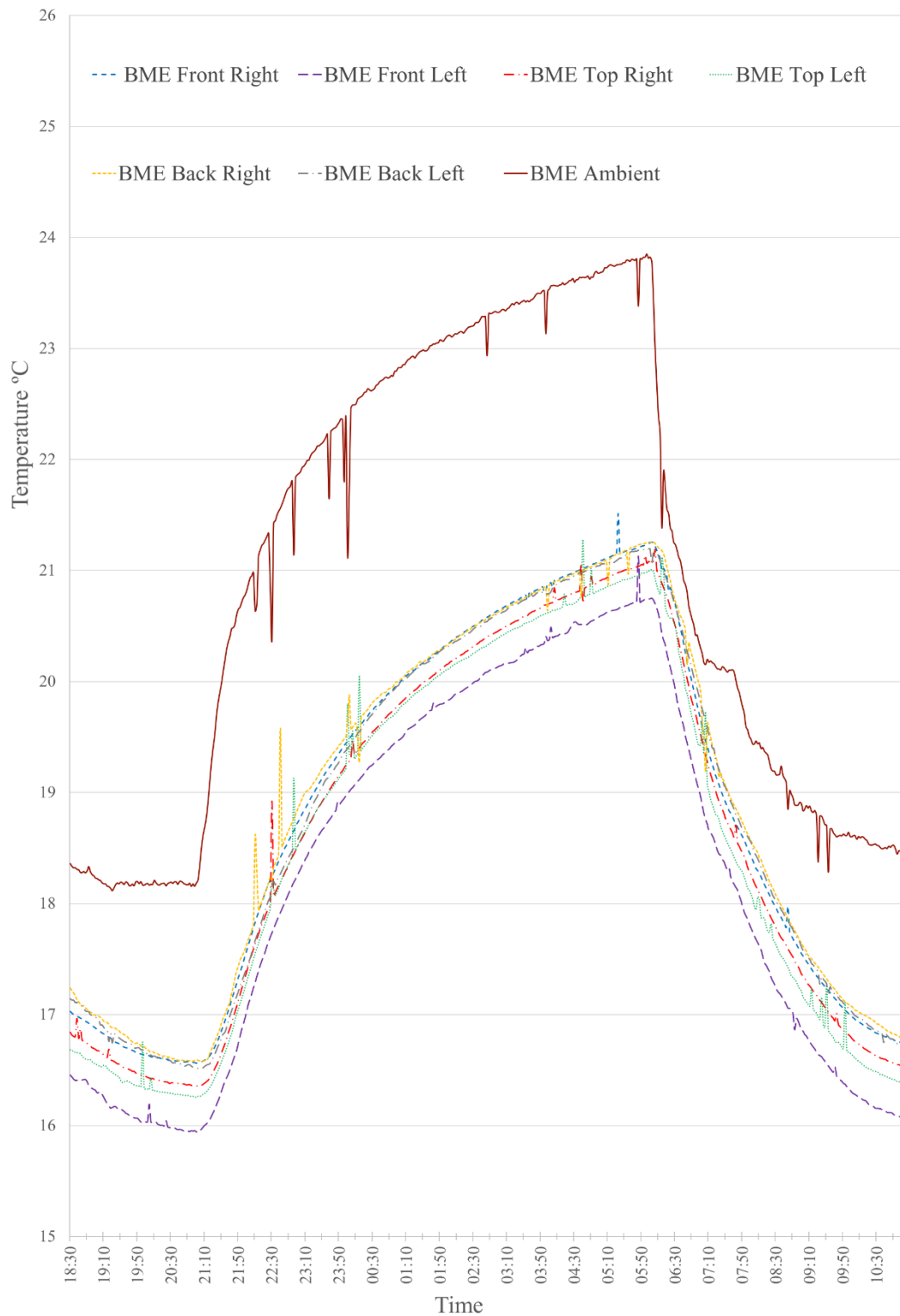
Figure 4-32. Graph showing temperature readings for *Nephropelis exaltata bostoniensis* between 6:30 pm and 11:00 am.

As for the unplanted module with growing medium only, it was tested dry and then saturated wet. When dry there was no significant change recorded in temperature as it only differed by less than 1°C during the night and by less than 0.5°C during the day. Humidity variation was

also low, about 5% during the day and 10% during the night. When saturated wet the variation in temperature and humidity has been similar to the other modules with plant species. This indicates that the plant transpiration has a very minor role and that the moisture content plays a major role in the temperature and humidity variations and that the plant species do not have a significant role. Tables 4-12 and 4-13 show the average temperature and humidity recorded by the BME sensors for the unplanted module when dry and when saturated wet.

| Plant type | Time | Temperature (°C) | | | | | | | |
		BME-F (Right)	BME-F (Left)	BME-T (Right)	BME-T (Left)	BME-B (Right)	BME-B (Left)	Ambient	Average Chamber
Dry Unplanted	Day	18.4	17.8	18.2	18.6	18.6	18.3	18.1	18.3
	Night	21.0	20.8	20.8	21.3	20.6	20.5	21.6	20.8
Wet Unplanted	Day	17.4	16.4	16.0	16.1	16.8	16.4	17.8	16.5
	Night	20.4	19.5	19.1	19.4	19.8	19.4	21.7	19.6

Table 4-12. Average temperature values recorded by BME sensors for unplanted module

| Plant type | Time | Humidity (%) | | | | | | | |
		BME-F (Right)	BME-F (Left)	BME-T (Right)	BME-T (Left)	BME-B (Right)	BME-B (Left)	Ambient	Average Chamber
Dry Unplanted	Day	69.1	69.4	68.3	68.7	68.8	67.7	63.7	68.7
	Night	81.7	78.5	80.5	80.7	84.1	81.7	70.2	81.2
Wet Unplanted	Day	82.0	84.5	91.2	99.2	89.4	90.4	68.9	89.5
	Night	87.8	90.9	96.1	99.0	94.3	95.4	70.9	93.9

Table 4-13. Average humidity values recorded by BME sensors for unplanted module

Figure 4-33 shows the graph of the temperatures for the unplanted module when saturated wet from midnight till 9:00 pm. The difference is approximately 1.5 °C during day time between the ambient temperature (higher) and the temperature inside the chamber, while this difference is about 2 °C during the night. The highest trace is the ambient temperature; the other lower traces are the temperatures from sensors inside the chamber.

173
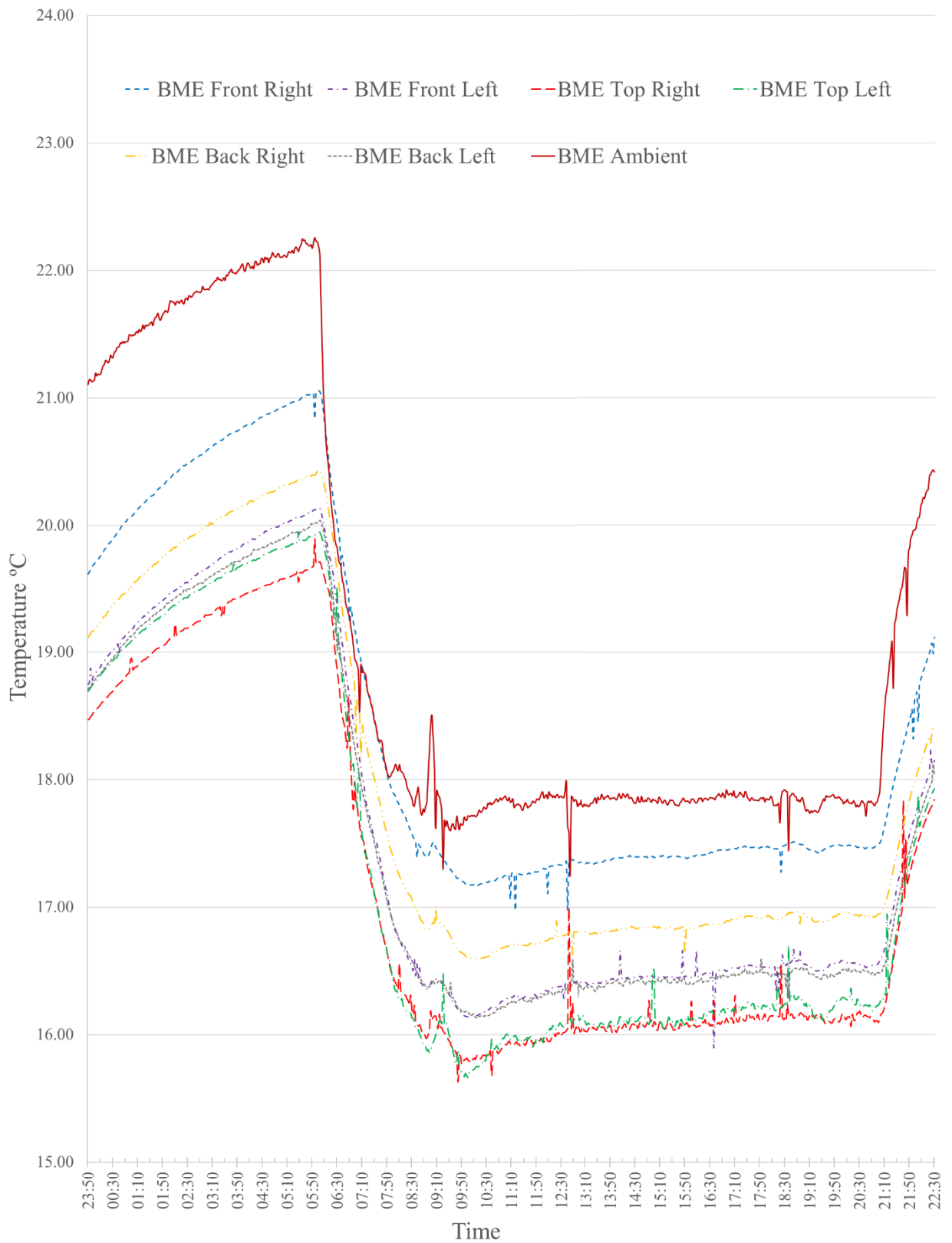
Figure 4-33. Graph showing temperature readings for the unplanted module between midnight and 10:30 pm.

Pressure difference across the different modules studied have been obtained and recorded in Table 4-14. The total flow rate is estimated based on the method described in section 4.1 [40, 140]. The Q-P relationship in all cases has trends agreeing with typical fan performance curves', namely as Q increases, P decreases [40, 140]. But it should also be noted that there is much back flow in all the cases considered.

Module Type	Pressure Difference (Pa)	Total Flow Rate (L/s)
Nematanthus glabra	23.8	16.0
Schefflera arboricola	25.7	15.3
Nephropelis exaltata bostoniensis	35.3	12.8
Nephrolepis cordifolia	28.2	14.5
Dry Unplanted	20.1	9.1
Wet Unplanted	24.5	15.8

Table 4-14. Pressure difference across the modules and corresponding total air flow rate

4.3.5 Results for passive green walls

For the three plant species studied, time-dependent temperature and humidity inside the acrylic chamber have been monitored and recorded. Similarly, the ambient conditions (temperature and humidity) were also recorded. Experiments were held during day time and during night time. Various averages have also been obtained such as the averages from all sensors inside the acrylic chamber at any particular time and the average from a particular sensor over a time period (day or night). Comparisons have been made especially between averages of the ambient and inside the chamber. The ambient temperature during day time was approximately 18-19 °C while at night it was approximately 22-22.5 °C. The ambient humidity during the day was approximately 58-62 % while during the night it was 66-72%. Table 4-15 shows the average temperature values recorded by the BME sensors during the day and night time; refer to Figure 4-31 for the location of the sensors inside the chamber. The average of the six sensors was also obtained and shown in Table 4-15 to indicate the temperature of the chamber. All of the sensors recorded lower temperatures than the ambient temperature and the

average difference was in the range of 0.5 – 1.5 °C during the day and in the range of 2 - 2.5 °C during the night.

Plant type	Time	Temperature (°C)							
		BME-F (Right)	BME-F (Left)	BME-T (Right)	BME-T (Left)	BME-B (Right)	BME-B (Left)	Ambient	Average Chamber
Nematanthus glabra	Day	18.6	18.3	18.4	18.3	18.8	18.7	19.1	18.5
	Night	20.9	20.6	20.5	20.5	20.7	20.4	22.2	20.6
Schefflera arboricola	Day	16.9	16.4	16.8	16.0	16.6	16.5	18.3	16.5
	Night	20.7	20.5	20.5	20.5	20.2	20.0	22.5	20.4
Nephrolepis cordifolia	Day	18.5	18.1	18.2	18.3	18.5	18.3	18.8	18.3
	Night	20.5	20.1	20.3	19.9	19.8	20.5	22.1	20.2

Table 4-15. Average temperature values recorded by BME sensors for different plant species

Table 4-16 shows the average humidity values recorded by the BME sensors during the day and night time. The average of the six sensors was also obtained and shown in Table 4-16 to indicate the average humidity inside the chamber.

Plant type	Time	Humidity (%)							
		BME-F (Right)	BME-F (Left)	BME-T (Right)	BME-T (Left)	BME-B (Right)	BME-B (Left)	Ambient	Average Chamber
Nematanthus glabra	Day	79.5	73.5	79.6	82.8	76.7	68.9	58.1	76.8
	Night	94.9	92.8	95.5	99.9	94.6	94.3	68.4	95.3
Schefflera arboricola	Day	85.7	83.6	84.5	96.5	88.5	88.6	61.6	87.9
	Night	92.0	89.3	91.2	98.9	95.2	95.4	71.3	93.7
Nephrolepis cordifolia	Day	89.7	88.3	90.7	97.4	90.4	91.6	61.0	91.4
	Night	89.6	94.5	89.0	96.5	91.5	93.0	66.7	92.4

Table 4-16. Average humidity values recorded by BME sensors for different plant species

All of the sensors has recorded higher humidity readings compared to the ambient and the average difference was approximately 20 - 25% during both day and night times. Higher humidity level has been expected due to the moisture content of the substrate which has been saturated 24 hours before the experiments.

Readings of the Vaisala sensors were recorded manually and compared to the readings recorded by the BME280 sensors for both temperature and humidity, the values compared varied by less than 2 %.

It is noted that none of the plant species had any preference except for some slight differences in the temperature and humidity which is probably due to the different moisture content of the substrate. In most of the cases, the sensors closest to the module (BME-T), has recorded higher humidity levels compared to other sensors.

Figure 4-34 shows the graph of the time-dependent temperatures for Schefflera arboricola between 9:30 pm till 6:00 am next day. As mentioned the difference is approximately 2 °C during night time between the ambient temperature (higher) and the temperature inside the chamber while this difference is about 1°C during the day as shown in Figure 4-35 for Nematanthus glabra between 9:30 am and 6:00 pm. The highest trace is the ambient temperature; the other lower traces are from sensors inside the acrylic chamber.
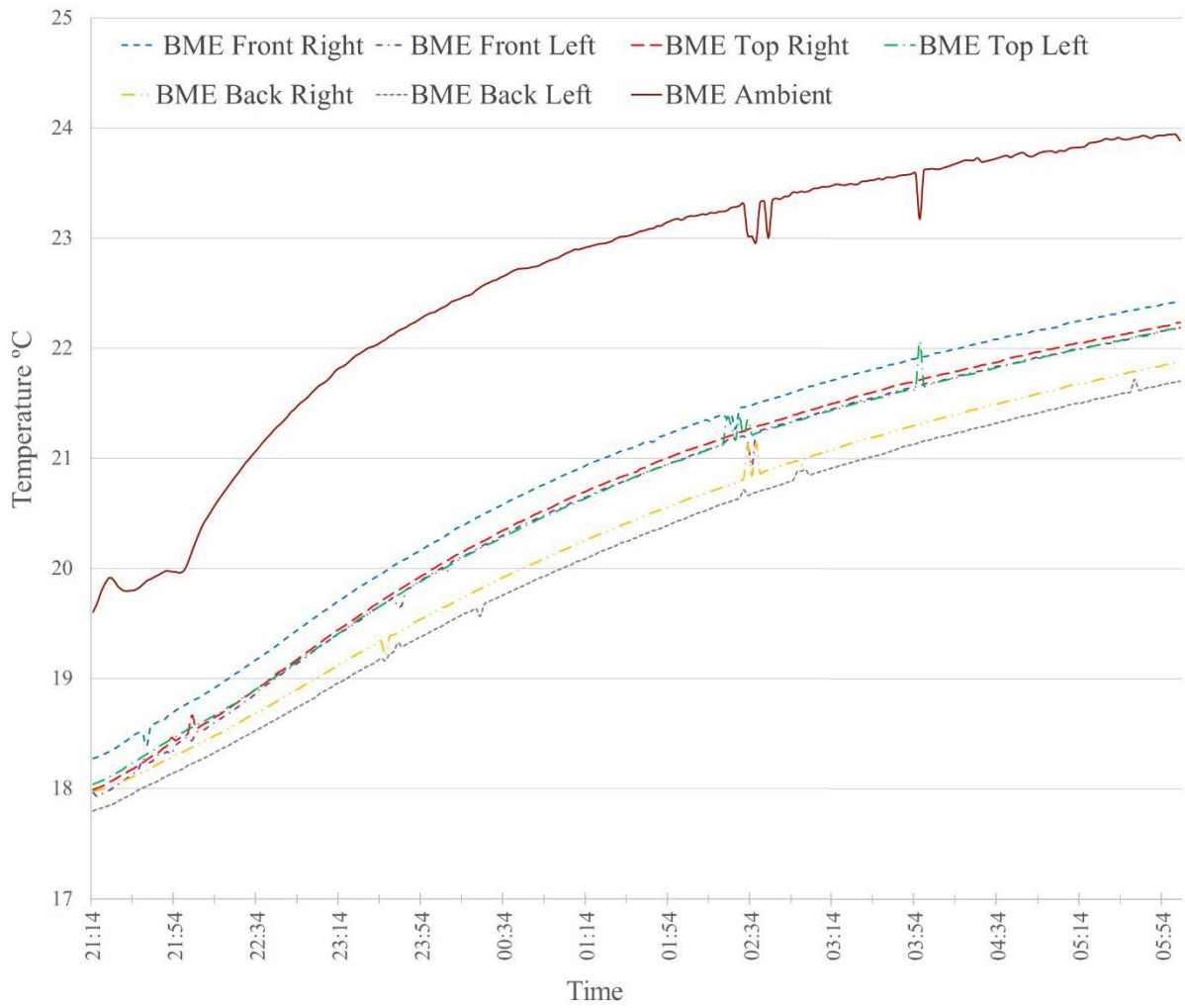
Figure 4-34. Graph showing temperature readings for *Schefflera arboricola* between 9:15 pm and 6:00 am.
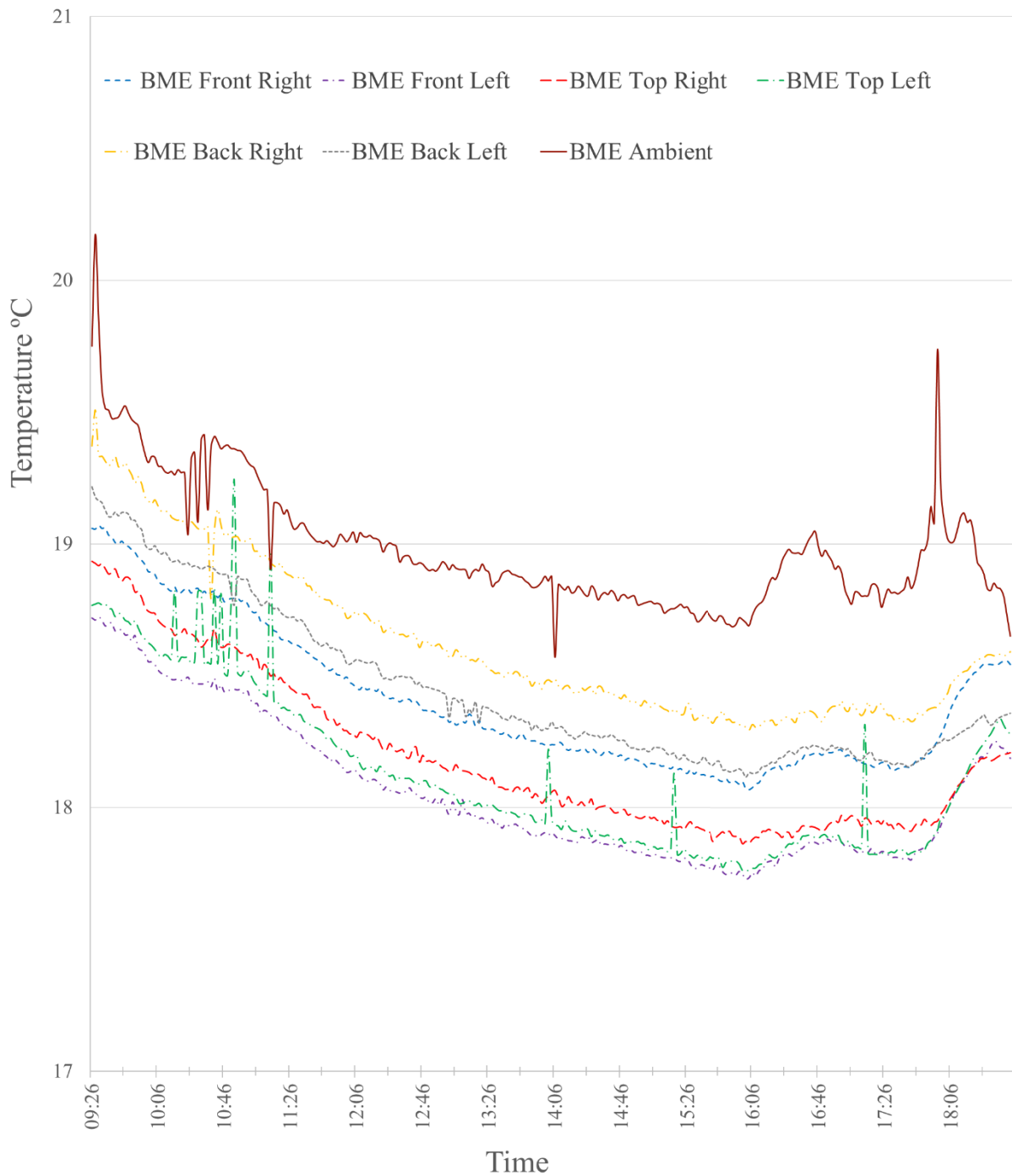
Figure 4-35. Graph showing temperature readings for *Nematanthus glabra* between 9:30 am and 6:00 pm.

4.3.6 Conclusion

The effect of active and passive green wall modules on the air temperature and humidity has been investigated. Cases for dry and wet (saturated) unplanted module, as well as saturated

planted modules with different plant species have been considered. The effect of different surrounding ambient conditions is also investigated.

For the active green wall modules, lower temperatures in the range of 1 to 3 °C, along with increased humidity levels have been noted when modules are saturated wet for cases of unplanted as well as planted modules with different plant species. While any of the plant species studied did not show any preference, an unplanted module with dry substrate did not cause any significant temperature variation indicating that the moisture content plays the major role in the temperature as well as humidity variations. With all the cases investigated Q-P relationship agrees with the typical fan performance curves', namely as Q increases, P decreases.

For the passive green wall modules, lower temperatures in the range of 0.5 to 2 °C, along with increased humidity levels have been noted when modules are saturated wet for planted modules with different plant species. None of the plant species studied showed any preference, indicating that the moisture content of the substrate plays the major role affecting the temperature and humidity variations.

Chapter 5 The effect of PCM incorporated in windcatcher

5.1 Introduction

The use of phase change material PCM in buildings is promising as a beneficial application that can decrease energy consumption, shift the peak loads of cooling energy demand, and decrease the temperature fluctuations while providing a thermally comfortable environment [147]. The performance of PCM as a sustainable passive cooling technique will be investigated in this study by integrating it within a windcatcher natural ventilation system.

Using PCM allows energy recycling. This cycling of thermal energy reduces energy consumption and air conditioning system run-time, maintenance and system size while enhancing thermal comfort. The biological components of Bio PCM contribute to CO_2 reduction and protection of the environment and climate significantly. They can be installed simply by unrolling the sheets and fixing them to the walls.

5.2 Materials and Devices

An experimental set up was arranged in the Metrology lab of the Faculty of Engineering and IT at UTS. An acrylic chamber fitted with a windcatcher was incorporated with phase change material and the temperature and humidity variations inside the chamber were monitored via BME sensors (Temperature, Pressure and Humidity). Air velocity sensors were also used to monitor the velocity inside the chamber at different locations.

5.2.1 Acrylic chamber fitted with a windcatcher

A 12 mm acrylic sheets chamber of dimensions 1250 x 1000 x 750 mm^3 has been used in this study to monitor the effect of PCM. The chamber has wheels as shown in Figure 5.1 for easy movement.

Figure 5-1. 12 mm acrylic sheets chamber (1250 x 1000 x 750 mm^3) with wheels.

The two sheets along the length of the chamber (right and left hand side) with dimensions of 1250 mm x 750 mm had several 12.7 mm holes. The distribution of the holes along with their locations are shown in Figure 5.2. Some of these holes were used to insert the sensors cables and probes into the chamber. The unused holes were closed with special plugs.
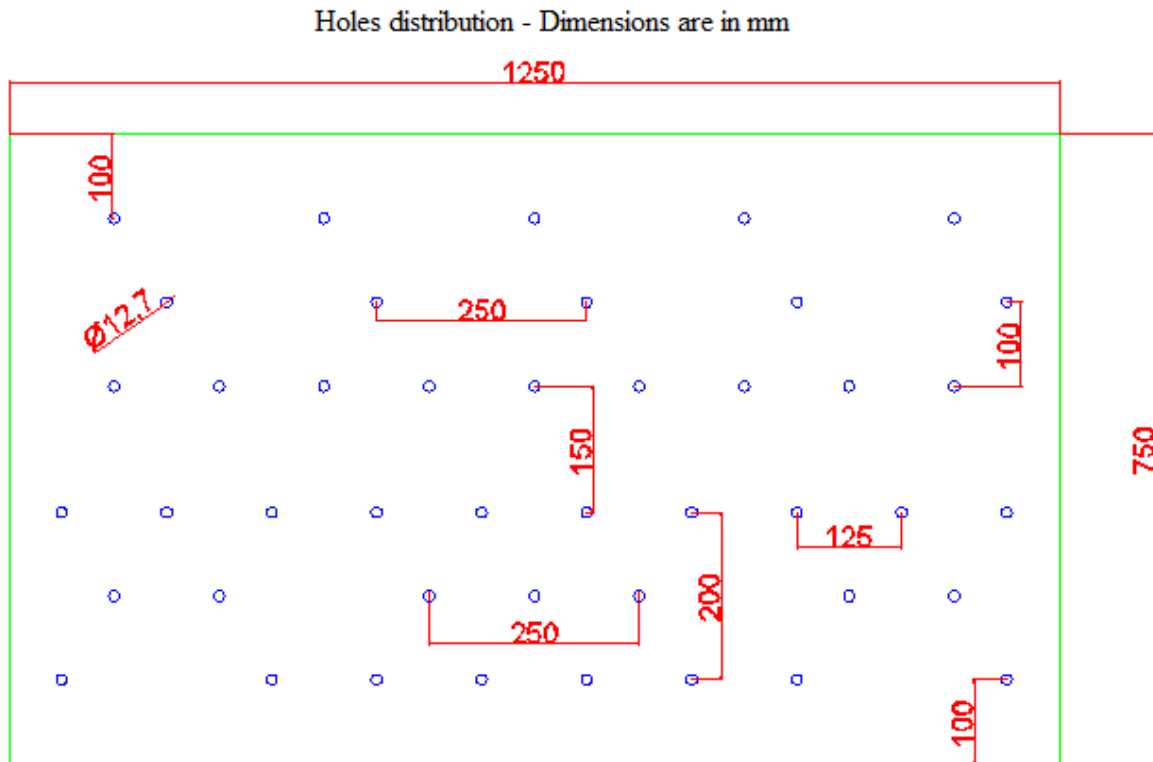
Figure 5-2. Distribution of 12.7 mm holes found in the right and left side sheets of the chamber.

A two sided windcatcher (figure 5-3) with two canal bottom shape is fitted on the roof of the acrylic chamber. The canals are curved with squared inlet/outlet shape and dimensions of 160 x 160 mm^2. The inlet and outlet are 400 mm above the roof of the chamber and the canals descend by only 100 mm inside the room. Figure 5-4 shows a three dimensional drawing of the acrylic chamber including the fitted two sided windcatcher along with their related dimensions.

Figure 5-3. Two sided windcatcher fitted on the acrylic chamber
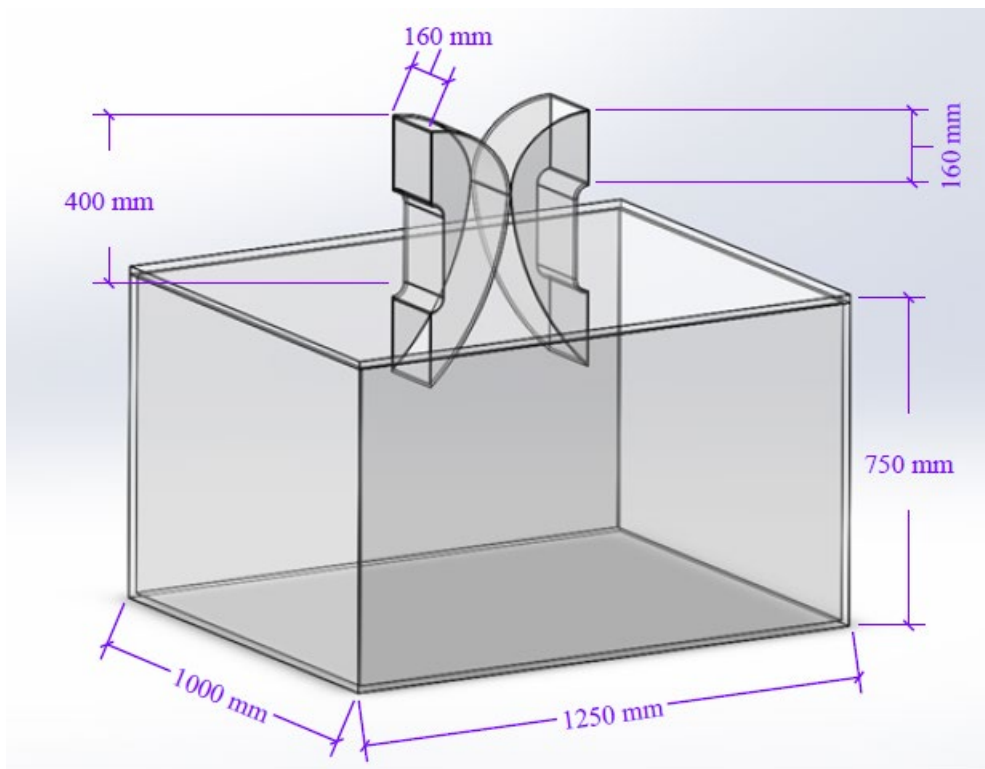
Figure 5-4. Three dimensional drawing of the acrylic chamber fitted with a two sided windcatcher

5.2.2 Plywood for insulating the acrylic chamber

Plywood of 6 mm thickness has been used as additional insulation for the acrylic chamber. Different plywood sheets has been cut to fit the chamber walls, floor and roof. Locations of sensors which required a gap in the plywood has been taken into consideration. Figure 5-5 shows the acrylic chamber with the insulation in place covering the floor and walls.

Figure 5-5 Acrylic chamber with plywood placed at the walls and the floor

5.2.3 Phase change material (PCM) used in this study

The phase change material used in this study is Bio PCM M51 Q24. Each carton contains 6 sheets (shown in figure 5-6) of dimensions 1050 mm x 480 mm with a total weight of 9Kg of active ingredients and a total energy capacity of 459 Wh/carton. Each sheet has seven pouches 110mm x 300mm. Its melt band is 20-24 ºC and it contains a fire retardant and a gelling agent. The energy generated from Bio PCM is approximately 4 KWhr.

Bio PCM is a passive solar system which acts like a rechargeable thermal storage that cycles daytime heat to night in winter and night time cool to day in summer. It provides thermal energy storage at the source of the load and greatly reduces wall heat flux and energy consumption.

Figure 5-6. Bio PCM M51 Q24 used in this study

The phase change sheets have been placed at different locations in the chamber for testing its effect. Mainly PCM was placed on the floor, attached to the walls, and covered the ceiling. Figure 5-7 shows the chamber with PCM on the floor and on the walls, while figure 5-8 shows the chamber with full coverage of PCM, floor, wall and ceiling (without the insulation for better visualization). In addition some experiments included PCM placed in the windcatcher's inlet channel as shown in figure 5-9.
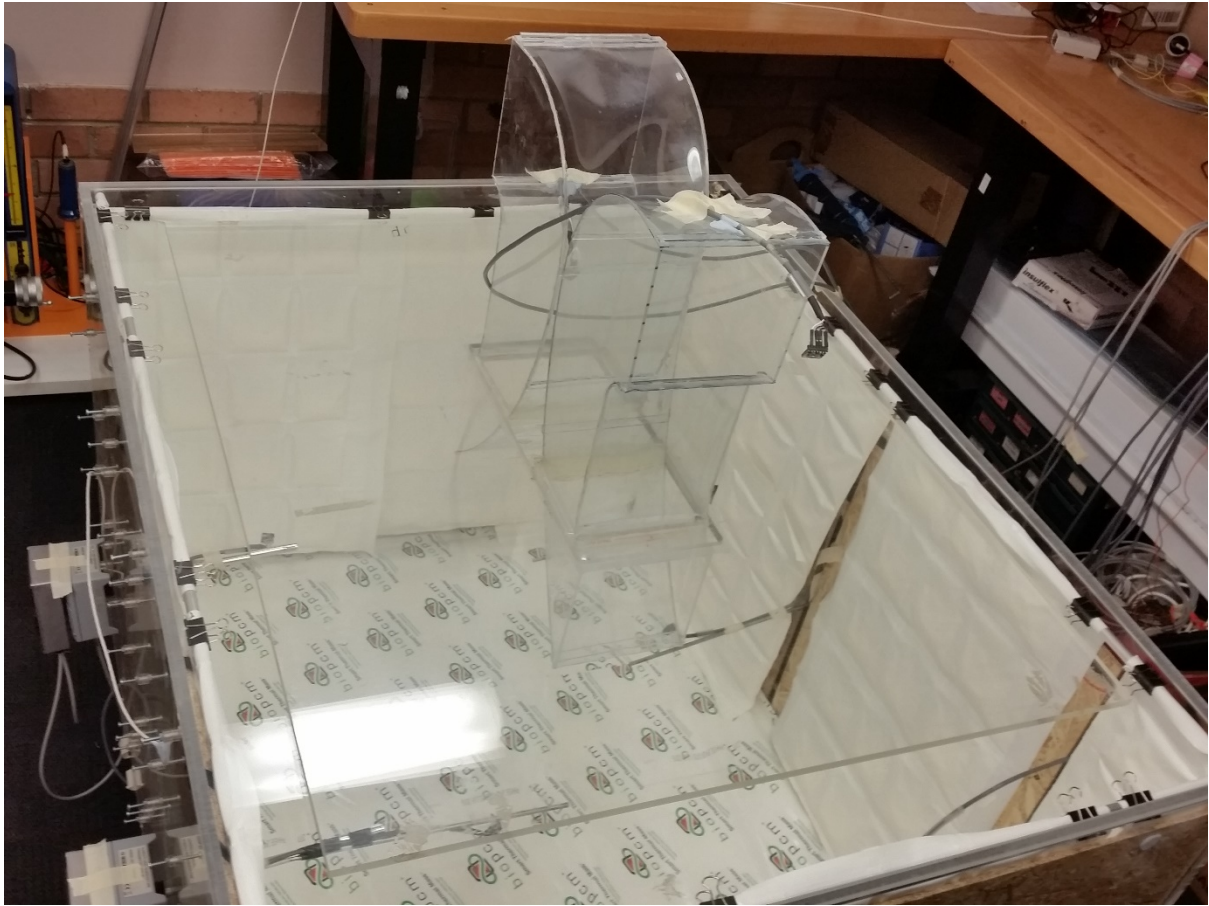
Figure 5-7Acrylic chamber with PCM on the floor and walls
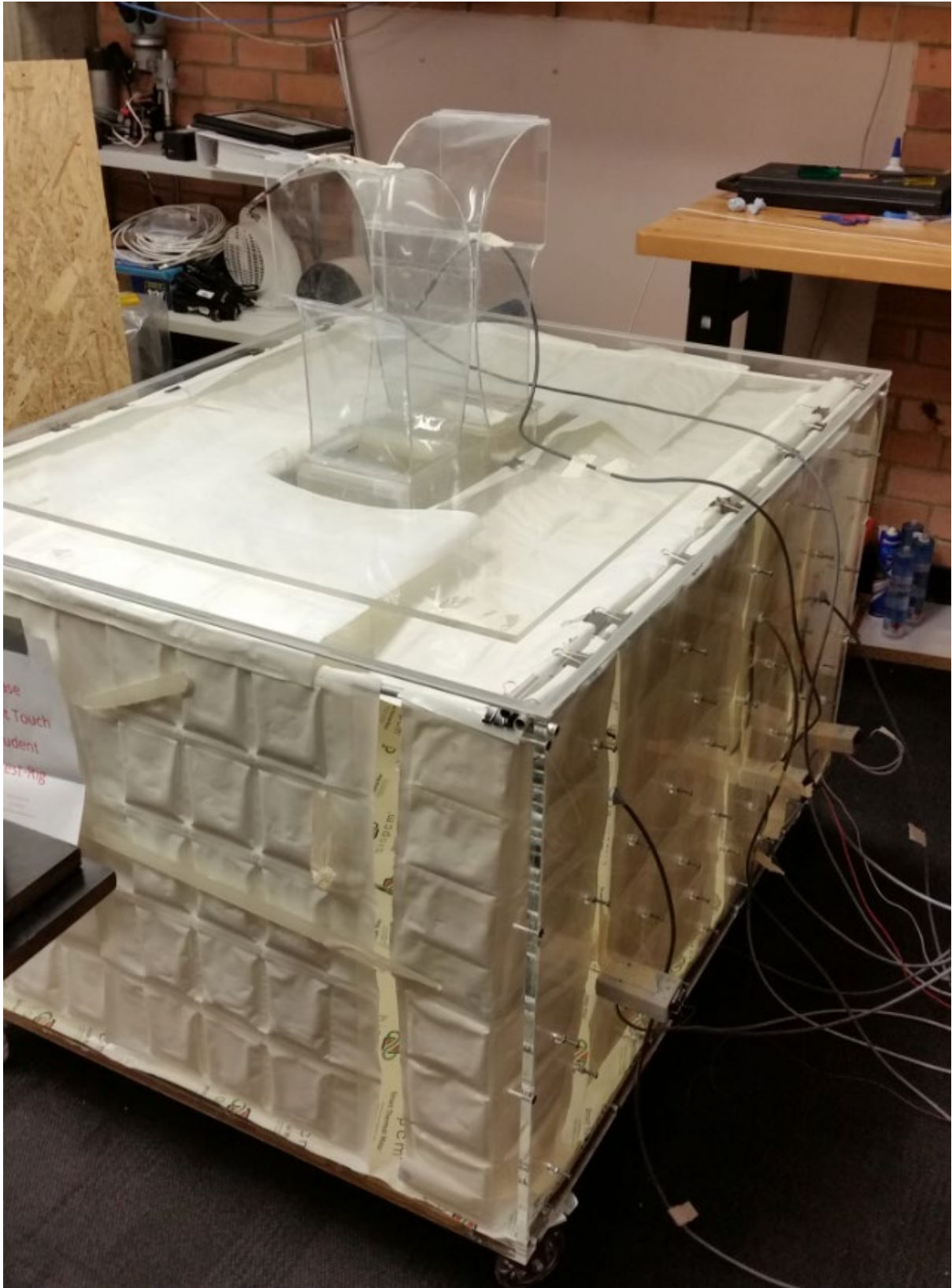
Figure 5-8 Chamber with PCM placed on floor, walls and covering the ceiling

Figure 5-9 PCM placed in the windcatcher's inlet channel

5.2.4 Generation of air flow- Hot Box Fan and ducts

A hot box, fan with heating elements manufactured by Thermal Electric Elements Australia has been used to generate air flow at different speeds and at different temperatures. The hot box has different stages as shown in Figure 5-10, each stage would add about 7 ℃ to the air temperature. Fan speed can also be regulated by setting the percentage as shown in the display. The hot box required three phase connection and was placed on a table 0.92 m high as shown in Figure 5-11.

Figure 5-10 Fan with heating elements control box

Figure 5-11 Set up for the Hot Box and ducts

Figure 5-11 shows the set up used to generate air flow. The hot air blown by the Hot Box fan was directed to the acrylic chamber through two ducts separated by a straightener. Both ducts have similar dimensions, their length is 500 mm and the internal dimensions of the ducts openings are 340 mm x 340 mm.

The straightener used STRA-R400x400 is manufactured by Dwyer (Figure 5-12). It is flanged to the ducts. The internal dimensions of the straightener are 400 mm x 400 mm. It is developed with a honeycomb airflow straightening section for use in duct systems having highly turbulent conditions at the point of measurement.

Figure 5-12 Straightener

5.2.4.1 Air velocity across the duct

The straightener used STRA-R400x400 is used to measure the air flow through the duct by simply connecting the tubing to the straightener fittings and then to a differential pressure sensor. Pressure difference was measured using the Sensirion digital sensor SDP610 – 125 Pa shown in figure 4-4. The pressure difference was measured for 100% fan speed of the total Hot Box fan speed. The following equation was then used to calculate the air velocity across the straightener and thus across the duct.

$$V = \sqrt{\frac{2\,\Delta P}{\rho}} \qquad \text{eq. 5-1}$$

Table 5-1 shows the calculated air velocity (m/s) corresponding to the average ΔP measured at full speed of the Hot Box fan.

Hot Box Fan speed	average ΔP (Pa)	Air velocity (m/s)
Full Fan speed 100 %	8.15	**3.65**

Table 5-1 Air velocity across the duct and straightener corresponding to Hot Box Fan speed

5.2.5 Sensors and Data acquisition system

Temperature, pressure and humidity variations were monitored via BME 280 sensors (Temperature, Pressure and Humidity). Air velocity sensors were also used to monitor the air velocity inside the chamber at different locations. A total of eight BME sensors and four air velocity sensors were used and their output connected to a Raspberry Pi 2 shown in figure 4-28. The software was set to record readings every 15 seconds and the data was exported to excel. Graphs showing the measurement were also downloaded from the software. During a course of recording, temporal readings varied by less than 3% about an average value for all of the sensors used.

The BME sensors used are the same used in the green walls experiment shown in Figure 4-26 and described in Chapter 4, section 4.3. Five BME sensors were distributed inside the chamber via the 12.7 mm holes from the right and left side sheets. Three sensors were inserted from the right side sheet, and two sensors from the left side sheet. The three sensors from the right are designated in the data acquisition system by Right front (Rt Fr), Right Back (Rt Bck) and Right Mid (Rt Mid), while the two sensors from the left side are designated by Left front (Lf Fr) and Left Back (Lf Bck). Four of these sensors (Rt Fr, Rt Mid, Lf Fr and Lf Bck) were placed at a height of 300 mm in the chamber. This height corresponds to 1.2 m high in a real sized room of 5x4x3 m^3. The sensor Rt Bck was placed at 200 mm high in the chamber, which corresponds to a height of 0.8 m in a real sized room. The probe of these sensors was placed at 200 mm away from the corresponding right or left wall respectively.

Two BME sensors were placed at the inlet and outlet of the windcatcher tunnel respectively. One sensor was placed at the inlet opening of the windcatcher slightly outside of the tunnel as shown in Figure 5-13. This sensor is used to measure the conditions (pressure, temperature and humidity) of the air blown through the windcatcher. It is designated (In) in the data acquisition system. Another sensor was placed inside the windtunnel and near the outlet opening. It is designated (Out) in the data acquisition system and is used to measure the condition of the air exiting the windcatcher after circulating in the chamber.

The eighth sensor is placed outside and away of the acrylic chamber. It is placed on a bench close to the Pi. This sensor is used to measure the ambient conditions in the lab and it is designated by (Amb) in the data acquisition system. Figure 5-13 shows the (In and Out) sensors as well as the bench at the back where the Computer screen, Rasbperry Pi and (Amb) sensor

are placed. Figure 5-13 also shows the set up when the chamber is close to the duct where the distance between the duct exit and the windcatcher inlet is 400 mm.

All the BME280 sensors were connected to a multiplexer and then to the computer (Raspberry Pi 2). Figure 5-15 shows a two dimensional schematic (top view) of the chamber with the locations of the sensors as well as the locations of the probes. BME sensors are indicated in green color.
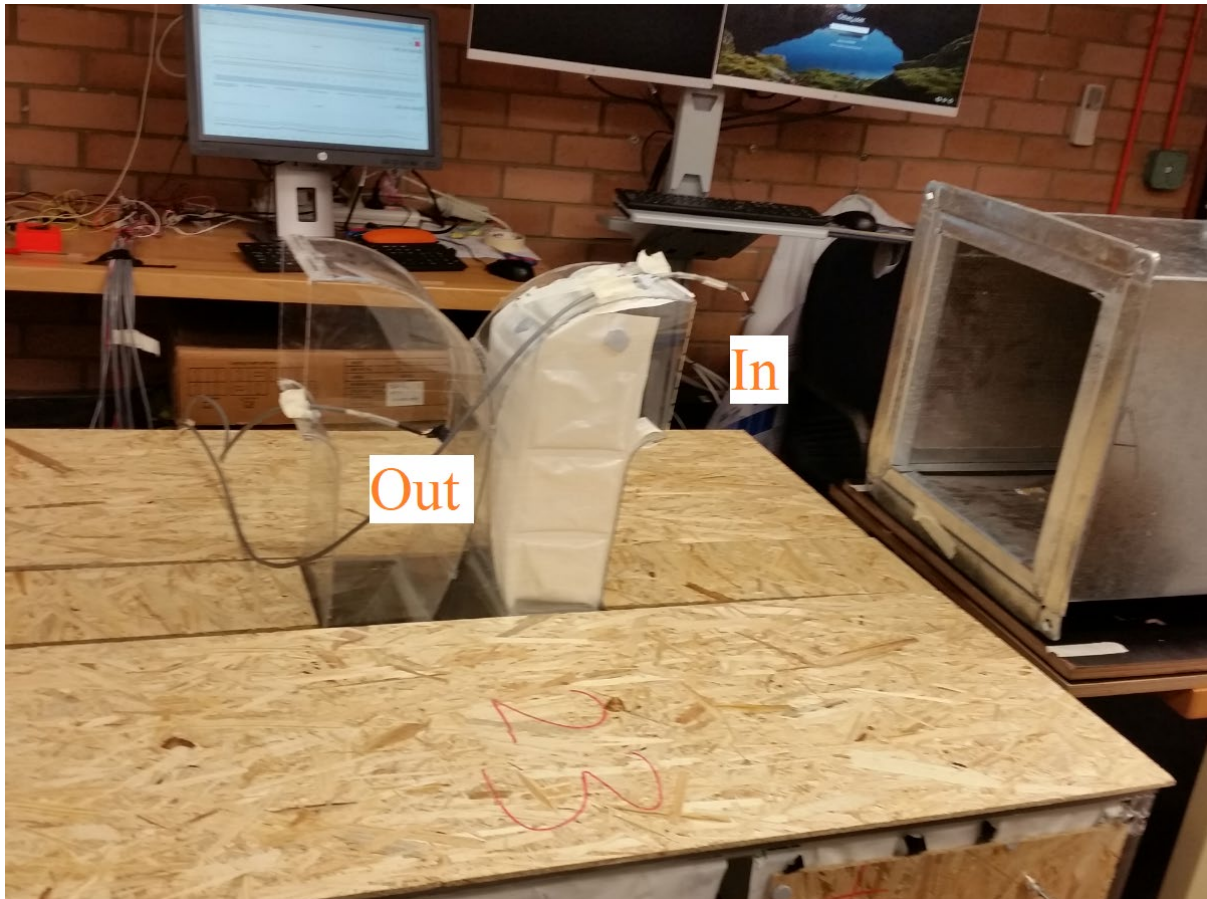
Figure 5-13 Set up shows (In and Out) sensors and the bench at the back where the Computer screen, Rasbperry Pi and (Amb) sensor are placed.

5.2.5.1 Air velocity sensors

Air velocity transducers (3xFMA904A-V1 and 1xFMA904R-V1) manufactured by Omega are used to monitor the air velocity. Three of these sensors have fixed probes, while the fourth has a remote probe. The fixed probe are of Stainless Steel of length 300 mm and the probe diameter is 6 mm. The remote probe has a fixed length of 305 mm with a 4.5 m shielded cable. The output of these sensors is linear 0 to 5 Volts DC. They have a hot wire air velocity sensor design

and they are 2% accurate at full scale. The air velocity range is 0 to 25.4 m/s. Figure 5-14 shows the air velocity transducer.

Figure 5-14 Omega air velocity transducer

Three sensors with fixed probe were inserted form the right side sheet through the 12.7 mm holes, while the sensor with the remote probe was inserted from the left side sheet. The sensors are designated Right front (Rt Fr), Right Mid (Rt Mid), Right Back (Rt Bck) and Left front (Lf Fr). Three of these sensors (Rt Fr, Rt Mid, Lf Fr) were placed at a height of 300 mm in the chamber. This height corresponds to 1.2 m high in a real sized room of 5x4x3 m^3. The sensor

Rt Bck was placed at 200 mm high in the chamber, which corresponds to a height of 0.8 m in a real sized room.

The output of the air velocity sensors was 0-5 volts and therefore they had to be connected to an Analog to Digital Convertor ADS1115, which was then connected to a multiplexer and then to the Raspberry Pi 2. Figure 5-15 shows a two dimensional schematic (top view) of the chamber with the locations of the sensors as well as the locations of the probes. BME sensors are indicated in green color, while the air velocity sensors are indicated in red
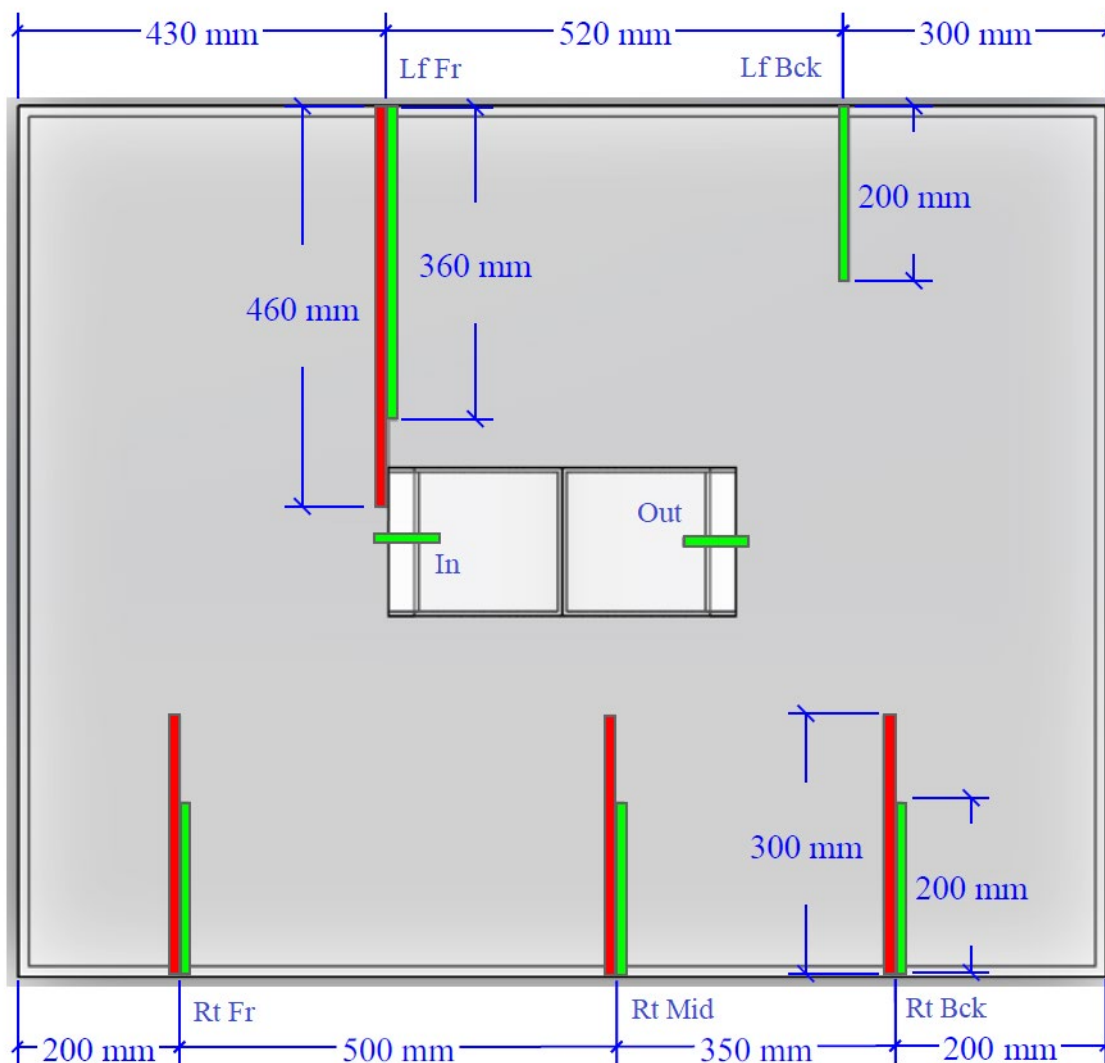
Figure 5-15 Top view of the chamber showing the locations of the sensors and their related probes. BME sensors are indicated in green color, while the air velocity sensors are indicated in red.

5.2.5.2 Set up for data acquisition system

Figure 5-16 shows a two dimensional schematic of the sensors locations and their connection with the Raspberry Pi through a multiplexer (MUX) and through an analogue to digital converter (ADC). The connections of the BME sensors are shown in green while the connections of the air velocity sensors are shown in red. Seven of the BME280 sensors are connected to a multiplexer and then to the computer (Raspberry Pi 2). BME sensor measuring the ambient is directly connected to the Raspberry Pi. The air velocity sensors were connected to the ADC and then to the multiplexer. The software was set to record readings every 15 seconds and the data was exported to excel.
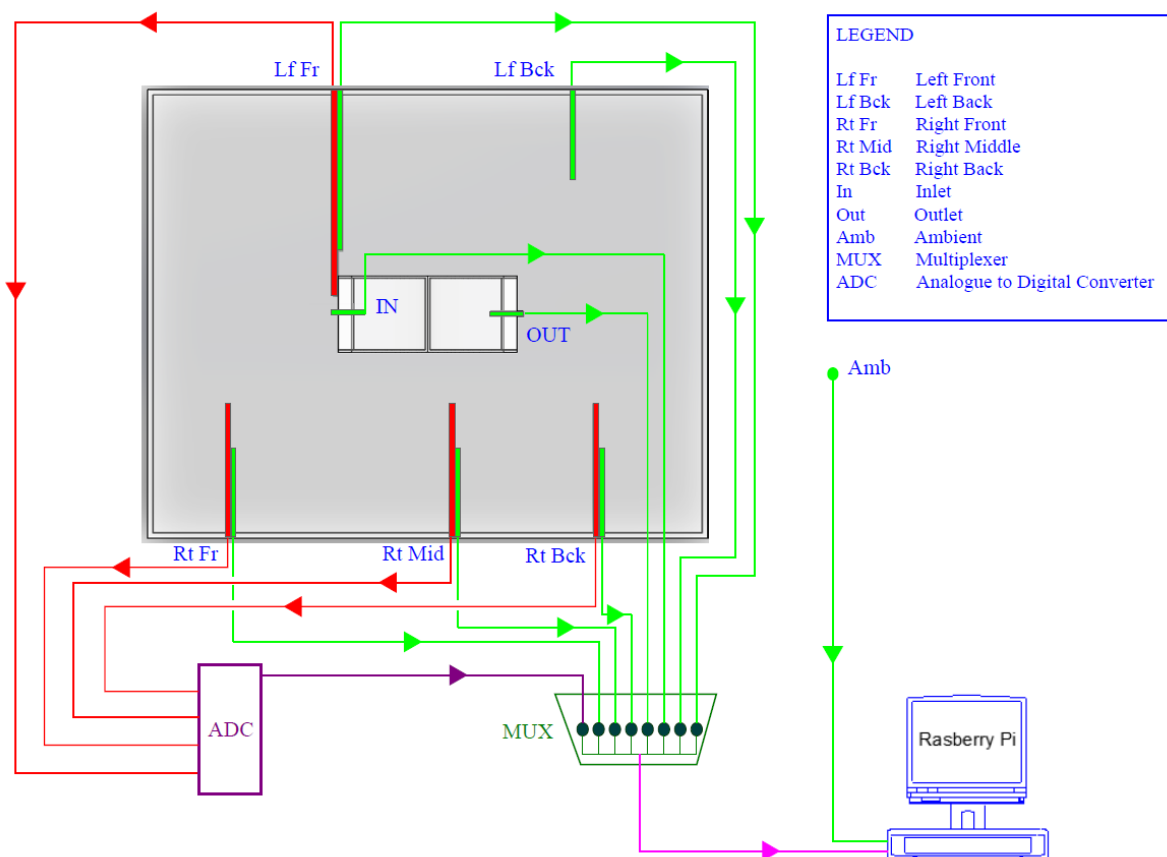
Figure 5-16 two dimensional schematic of the sensors locations and their connection with the Raspberry Pi through the multiplexer and the ADC

5.3 Methods

To investigate the effect of phase change material incorporated with a windcatcher, different models with different locations of PCM have been used. Experiments have been conducted

when the acrylic chamber is empty and also when it contains PCM sheets in several locations. The following models have been investigated:

1. No PCM: chamber empty
2. PCM Walls only
3. PCM Floor and walls
4. PCM Full: PCM found on floor, ceiling and walls
5. PCM Full + windcatcher: PCM found on floor, ceiling, walls and the windcatcher's inlet channel.

5.3.1 Chamber's location with respect to the duct's outlet

During the experiments, ply wood covered all the sides of the chamber. The chamber was placed away from the ducts exit to demonstrate free flow through the windcatcher. The distance between the duct's exit and the windcatchers inlet was 850 mm as shown in figure 5-17.

Figure 5-17 Chamber location at 850 mm from the duct's outlet.

A different location was also used (Figure 5-13), with the chamber pushed as close as possible to the duct which minimized the distance between the duct outlet and the windcatcher's opening to 400 mm.

5.3.2 Discharging process (Cooling of air)

To investigate the discharging process of the PCM, the hot box fan was operated with two different stages (stage 1 and stage 2). Each stage adds approximately 7 ºC to the ambient temperature in the lab. The maximum speed of the hot box fan was used and set using the control box shown in figure 5-10.

5.3.3 Charging process (Solidification of PCM)

After the discharging process, charging process of the PCM had to take place. Cooling down the lab was necessary to decrease the temperatures to levels lower than 20 ºC (lower than the melting temperature of the used PCM). An air conditioning unit found in the lab was used to cool down the lab and a 16 Watt small desk fan with 15 cm diameter was used to direct the cold air into the chamber through the wind catcher inlet. The small fan was placed about 300 mm away from the windcatcher's inlet as shown in figure 5-18.

Figure 5-18 Set up used for solidification of PCM (charging process)

5.3.4 Statistical analysis

Box plots and cumulative frequency distributions were used to compare the results obtained for the different studied models. This analysis has been used due to the variations in the initial conditions of the lab before the experiment started which made it difficult to compare the results at a certain time (after 30 or 45 minutes for example). Figure 5-19 shows an example of a box plot indicating the average value (about 35 ºC) and the different quartiles (Q1, Q2, Q3 and Q4) which correspond respectively to (25%, 50%, 75%, 100%) of the data.
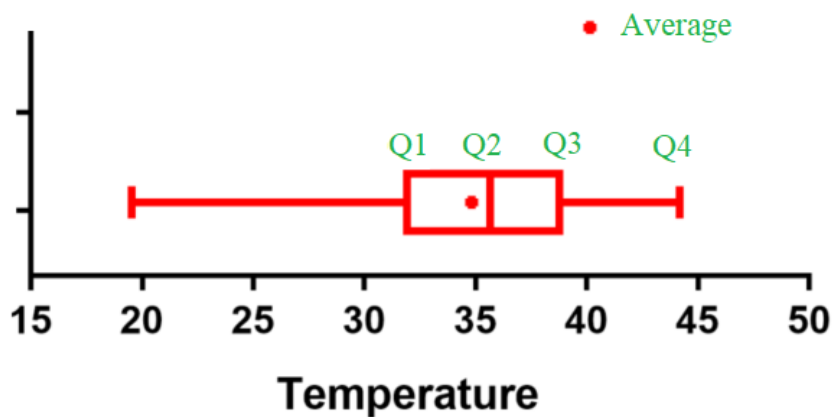
Figure 5-19 Box plot indicating the average value and the different quartiles

5.4 Results

To investigate the effect of phase change material incorporated with a windcatcher, different models with different locations of PCM have been used. Experiments have been conducted when the acrylic chamber is empty and also when it contains PCM sheets.

The following models have been investigated:
1. No PCM: chamber empty
2. PCM Walls only
3. PCM Floor and walls
4. PCM Full: PCM found on floor, ceiling and walls
5. PCM Full + windcatcher: PCM found on floor, ceiling, walls and the windcatcher's inlet channel.

Values for temperature, humidity and pressure were recorded by the BME sensors during operation of the models mentioned above. Most of the experiments lasted at least 5 hours each.

During the discharging process, the hot box fan was operated with two different stages (stage 1 and stage 2) and at maximum speed (100%) of the Hot Box fan. The chamber was also located at two different locations, the first location with a distance between the duct's exit and the windcatchers inlet of 850 mm as shown in figure 5-17, and the second location with a minimum distance between the duct outlet and the windcatcher's inlet of 400 mm.

Table 5-2 provides the total flow rate Q (m^3/s) and the average velocity (m/s) calculated at the windcatchers inlet for the two locations of the chamber. It is noted that with the hot box fan speed of 100% the windcatcher captures more air (0.0382 m^3/s) when the chamber is closer (at 400 mm distance) to the duct with an increase of about 6.5 % compared to the flow rate captured by the windcatcher (0.0357 m^3/s) when the chamber is at 800 mm.

Fan speed (%)	Average velocity through windcatcher (m/s)		Total Flow Rate Q through windcatcher (m^3/s)	
	Room at 850 mm	Room at 400 mm	Room at 850 mm	Room at 400 mm
100%	1.4	1.49	0.0357	0.0382

Table 5-2 Total flow rate Q and average velocity through the windcatcher during discharging

During the charging process (solidification of PCM), a small desk fan with 15 cm diameter was used to direct the cold air into the chamber through the wind catcher. The small fan was placed about 300 mm away from the windcatcher's inlet as shown in figure 5-18. During charging the total flow rate Q captured by the windcatcher was 0.0145 m³/s and the average velocity was 0.56 m/s.

5.4.1 Temperature variation during discharging process with stage1 heating element

To investigate the effect of the discharging process on the temperature inside the chamber with heating element at stage 1 and a fan speed of 100% all the five models have been used, and the results obtained and compared. The experiments lasted at least five hours for each of the models.

Table 5-3 shows the temperatures recorded every 15 minutes when the chamber is empty (No PCM) by the different BME sensors as well as the average of each sensor and the average inside the room. Figure 5-20 shows the plot of the temperature versus the time of the experiment from the start and till after 135 minutes with No PCM.

No PCM	Temperature, °C								
	Amb H1	In C8	Out E7	Lf Fr G4	Lf Bck F9	Rt Fr B6	Rt Bck D10	Rt Mid A5	Room Average
start	20.70	20.72	20.32	20.22	20.18	20.46	20.32	20.45	20.38
15 min	23.76	28.84	25.82	25.35	24.48	25.31	24.75	25.32	25.70
30 min	24.60	29.86	27.17	26.74	26.07	26.72	26.24	26.73	27.08
45 min	25.22	30.39	28.06	27.66	27.00	27.67	27.20	27.67	27.95
60 min	25.73	30.96	28.81	28.46	27.80	28.46	28.04	28.45	28.71
75 min	26.21	31.39	29.45	29.11	28.56	29.11	28.75	29.12	29.36
90 min	26.60	31.77	29.93	29.64	29.17	29.62	29.26	29.64	29.86
105 min	26.96	32.04	30.35	30.05	29.53	30.05	29.73	30.05	30.26
120 min	27.34	32.30	30.69	30.41	29.98	30.41	30.09	30.41	30.61
135 min	27.46	32.47	30.88	30.61	30.12	30.60	30.31	30.61	30.80
150 min	27.66	32.77	31.11	30.80	30.24	30.80	30.36	30.80	30.98
165 min	27.85	32.05	31.31	30.95	30.36	30.95	30.42	30.95	31.00
180 min	28.02	32.33	31.52	31.15	30.47	31.15	30.47	31.15	31.18
195 min	28.23	32.50	31.71	31.30	30.62	31.30	30.62	31.30	31.34
210 min	28.45	32.82	31.93	31.44	30.77	31.44	30.77	31.44	31.52
225 min	28.65	33.05	32.11	31.59	30.91	31.59	30.91	31.59	31.68

240 min	28.74	33.34	32.33	31.73	31.05	31.73	31.05	31.73	31.85
255 min	28.94	33.54	32.53	31.93	31.25	31.93	31.25	31.93	32.05
270 min	29.14	33.74	32.73	32.13	31.45	32.13	31.45	32.13	32.25
285 min	29.34	33.94	32.93	32.33	31.65	32.33	31.65	32.33	32.45
average	26.98	31.54	30.08	29.68	29.08	29.69	29.18	29.69	29.85

Table 5-3 Temperature readings for empty chamber (No PCM) with stage 1 heating element
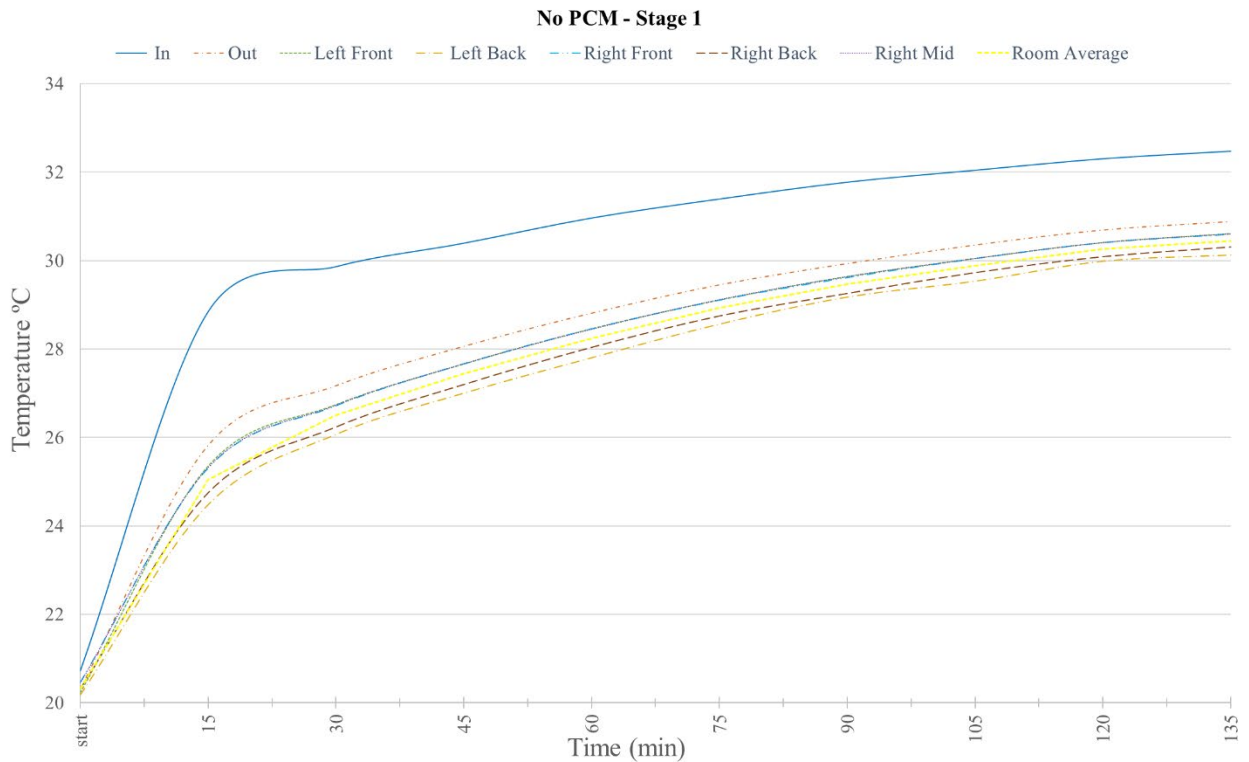
Figure 5-20 Temperature plots for empty chamber (No PCM) with stage 1 heating element

Figures 5-21 till 5-24 show the plots of the temperature versus the time of the experiment for the remaining models. The tables related to these plots are similar in structure to Table 5-3 and are found in the appendix, refer to tables A-1 to A-4. As the plots of the temperatures versus time are all similar to Figure 5-20 for the whole time of the experiments, each of these plots covered a certain range of time in order to show clearly the variations of temperatures.

Figure 5-21 shows the temperature for the chamber with PCM Walls only from 60 minutes after the start till 210 minutes. Figure 5-22 shows the temperature for the chamber with PCM Floor and Walls from the start till after 45 minutes. Figure 5-23 shows the temperature for the chamber with PCM Full from 150 minutes after the start till 210 minutes. Figure 5-24 shows

the temperature for the chamber with PCM Full plus windcatcher from the start till 180 minutes.
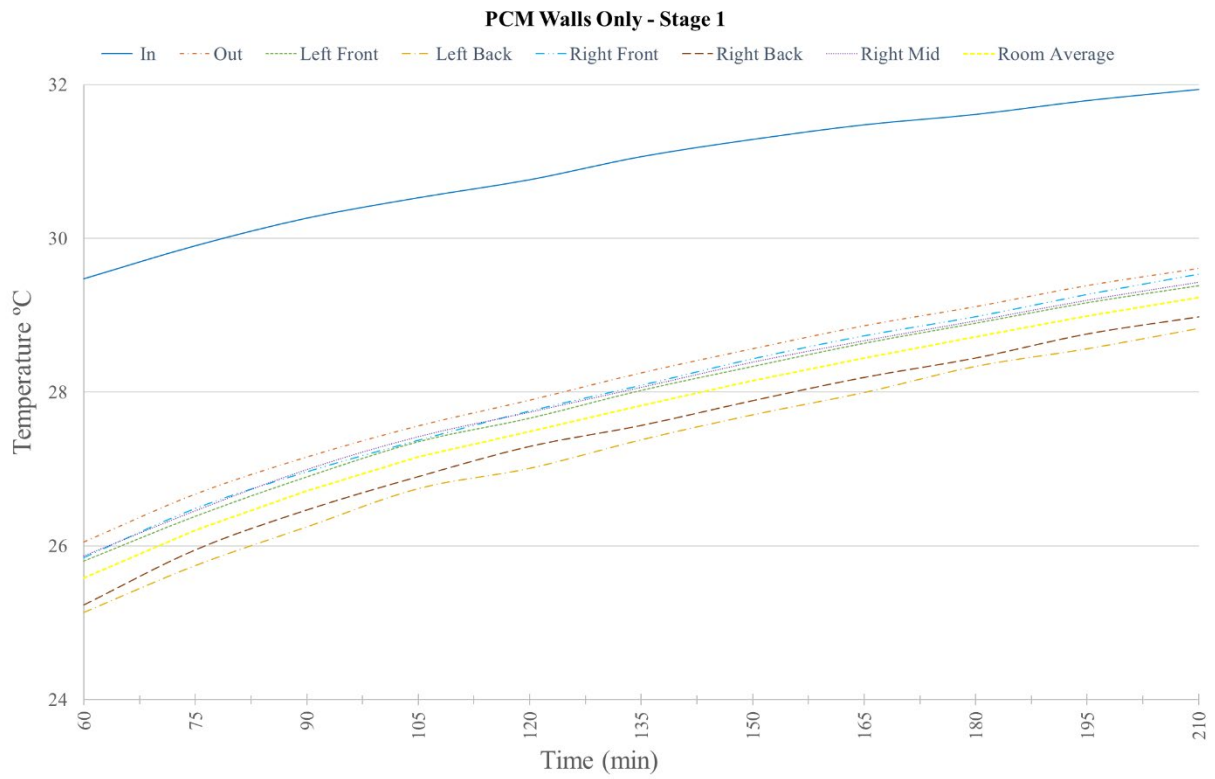
Figure 5-21 Temperature plots for chamber with PCM Walls Only and with stage 1 heating element
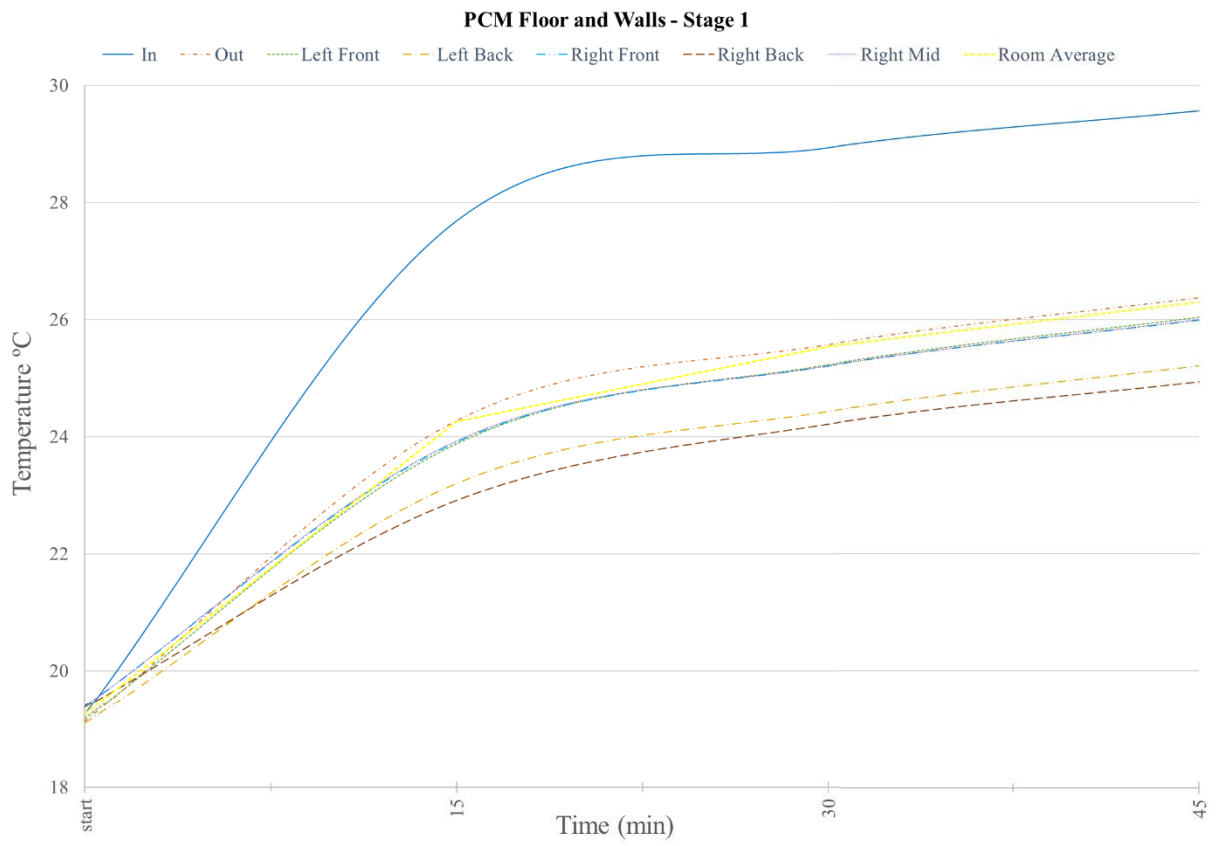
Figure 5-22 Temperature plots for chamber with PCM Floor and Walls and with stage 1 heating element
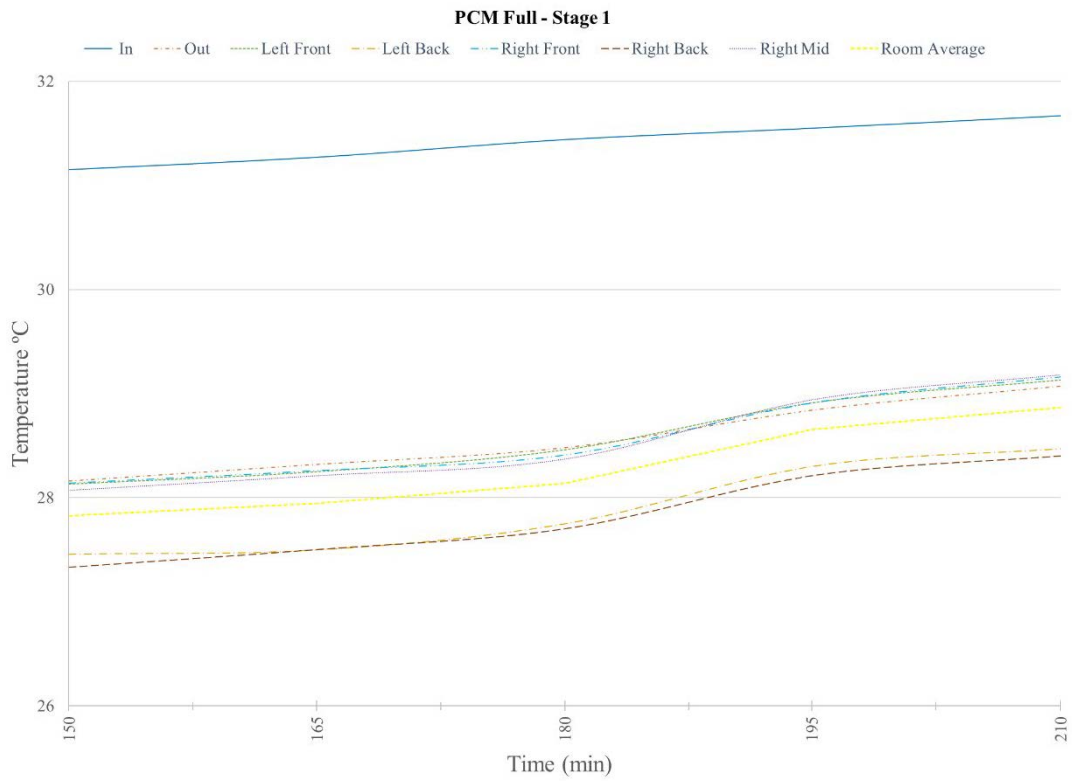
Figure 5-23 Temperature plots for chamber with PCM Full and with stage 1 heating element
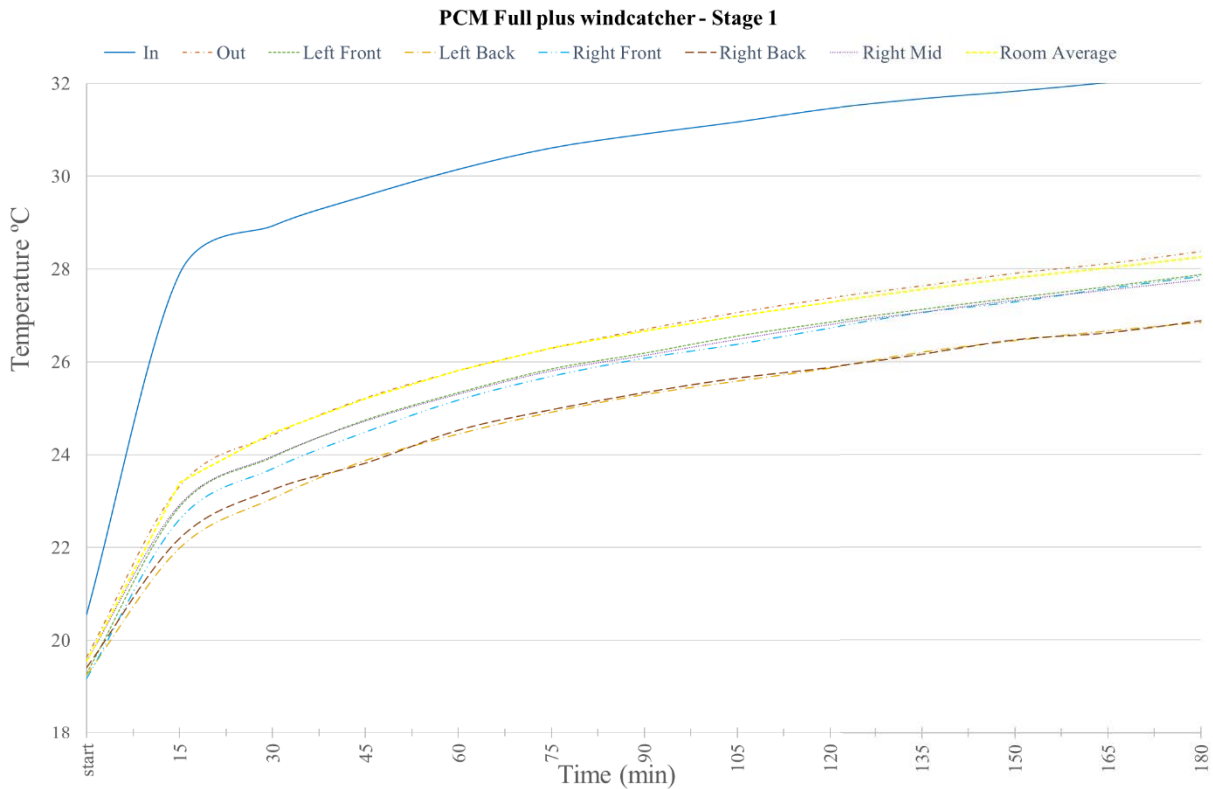
Figure 5-24 Temperature plots for chamber with PCM Full plus windcatcher and with stage 1 heating element

The above figures 5-21 till 5-24 indicate that the temperatures recorded at the front (Left front and right front) are higher than the temperatures recorded at the back (Left back and right back). This is noted for all the models with PCM and the highest difference is observed for the model with PCM full plus windcatcher, however this variation is not observed for the model with No PCM (Figure 5-20).

Table 5-4 summarizes the average temperatures in the chamber for the different models. It shows the difference in the average temperature (in ºC) between the different models with respect to the model with (No PCM) as well as the corresponding difference in percentage. Figure 5-25 shows the average temperature plots inside the chamber for the different models studied from the start till 285 minutes. The average temperature for the model with empty chamber is the higher trace while the lower trace is for the model with PCM Full plus windcatcher.

Temperature, °C	No PCM	PCM Walls Only	PCM Floor and Walls	PCM Full	PCM Full + windcatcher
Room average	29.85	27.54	28.05	27.74	27.07
Difference °C	---	2.31	1.80	2.11	2.78
Difference %	---	7.74%	6.04%	7.08%	9.33%

Table 5-4 Average temperature in the chamber for the different models with stage 1 heating element
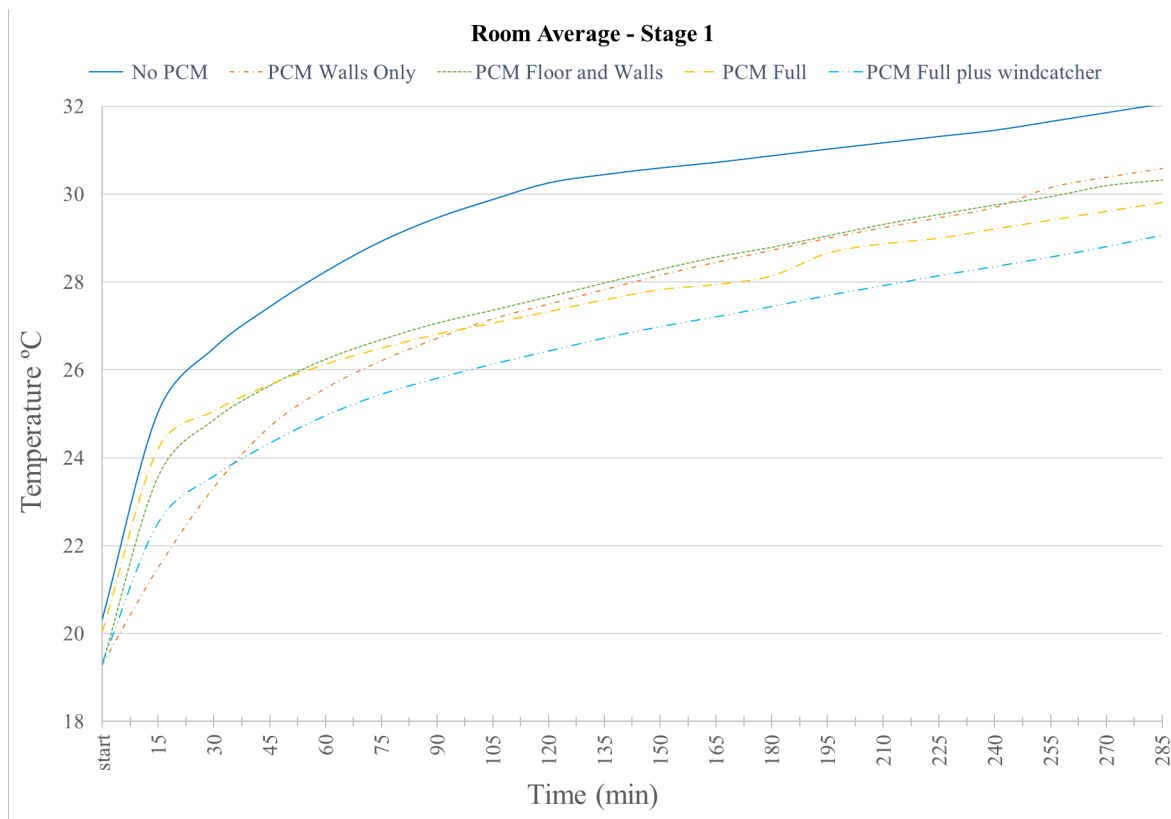
Figure 5-25 Average temperature plots of the Room for all the models with stage 1 heating element.

It is noted that with all the models containing PCM the average temperature inside the chamber drops compared to the model with No PCM. The difference ranges from 1.8 ºC (PCM Floor and Walls) and up to 2.78 ºC (PCM Full + windcatcher).

Comparing the model with (PCM Full + windcatcher) with the other models, we observe about 0.7 ºC reduction in temperature with respect to the model with PCM Full while the reduction in average temperature with respect to No PCM is about 2.75 ºC.

Figure 5-26 summarizes the results showing the box plot for the five models. It shows the average temperature inside the chamber as well as the minimum and maximum temperatures and the corresponding quartiles values. The model with the PCM located in the floor, ceiling and walls as well as in the windcatcher's inlet channel has shown the best performance compared to the other models and the reduction of average temperatures observed is significant with respect to the model with No PCM. This reduction of 2.78 ºC is equivalent to 9.33 % difference as shown in table 5-8.
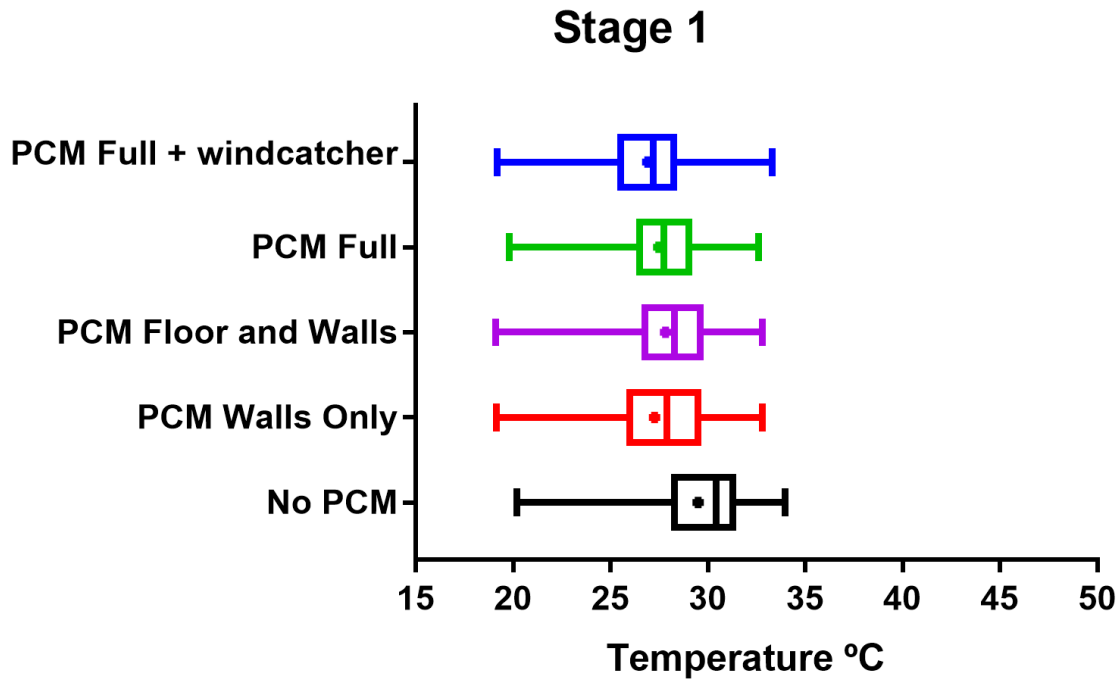
Figure 5-26 Box plot of the five models with stage 1 heating element.

Figure 5-27 shows the distribution of the temperatures with respect to the time of the experiment (frequency) for each of the models. It is evident that all of the models with PCM has shown lower temperature values compared to the model with No PCM (shown in black in figure 5-27). At 50% of the total time which corresponds to 2.5 hours the average temperature of the model with NO PCM is approximately 30.5 ºC while the average temperature of the model with PCM full + windcatcher is approximately 27 ºC.

At 25% of the total time which corresponds to 1.25 hours the average temperature of the model with NO PCM is approximately 28 ºC while the average temperature of the model with PCM full + windcatcher is approximately 25.5 ºC. It is also clear that the model with PCM full + windcatcher shows the best performance as its corresponding graph (shown in blue in figure 5-27) is the farthest with respect to No PCM.
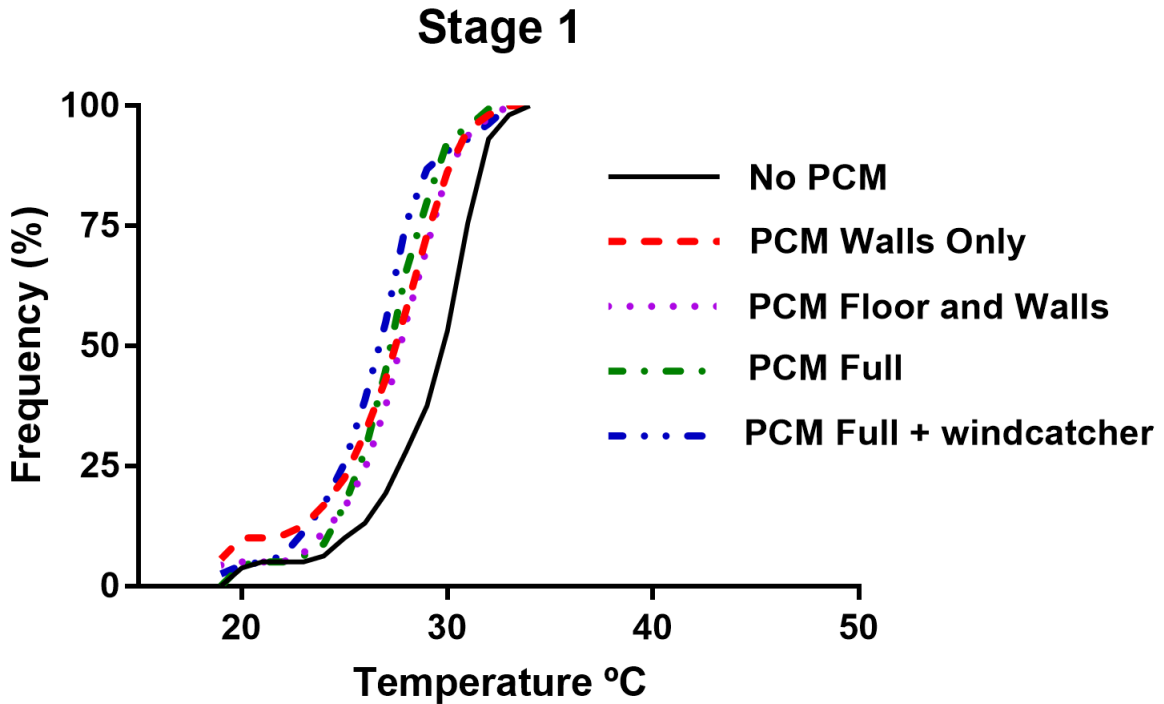
Figure 5-27 Distribution of temperatures for the five models with stage 1 heating element

5.4.2 Temperature variation during discharging process with stage 2 heating element

To investigate the effect of the discharging process on the temperature inside the chamber with heating element at stage 2 and a fan speed of 100% all the five models have been used, and the results obtained and compared. The experiments lasted at least five hours for each of the models. The tables showing the results of these experiments are similar in structure to Table 5-3 and are found in the appendix, refer to Tables A-5 to A-9.

Figure 5-28 shows the plot of the temperature versus the time of the experiment from the start and till after 135 minutes with empty chamber (No PCM).
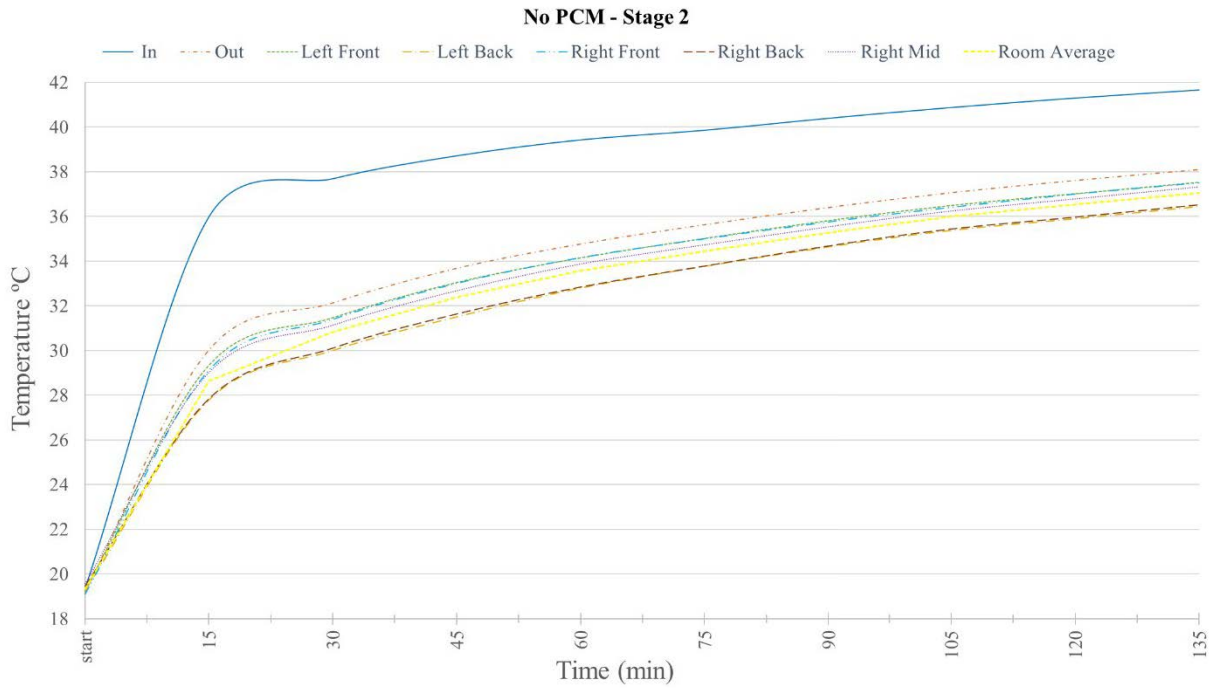
Figure 5-28 Temperature plots for empty chamber (No PCM) with stage 2 heating element

Figures 5-29 till 5-32 show the plots of the temperature versus the time of the experiment for the remaining models. As the plots of the temperatures versus time are all similar to Figure 5-29 for the whole time of the experiments, each of these plots covered a certain range of time in order to show clearly the variations of temperatures.

Figure 5-29 shows the temperature for the chamber with PCM Walls only from 60 minutes after the start till 210 minutes. Figure 5-30 shows the temperature for the chamber with PCM Floor and Walls from the start till after 45 minutes. Figure 5-31 shows the temperature for the chamber with PCM Full from 150 minutes after the start till 210 minutes. Figure 5-32 shows the temperature for the chamber with PCM Full plus windcatcher from the start till 180 minutes.
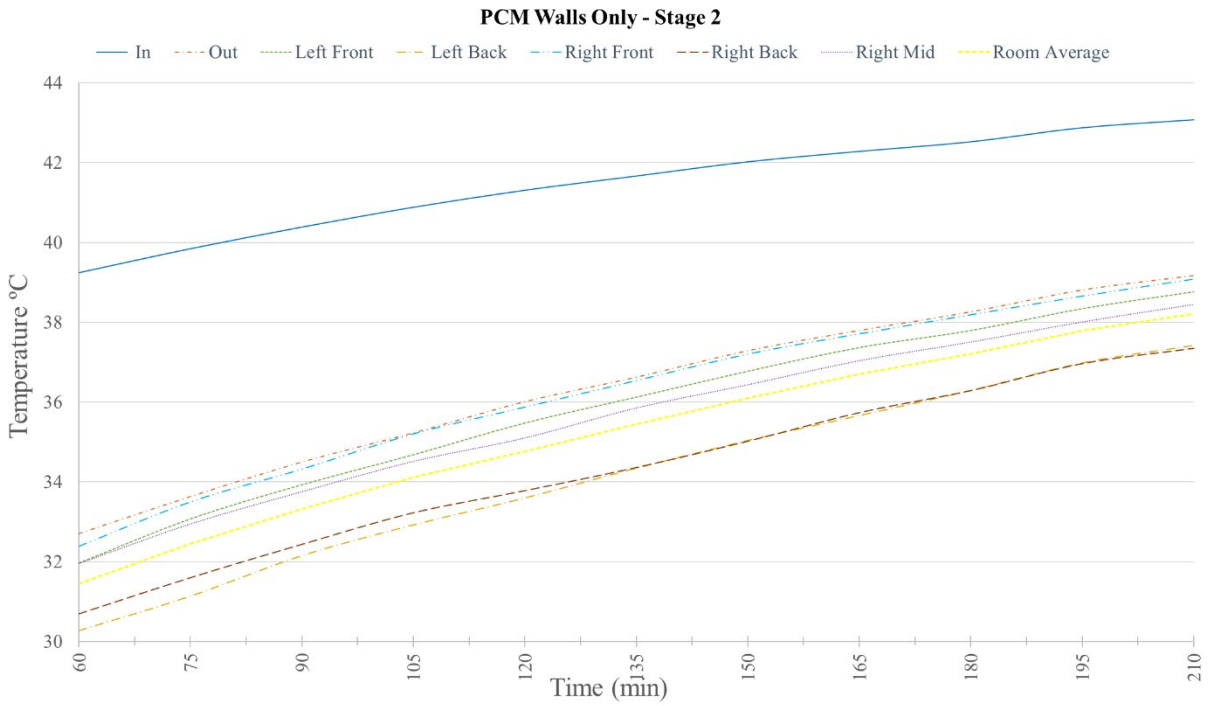
Figure 5-29 Temperature plots for chamber with PCM Walls Only and with stage 2 heating element

Figure 5-30 Temperature plots for chamber with PCM Floor and Walls and with stage 2 heating element

212

Figure 5-31 Temperature plots for chamber with PCM Full and with stage 2 heating element
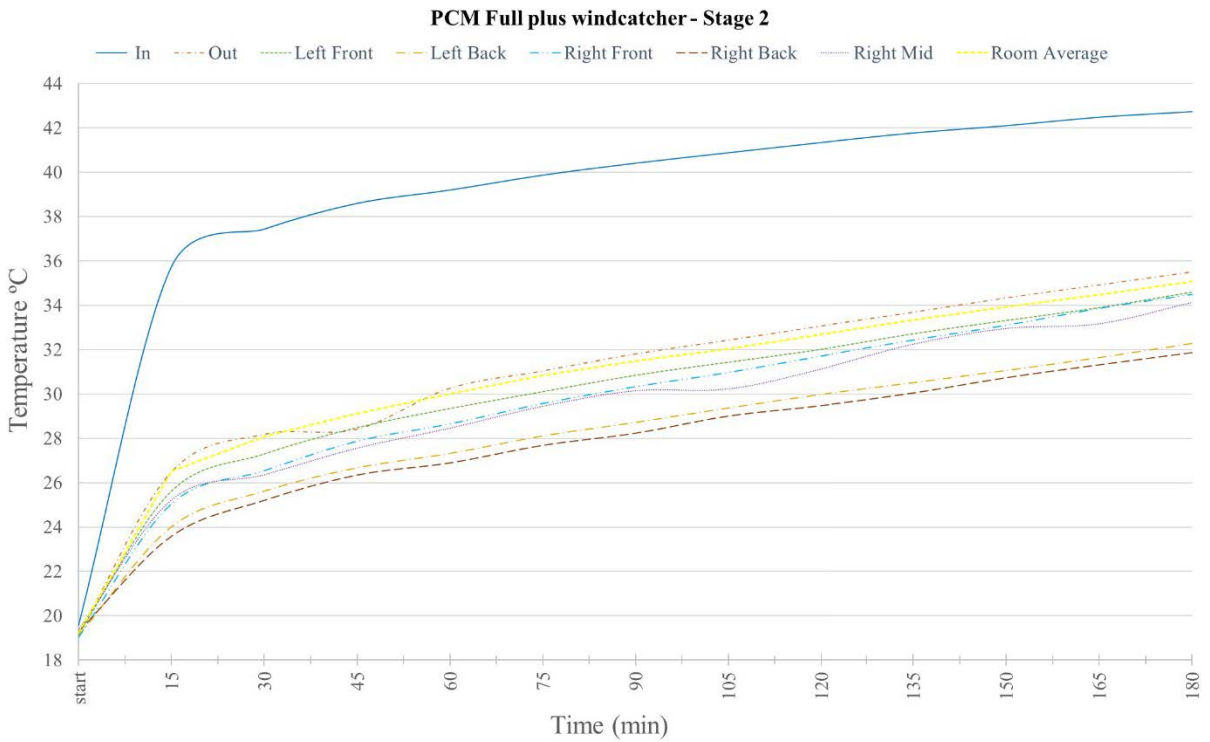
Figure 5-32 Temperature plots for chamber with PCM Full plus windcatcher and with stage 2 heating element

213

The above figures 5-29 till 5-32 indicate that the temperatures recorded at the front (Left front and right front) are higher than the temperatures recorded at the back (Left back and right back). This is noted for all the models with PCM and the highest difference is observed for the model with PCM full plus windcatcher, however this variation is not observed for the model with No PCM (Figure 5-28). This observation is consistent with the results founds when the experiment was conducted with stage 1 heating element.

Table 5-5 summarizes the average temperatures in the chamber for the different models. It shows the difference in the average temperature (in °C) between the different models with respect to the model with (No PCM) as well as the corresponding difference in percentage.

Temperature, °C	No PCM	PCM Walls Only	PCM Floor and Walls	PCM Full	PCM Full + windcatcher
Room average	36.52	35.61	36.33	35.32	32.90
Difference °C	---	0.91	0.19	1.20	3.61
Difference %	---	2.49%	0.52%	3.28%	9.90%

Table 5-5 Average temperature in the chamber for the different models with stage 2 heating element

It is noted that with all the models containing PCM the average temperature inside the chamber drops compared to the model with No PCM. The difference is about 1 °C for the model with PCM Walls only and for PCM Full. No significance difference has been observed for the PCM Floor and Walls model compared to No PCM, the reason for this insignificant difference is to be investigated. It might be due to the strong buoyancy effects in the room with high temperature of the air supply generated by stage 2 of the fan. Comparing the model PCM Full + windcatcher with the other models, we observe that it has provided the largest reduction in temperature (3.61 °C) with respect to the model with No PCM.

Figure 5-33 summarizes the results showing the box plot for the five models. It shows the average temperature inside the chamber as well as the minimum and maximum temperatures and the corresponding quartile values. The model with the PCM located in the floor, ceiling and walls as well as in the windcatcher has shown the best performance compared to the other models and the reduction of average temperatures observed is significant with respect to the

model with No PCM. This reduction of 3.61 ºC is equivalent to 9.90 % difference as shown in table 5-5.

Stage 2

Figure 5-33 Box plot of the five models with stage 2 heating element

Figure 5-34 shows the distribution of the temperatures with respect to the time of the experiment for each of the models. It is evident that all of the models with PCM has shown lower temperature values compared to the model with No PCM (shown in black in figure 5-34). At 50% of the total time which corresponds to 2.5 hours, the average temperature of the model with NO PCM is approximately 38 ºC while the average temperature of the model with PCM full + windcatcher is approximately 32 ºC.

At 25% of the total time which corresponds to 1.25 hours the average temperature of the model with NO PCM is approximately 33 ºC while the average temperature of the model with PCM full + windcatcher is approximately 28 ºC.

It is also clear that the model with PCM full + windcatcher shows the best performance as its corresponding graph (shown in blue in figure 5-24) is the farthest with respect to No PCM.

Figure 5-34 Distribution of temperatures for the five models with stage 2 heating element

5.4.3 Temperature variation during discharging process with stage1 heating element and room location closer to fan

To investigate the effect of the discharging process on the temperature inside the chamber located closer to the hot box fan at 400 mm with heating element at stage 1, two models have been used (No PCM and PCM full + windcatcher), and the results obtained and compared. The experiments lasted at least four hours for each of the models. The tables showing the results of these experiments are similar in structure to Table 5-3 and are found in the appendix, refer to Tables A-10 and A-11.

Figure 5-35 shows the plot of the temperature versus the time of the experiment from the start and till after 45 minutes with empty chamber (No PCM). Figure 5-36 shows the temperature for the chamber with PCM Full plus windcatcher from the start also till 45 minutes.
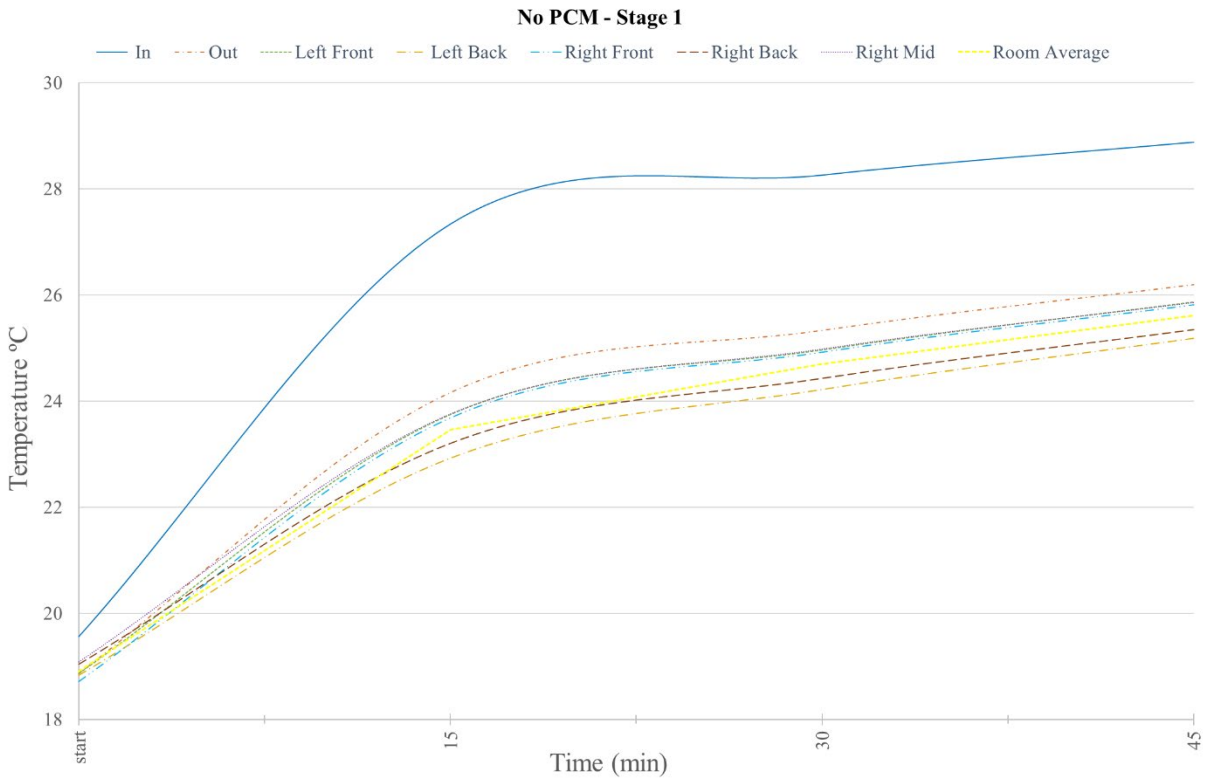
Figure 5-35 Temperature plots for empty chamber (No PCM) located closer to fan with stage 1 heating element
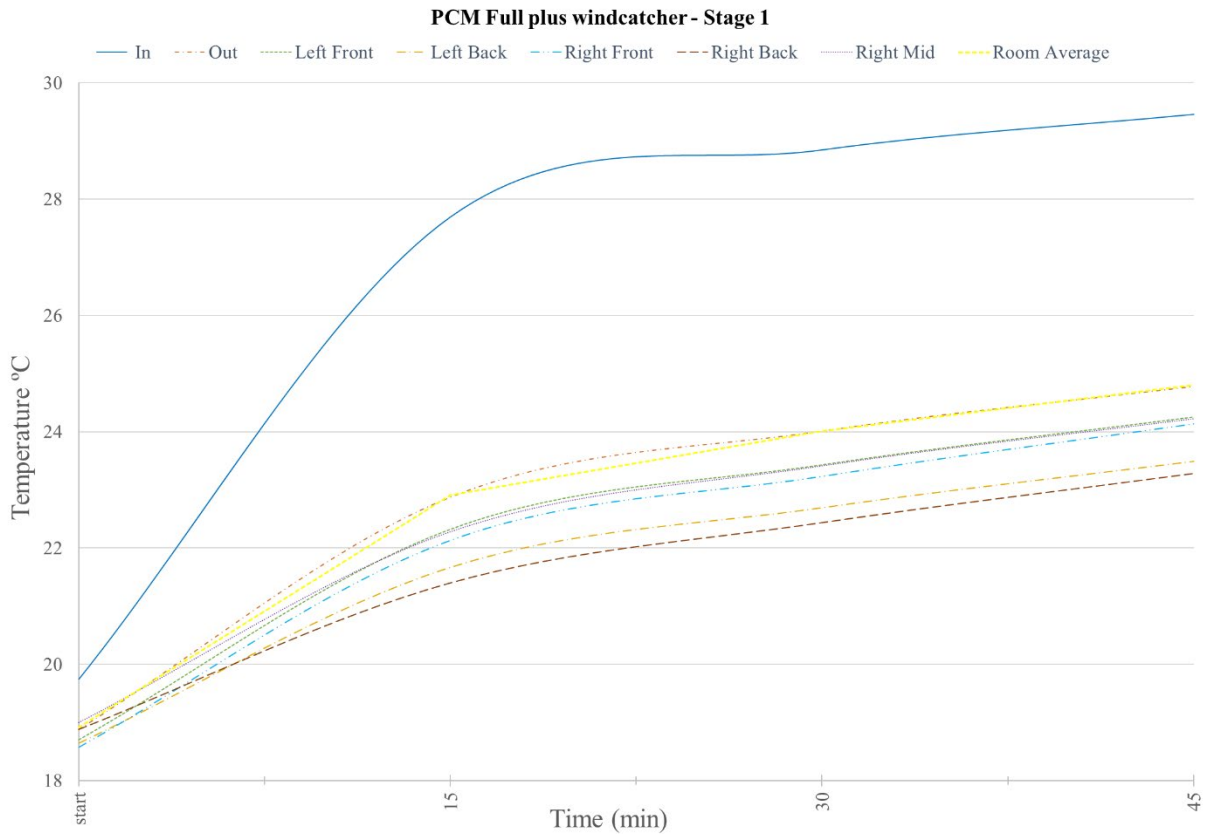
Figure 5-36 Temperature plots for chamber with PCM Full plus windcatcher located closer to fan and with stage 1 heating element

Table 5-6 summarizes the average temperatures in the chamber for the different models. It shows the difference in the average temperature (in ℃) between the two models as well as the corresponding difference in percentage. Figure 5-37 shows the average temperature plots inside the chamber for the two models studied from the start till 240 minutes. The average temperature for the model with empty chamber is the higher trace while the lower trace is for the model with PCM Full plus windcatcher.

Temperature, °C	No PCM	PCM Full + windcatcher
Room average	27.66	26.21
Difference °C	---	1.45
Difference %	---	5.24%

Table 5-6 Average temperature in the chamber located closer to fan with stage 1 heating element
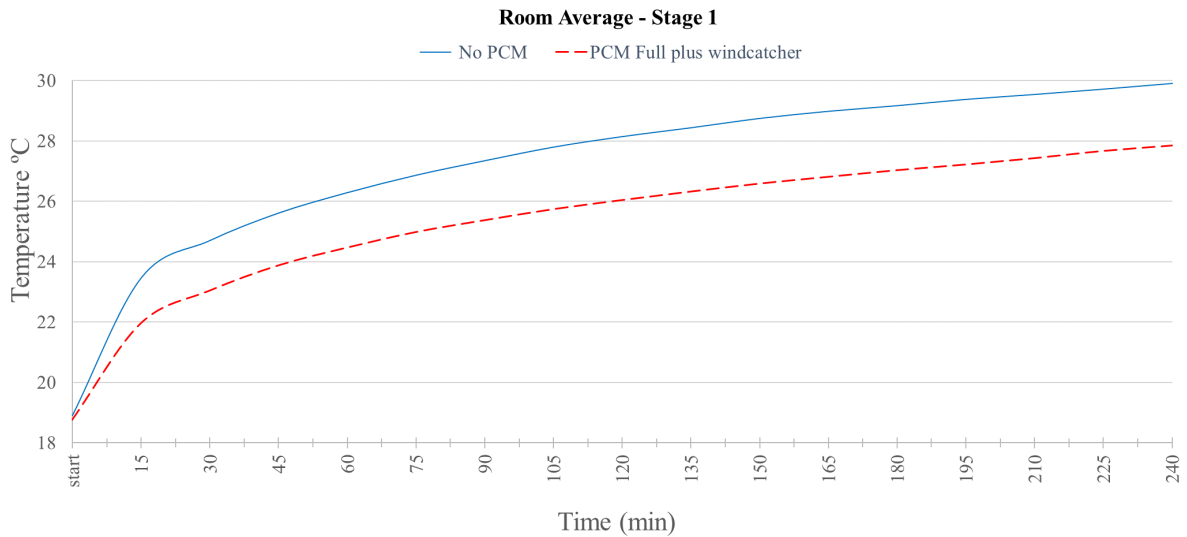
Figure 5-37 Average temperature plots of the room located closer to fan with stage 1 heating element.

Figure 5-38 summarizes the results showing the box plot for the two models. It shows the average temperature inside the chamber as well as the minimum and maximum temperatures and the corresponding quartile values. The model with the PCM located in the floor, ceiling and walls as well as in the wind tunnel has provided a reduction of average temperature of about 1.45 ºC which is equivalent to 5.24 % difference as shown in table 5-6.
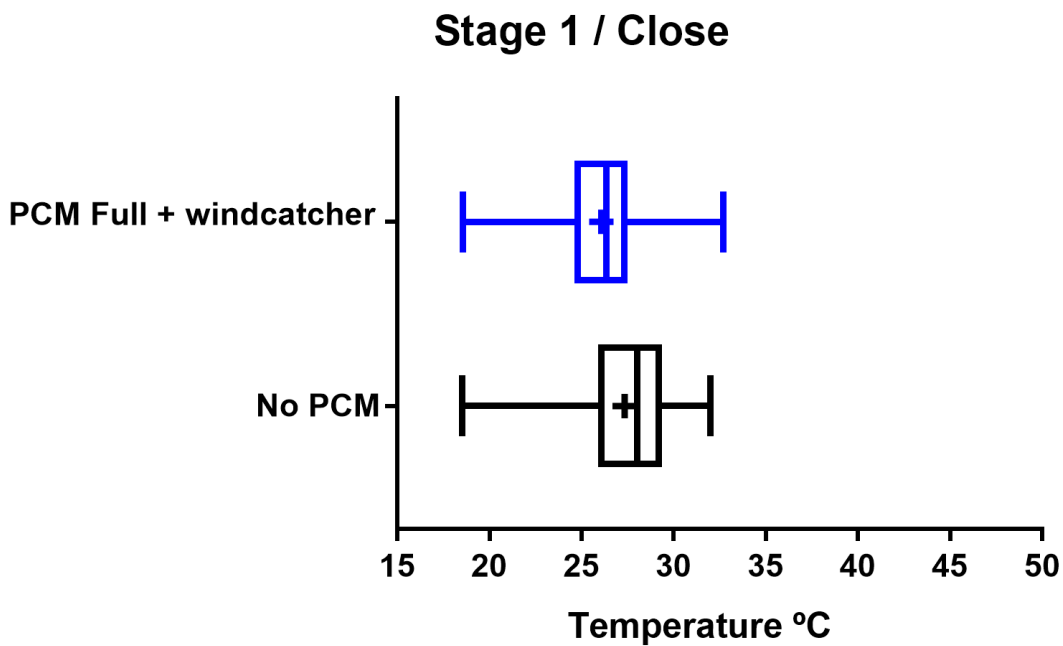
Figure 5-38 Box plot of the two models with stage 1 heating element and room close to fan

Figure 5-39 shows the distribution of the temperatures with respect to the time of the experiment for each of the models. It is evident that the model with PCM plus windcatcher has shown lower temperature values compared to the model with No PCM. At 50% of the total time which corresponds to 2 hours the average temperature of the model with NO PCM is approximately 27.5 ºC while the average temperature of the model with PCM full + windcatcher is approximately 25.5 ºC.

At 25% of the total time which corresponds to 1 hour the average temperature of the model with NO PCM is approximately 26 ºC while the average temperature of the model with PCM full + windcatcher is approximately 25 ºC.
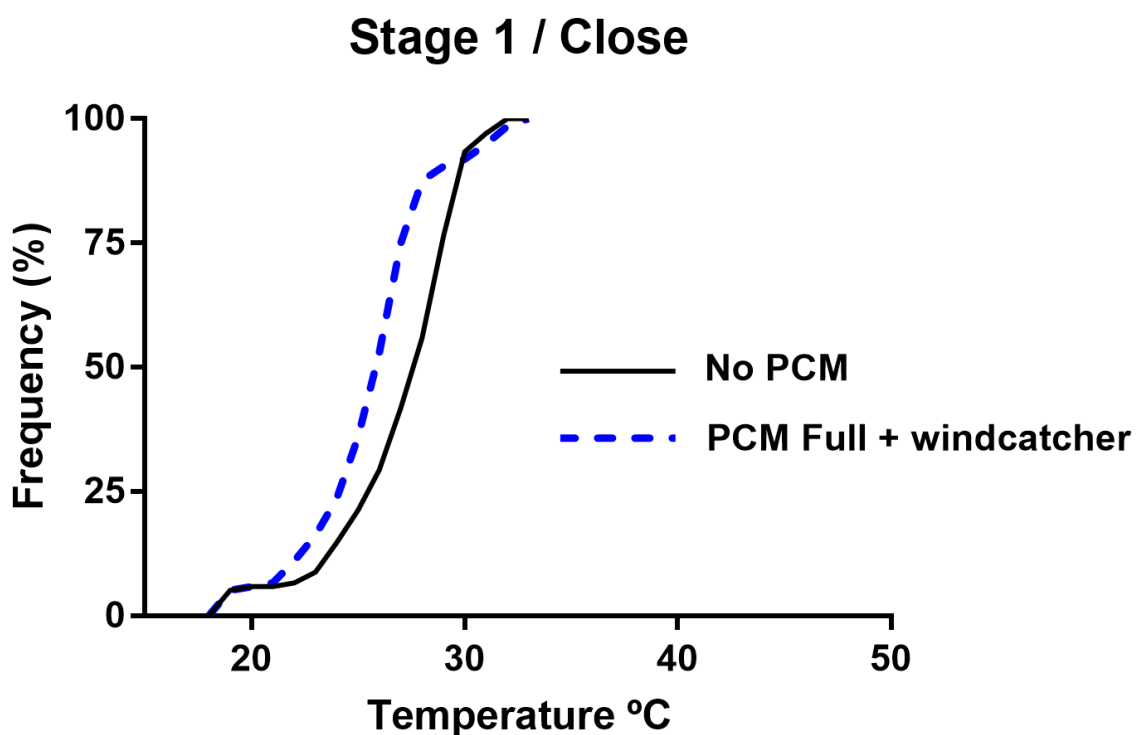
Figure 5-39 Distribution of temperatures for the two models with stage 1 heating element and room located closer to fan

5.4.4 Temperature variation during discharging process with stage2 heating element and room location closer to fan

To investigate the effect of the discharging process on the temperature inside the chamber located closer to the hot box fan at 400 mm with heating element at stage 2, two models have been used (No PCM and PCM full + windcatcher), and the results obtained and compared. The experiments lasted at least four hours for each of the models. The tables showing the results of these experiments are similar in structure to Table 5-3 and are found in the appendix, refer to tables A-12 and A-13.

Figure 5-40 shows the plot of the temperature versus the time of the experiment from 60 minutes after the start and till 150 minutes with empty chamber (No PCM). Figure 5-41 shows the temperature for the chamber with PCM Full plus windcatcher.
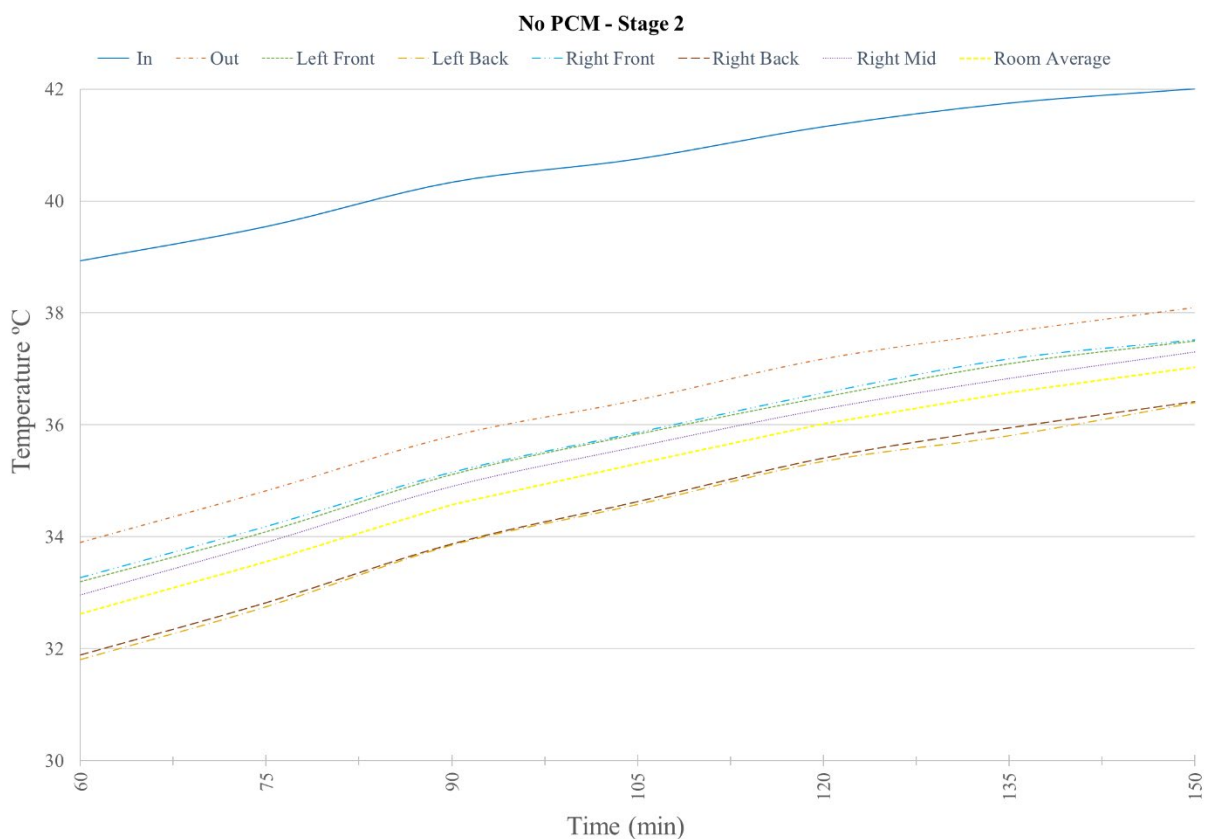
Figure 5-40 Temperature plots for empty chamber (No PCM) located closer to fan with stage 2 heating element
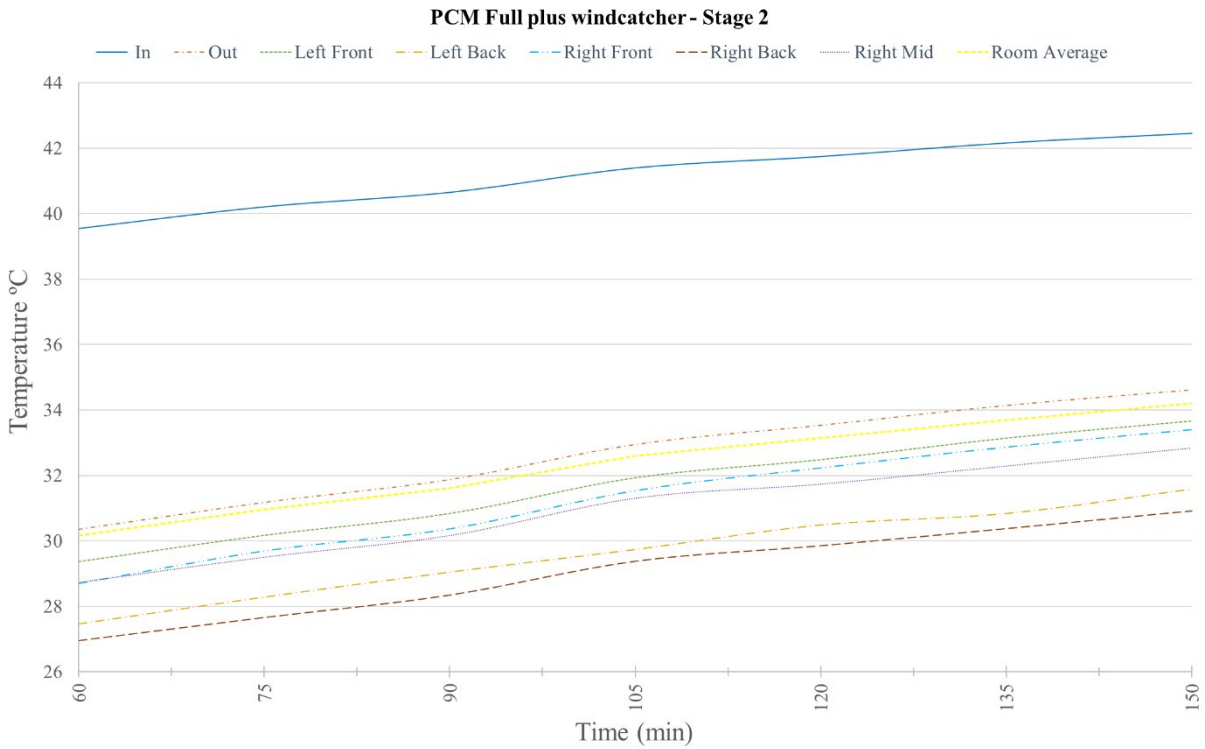
Figure 5-41 Temperature plots for chamber with PCM Full plus windcatcher located closer to fan and with stage 2 heating element

Table 5-7 summarizes the average temperatures in the chamber for the different models. It shows the difference in the average temperature (in ºC) between the two models as well as the corresponding difference in percentage. Figure 5-42 shows the average temperature plots inside the chamber for the two models studied from the start till 240 minutes. The average temperature for the model with empty chamber is the higher trace while the lower trace is for the model with PCM Full plus windcatcher.

Temperature, °C	No PCM	PCM Full + windcatcher
Room average	35.13	32.10
Difference °C	---	3.03
Difference %	---	8.63%

Table 5-7 Average temperature in the chamber located closer to fan with stage 1 heating element
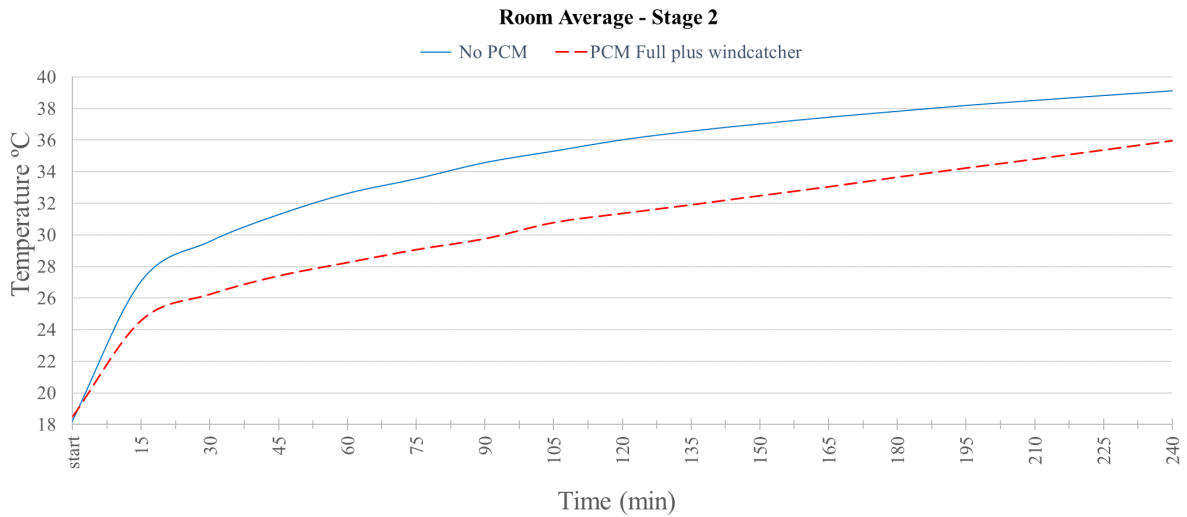
Figure 5-42 Average temperature plots of the room located closer to fan with stage 2 heating element.

Figure 5-43 summarizes the results showing the box plot for the two models. It shows the average temperature inside the chamber as well as the minimum and maximum temperatures and the corresponding quartile values. The model with the PCM located in the floor, ceiling and walls as well as in the windcatcher's inlet channel has provided a reduction of average temperature of about 3.03 ºC which is equivalent to 8.63 % difference as shown in table 5-7.
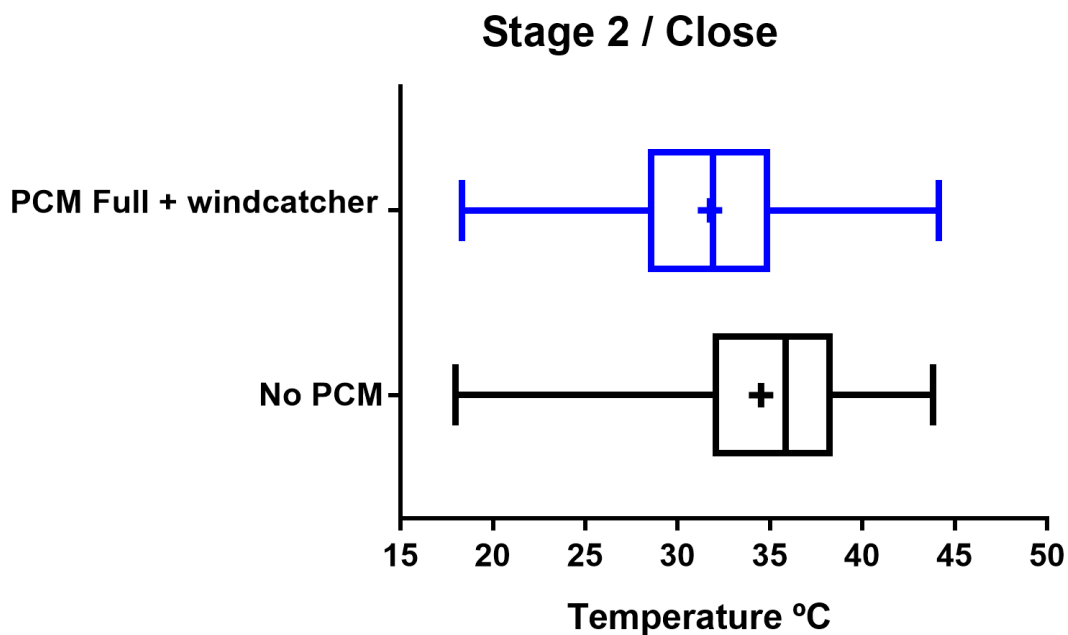
Figure 5-43 Box plot of the two models with stage 2 heating element and room located closer to the fan

Figure 5-44 shows the distribution of the temperatures with respect to the time of the experiment for each of the models. It is evident that the model with PCM plus windcatcher has shown lower temperature values compared to the model with No PCM. At 50% of the total time of the experiment which corresponds to 2 hours the average temperature of the model with NO PCM is approximately 36 ºC while the average temperature of the model with PCM full + windcatcher is approximately 32 ºC.

At 25% of the total time of the experiment which corresponds to 1 hour the average temperature of the model with NO PCM is approximately 31.5 ºC while the average temperature of the model with PCM full + windcatcher is approximately 27.5 ºC.

Figure 5-44 Distribution of temperatures for the two models with stage 2 heating element and room close to fan

5.4.5 Effect of chamber location on temperature variation during discharging process

To investigate the effect of the room location on the discharging process with stage 2 heating elements, two models have been used (No PCM and PCM full + windcatcher) and the temperature inside the chamber was obtained and compared. The experiments lasted at least four hours for each of the models. The room was located far from the duct at 850mm and at a closer distance at 400 mm. These models are represented by figures 5-28 and 5-32 when the room is located at 850 mm distance from the duct and figures 5-40 and 5-41 when the room is closer at 400 mm duct. As indicated in table 5-2, with the hot box fan speed of 100% the windcatcher captures more air (0.0382 m^3/s) when the chamber is closer (at 400 mm distance) to the duct with an increase of about 6.5 % compared to the flow rate captured by the windcatcher (0.0357 m^3/s) when the chamber is at 800 mm. Thus the comparison due to the different locations of the chamber would indicate the effect of different air velocity and total flow rate captured by the windcatcher on the performance of PCM.

Table 5-8 summarizes the average temperatures related to the studied models. It shows the difference in the average temperature (in ºC) between the two models as well as the corresponding difference in percentage.

Temperature, °C	fan far		close fan	
	No PCM	PCM Full + windcatcher	No PCM	PCM Full + windcatcher
Room average	36.52	32.9	35.13	32.1
Difference °C	---	3.62	---	3.03
Difference %	---	9.91%	---	8.63%

Table 5-8 Average temperature in the chamber at both locations with stage 2 heating element

With both locations the model PCM Full + windcatcher has provided a reduction in average temperature more than 3 ºC as shown in table 5-8.
Figure 5-45 summarizes the results showing the related box plot. It shows the average temperature inside the chamber as well as the minimum and maximum temperatures and the corresponding quartile values. It is noted that the differences based on the locations of the room is not significant as the average temperature was in the same range for both locations. This is also shown in figure 5-46 which shows the distribution of the temperatures with respect to the

time of the experiment for each of the models. Figures 5-46 shows that the graphs related to the models with No PCM (red and blue) are close to each while the graphs related to the other models with PCM Full plus windcatcher (black and yellow) are also close to each, which indicates that the effect of changing the location of the chamber with respect to the duct outlet did not have a significant effect on the temperature inside the room and thus on the performance of the PCM. Consequently it is concluded that the variation in the flow rate captured by the windcatcher of about 6.5% did not have any significant effect on the temperature inside the chamber and thus had no effect on the performance of the PCM.
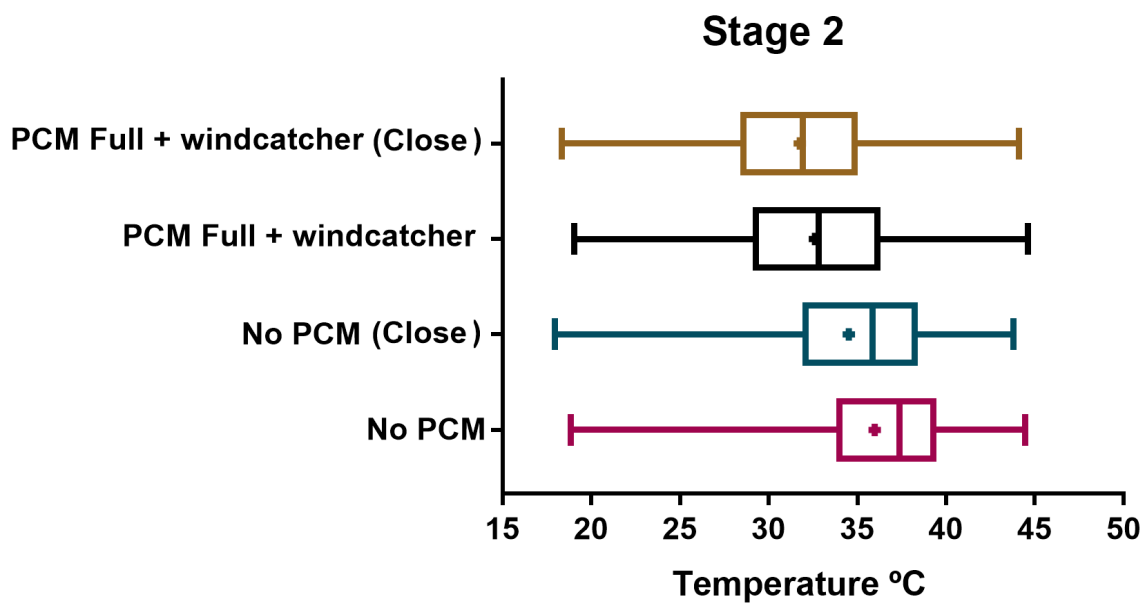
Figure 5-45 Box plot comparing temperatures at two locations of the room with stage 2 heating element
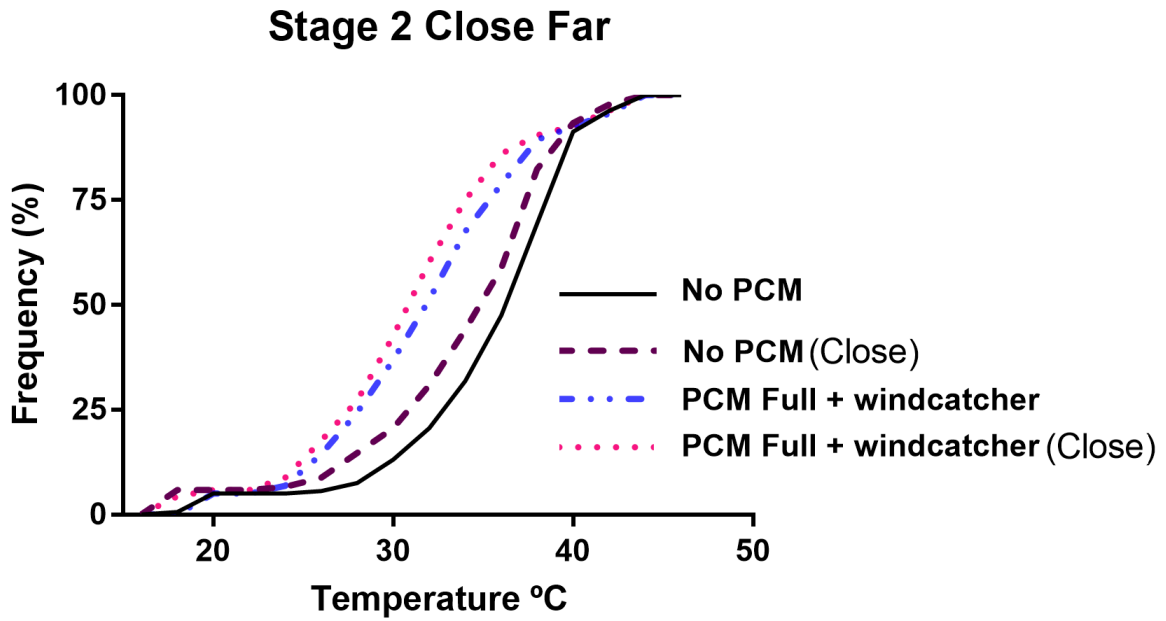
Figure 5-46 Distribution of temperatures at two locations of the room with stage 2 heating element

5.4.6 Humidity variation during discharging process with stage 2 heating element

To investigate the effect of the discharging process on the humidity inside the chamber with heating element at stage 2 and a fan speed of 100% all the five models have been used, and the results obtained and compared. The experiments lasted at least five hours for each of the models. The tables showing the results of these experiments are similar in structure to Table 5-3 and are found in the appendix, refer to Tables A-14 to A-18.

Figure 5-47 shows the plot of the humidity versus the time of the experiment from the start and till after 135 minutes with empty chamber (No PCM).
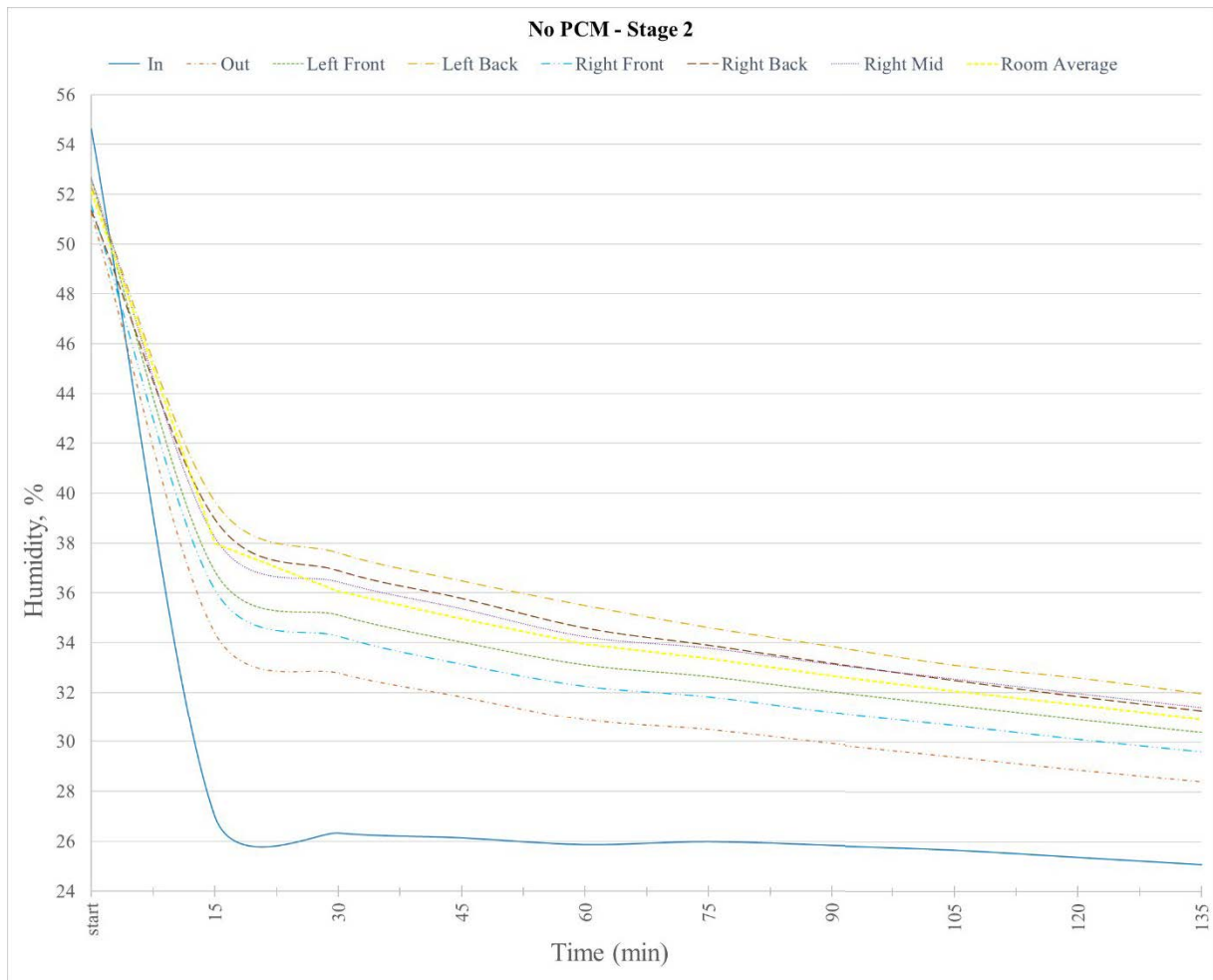
Figure 5-47 Humidity plots for empty chamber (No PCM) with stage 2 heating element

Figures 5-48 till 5-51 show the plots of the humidity versus the time of the experiment for the remaining models. As the plots of the humidity versus time are all similar to Figure 5-47 for the whole time of the experiments, each of these plots covered a certain range of time in order to show clearly the variations of temperatures.

Figure 5-48 shows the temperature for the chamber with PCM Walls only from 60 minutes after the start till 210 minutes. Figure 5-49 shows the temperature for the chamber with PCM Floor and Walls from the start till after 45 minutes. Figure 5-50 shows the temperature for the chamber with PCM Full from 150 minutes after the start till 210 minutes. Figure 5-51 shows the temperature for the chamber with PCM Full plus windcatcher from the start till 180 minutes.
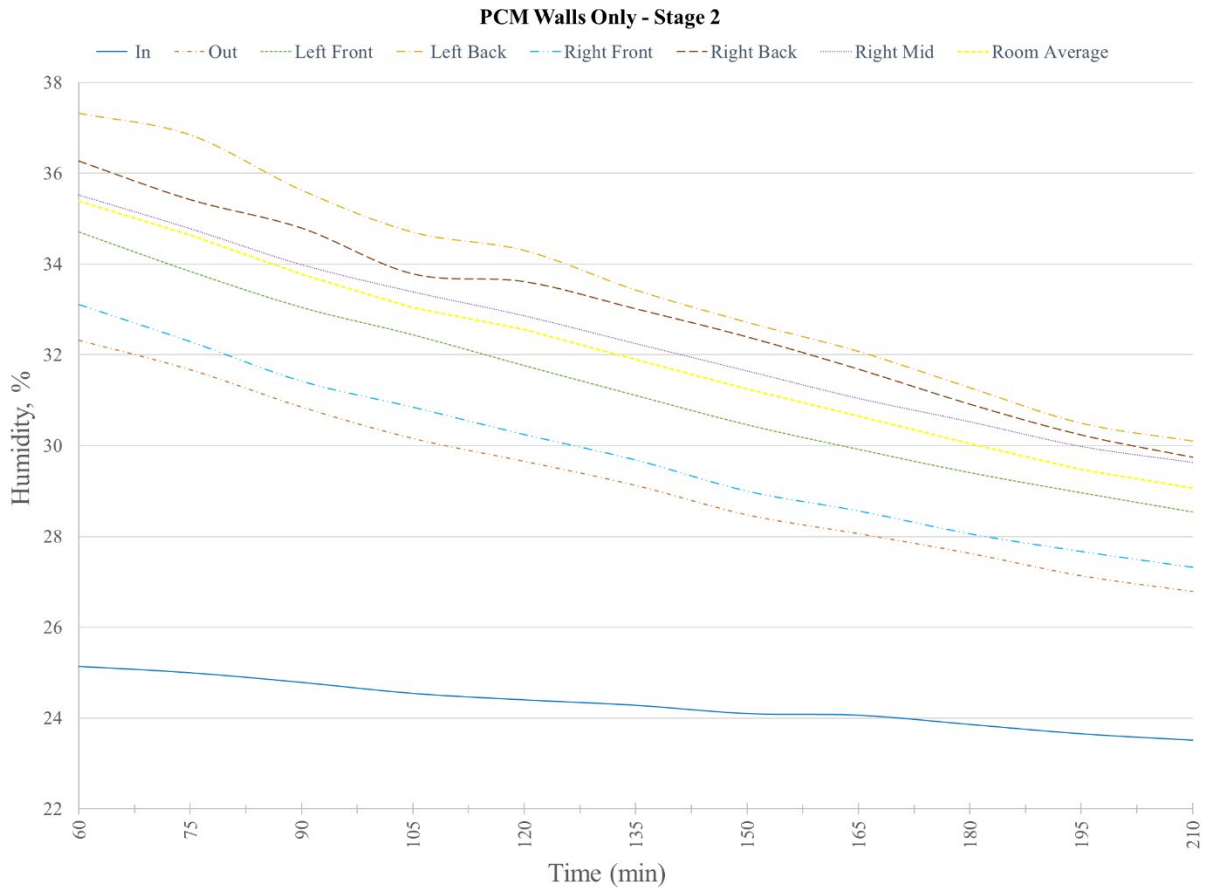
Figure 5-48 Humidity plots for chamber with PCM Walls Only and with stage 2 heating element
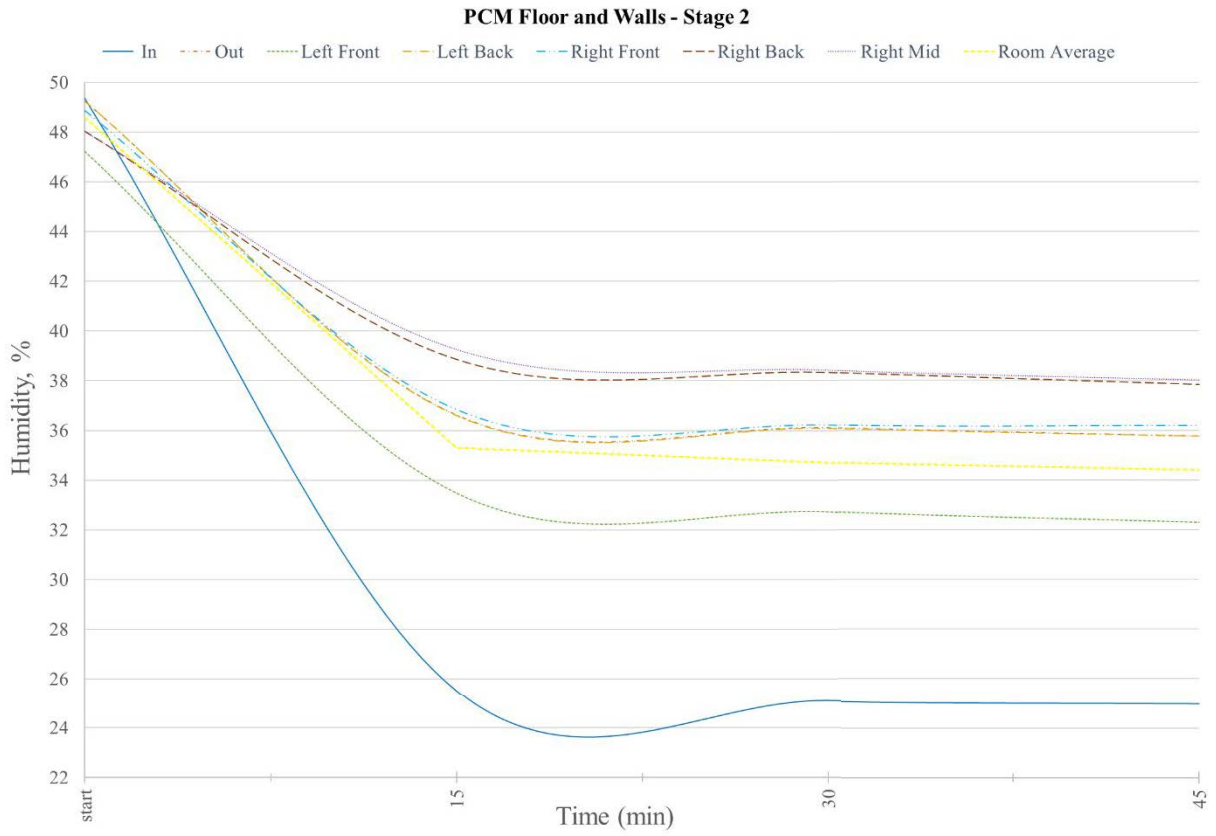
Figure 5-49 Humidity plots for chamber with PCM Floor and Walls and with stage 2 heating element
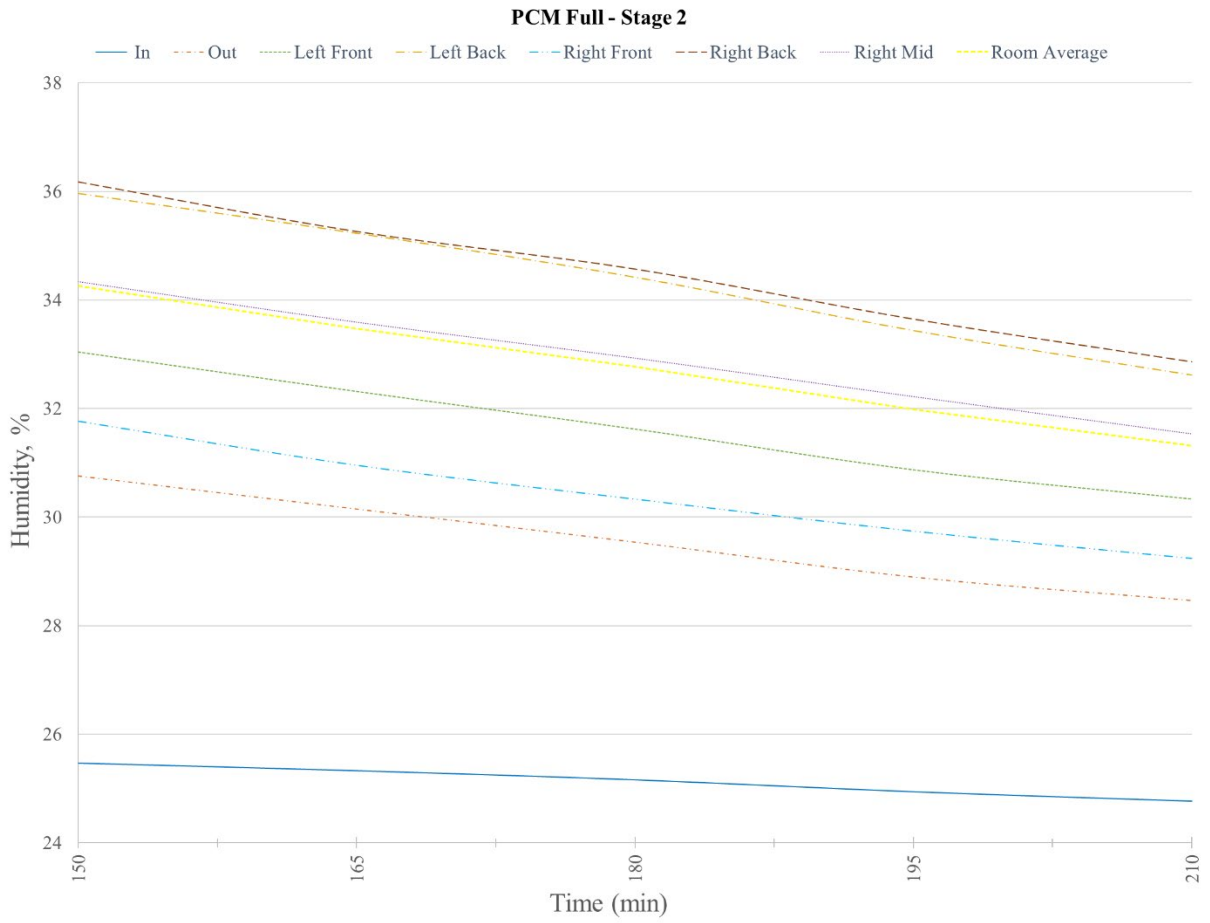
Figure 5-50 Humidity plots for chamber with PCM Full and with stage 2 heating element
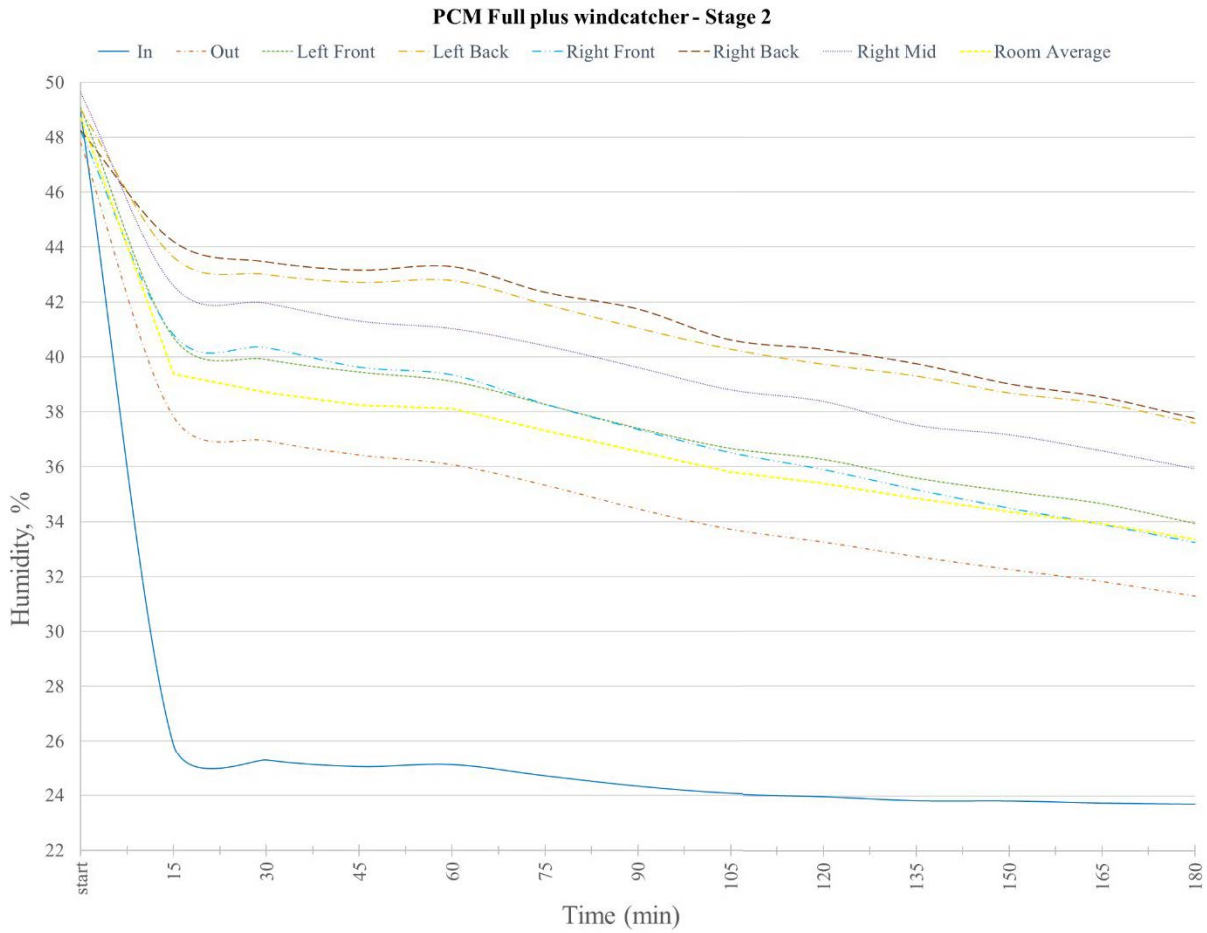
Figure 5-51 Humidity plots for chamber with PCM Full plus windcatcher and with stage 2 heating element

Table 5-9 summarizes the average humidity values in the chamber for the different models. It shows the difference in the average humidity between the different models with respect to the model with (No PCM). Figure 5-52 shows the average temperature plots inside the chamber for the different models studied from the start till 285 minutes. The average temperature for the model with empty chamber is the higher trace while the lower trace is for the model with PCM Full plus windcatcher.

Humidity, %	No PCM	PCM Walls Only	PCM Floor and Walls	PCM Full	PCM Full + windcatcher
Room average	31.12	30.89	32.01	33.65	35
Difference	---	0.23	-0.89	-2.53	-3.88

Table 5-9 Average humidity in the chamber for the different models with stage 2 heating element
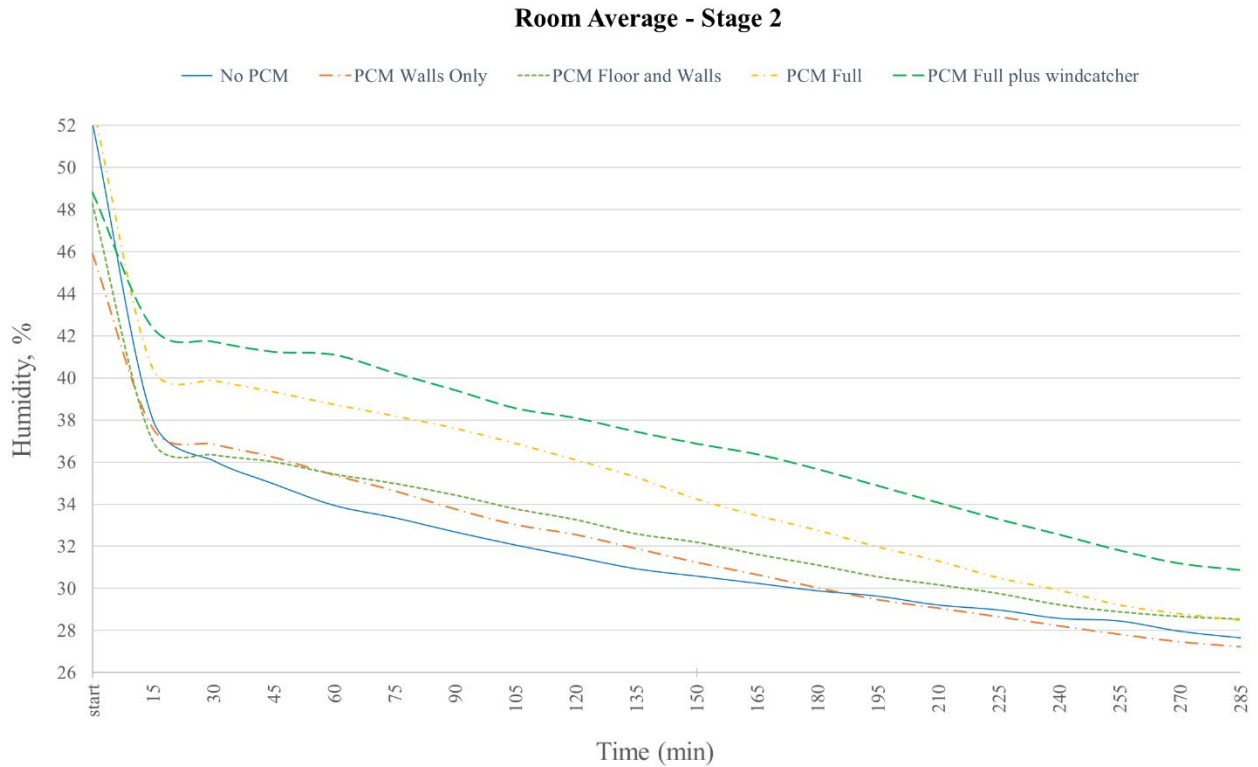
Figure 5-52 Average humidity plots of the room for all the models studied with stage 2 heating element.

It is noted that with all the models containing PCM the average humidity inside the chamber increased slightly compared to the model with No PCM. The difference ranged between 0 and 3.88% which indicates that the humidity variations are not significant.

Figure 5-53 summarizes the results showing the box plot for the five models. It shows the average humidity inside the chamber as well as the minimum and maximum humidity values.
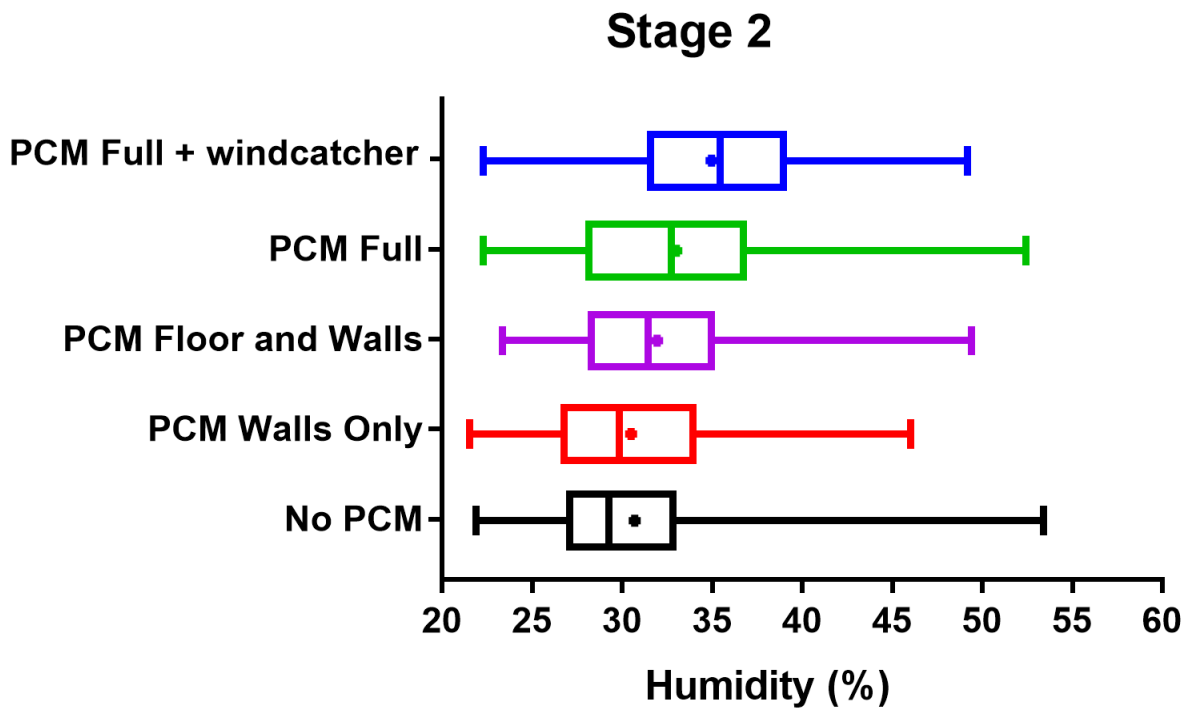
Figure 5-53 Box plot of the five models with stage 2 heating element

Figure 5-54 shows the distribution of the humidity values with respect to the time of the experiment for each of the models. The differences between the humidity values as the time changes is in a maximum range of about 5-6%. At 50% of the total time which corresponds to 2.5 hours, the average humidity of the model with NO PCM is approximately 29% while the average humidity of the model with PCM full + windcatcher is approximately 35%.

At 25% of the total time which corresponds to 1.25 hours the average temperature of the model with NO PCM is approximately 27% while the average temperature of the model with PCM full + windcatcher is approximately 32%.
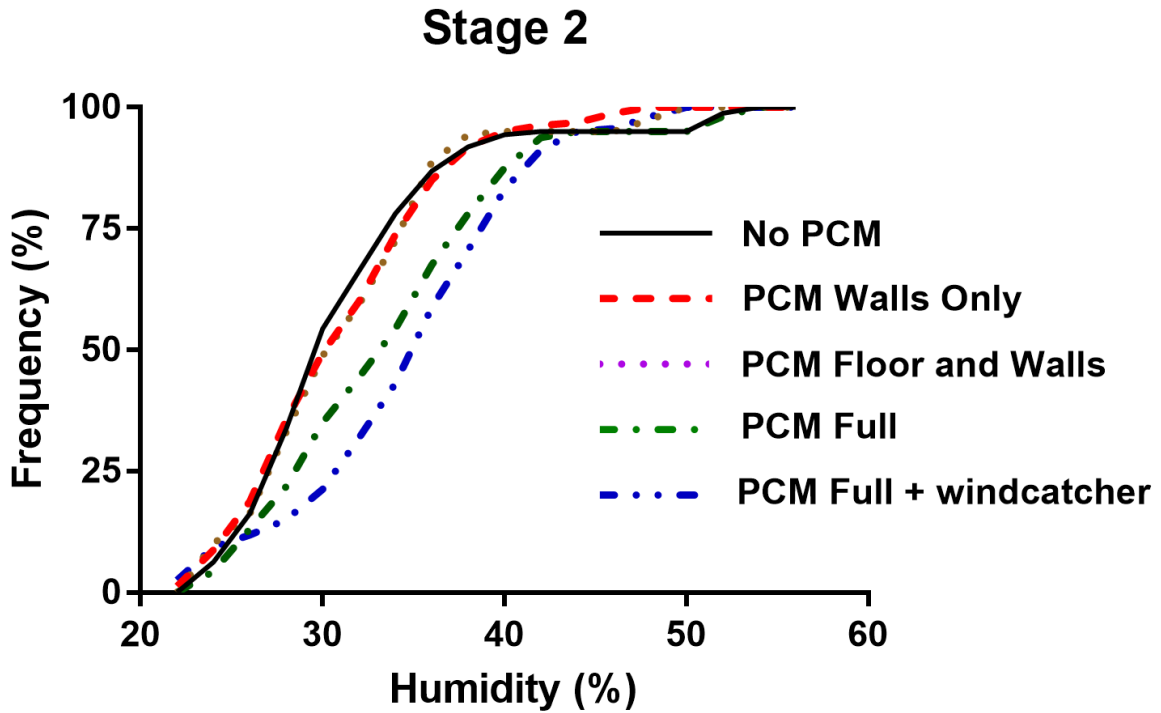
Figure 5-54 Distribution of humidity for the five models with stage 2 heating element

5.4.7 Temperature variation during charging process (solidification of PCM)

To investigate the effect of the charging process (solidification of PCM) on the temperature inside the chamber, an air conditioning unit was used to cool down the lab and a small fan placed about 300 mm from the windcatcher inlet as shown in figure 5-18. All the five models have been used, and the results obtained and compared. The experiments lasted at least five hours for each of the models. The tables related to these plots are similar in structure to Table 5-3 and are found in the appendix, refer to Tables A-19 to A-23.

Figure 5-55 shows the plot of the temperature versus the time of the experiment from the start and till after 135 minutes with No PCM.
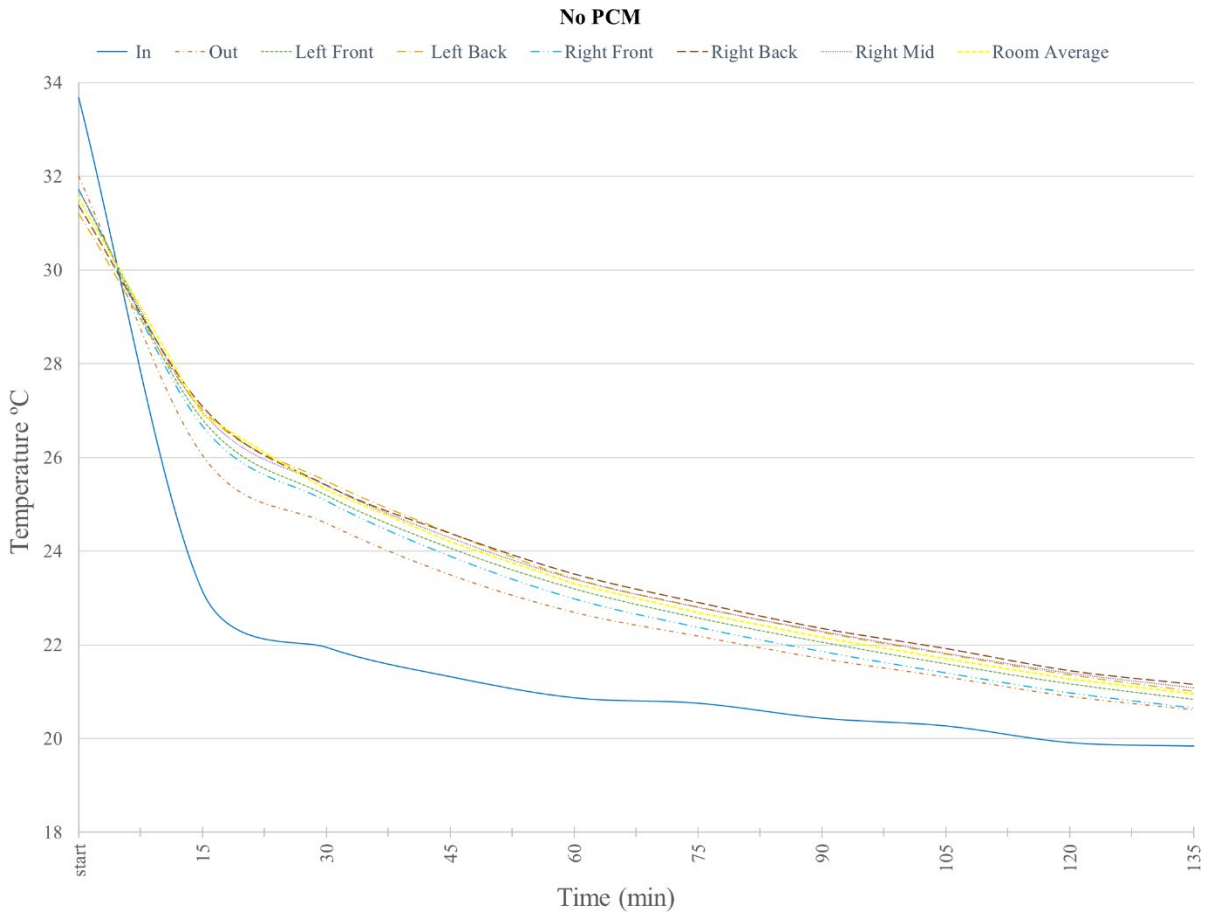
Figure 5-55 Temperature plots for empty chamber (No PCM) during charging process

Figures 5-56 till 5-59 show the plots of the temperature versus the time of the experiment for the remaining models. As the plots of the temperatures versus time are all similar to Figure 5-55 for the whole time of the experiments, each of these plots covered a certain range of time in order to show clearly the variations of temperatures. Figure 5-56 shows the temperature for the chamber with PCM Walls only from 60 minutes after the start till 210 minutes. Figure 5-57 shows the temperature for the chamber with PCM Floor and Walls from the start till after 45 minutes. Figure 5-58 shows the temperature for the chamber with PCM Full from 150 minutes after the start till 210 minutes. Figure 5-59 shows the temperature for the chamber with PCM Full plus windcatcher from the start till 180 minutes.
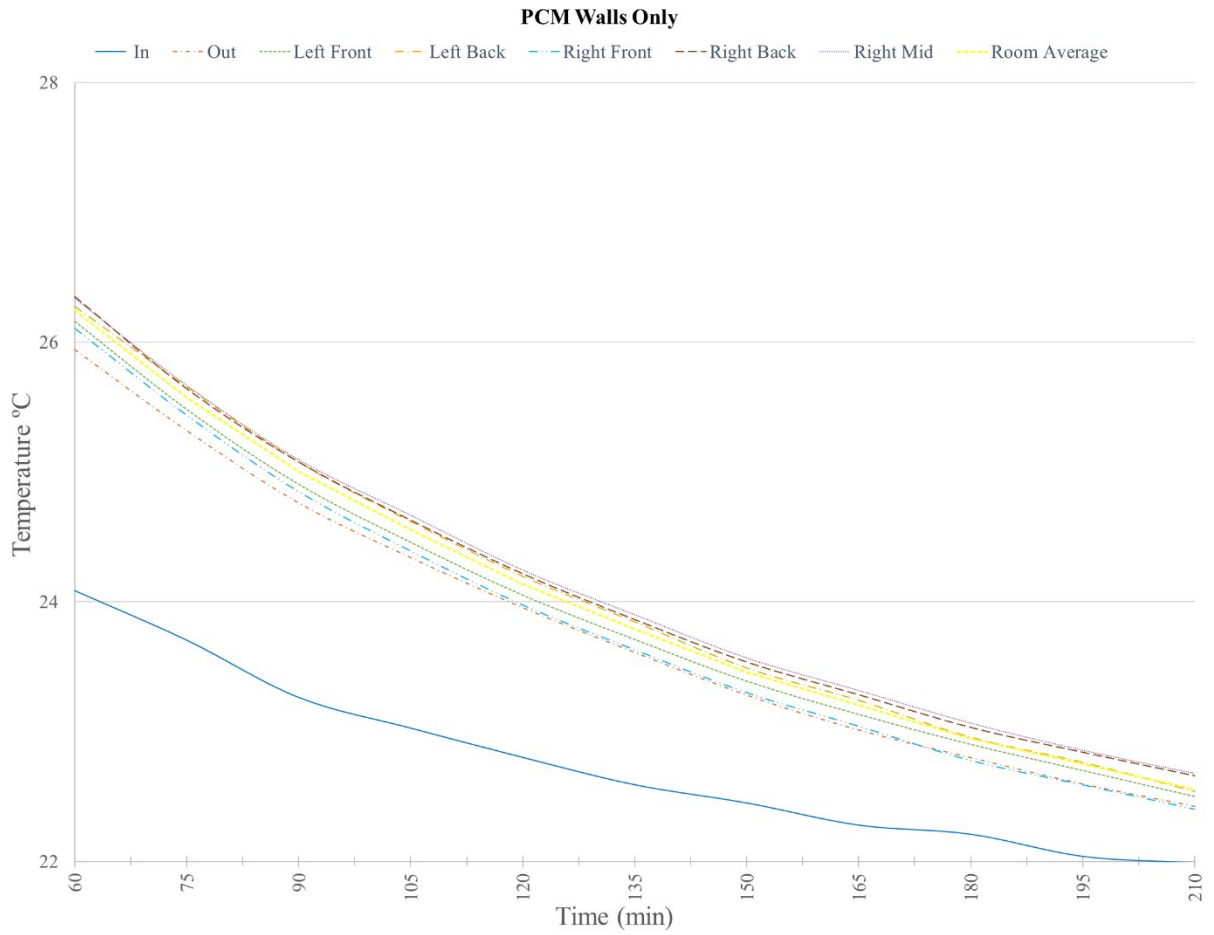
Figure 5-56 Temperature plots for chamber with PCM Walls Only during charging process
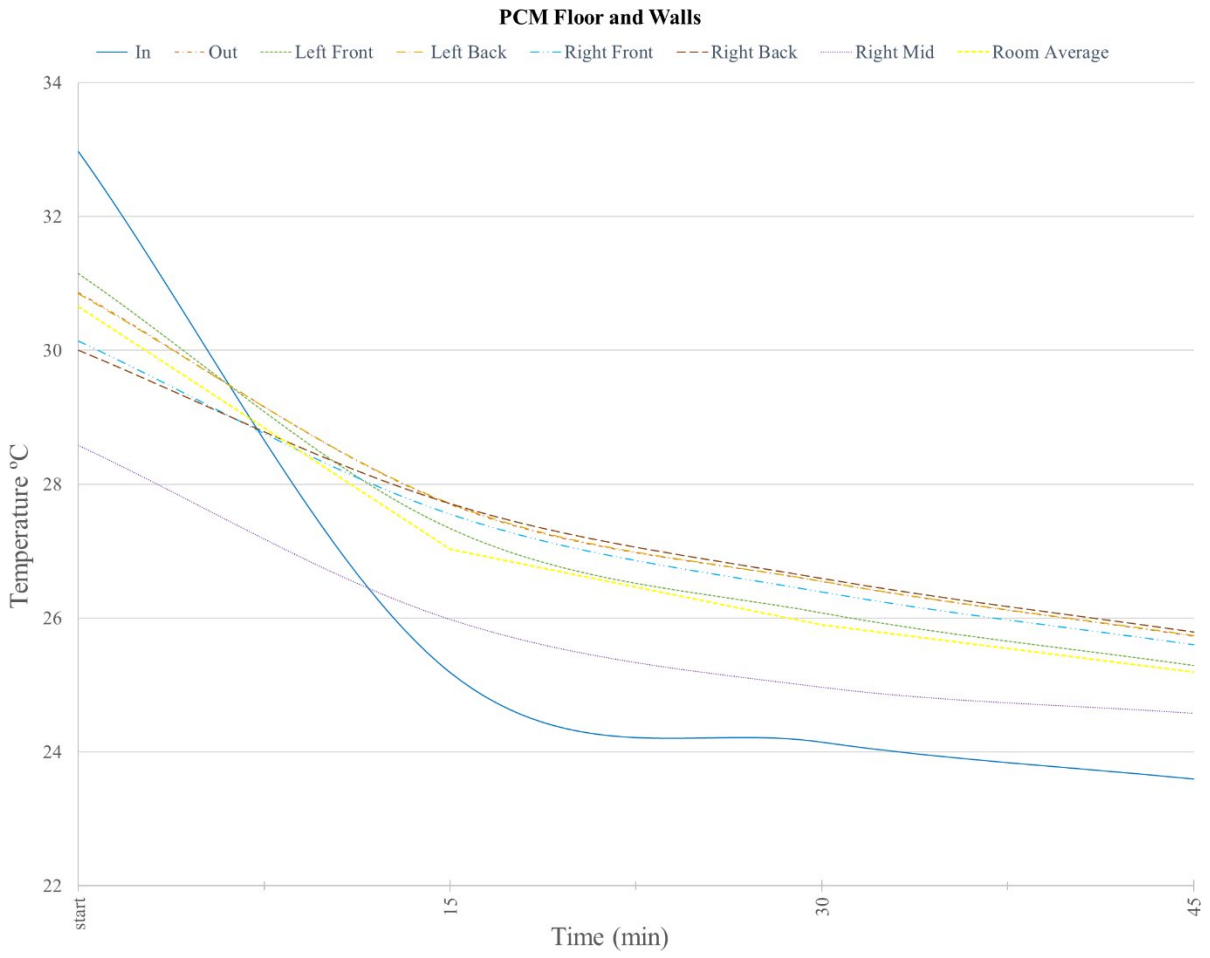
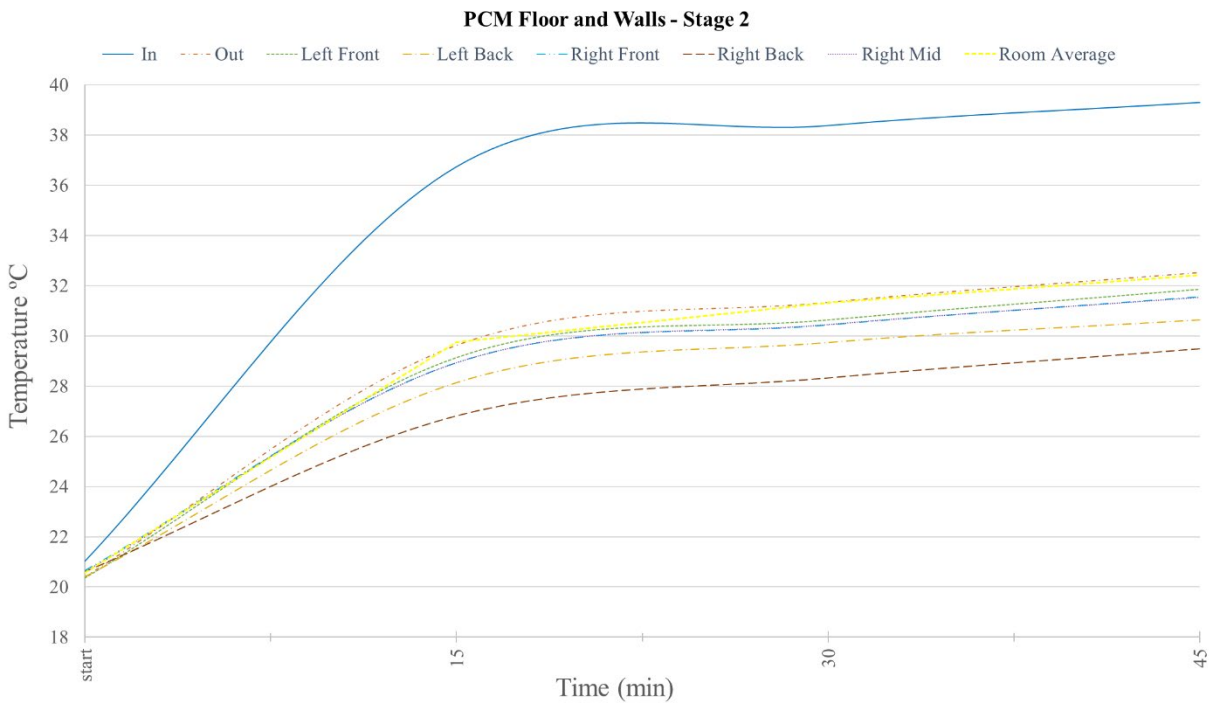Figure 5-57 Temperature plots for chamber with PCM Floor and Walls during charging process

238
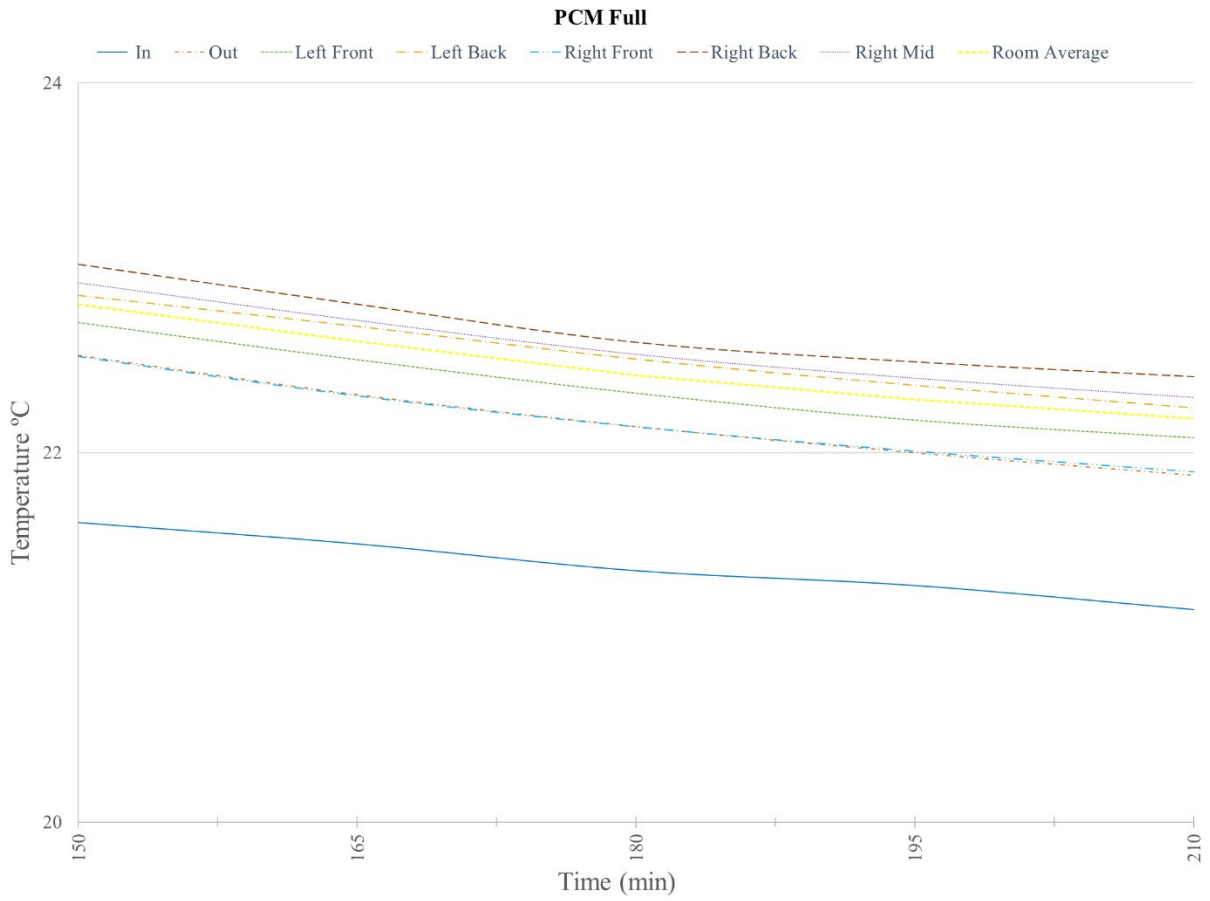
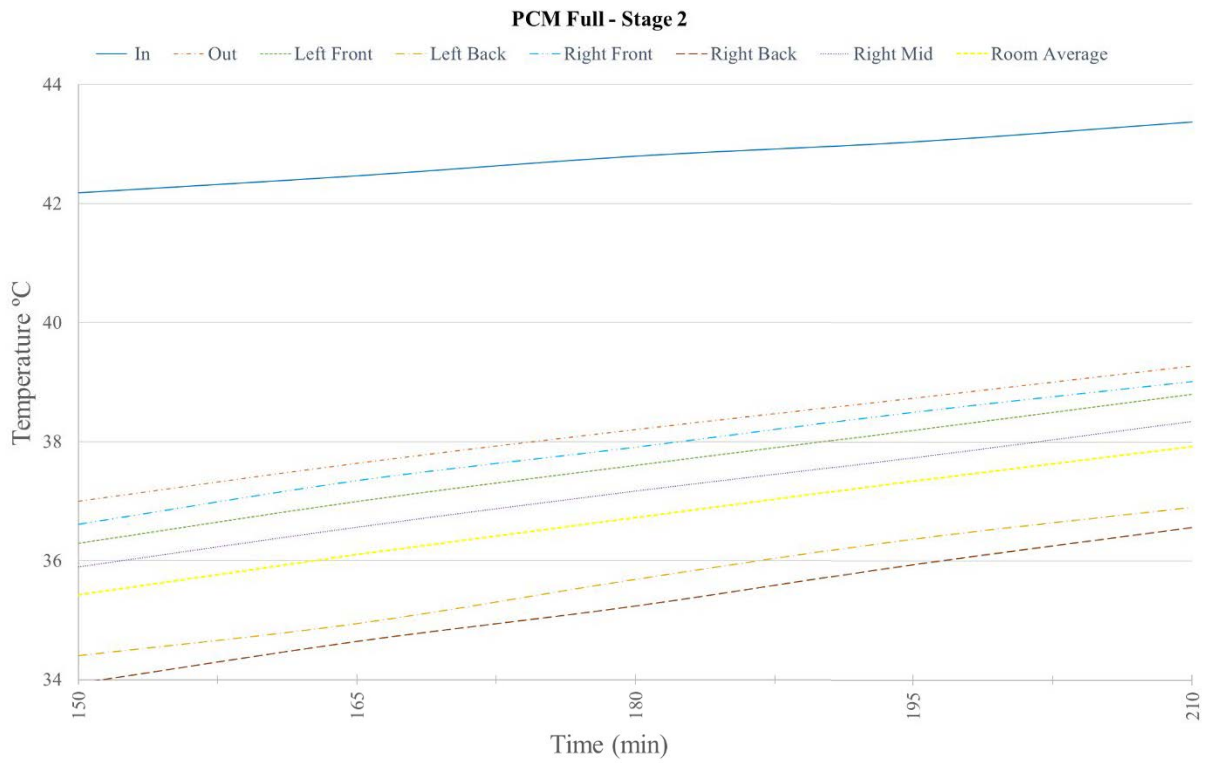Figure 5-58 Temperature plots for chamber with PCM Full during charging process
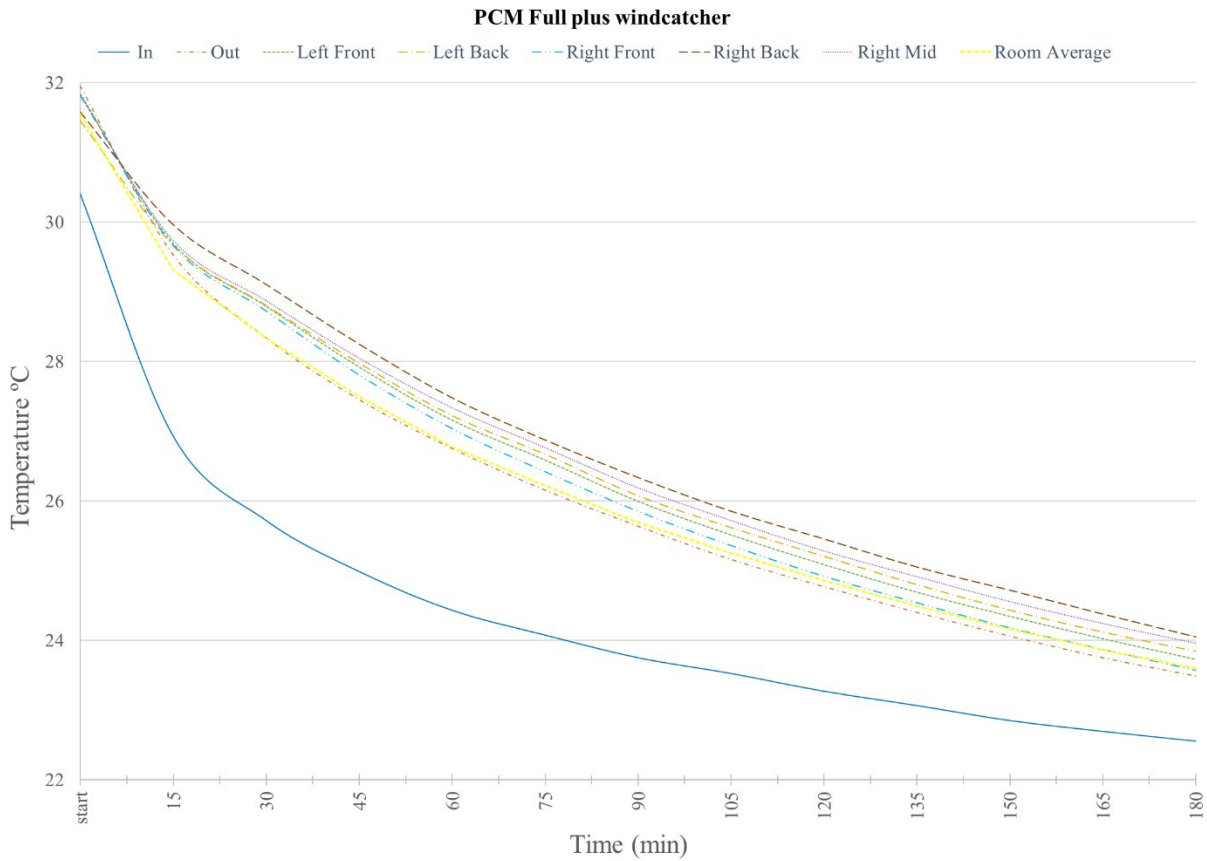
Figure 5-59 Temperature plots for chamber with PCM Full plus windcatcher during charging process

Table 5-10 summarizes the average temperatures in the chamber for the different models. It shows the difference in the average temperature (in ºC) between the different models with respect to the model with (No PCM) as well as the corresponding difference in percentage. Figure 5-60 shows the average temperature plots inside the chamber for the different models studied from the start till 285 minutes. The average temperature for the model with empty chamber is the lower trace while the higher trace is for the model with PCM Full plus windcatcher.

Temperature, °C	No PCM	PCM Walls Only	PCM Floor and Walls	PCM Full	PCM Full + windcatcher
Room average	21.66	24.40	23.94	23.59	25.06
Difference °C	---	2.74	2.28	1.93	3.40
Difference %	---	12.65%	10.53%	8.91%	15.70%

Table 5-10 Average temperature during solidification in the chamber for the different models
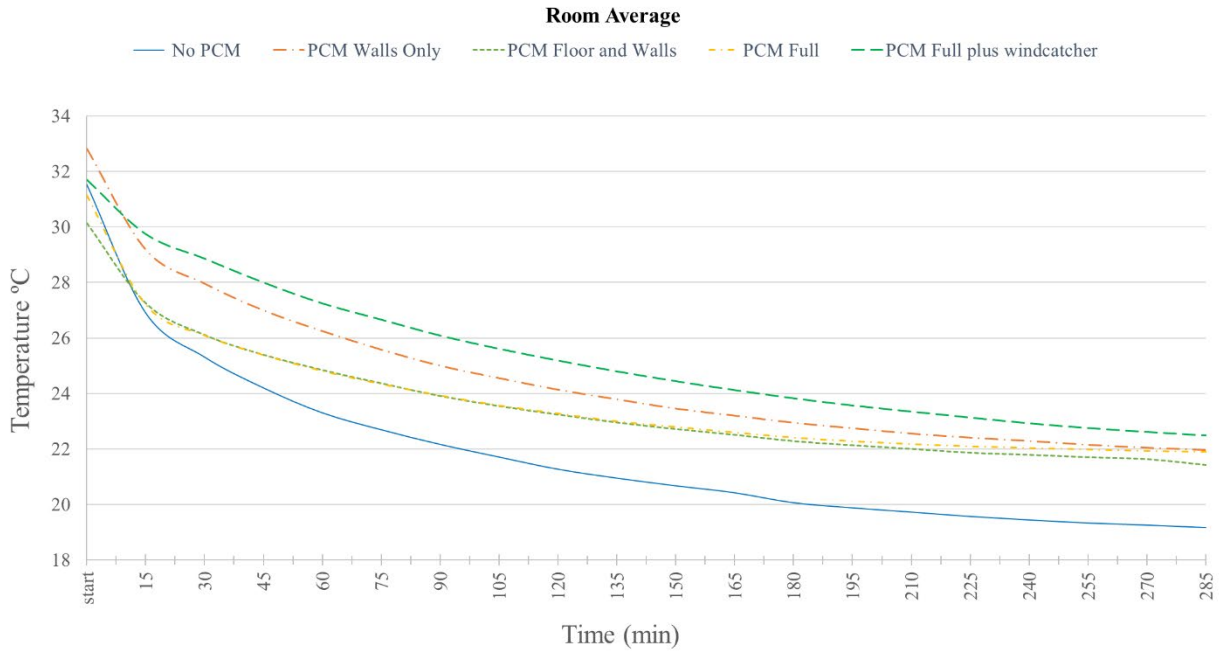
Figure 5-60 Average temperature plots of the Room for all the models during charging process.

It is noted that with all the models containing PCM the average temperature inside the chamber increased compared to the model with No PCM. Comparing the model PCM Full + windcatcher with the other models, we observe that it has provided the largest increase in temperature (3.40 ºC) with respect to the model with No PCM.

Figure 5-61 summarizes the results showing the box plot for the five models. It shows the average temperature inside the chamber as well as the minimum and maximum temperatures and the quartile values. The model with the PCM located in the floor, ceiling and walls as well as in the windcatcher's inlet channel has shown the best performance compared to the other models and the increase of average temperatures observed is significant with respect to the model with No PCM. This increase of 3.40 ºC is equivalent to 15.70 % difference as shown in table 5-10.
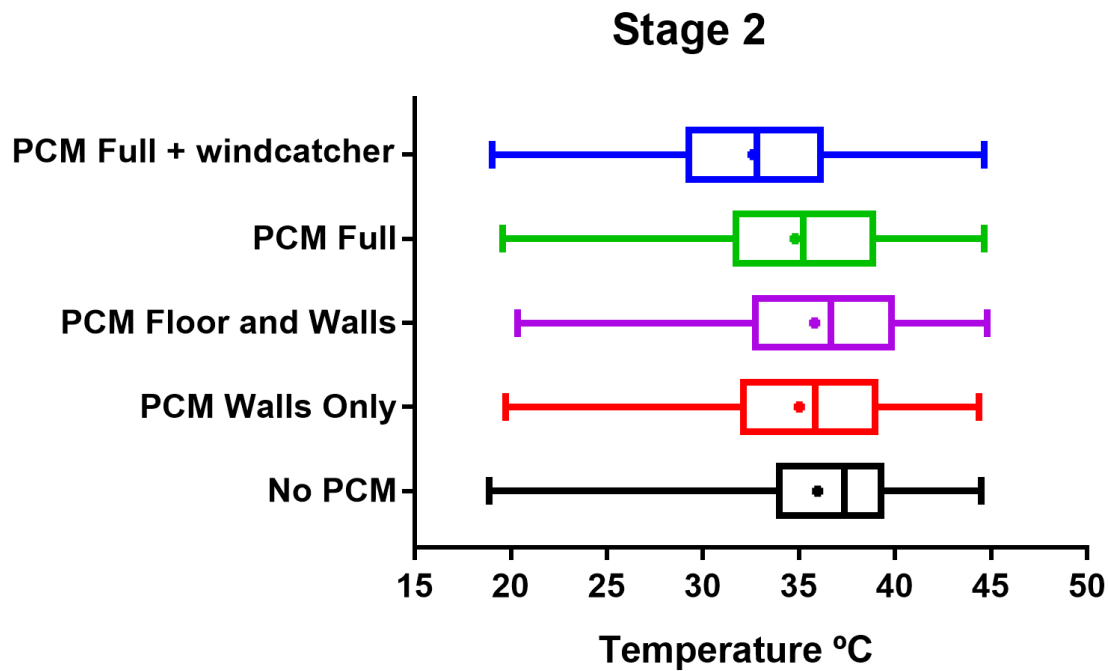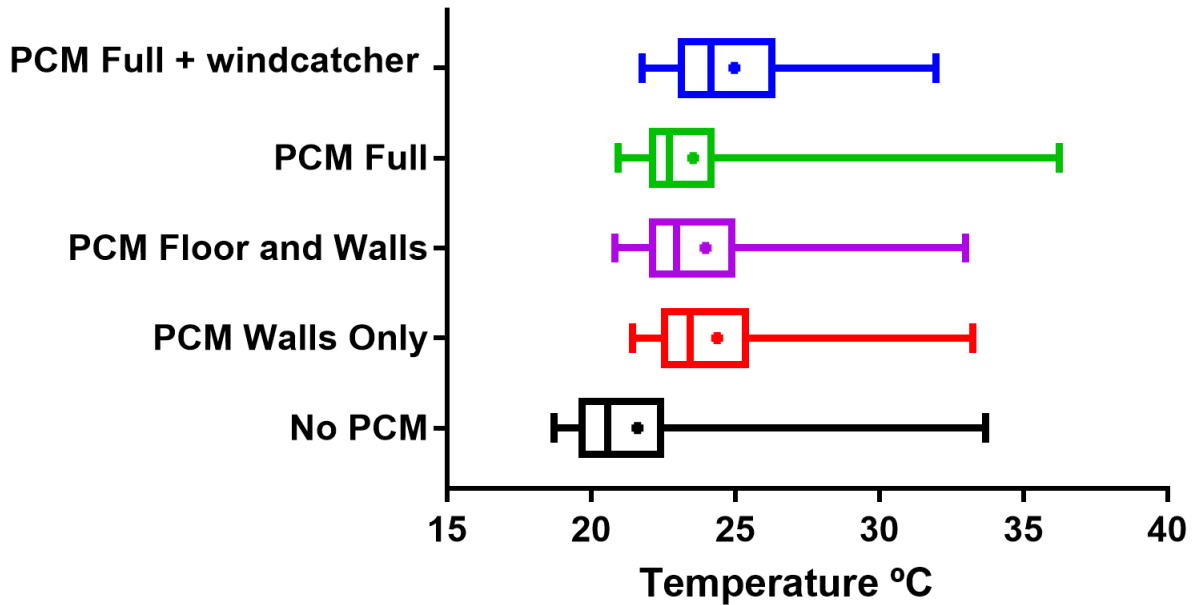
Figure 5-61 Box plot of the five models during charging process

Figure 5-62 shows the distribution of the temperatures during the charging process with respect to the time of the experiment for each of the models. It is evident that all of the models with PCM has shown higher temperature values compared to the model with No PCM (shown in black in figure 5-62). At 50% of the total time of the experiment which corresponds to 2.5 hours, the average temperature of the model with NO PCM is approximately 21 ºC while the average temperature of the model with PCM full + windcatcher is approximately 24 ºC.

It is also clear that the model with PCM full + windcatcher shows the best performance as its corresponding graph (shown in blue in figure 5-62) is the farthest with respect to No PCM.
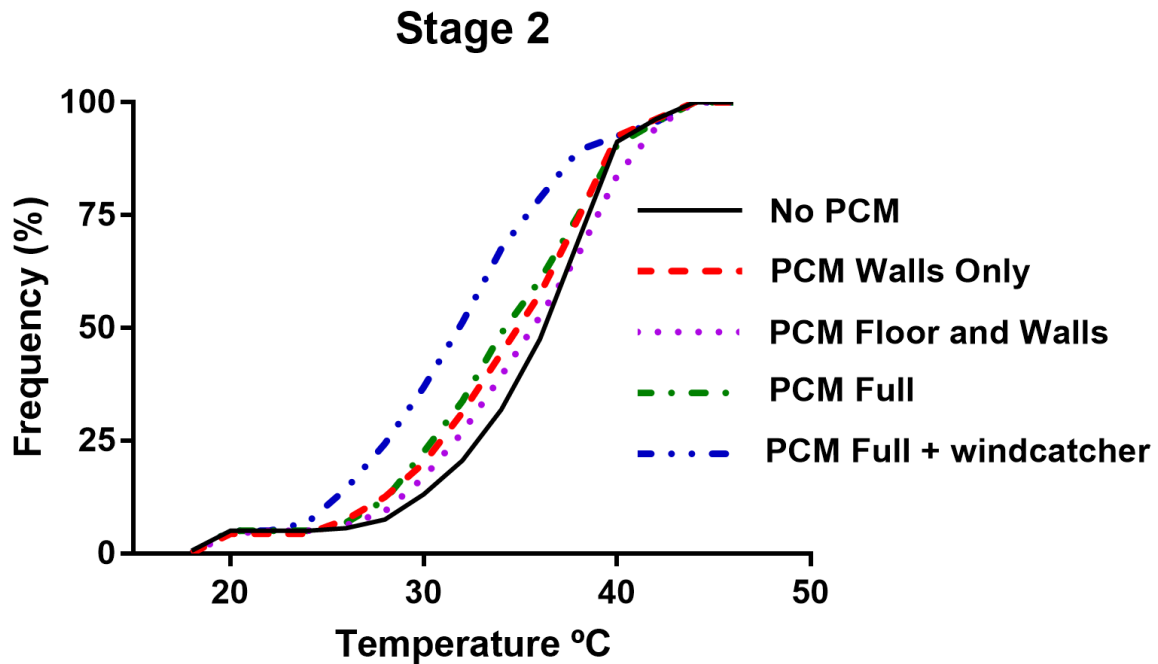
Stage 1
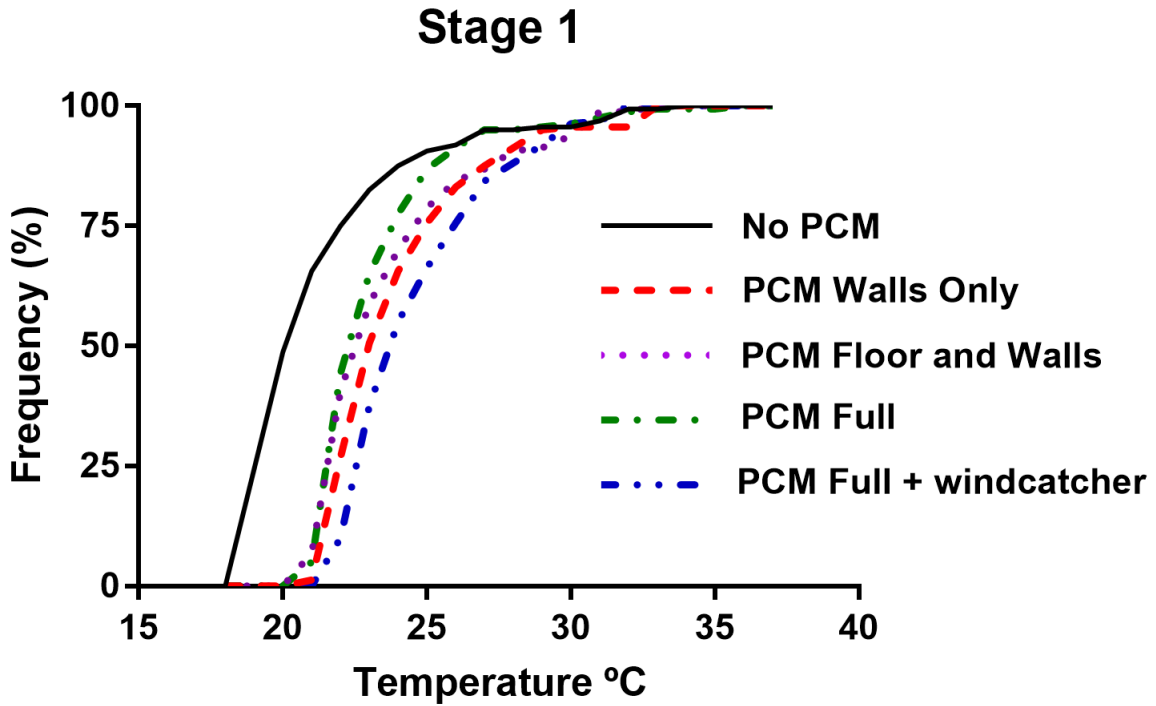
Figure 5-62 Distribution of temperatures during charging process for the five models

5.4.8 Air Velocity inside the chamber

Air velocity transducers (Figure 5-14) have been used to record the air velocity inside the chamber. The locations of the sensors are shown in figure 5-15.

During discharging the hot box fan was operated at 100% speed. Table 5-41 shows the average values for the air velocity recorded by the sensors for both locations of the chamber. It was noted that the average velocities did not change with the different models studied which indicates that the presence of the PCM did not affect flow pattern through the chamber.

Fan location and speed	Average Velocity, m/s			
	Rt Fr A0	Rt Mid A1	Rt Bck A2	Lf Fr A3
Hot box fan far 100%	0.61	0.60	0.54	0.67
Hot box fan close 100%	0.63	0.56	0.41	0.68

Table 5-11 Average velocity inside the chamber during discharging

Figure 5-63 shows the air velocities recorded inside the chamber (when far from the duct placed at 850 mm distance) during the discharging process with the hot box fan speed of 100%. It is noted from table 5-11 that the speed inside the chamber did not vary much with the different locations of the chamber except for the sensor right back (Rt Bck).
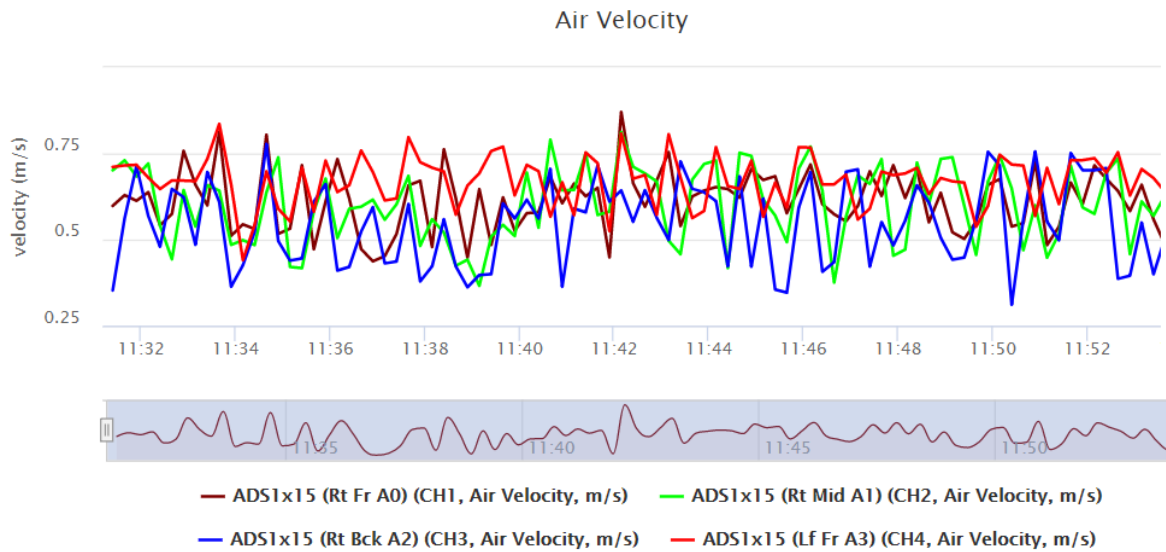
Figure 5-63 Air velocities inside the chamber during discharging process

Table 5-12 shows the average values for the air velocity during the charging process (solidification of PCM). It was also noted that the average velocities did not change with the different models studied which indicates that the presence of the PCM did not affect the flow pattern through the chamber. Figure 5-64 shows the air velocities recorded inside the chamber during the charging process.

Small fan - solidification	Sensor			
	Rt Fr A0	Rt Mid A1	Rt Bck A2	Lf Fr A3
Average Velocity, m/s	0.32	0.38	0.29	0.32

Table 5-12 Average velocity inside the chamber during charging process
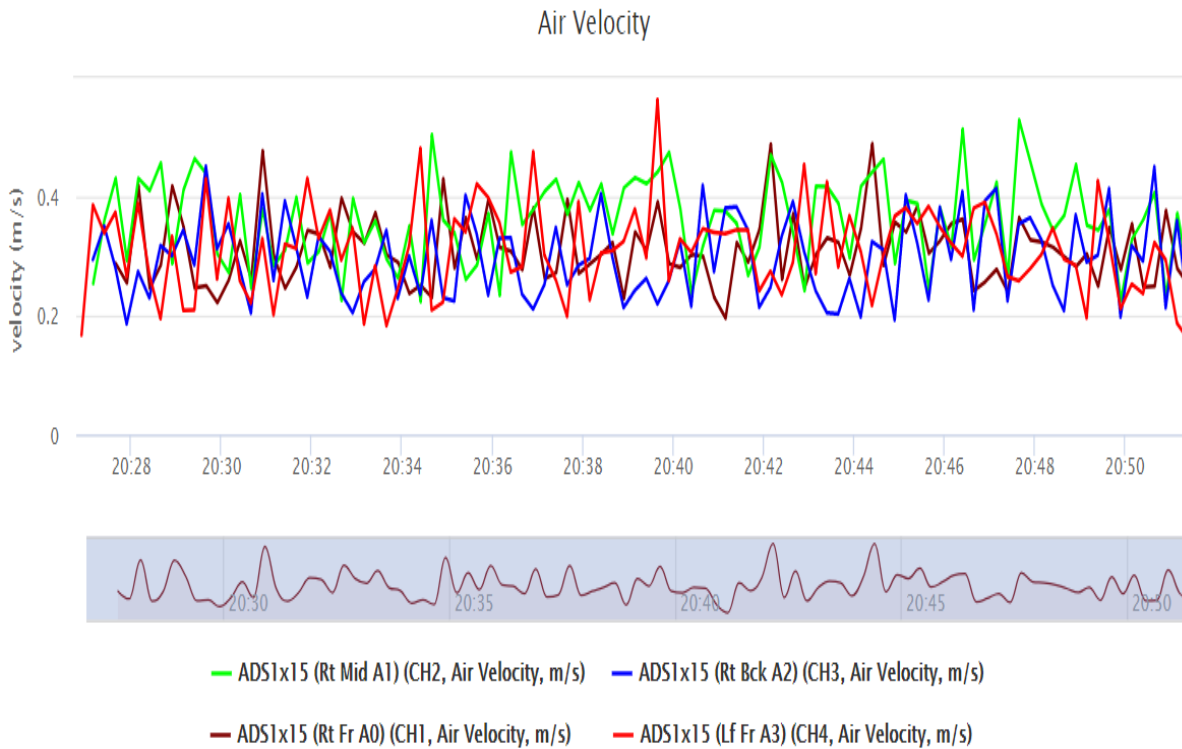
Figure 5-64 Air velocities inside the chamber during charging process

5.5 Conclusion

The effect of phase change material PCM on the temperature and humidity in a room fitted with a windcatcher is investigated. PCM is integrated respectively at the walls of the room, its floor and ceiling and within the windcatchers inlet chanel. Five models are investigated and the results compared, one model when the room is empty (No PCM), another model when PCM is found on the walls only, a third model is with the PCM placed on the floor and walls of the room, a fourth model is with the room full with PCM (PCM on floor, walls and ceiling). The fifth model included the PCM located in the inlet of the windcatcher in addition to the floor, ceiling and walls of the room.

During the discharging process wind is blown through the room using a fan with heating elements and the temperature is measured at different locations inside the chamber. Average temperatures corresponding to the different models are obtained and compared. Two stages of the heating elements are used, each stage added about 7 ºC to the ambient temperature in the lab. The model with the PCM located in the floor, ceiling and walls as well as in the windcatcher's inlet channel has shown the best performance compared to the other models and the reduction of temperatures observed is significant (about 2.75 ºC which is equivalent to 9.33%) with respect to the model with No PCM when stage 1 heating element was used. With stage 2 heating element the model with Full PCM plus windcatcher has also provided the best performance with a significant reduction of temperature 3.61 ºC which is equivalent to 9.90 %.

During the discharging process the room was also located in two positions with respect to the duct's outlet to investigate the effect of the flow rate captured by the windcatcher on the performance of the PCM. It is noted that the differences based on the locations of the room is not significant as the average temperature differed by about 1.25% only for both locations. It is concluded that the variation of about 6.5 % in the flow rate captured by the windcatcher did not have any significant effect on the temperature inside the chamber and thus had little effect on the performance of the PCM.

During the discharging process the variation of humidity is also investigated with stage 2 heating element and it is noted that with all the models containing PCM the average humidity inside the chamber increased slightly compared to the model with No PCM. The difference ranged between 0 and 3.88% which indicates that the humidity variations are not significant.

During the charging process (solidification of PCM) an air conditioning unit was used to cool down the lab and a small fan was used to direct the cool air through the windcatcher inlet. All the five models have been used, and the results obtained and compared. It is noted that with all the models containing PCM the average temperature inside the chamber increased significantly compared to the model with No PCM with a minimum increase of about 2 ºC. The model with the PCM located in the floor, ceiling and walls as well as in the windcatcher's inlet channel has shown the best performance compared to the other models and the increase of average temperatures observed (3.40 ºC equivalent to 15.70 %) is significant with respect to the model with No PCM.

Real buildings should make use of the phase change material combined with natural ventilation to enhance the indoor environment. The main difficulty for using PCM remains in the solidification process as there is no guarantee that during night time the temperatures would drop down to level low enough for complete solidification of PCM. Other difficulties may be due to the current high cost of PCM.

Chapter 6 Summary and conclusions

6.1 Summary

As mentioned in the introduction section more than 40% of the total world energy consumption is allocated to the building sector, of which more than 60% [1] of the total building sector energy consumption is used for heating, ventilation and cooling. Thus the approach to building design is essential in producing buildings that are energy efficient. Windcatcher is one of the green features for providing natural ventilation using wind power. Natural ventilation has some disadvantages and may not be suitable for regions with cold climate or for regions with hot windless weather. When buildings are located in polluted areas, natural ventilation may cause some health risks to the occupants. The variation of wind speeds may as well lead to air quality problems [45]. Heat stress in cities can be addressed by increasing green spaces and using green walls and green roofs [47]. The integration of vegetation in urban areas has several environmental benefits, contributing to the improvement of air quality. Green walls have recently been used to help with this and even thermal comfort. Phase change material (PCM) has been recently regarded as a sustainable passive cooling method [51]. PCM shows promise when combined with windcatchers to be very effective at providing both cooling and ventilation in a sustainable system.

The ultimate aim of this research is to develop a natural ventilating system to enhance a healthy, comfortable and energy efficient indoor environment. A two sided windcatcher is used to investigate the performance of windcatchers. PCMs and green wall modules are also investigated in this thesis. Green walls represent an emerging technology for the removal of pollutants present in air streams, with many conventional analyses yet to be applied to these systems. This work provides an initial study directed at optimizing the airflow characteristics through a green wall module and investigating the effect of these green walls on indoor thermal comfort (temperature and humidity). The effect of using phase change material (PCM) as a passive cooling technique on the performance of a windcatcher is also studied in this research.

In light of the above, this thesis has asked the following questions (refer to section 1.7):

1. *How to enhance the performance of a two sided windcatcher and what are the effects of its inlet design and of combining the buoyancy driven ventilation with the winddriven ventilation on the air flow through the windcatcher and on the human thermal comfort?*

This question is answered in Chapter 3 using two dimensional and three dimensional simulations. Three inlet designs (Uniform, divergent and bulging convergent) have been studied in sections 3.1 (2D) and 3.3 (3D). Combining buoyancy driven and winddriven ventilation has also been studied in sections 3.2 (2D) and 3.4 (3D).

2. *What are the effects of green walls systems on indoor thermal comfort and what are the parameters affecting the evaluation and distribution of air flow through an active green wall module?*

This question is answered in Chapter 4 using experimental methods. Air flow through an active green wall biofilter has been evaluated in section 4.1 and the parameters affecting the airflow and its distribution such as plant roots, moisture content, and the modules geometry have been considered. Section 4.2 also investigates the effect of fan speeds on air flow through an active green wall module, and section 4.3 investigates the effect of active and passive green walls on temperature and humidity.

3. *What is the effect of using PCM (phase change material) on the performance of a two sided windcatcher and how to incorporate it effectively?*

This question is answered in Chapter 5 using experiments. PCM is incorporated in several locations in a room fitted with a windcatcher and its effect on temperature and humidity has been investigated. Five models are investigated and the results compared, one model when the room is empty (No PCM), another model when PCM is found on the walls only, a third model is with the PCM placed on the floor and walls of the room, a fourth model is with the room full with PCM (PCM on floor, walls and ceiling). The fifth model included the PCM located in the windcatcher's inlet channel in addition to the floor, ceiling and walls of the room. Both charging and discharging processes were considered. During discharging, different wind temperatures were applied using two stages of heating elements in the fan and two locations of the room were studied to investigate the effect of two different wind speeds.

Based on the above research questions, this thesis makes the following contributions:

Contribution 1: A divergent inlet captures the highest air flow through a room fitted with a windcatcher compared to a uniform and to a bulging convergent inlet. It provides higher average velocity at 1.2 m high in the room enhancing the thermal comfort where most of the human occupancy occurs.

Cases for three inlet shapes, uniform, divergent and bulging-convergent have been simulated using Ansys Fluent as discussed in section 3.1 using a two dimensional analysis and in section 3.3 using a three dimensional analysis. The pattern of the flow for the three inlets has provided full ventilation inside the room especially in the living area. With the two dimensional computations and an applied wind velocity of 3 m/s, the divergent inlet has captured the highest air flow with a difference of approximately 3% compared to the uniform inlet and 8% difference compared to the bulging-convergent inlet. With the three dimensional simulations which reflect real life situation, wind velocities of 1, 2, 3 and 6 m/s have been applied. The divergent inlet design has captured the highest air flow through the room and provided higher average velocity at 1.2 m high enhancing the thermal comfort where most of the human occupancy occurs. With 6 m/s wind velocity the divergent inlet has captured 7.16% more flow rate compared to the uniform inlet and 8.44% compared to the bulging convergent inlet, and also it provided an average velocity at 1.2 m high in the room of 2.65% higher than the uniform inlet and 4.58% higher than the bulging convergent inlet.

Contribution 2: With combined buoyancy driven and winddriven ventilation, as the wind speed increases the winddriven ventilation dominates the flow and reduces the effect of the buoyancy forces. Buoyancy driven ventilation is effective at low wind speeds especially with wind speeds less than 1 m/s.

Cases for winddriven ventilation and combined winddriven and buoyancy driven ventilation for a uniform inlet has been simulated as discussed in section 3.2 using a two dimensional analysis and in section 3.4 using a three dimensional analysis.. The average velocity at 1.2 m height inside the room in the cases studied satisfied the human thermal comfort conditions. With the three dimensional simulations using Ansys Fluent, temperatures of 350 K and 400 K are applied at the windcatchers outlet to simulate the buoyant effect, and different wind speeds between 0 up to 3 m/s are applied. The combined solar windcatcher provided the highest

increase in flow rate of 23.16 % when wind speed is 0.25m/s, this percentage drops till about 1% when the wind speed is 1m/s and to about 0.33% as the wind speed increases to 2.5 m/s. At 3 m/s wind speed the differences are almost negligible. This indicates that as the wind speed increases the winddriven ventilation dominates the flow and reduces the effect of the buoyancy forces. The combined solar windcatcher is useful however when the wind speeds are lower than 1 m/s.

Contribution 3: The primary observation of the current work in relation to active green walls is that more air will pass through a typical green wall substrate, and hence become cleansed, when the substrate is saturated with water than when it is dry.

Air flow through an active green wall biofilter has been evaluated in section 4.1. This study evaluated the air flow characteristics through an active green wall module and investigated the air flow distribution, the effect of wetting the substrate and the effect of adding a top cover to the module's open top face. Four cases of both planted and unplanted modules under both dry and wet conditions are considered. The primary observations of the current work are that more air will pass through a typical green wall substrate, and hence become cleansed, when the substrate is saturated with water than when it is dry. The increase was substantial at approximately 50% more with 14.9 L/s total air flow rate passing through the wet planted module versus 10 L/s when dry. Plant roots themselves, on the other hand, play minor roles in creating resistance to the air flow, indicating that root morphology may not be of prime importance in plant selection, allowing other criteria to be used, such as pollution tolerance, low maintenance or longevity, low watering needs for eco-efficiency, or pollutant removal effects.

Contribution 4: Adding a top cover to the module having six 10 mm diameter holes for irrigation decreased the air flow through the top by 6 %, and directed it instead through the filter increasing the percentage of air flow passing through the front openings from 79 % to 85 %.

Section 4.1 has also investigated the air flow distribution through the active green wall module. Airflow distribution within the system tested was reasonably even, despite the absence of a complex baffle system in the green wall air intake plenum, indicating that plenum design can be simplified, potentially reducing system cost both through cheaper design and back pressure

reduction. Reducing the 15.5 % of polluted air that bypasses the substrate and plant canopy in green walls will clearly improve their filtration performance. Adding a top cover to the module having six 10 mm diameter holes for irrigation decreased the air flow through the top (and thus returning to atmosphere with much less filtration) by 6 %, and directed it instead through the filter increasing the percentage of air flow passing through the front openings from 79 % to 85 %. The top cover's presence had little effect on the total air-flow rate through the module, and the pressure drop across it.

Contribution 5: As the fan speeds increased, the pressure difference across the module increased, as well as the corresponding air flow rate. The distribution of airflow through the module openings under the same plant-growing medium was approximately the same for different fan speeds.

Section 4.2 investigates the effect of fan speeds on air flow through an active green wall module. Cases of different fan speeds were considered, and the corresponding air-flow rates and pressure difference compared. As the fan speeds increased, the pressure difference across the module increased, as well as the corresponding air flow rate. The distribution of airflow through the module openings under the same plant-growing medium was approximately the same for different fan speeds. With all the cases investigated, the Q-P relationship (curve of flow-rate versus pressure) agreed with the typical fan performance curves, namely as Q increased, P decreased.

Contribution 6: Both active and passive green walls affect the temperature and humidity. Lower temperatures in the range of 1 to 3 °C are observed along with increased levels of humidity.

Section 4.3 investigated the effect of active and passive green walls on temperature and humidity. Cases for dry and wet (saturated) unplanted module, as well as saturated planted modules with different plant species have been considered. The effect of different surrounding ambient conditions is also investigated.

For the active green wall modules, lower temperatures in the range of 1 to 3 °C, along with increased humidity levels have been noted when modules are saturated wet for cases of

unplanted as well as planted modules with different plant species. While any of the plant species studied did not show any preference, an unplanted module with dry substrate did not cause any significant temperature variation indicating that the moisture content plays the major role in the temperature as well as humidity variations.

For the passive green wall modules, lower temperatures in the range of 0.5 to 2 °C, along with increased humidity levels have been noted when modules are saturated wet for planted modules with different plant species. None of the plant species studied showed any preference, indicating that the moisture content of the substrate plays the major role affecting the temperature and humidity variations.

Contribution 7: PCM located in the floor, ceiling and walls as well as in the windcatcher's inlet channel has shown the best performance with respect to the temperature variations during both discharging and charging processes. The difference was significant, about 3 ºC, compared to a room fitted with the windcatcher with No PCM.

The effect of using phase change material (PCM) as a passive cooling technique on the performance of a two sided windcatcher is studied in chapter 5. PCM is integrated respectively at the walls of the room, its floor and ceiling and within the windcatchers inlet tunnel. Five models are investigated and the results compared during charging and discharging.

During the discharging process the model with the PCM located in the floor, ceiling and walls as well as in the wind tunnel has shown the best performance compared to the other models and the reduction of temperatures observed is significant (about 2.75 ºC which is equivalent to 9.33%) with respect to the model with No PCM when stage 1 heating element was used. Each stage of heating elements adds approximately 7 ºC to the ambient temperature in the lab. With stage 2 heating element the model with Full PCM plus windtunnel has also provided the best performance with a significant reduction of 3.61 ºC which is equivalent to 9.90 %. The room was also located in two positions with respect to the fan duct's outlet to investigate the effect of the flow rate captured by the windcatcher on the performance of the PCM. It is noted that the differences based on the locations of the room is not significant as the average temperature differed by about 1.25% only for both locations. It is concluded that the variation of about 6.5 % in the flow rate captured by the windcatcher did not have any significant effect on the temperature inside the chamber and thus had little effect on the performance of the PCM. It was also noted in section 5.4.8 that the average velocities inside the room did not change with

the different models studied which indicates that the presence of the PCM did not affect flow pattern through the room.

During the charging process (solidification of PCM), all the models containing PCM provided an increased average temperature inside the room compared to the model with No PCM and the minimum increase was about 2 ºC. The model with the PCM located in the floor, ceiling and walls as well as in the wind tunnel has shown the best performance compared to the other models and the increase of average temperatures observed (3.40 ºC equivalent to 15.70 %) is significant with respect to the model with No PCM.

Contribution 8: Humidity variation due to the integration of PCM is not significant. The average humidity inside the room increased slightly (between 0 and 3.88%) compared to the model with No PCM.

Section 5.4.6 investigates the effect of PCM on the humidity variations during the discharging process. It is noted that with all the models containing PCM the average humidity inside the chamber increased slightly compared to the model with No PCM. The difference ranged between 0 and 3.88% which indicates that the humidity variations are not significant.

6.2 Conclusion

Using windcatchers would decrease the consumption of non-renewable energies by buildings. It would be an efficient sustainable method to preserve the environment and a major help in managing the limited available non-renewable energy resources. Applying a divergent inlet would provide additional airflow and contribute to enhancing the thermal comfort of the occupants and increase the windcatcher's ability to capture more airflow. Combining the winddriven and buoyancy driven ventilation would also increase the effectiveness of windcatchers especially with low wind speeds less than 1 m/s.

If active green walls are to be used as air cleaning devices, the airflow through these systems must be maximized so as to provide maximized air cleaning efficiency, with minimal energy wastage. The primary observations of the current work are that more air will pass through a typical green wall substrate, and hence become cleansed, when the substrate is saturated with water than when it is dry. The increase was substantial at approximately 50% more with 14.9

L/s total air flow rate passing through the wet planted module versus 10 L/s when dry. Adding a top cover to the module having six 10 mm diameter holes for irrigation decreased the air flow through the top by 6 %, and directed it instead through the filter increasing the percentage of air flow passing through the front openings from 79 % to 85 %. Active and passive green walls affect the temperature and humidity of the air layers surrounding them, as lower temperature in the range of 1 to 3 °C is observed along with increased levels of humidity.

PCM located in the floor, ceiling and walls of a room fitted with a windcatcher as well as in the wind tunnel has shown the best performance with respect to the temperature variations during both discharging and charging processes. The difference was significant, about 3 ºC, compared to a room fitted with a windcatcher with No PCM. Humidity variation on the other hand due to the integration of PCM is not significant. The average humidity increased slightly (between 0 and 3.88%) compared to the model with No PCM. The average velocities inside the room did not change with the different models studied during charging and discharging processed which indicates that the presence of the PCM did not affect flow pattern through the room.

The techniques proposed in this research would complement each other to enhance a healthy, comfortable and energy efficient indoor environment. Combining winddriven and buoyancy driven ventilation increases the air flow rate captured by windcatchers and especially for low wind speeds less than 1 m/s, while using a divergent inlet would allow for an increase in the flow rates through the windcatcher. Green walls would enhance the indoor temperature and humidity, and would improve the indoor air quality by reducing the concentration of CO_2 and other pollutants such as VOCs and PMs. Using a windcatcher with a long inlet channel is recommended to incorporate PCM. As this research concluded that incorporating PCM in the windcatcher's inlet channel as well as inside the room has shown the best performance, it is recommended to lengthen the inlet channel so it serves as a storage area where PCM would be mainly placed to provide the required energy conservation and enhance the thermal needs of indoor occupants. This may also create the opportunity to increase the buoyant effect as more area for temperature / heat flux would be available at the outlet channel of the windcatcher. Using the three proposed techniques (windcatcher, green walls and PCM) requires coordination from the early design stages of new buildings. Implementing the three methods may be possible in practice however some difficulties may arise due to the building constraints, special design requirements, cost of PCM and green walls as well as cost of refurbishment of existing buildings.

6.3 Limitations and recommendations for future work

Further studies are recommended in relation to the performance of a windcatcher such as investigating the effect of variable wind directions and wind speeds, both computationally and experimentally. An experimental validation of our three dimensional computations is also recommended as well as applying different computational techniques such as using LES (Large Eddy Simulation) method and comparing these findings with our current results. Our main limitations in relation to the validation of our simulations was the lack of space and resources to conduct an experiment on a scaled model. On the other hand, with the exception of only one study, the literature did not contain previous studies with conditions similar to ours, such as the dimensions of the real room studied, shape and size of the windcatcher inlet and outlet, inlet shapes design and locations and magnitude of the temperature/heat flux used to generate the buoyant effect.

The primary limitation of our study with the green walls is related to the use of a single, undeveloped active green wall system. A sequence of modification and retesting could have yielded greater performance, although this was beyond the scope of our current study, which was directed at testing an existing, commercially successful system. Testing other systems, with different substrate types, module casings and plant species would be of additional value. With the robust experimental procedure described in this thesis, this should enable green wall researchers to characterise the airflow of other systems, and thus provide comparative data in this otherwise undeveloped field. The long-term objective of this work is to improve the functionality of active green wall systems and thus to enhance the environmental quality of their surroundings. Once developments have occurred regarding system structure, Computational Fluid Dynamics (CFD) simulation needs to be conducted to test the effects of the modifications. Further CFD simulations, such as Large Eddy Simulations (LES) is then recommended to model the effectiveness of the active green wall at filtering air pollutants on a building/room scale.

Using a different larger windcatcher with a longer wind tunnel is recommended to further investigate the effect of incorporating PCM. Computational Fluid Dynamics (CFD) simulation needs also to be conducted to test the effects of the modifications on the performance of PCM and on the ventilation flow through a real sized room.

Additional suggestions related to the performance of windcatchers may be considered as future research work as follows:

- The windcatcher surrounding such as buildings and other structures which can change the wind magnitude and direction and ultimately affects the performance of a windcatcher.
- Investigate the performance of a multiple inlet/outlet (4, 6, and 8) of a windcatcher computationally and experimentally if possible.
- Investigate the effect of the internal arrangement of partitions, furniture and other accessories which may affect the flow pattern and circulation quality.
- Investigate the effect of location and sizes of doors and windows in buildings which can change the ventilation quality due to cross ventilation.

References

[1]   Saadatian, O., L.C. Haw, K. Sopian, and M.Y. Sulaiman, *Review of windcatcher technologies*. Renewable and Sustainable Energy Reviews, 2012. **16**(3): p. 1477-1495.

[2]   Santamouris, M., G. Mihalakakou, and D.N. Asimakopoulos, *On the coupling of thermostatically controlled buildings with ground and night ventilation passive dissipation techniques*. Solar Energy, 1997. **60**(3): p. 191-197.

[3]   Angelis, N., *Solar chimney design: Investigating natural ventilation and cooling in offices with the aid of computer simulation*. 2005, University of London, University College London (United Kingdom): Ann Arbor.

[4]   Stavridou, A.D., *Breathing architecture: Conceptual architectural design based on the investigation into the natural ventilation of buildings*. Frontiers of Architectural Research, 2015. **4**(2): p. 127-145.

[5]   Santamouris, M., N. Papanikolaou, I. Livada, I. Koronakis, C. Georgakis, A. Argiriou, and D.N. Assimakopoulos, *On the impact of urban climate on the energy consumption of buildings*. Solar Energy, 2001. **70**(3): p. 201-216.

[6]   Lakkas, T., *Sustainable cooling techniques the state of art*. 2008, University of London, University College London (United Kingdom): Ann Arbor.

[7]   Kolokotroni, M., I. Giannitsaris, and R. Watkins, *The effect of the London urban heat island on building summer cooling demand and night ventilation strategies*. Solar Energy, 2006. **80**(4): p. 383-392.

[8]   Ghiaus, C., F. Allard, M. Santamouris, C. Georgakis, and F. Nicol, *Urban environment influence on natural ventilation potential*. Building and Environment, 2006. **41**(4): p. 395-406.

[9]   PROCESS, S.T.C. *SOLAR/THERMAL CHIMNEY PROCESS*. [website]; Available from: http://ae390-systemsvariety-group6.weebly.com/solarthermal-chimney.html#Solar/Thermal_Chimney_Process.

[10]   Monodraught. *Windcatcher, top-down natural ventilation*. [website]; Available from: https://www.monodraught.com/.

[11]   Hughes, B.R., H.N. Chaudhry, and S.A. Ghani, *A review of sustainable cooling technologies in buildings*. Renewable and Sustainable Energy Reviews, 2011. **15**(6): p. 3112-3120.

[12]   Yaghoubi, M.A., A. Sabzevari, and A.A. Golneshan, *Wind towers: Measurement and performance*. Solar Energy, 1991. **47**(2): p. 97-106.

[13]   Afshin, M., A. Sohankar, M.D. Manshadi, and M.K. Esfeh, *An experimental study on the evaluation of natural ventilation performance of a two-sided wind-catcher for various wind angles*. Renewable Energy, 2016. **85**: p. 1068-1078.

[14]   Niktash, A. and P. Huynh. *Numerical simulation and analysis of the two-sided windcatcher inlet\outlet effect in ventilation flow through a three dimensional room*. in *Proceedings of the ASME 2014 Power Conference*. 2014. Baltimore, Maryland, USA.

[15]   Hughes, B.R., J.K. Calautit, and S.A. Ghani, *The development of commercial wind towers for natural ventilation: A review*. Applied Energy, 2012. **92**: p. 606-627.

[16]   Hosseini, S.H., E. Shokry, A.J. Ahmadian Hosseini, G. Ahmadi, and J.K. Calautit, *Evaluation of airflow and thermal comfort in buildings ventilated with wind catchers: Simulation of conditions in Yazd City, Iran*. Energy for Sustainable Development, 2016. **35**: p. 7-24.

[17]   Short, C.A., *The recovery of natural environments in architecture: Delivering the recovery*. Journal of Building Engineering, 2018. **15**: p. 328-333.

[18]   Abdo, P., R. Taghipour, and B.P. Huynh. *EFFECT OF WINDCATCHER'S INLET SHAPE ON VENTILATION FLOW THROUGH A TWO DIMENSIONAL ROOM*. in *Proceedings of the ASME 2018 5th Joint US-European Fluids Engineering Summer Conference FEDSM2018*. 2018. July 15-20, 2018, Montreal, Quebec, Canada: American Society of Mechanical Engineers.

[19]   Taghipour, R., P. Abdo, and B.P. Huynh. *EFFECT OF WIND SPEED ON VENTILATION FLOW THROUGH A TWO DIMENSIONAL ROOM FITTED WITH A WINDCATCHER*. in *Proceedings of the ASME 2018 International Mechanical Engineering Congress and Exposition IMECE2018*. 2018. November 9-15, 2018, Pittsburgh, PA, USA: American Society of Mechanical Engineers.

[20]   Abdo, P., R. Taghipour, and B.P. Huynh. *THREE DIMENSIONAL SIMULATION OF THE EFFECT OF WINDCATCHER`S INLET SHAPE*. in *The ASME - JSME - KSME Joint Fluids Engineering Conference 2019, AJKFLUIDS2019*. 2019. San Francisco, CA, USA.

[21] Abdo, P. and B.P. Huynh. *Effect of Combining Buoyancy Driven and Winddriven Ventilation in a Two Dimensional Room Fitted With a Windcatcher*. in *ASME International Mechanical Engineering Congress and Exposition, IMECE2017, Tampa, Florida, USA*. 2017. Tampa, Florida, USA, November 3–9, 2017: American Society of Mechanical Engineers.

[22] Abdo, P., R. Taghipour, and B.P. Huynh. *Simulation of Buoyancy Driven and Winddriven Ventilation Flow in a Three Dimensional Room Fitted with a Windcatcher*. in *21st Australasian Fluid Mechanics Conference, 2018*. 2018. Adelaide, Australia.

[23] Abdo, P., R. Taghipour, and B.P. Huynh. *THREE DIMENSIONAL SIMULATION OF VENTILATION FLOW THROUGH A SOLAR WINDCATCHER*. in *The ASME - JSME - KSME Joint Fluids Engineering Conference 2019, AJKFLUIDS2019*. 2019. San Francisco, CA, USA.

[24] Dehghani-sanij, A.R., M. Soltani, and K. Raahemifar, *A new design of wind tower for passive ventilation in buildings to reduce energy consumption in windy regions*. Renewable and Sustainable Energy Reviews, 2015. **42**: p. 182-195.

[25] Manso, M. and J. Castro-Gomes, *Green wall systems: A review of their characteristics*. Renewable and Sustainable Energy Reviews, 2015. **41**: p. 863-871.

[26] Lohr, V.L., C.H. Pearson-Mims, and G.K. Goodwin, *Interior plants may improve worker productivity and reduce stress in a windowless environment*. Journal of Environmental Horticulture, 1996. **14**: p. 97-100.

[27] Fjeld, T., *The effect of interior planting on health and discomfort among workers and school children*. Hortscience, 2000. **10**(1): p. 46-52.

[28] Park, J.H., J.M. Cox-Ganser, K. Kreiss, S.K. White, and C.Y. Rao, *Hydrophilic fungi and ergosterol associated with respiratory illness in a water-damaged building*. Environmental Health Perspectives, 2008. **116**: p. 45-50.

[29] Bringslimark, T., T. Hartig, and G.G. Patil, *The psychological benefits of indoor plants: A critical review of the experimental literature*. Journal of Environmental Psychology, 2009. **29**(4): p. 422-433.

[30] Irga, P.J., N.J. Paull, P. Abdo, B.P. Huynh, V. Avakian, T. Nguyen, and F. Torpy, *DEVELOPING THE JUNGLEFY BREATHING WALL FOR ENHANCED INDOOR AIR QUALITY REMEDIATION*. 2017: Sydney, Australia.

[31] Pettit, T., P. Irga, P. Abdo, B. Huynh, J. Stephen, and F.R. Torpy, *DEVELOPMENT AND AUGMENTATION THE JUNGLEFY BREATHING WALL*. 2017, UTS: Sydney, Australia.

[32] Torpy, F.R., M. Zavattaro, P.J. Irga, and M.D. Burchett, *Assessing the air quality remediation capacity of the JUNGLEFY breathing wall - Modular plant wall system.*, in *Research Report*. 2015, School of Life Sciences, Faculty of Science, University of Technology Sydney.

[33] Irga, P.J., P. Abdo, M. Zavattaro, and F.R. Torpy, *An assessment of the potential fungal bioaerosol production from an active living wall*. Building and Environment, 2017. **111**: p. 140-146.

[34] Pettit, T., P.J. Irga, P. Abdo, and F.R. Torpy, *Do the plants in functional green walls contribute to their ability to filter particulate matter?* Building and Environment, 2017. **125**(Supplement C): p. 299-307.

[35] Kontoleon, K.J. and E.A. Eumorfopoulou, *The effect of the orientation and proportion of a plant-covered wall layer on the thermal performance of a building zone*. Building and Environment, 2010. **45**(5): p. 1287-1303.

[36] Abdo, P. and B.P. Huynh. *Effect of Passive Green Wall Modules on Air Temperature and Humidity*. in *Proceedings of the ASME 2018 International Mechanical Engineering Congress and Exposition IMECE2018*. 2018. November 9-15, 2018, Pittsburgh, PA, USA: American Society of Mechanical Engineers.

[37] Abdo, P., B.P. Huynh, and V. Avakian. *Effect of Green Wall Modules on Air Temperature and Humidity*. in *Proceedings of the ASME 2018 5th Joint US-European Fluids Engineering Summer Conference FEDSM2018*. 2018. July 15-20, 2018, Montreal, Quebec, Canada: American Society of Mechanical Engineers.

[38] Pérez, G., L. Rincón, A. Vila, J.M. González, and L.F. Cabeza, *Green vertical systems for buildings as passive systems for energy savings*. Applied Energy, 2011. **88**(12): p. 4854-4859.

[39] Darlington, A., M.A. Dixon, and C. Pilger, *The use of biofilters to improve indoor air quality: the removal of toluene, TCE, and formaldehyde*. Life support & biosphere science : international journal of earth space, 1998. **5**(1): p. 63-69.

[40] Abdo, P., B.P. Huynh, and V. Avakian. *Distribution of Air Flow Through a Green Wall Module*. in *ASME 2017 Fluids Engineering Division Summer Meeting*. 2017. Waikoloa, Hawaii, USA: American Society of Mechanical Engineers.

[41]   Abdo, P., B.P. Huynh, and V. Avakian. *EFFECT OF FAN SPEED ON AIR FLOW THROUGH A GREEN WALL MODULE*. in *Proceedings of the ASME 2018 5th Joint US-European Fluids Engineering Summer Conference FEDSM2018*. 2018. July 15-20, 2018, Montreal, Quebec, Canada: American Society of Mechanical Engineers.

[42]   Abdo, P., B.P. Huynh, P.J. Irga, and F.R. Torpy, *Evaluation of air flow through an active green wall biofilter.* Urban Forestry & Urban Greening, 2019. **41**: p. 75-84.

[43]   Abhat, A., *Low temperature latent heat thermal energy storage: Heat storage materials.* Solar Energy, 1983. **30**(4): p. 313-332.

[44]   Zhou, D., C.Y. Zhao, and Y. Tian, *Review on thermal energy storage with phase change materials (PCMs) in building applications.* Applied Energy, 2012. **92**: p. 593-605.

[45]   Laxen, D.P.H. and E. Noordally, *Nitrogen dioxide distribution in street canyons.* Atmospheric Environment (1967), 1987. **21**(9): p. 1899-1903.

[46]   Porritt, J., *Capitalism As If the World Matters*. Vol. Rev. pbk. ed. 2007, Sterling, VA: Routledge.

[47]   Manso, M. and J.P. Castro-Gomes, *Thermal analysis of a new modular system for green walls.* Journal of Building Engineering, 2016. **7**: p. 53-62.

[48]   Wong, N.H., A.Y. Kwang Tan, P.Y. Tan, K. Chiang, and N.C. Wong, *Acoustics evaluation of vertical greenery systems for building walls.* Building and Environment, 2010. **45**(2): p. 411-420.

[49]   Alraddadi, O.L., Hannes; Boor, Brandon; Rajkhowa, Bhargav; Hutzel, William; and Dana, Michael, . *Air Cleaning Performance of a Biowall for Residential Applications*. in *International High Performance Buildings Conference*. 2016. Purdue, USA.

[50]   Irga, P.J. and F.R. Torpy. *Reducing indoor air pollutants through horticultural biotechnology*. in *Green Infrastructure: Nature Based Solutions For Sustainable and Resilient Cities*. 2017. Orvieto, Italy, 2017.

[51]   Akeiber, H., P. Nejat, M.Z.A. Majid, M.A. Wahid, F. Jomehzadeh, I. Zeynali Famileh, J.K. Calautit, B.R. Hughes, and S.A. Zaki, *A review on phase change material (PCM) for sustainable passive cooling in building envelopes.* Renewable and Sustainable Energy Reviews, 2016. **60**: p. 1470-1497.

[52]   CFD-ACE, *CFD-ACE_V2013.3_Modules_Manual*. 2013, ESI Group.

[53]   Coddington, O., J.L. Lean, P. Pilewskie, M. Snow, and D. Lindholm, *A Solar Irradiance Climate Data Record.* Bulletin of the American Meteorological Society, 2016. **97**(7): p. 1265-1282.

[54]   ANSYS, *ANSYS Fluent (Including Ansys CFD-Post) Release 18.2*. 2018.

[55]   Davies, M., M. Ucci, M. Mccarthy, T. Oreszczyn, I. Ridley, D. Mumovic, J. Singh, and S. Pretlove, *A review of evidence linking ventilation rates in dwellings and respiratory health: a focus on house dust mites and mould.* 2004, International Journal of Ventilation , 3 (2) pp. 155-168. (2004): International Journal of Ventilation , 3 (2) pp. 155-168. (2004).

[56]   Molloy, S.B., M. Cheng, I.E. Galbally, M.D. Keywood, S.J. Lawson, J.C. Powell, R. Gillett, E. Dunne, and P.W. Selleck, *Indoor air quality in typical temperate zone Australian dwellings.* Atmospheric Environment, 2012. **54**: p. 400-407.

[57]   Newton, P., *Human Settlements, Australian State of the Environment Report 2001 (Theme Report)*. 2001, CSIRO Publishing on behalf of the Department of the Environment and Heritage, Canberra, Australia.

[58]   Marchetti, N., A. Cavazzini, L. Pasti, M. Catani, C. Malagu, and V. Guidi. *A campus sustainability initiative: Indoor air quality monitoring in classrooms*. in *AISEM Annual Conference, 2015 XVIII*. 2015.

[59]   Irga, P.J., *Investigations into air pollutant concentrations across inner Sydney and their relationships with urban forestry*. 2016: Sydney, Australia: University of Technology Sydney.

[60]   Hedge, A., *Indoor Work and Living Environments: Health, Safety and Peformance*, in *Indoor Air Quality, Health and Productivity*. 2009, Science publishers Inc: Ithaca, New York. p. 247-267.

[61]   Engvall, K., P. Wickman, and D. Norbäck, *Sick building syndrome and perceived indoor environment in relation to energy saving by reduced ventilation flow during heating season: a 1 year intervention study in dwellings.* Indoor Air, 2005. **15**(2): p. 120-126.

[62]   Wang, B.-L., T. Takigawa, Y. Yamasaki, N. Sakano, D.-H. Wang, and K. Ogino, *Symptom definitions for SBS (sick building syndrome) in residential dwellings.* International Journal of Hygiene and Environmental Health, 2008. **211**(1–2): p. 114-120.

[63]   Fisk, W.J., A.G. Mirer, and M.J. Mendell, *Quantitative relationship of sick building syndrome symptoms with ventilation rates.* Indoor Air, 2009. **19**(2): p. 159-165.

[64]   Tippayawong, N., P. Khuntong, C. Nitatwichit, Y. Khunatorn, and C. Tantakitti, *Indoor/outdoor relationships of size-resolved particle concentrations in naturally ventilated school environments.* Building and Environment, 2009. **44**(1): p. 188-197.

[65] Mitchell, B., *Building Materials Can Be a Major Source of Indoor Air Pollution.* Occupational Health & Safety, 2013. **82**(9): p. 62-64.

[66] Thevenet, F., L. Sivachandiran, O. Guaitella, C. Barakat, and A. Rousseau, *Plasma–catalyst coupling for volatile organic compound removal and indoor air treatment: a review.* Journal of Physics D: Applied Physics, 2014. **47**(22): p. 224011.

[67] Soreanu, G., M. Dixon, and A. Darlington, *Botanical biofiltration of indoor gaseous pollutants – A mini-review.* Chemical Engineering Journal, 2013. **229**: p. 585-594.

[68] Seow, W.J., G.S. Downward, H. Wei, N. Rothman, B. Reiss, J. Xu, B.A. Bassig, J. Li, J. He, H.D. Hosgood, G. Wu, R.S. Chapman, L. Tian, F. Wei, N.E. Caporaso, R. Vermeulen, and Q. Lan, *Indoor concentrations of nitrogen dioxide and sulfur dioxide from burning solid fuels for cooking and heating in Yunnan Province, China.* Indoor Air, 2016. **26**(5): p. 776-783.

[69] Torpy, F.R., P.J. Irga, and M.D. Burchett, *Reducing Indoor Air Pollutants Through Biotechnology*, in *Biotechnologies and Biomimetics for Civil Engineering*, F. Pacheco Torgal, et al., Editors. 2015, Springer International Publishing. p. 181-210.

[70] Erdmann, C.A. and M.G. Apte, *Mucous membrane and lower respiratory building related symptoms in relation to indoor carbon dioxide concentrations in the 100-building BASE dataset.* Indoor Air, 2004. **14**: p. 127-134.

[71] Ozgok-Kangal, K., İ. Arziman, G. Uzun, and Ş. Yildiz, *Carbon monoxide poisoning in the workplace: A hidden danger.* Apollo Medicine, 2016. **13**(3): p. 196-197.

[72] Naima, B., H. Henrietta, H. Greg, K. Robie, K. Andrew, and M. Virginia, *Essentials of Environmental Public Health ScienceA Handbook for Field Professionals.* 2012, 'Oxford University Press': Oxford, UK.

[73] Powe, N.A. and K.G. Willis, *Mortality and morbidity benefits of air pollution (SO2 and PM10) absorption attributable to woodland in Britain.* Journal of Environmental Management, 2004. **70**(2): p. 119-128.

[74] Li, L. and C.M. Mak, *The assessment of the performance of a windcatcher system using computational fluid dynamics.* Building and Environment, 2007. **42**(3): p. 1135-1141.

[75] Elmualim, A.A., *Verification of Design Calculations of a Wind Catcher/Tower Natural Ventilation System with Performance Testing in a Real Building.* International Journal of Ventilation, 2006. **4**(4): p. 393-404.

[76] Hadley-Goggin, J. *The Need for the Fall of Air Conditioning.* [website]; Available from: https://joshhg.wordpress.com/page/2/.

[77] Afonso, C. and A. Oliveira, *Solar chimneys: simulation and experiment.* Energy and Buildings, 2000. **32**(1): p. 71-79.

[78] Elmualim, A.A. and H.B. Awbi, *Wind Tunnel and CFD Investigation of the Performance of "Windcatcher" Ventilation Systems.* International Journal of Ventilation, 2002. **1**(1): p. 53-64.

[79] AboulNaga, M.M. and S.N. Abdrabboh, *Improving night ventilation into low-rise buildings in hot-arid climates exploring a combined wall–roof solar chimney.* Renewable Energy, 2000. **19**(1–2): p. 47-54.

[80] Ding, W., Y. Hasemi, and T. Yamada, *Natural ventilation performance of a double-skin façade with a solar chimney.* Energy and Buildings, 2005. **37**(4): p. 411-418.

[81] Niktash, A.R., *Investigation into two-sided windcatchers used for room ventilation.* 2016: Sydney, Australia: University of Technology Sydney.

[82] Munson, B.R., A.P. Rothmayer, T.H. Okiishi, and W.W. Huebsch, *Fundamentals of Fluid Mechanics.* 7th ed. 2013: Wiley.

[83] Montazeri, H., F. Montazeri, R. Azizian, and S. Mostafavi, *Two-sided wind catcher performance evaluation using experimental, numerical and analytical modeling.* Renewable Energy, 2010. **35**(7): p. 1424-1435.

[84] Evola, G. and V. Popov, *Computational analysis of wind driven natural ventilation in buildings.* Energy and Buildings, 2006. **38**(5): p. 491-501.

[85] Tu, J., G.H. Yeoh, and C. Liu, *Computational Fluid Dynamics - A Practical Approach (2nd Edition).* 2012, Elsevier.

[86] Harlow, F.H. and P.I. Nakayama, *Turbulence Transport Equations.* The Physics of Fluids, 1967. **10**(11): p. 2323-2332.

[87] Launder, B.E. and D.B. Spalding, *The numerical computation of turbulent flows.* Computer Methods in Applied Mechanics and Engineering, 1974. **3**(2): p. 269-289.

[88]   Yakhot, V., S.A. Orszag, S. Thangam, T.B. Gatski, and C.G. Speziale, *Development of turbulence models for shear flows by a double expansion technique.* Physics of Fluids A: Fluid Dynamics, 1992. **4**(7): p. 1510-1520.

[89]   Jones, B.M. and R. Kirby, *Quantifying the performance of a top–down natural ventilation Windcatcher™.* Building and Environment, 2009. **44**(9): p. 1925-1934.

[90]   Hughes, B.R. and S.A.A.A. Ghani, *Investigation of a windvent passive ventilation device against current fresh air supply recommendations.* Energy and Buildings, 2008. **40**(9): p. 1651-1659.

[91]   Ahmed Kabir, I.F.S., S. Kanagalingam, and F. Safiyullah, *Performance evaluation of air flow and thermal comfort in the room with Wind-Catcher using different CFD techniques under neutral Atmospheric Boundary Layer.* Energy Procedia, 2017. **143**: p. 199-203.

[92]   Spentzou, E., M.J. Cook, and S. Emmitt, *Natural ventilation strategies for indoor thermal comfort in Mediterranean apartments.* Building Simulation, 2018. **11**(1): p. 175-191.

[93]   Bahadori, M.N., *An improved design of wind towers for natural ventilation and passive cooling.* Solar Energy, 1985. **35**(2): p. 119-129.

[94]   E. Jazayeri, A.G., Islamic Azad University, Tehran, Iran, *Construction of windcatcher and necessity of enhancing the traditional windcatcher.* Magazine of Civil Engineering, 2011. **2011**(6).

[95]   Bansal, N.K., R. Mathur, and M.S. Bhandari, *A study of solar chimney assisted wind tower system for natural ventilation in buildings.* Building and Environment, 1994. **29**(4): p. 495-500.

[96]   Hunt, G.R. and P.P. Linden, *The fluid mechanics of natural ventilation—displacement ventilation by buoyancy-driven flows assisted by wind.* Building and Environment, 1999. **34**(6): p. 707-720.

[97]   Leng, P.C., M.H. Ahmad, D.R. Ossen, and M. Hamid, *TOWARDS SUSTAINABLE ARCHITECTURE: THE EFFECT OF THE SOLAR CHIMNEY MATERIAL ON THERMAL PERFORMANCE BASED ON CFD SIMULATION*, in *International Conference on Sustainable Urban Design for Liveable Cities (SUDLiC 2014)*. 2014.

[98]   Liu, J., T. Shui, and F. Ma, *Analysis of natural cross-ventilation in buildings driven by wind and buoyancy forces.* Applied Mechanics and Materials, 2013. **353-356**: p. 3001-3004.

[99]   Gan, G., *Interaction Between Wind and Buoyancy Effects in Natural Ventilation of Buildings.* The Open Construction and Building Technology Journal, 2010. **4**: p. 134-145.

[100]   Hughes, B.R. and M. Cheuk-Ming, *A study of wind and buoyancy driven flows through commercial wind towers.* Energy and Buildings, 2011. **43**(7): p. 1784-1791.

[101]   Wood, R.A., M.D. Burchett, R. Alquezar, R.L. Orwell, J. Tarran, and F. Torpy, *The potted-plant microcosm substantially reduces indoor air VOC pollution: I. Office field-study.* Water, Soil and Air Pollution, 2006. **175**: p. 163-180.

[102]   Yoo, M.H., Y.J. Kwon, K.-C. Son, and S.J. Kays, *Efficacy of Indoor Plants for the Removal of Single and Mixed Volatile Organic Pollutants and the Physiological Effects of the Volatiles on the Plants.* Journal for the American Society for Horticultural Science, 2006. **131**(4): p. 452-458.

[103]   Irga, P.J., F.R. Torpy, and M.D. Burchett, *Can hydroculture be used to enhance the performance of indoor plants for the removal of air pollutants?* Atmospheric Environment, 2013. **77**(0): p. 267-271.

[104]   Oh, G., G. Jung, M. Seo, and Y. Im, *Experimental study on variations of CO2 concentration in the presence of indoor plants and respiration of experimental animals.* Horticulture, Environment, and Biotechnology, 2011. **52**(3): p. 321-329.

[105]   Xu, Z., L. Wang, and H. Hou, *Formaldehyde removal by potted plant–soil systems.* Journal of Hazardous Materials, 2011. **192**(1): p. 314-318.

[106]   Torpy, F.R., P.J. Irga, and M.D. Burchett, *Profiling indoor plants for the amelioration of high CO2 concentrations.* Urban Forestry & Urban Greening, 2014. **13**(2): p. 227-233.

[107]   Irga, P.J., N.J. Paull, P. Abdo, and F.R. Torpy, *An assessment of the atmospheric particle removal efficiency of an in-room botanical biofilter system.* Building and Environment, 2017. **115**: p. 281-290.

[108]   Gawrońska, H. and B. Bakera, *Phytoremediation of particulate matter from indoor air by Chlorophytum comosum L. plants.* Air Quality, Atmosphere & Health, 2014: p. 1-8.

[109]   Darlington, A.B., J.F. Dat, and M.A. Dixon, *The Biofiltration of Indoor Air: Air Flux and Temperature Influences the Removal of Toluene, Ethylbenzene, and Xylene.* Environmental Science & Technology, 2001. **35**(1): p. 240-246.

[110]   Wang, Z., J. Pei, and J.S. Zhang, *Experimental investigation of the formaldehyde removal mechanisms in a dynamic botanical filtration system for indoor air purification.* Journal of Hazardous Materials, 2014. **280**(Supplement C): p. 235-243.

[111] Wang, Z. and J.S. Zhang, *Characterization and performance evaluation of a full-scale activated carbon-based dynamic botanical air filtration system for improving indoor air quality.* Building and Environment, 2011. **46**(3): p. 758-768.

[112] Hee Lee, C., B. Choi, and M. Young Chun, *Stabilizing Soil Moisture and Indoor Air Quality Purification in a Wall-typed Botanical Biofiltration System Controlled by Humidifying Cycle.* Vol. 33. 2015. 605-617.

[113] Torpy, F.R., M. Zavattaro, and P.J. Irga, *Green wall technology for the phytoremediation of indoor air: a system for the reduction of high CO2 concentrations.* Air Quality, Atmosphere & Health, 2017. **10**(5): p. 575-585.

[114] Pérez-Urrestarazu, L., R. Fernández-Cañero, A. Franco, and G. Egea, *Influence of an active living wall on indoor temperature and humidity conditions.* Ecological Engineering, 2016. **90**(Supplement C): p. 120-124.

[115] Irga, P.J., T.J. Pettit, and F.R. Torpy, *The phytoremediation of indoor air pollution: a review on the technology development from the potted plant through to functional green wall biofilters.* Reviews in Environmental Science and Bio/Technology, 2018.

[116] D'Alessandro, F., F. Asdrubali, and N. Mencarelli, *Experimental evaluation and modelling of the sound absorption properties of plants for indoor acoustic applications.* Building and Environment, 2015. **94**: p. 913-923.

[117] Azkorra, Z., G. Pérez, J. Coma, L.F. Cabeza, S. Bures, J.E. Álvaro, A. Erkoreka, and M. Urrestarazu, *Evaluation of green walls as a passive acoustic insulation system for buildings.* Applied Acoustics, 2015. **89**: p. 46-56.

[118] Davis, M.J.M., M.J. Tenpierik, F.R. Ramírez, and M.E. Pérez, *More than just a Green Facade: The sound absorption properties of a vertical garden with and without plants.* Building and Environment, 2017. **116**: p. 64-72.

[119] Coma, J., G. Pérez, A. de Gracia, S. Burés, M. Urrestarazu, and L.F. Cabeza, *Vertical greenery systems for energy savings in buildings: A comparative study between green walls and green facades.* Building and Environment, 2017. **111**: p. 228-237.

[120] Wong, N.H., A.Y.K. Tan, P.Y. Tan, and N.C. Wong, *Energy simulation of vertical greenery systems.* Energy and Buildings, 2009. **41**(12): p. 1401-1408.

[121] Pérez, G., J. Coma, I. Martorell, and L.F. Cabeza, *Vertical Greenery Systems (VGS) for energy saving in buildings: A review.* Renewable and Sustainable Energy Reviews, 2014. **39**: p. 139-165.

[122] De Gracia, A., L. Navarro, J. Coma, S. Serrano, J. Romaní, G. Pérez, and L.F. Cabeza, *Experimental set-up for testing active and passive systems for energy savings in buildings – Lessons learnt.* Renewable and Sustainable Energy Reviews, 2018. **82**: p. 1014-1026.

[123] Perini, K., F. Bazzocchi, L. Croci, A. Magliocco, and E. Cattaneo, *The use of vertical greening systems to reduce the energy demand for air conditioning. Field monitoring in Mediterranean climate.* Energy and Buildings, 2017. **143**: p. 35-42.

[124] Soares, N., J.J. Costa, A.R. Gaspar, and P. Santos, *Review of passive PCM latent heat thermal energy storage systems towards buildings' energy efficiency.* Energy and Buildings, 2013. **59**: p. 82-103.

[125] Hed, G. and R. Bellander, *Mathematical modelling of PCM air heat exchanger.* Energy and Buildings, 2006. **38**(2): p. 82-89.

[126] Waqas, A. and Z. Ud Din, *Phase change material (PCM) storage for free cooling of buildings—A review.* Renewable and Sustainable Energy Reviews, 2013. **18**: p. 607-625.

[127] Butala, V. and U. Stritih, *Experimental investigation of PCM cold storage.* Energy and Buildings, 2009. **41**(3): p. 354-359.

[128] Baetens, R., B.P. Jelle, and A. Gustavsen, *Phase change materials for building applications: A state-of-the-art review.* Energy and Buildings, 2010. **42**(9): p. 1361-1368.

[129] Tyagi, V.V. and D. Buddhi, *PCM thermal storage in buildings: A state of art.* Renewable and Sustainable Energy Reviews, 2007. **11**(6): p. 1146-1166.

[130] Verma, P., Varun, and S.K. Singal, *Review of mathematical modeling on latent heat thermal energy storage systems using phase-change material.* Renewable and Sustainable Energy Reviews, 2008. **12**(4): p. 999-1031.

[131] Zhang, Y., K. Lin, Q. Zhang, and H. Di, *Ideal thermophysical properties for free-cooling (or heating) buildings with constant thermal physical property material.* Energy and Buildings, 2006. **38**(10): p. 1164-1170.

[132] Ramakrishnan, S., X. Wang, M. Alam, J. Sanjayan, and J. Wilson, *Parametric analysis for performance enhancement of phase change materials in naturally ventilated buildings.* Energy and Buildings, 2016. **124**: p. 35-45.

[133] Álvarez, S., L.F. Cabeza, A. Ruiz-Pardo, A. Castell, and J.A. Tenorio, *Building integration of PCM for natural cooling of buildings.* Applied Energy, 2013. **109**: p. 514-522.

[134] Mosaffa, A.H., C.A. Infante Ferreira, F. Talati, and M.A. Rosen, *Thermal performance of a multiple PCM thermal storage unit for free cooling.* Energy Conversion and Management, 2013. **67**: p. 1-7.

[135] Kivva, T., B.P. Huynh, M. Gaston, and D. Munn, *A numerical study of ventilation flow through a 3-dimensional room with a fan.* ICHMT DIGITAL LIBRARY ONLINE, 2009.

[136] Niktash, A.R. and B.P. Huynh. *Numerical Study of Ventilation Flow Through a Two Dimensional Room Fitted With a Windcatcher.* in *ASME 2011 International Mechanical Engineering Congress & Exposition.* 2011. Denver, Colorado, USA.

[137] ASHRAE, *ANSI/ASHRAE standard 55-2010 : thermal environmental conditions for human occupancy.* 2010.

[138] Esfeh, M.K., A.A. Dehghan, M.D. Manshadi, and S. Mohagheghian, *Visualized flow structure around and inside of one-sided wind-catchers.* Energy and Buildings, 2012. **55**: p. 545-552.

[139] Niktash, A. and B.P. Huynh, *ICCM2015: A Comparison of RANS and LES Computational Methods in Analyzing Ventilation Flow Through a Room Fitted with a Two-Sided Windcatcher.* International Journal of Computational Methods, 2017. **14**(03): p. 1750021.

[140] Abdo, P., B.P. Huynh, V. Avakian, T. Nguyen, J. Gammon, F.R. Torpy, and P.J. Irga. *Measurement of air flow through a green-wall module.* in *20th Australasian Fluid Mechanics Conference.* 2016. Perth, Australia.

[141] Oh, G.S., G.J. Jung, M.H. Seo, and Y.B. Im, *Experimental study on variations of CO_2 concentration in the presence of indoor plants and respiration of experimental animals.* Horticulture, Environment, and Biotechnology, 2011. **52**(3): p. 321-329.

[142] Huynh, B.P., *Private communication.* 2016.

[143] Huynh, B.P., *Private communication.* 2018.

[144] Petterson, T., *Variation of energy consumption in dwellings due to climate, building and inhabitants.* Energy and Buildings, 1994. **21**: p. 209-218.

[145] Lam, J.C., R.Y.C. Chan, C.L. Tsang, and D.H.W. Li, *Electricity use characteristics of purpose-built office buildings in subtropical climates.* Energy Conversion and Management, 2004. **45**(6): p. 829-844.

[146] Zhai, J., S.N. Al Saadi, M. El Mankibi, and R. Slowinski, *Breathing and Living Walls,* in *Advanced Energy Efficient Building Envelope Systems*, M. Krarti, Editor. 2017, ASME: New York, NY.

[147] Souayfane, F., F. Fardoun, and P.-H. Biwole, *Phase change materials (PCM) for cooling applications in buildings: A review.* Energy and Buildings, 2016. **129**: p. 396-431.

Appendix

The following tables are related to the results of Chapter 5. All of these tables are referenced in the text and are shown by graphs.

PCM Walls Only	Temperature, °C								
	Amb H1	In C8	Out E7	Lf Fr G4	Lf Bck F9	Rt Fr B6	Rt Bck D10	Rt Mid A5	Room Average
start	19.81	19.65	19.23	19.26	19.20	19.13	19.47	19.46	19.34
15 min	19.86	19.96	19.51	19.34	19.35	19.20	19.58	19.61	19.51
30 min	22.49	27.64	23.93	23.56	22.92	23.60	22.93	23.63	24.03
45 min	23.35	28.80	25.26	24.94	24.24	25.01	24.36	25.00	25.37
60 min	24.00	29.47	26.05	25.80	25.14	25.85	25.24	25.87	26.20
75 min	24.52	29.90	26.68	26.39	25.75	26.49	25.95	26.45	26.80
90 min	24.85	30.26	27.16	26.90	26.25	26.97	26.47	26.99	27.29
105 min	25.31	30.53	27.56	27.36	26.75	27.38	26.90	27.42	27.70
120 min	25.59	30.76	27.90	27.66	27.01	27.76	27.30	27.74	28.02
135 min	25.82	31.06	28.25	28.02	27.38	28.09	27.57	28.06	28.35
150 min	26.06	31.29	28.57	28.33	27.71	28.44	27.89	28.39	28.66
165 min	26.26	31.48	28.87	28.64	28.00	28.74	28.19	28.67	28.94
180 min	26.55	31.62	29.12	28.90	28.34	28.99	28.44	28.93	29.19
195 min	26.83	31.80	29.39	29.16	28.57	29.28	28.76	29.19	29.45
210 min	26.94	31.94	29.61	29.38	28.83	29.54	28.98	29.43	29.67
225 min	27.21	32.11	29.87	29.64	29.05	29.76	29.17	29.67	29.90
240 min	27.33	32.23	30.08	29.85	29.25	30.02	29.48	29.88	30.11
255 min	27.63	32.50	30.50	30.31	29.78	30.44	29.90	30.30	30.53
270 min	27.72	32.67	30.73	30.50	30.02	30.68	30.17	30.52	30.76
285 min	27.90	32.81	30.92	30.74	30.20	30.85	30.35	30.74	30.94
average	25.30	29.92	27.46	27.23	26.69	27.31	26.85	27.30	27.54

Table A-0-1 Temperature readings for chamber with PCM Walls and stage 1 heating element

PCM Floor and Walls	Temperature, °C								
	Amb H1	In C8	Out E7	Lf Fr G4	Lf Bck F9	Rt Fr B6	Rt Bck D10	Rt Mid A5	Room Average
start	19.83	19.24	19.12	19.17	19.09	19.39	19.37	19.39	19.25
15 min	22.78	27.68	24.27	23.88	23.2	23.91	22.91	23.93	24.25
30 min	23.83	28.93	25.57	25.23	24.43	25.21	24.21	25.21	25.54
45 min	24.53	29.56	26.37	26.04	25.21	25.99	24.93	26	26.30
60 min	25.01	30.09	26.96	26.64	25.82	26.62	25.5	26.6	26.89
75 min	25.44	30.42	27.42	27.09	26.16	27.08	26	27.08	27.32
90 min	25.77	30.6	27.77	27.46	26.58	27.42	26.4	27.44	27.67
105 min	26.18	30.86	28.09	27.75	26.84	27.71	26.75	27.72	27.96
120 min	26.36	31.15	28.44	28.08	27.22	27.99	27	28	28.27

135 min	26.7	31.36	28.73	28.39	27.53	28.3	27.33	28.31	28.56
150 min	26.97	31.66	29.05	28.71	27.83	28.64	27.59	28.63	28.87
165 min	27.16	31.81	29.31	28.99	28.15	28.92	27.86	28.89	29.13
180 min	27.35	31.97	29.54	29.23	28.33	29.13	28.12	29.12	29.35
195 min	27.64	32.12	29.82	29.49	28.53	29.41	28.39	29.41	29.60
210 min	27.81	32.26	30.05	29.74	28.87	29.65	28.62	29.65	29.83
225 min	27.94	32.4	30.24	29.94	29.05	29.89	28.89	29.89	30.04
240 min	28.09	32.5	30.46	30.17	29.31	30.09	29.1	30.08	30.24
255 min	28.26	32.62	30.65	30.39	29.39	30.29	29.31	30.31	30.42
270 min	28.33	32.77	30.87	30.61	29.77	30.49	29.57	30.5	30.65
285 min	28.44	32.8	30.94	30.71	29.9	30.63	29.7	30.63	30.76
average	26.22	30.64	28.18	27.89	27.06	27.84	26.88	27.84	28.05

Table A-0-2 Temperature readings for chamber with PCM Floor and Walls and stage 1 heating element

PCM Full	Temperature, °C								
	Amb H1	In C8	Out E7	Lf Fr G4	Lf Bck F9	Rt Fr B6	Rt Bck D10	Rt Mid A5	Room Average
start	19.80	20.80	20.09	20.01	19.90	19.91	20.12	20.22	20.15
15 min	22.68	27.89	24.68	24.50	23.89	24.42	23.72	24.51	24.80
30 min	23.44	28.70	25.52	25.35	24.76	25.30	24.57	25.33	25.65
45 min	24.01	29.27	26.12	25.95	25.34	25.90	25.17	25.96	26.24
60 min	24.51	29.63	26.54	26.40	25.80	26.37	25.71	26.37	26.69
75 min	24.89	29.96	26.86	26.76	26.20	26.76	26.02	26.74	27.04
90 min	25.22	30.27	27.17	27.10	26.49	27.08	26.30	27.09	27.36
105 min	25.60	30.44	27.37	27.35	26.74	27.34	26.57	27.32	27.59
120 min	25.83	30.65	27.56	27.63	26.98	27.61	26.85	27.56	27.83
135 min	26.04	30.93	27.86	27.89	27.26	27.89	27.10	27.84	28.11
150 min	26.33	31.15	28.16	28.13	27.46	28.14	27.33	28.07	28.35
165 min	26.53	31.27	28.32	28.25	27.50	28.26	27.50	28.21	28.47
180 min	26.62	31.44	28.48	28.46	27.75	28.41	27.70	28.37	28.66
195 min	26.90	31.55	28.84	28.91	28.30	28.91	28.21	28.94	29.09
210 min	27.03	31.67	29.07	29.13	28.47	29.16	28.40	29.18	29.30
225 min	27.27	31.83	29.47	29.34	28.67	29.34	28.46	29.17	29.47
240 min	27.44	32.01	29.71	29.50	28.90	29.55	28.69	29.40	29.68
255 min	27.64	32.21	29.91	29.70	29.10	29.75	28.89	29.60	29.88
270 min	27.84	32.41	30.11	29.90	29.30	29.95	29.09	29.80	30.08
285 min	28.04	32.61	30.31	30.10	29.50	30.15	29.29	30.00	30.28
average	25.68	30.33	27.61	27.52	26.92	27.51	26.78	27.48	27.74

Table A-0-3 Temperature readings for chamber with PCM full and stage 1 heating element

PCM Full plus Windcatcher	Temperature, °C								
	Amb H1	In C8	Out E7	Lf Fr G4	Lf Bck F9	Rt Fr B6	Rt Bck D10	Rt Mid A5	Room Average
start	19.86	20.56	19.64	19.29	19.25	19.18	19.42	19.55	19.56
15 min	22.64	27.90	23.32	22.88	21.99	22.61	22.20	22.92	23.40
30 min	23.44	28.93	24.42	23.95	23.06	23.70	23.25	23.97	24.47
45 min	24.00	29.58	25.22	24.75	23.88	24.49	23.82	24.73	25.21
60 min	24.62	30.15	25.81	25.34	24.45	25.18	24.53	25.31	25.82
75 min	25.03	30.61	26.29	25.85	24.92	25.69	24.97	25.81	26.31
90 min	25.39	30.91	26.70	26.19	25.30	26.08	25.34	26.14	26.67
105 min	25.71	31.17	27.06	26.56	25.59	26.38	25.65	26.49	26.99
120 min	26.03	31.46	27.37	26.86	25.87	26.73	25.88	26.81	27.28
135 min	26.32	31.67	27.63	27.13	26.21	27.06	26.16	27.07	27.56
150 min	26.59	31.83	27.90	27.38	26.46	27.29	26.47	27.33	27.81
165 min	26.78	32.02	28.11	27.62	26.67	27.58	26.62	27.55	28.02
180 min	27.02	32.22	28.37	27.88	26.85	27.84	26.88	27.77	28.26
195 min	27.22	32.44	28.60	28.13	27.05	28.11	27.12	28.06	28.50
210 min	27.38	32.56	28.82	28.30	27.34	28.36	27.35	28.24	28.71
225 min	27.65	32.73	29.09	28.59	27.58	28.58	27.55	28.43	28.94
240 min	27.77	32.84	29.26	28.78	27.73	28.86	27.72	28.66	29.12
255 min	27.85	32.99	29.51	28.98	27.97	29.06	27.95	28.88	29.33
270 min	28.10	33.13	29.75	29.27	28.21	29.33	28.08	29.12	29.56
285 min	28.25	33.29	29.98	29.49	28.43	29.59	28.43	29.38	29.80
average	25.88	30.95	27.14	26.66	25.74	26.59	25.77	26.61	27.07

Table A-0-4 Temperature readings for chamber with PCM full plus windcatcher and stage 1 heating element

No PCM	Temperature, °C								
	Amb H1	In C8	Out E7	Lf Fr G4	Lf Bck F9	Rt Fr B6	Rt Bck D10	Rt Mid A5	Room Average
start	18.85	19.36	19.22	19.26	19.26	19.10	19.48	19.58	19.32
15 min	26.67	35.99	30.03	29.35	27.79	29.13	27.85	29.03	29.88
30 min	28.25	37.69	32.13	31.47	30.00	31.40	30.12	31.13	31.99
45 min	29.36	38.72	33.68	33.05	31.50	33.01	31.64	32.68	33.47
60 min	30.23	39.43	34.76	34.15	32.79	34.16	32.85	33.87	34.57
75 min	30.88	39.86	35.63	35.02	33.76	35.01	33.78	34.72	35.40
90 min	31.49	40.39	36.39	35.82	34.63	35.76	34.68	35.53	36.17
105 min	32.07	40.87	37.05	36.49	35.37	36.42	35.44	36.24	36.84
120 min	32.61	41.30	37.60	37.02	35.89	37.01	35.97	36.78	37.37
135 min	33.02	41.66	38.09	37.53	36.44	37.51	36.52	37.32	37.87
150 min	33.39	41.99	38.49	37.98	36.87	37.96	36.85	37.71	38.26
165 min	33.81	42.29	38.88	38.38	37.37	38.31	37.39	38.13	38.68
180 min	34.15	42.60	39.25	38.73	37.79	38.66	37.78	38.49	39.04
195 min	34.42	42.84	39.58	39.06	38.12	38.95	38.11	38.81	39.35

210 min	34.76	43.17	39.87	39.39	38.34	39.30	38.43	39.14	39.66
225 min	35.01	43.43	40.16	39.64	38.61	39.61	38.70	39.41	39.94
240 min	35.40	43.83	40.52	40.02	38.94	39.97	38.99	39.73	40.29
255 min	35.57	43.92	40.71	40.23	39.16	40.15	39.20	39.94	40.47
270 min	35.88	44.17	41.00	40.49	39.46	40.43	39.52	40.24	40.76
285 min	36.11	44.46	41.24	40.73	39.71	40.67	39.79	40.44	41.01
average	32.10	40.40	36.71	36.19	35.09	36.13	35.15	35.95	36.52

Table A-0-5 Temperature readings for empty chamber (No PCM) with stage 2 heating element

PCM Walls Only	Temperature, °C								
	Amb H1	In C8	Out E7	Lf Fr G4	Lf Bck F9	Rt Fr B6	Rt Bck D10	Rt Mid A5	Room Average
start	19.92	25.46	20.89	20.12	19.72	20.01	20.06	20.51	20.97
15 min	25.18	35.87	28.63	27.88	26.16	28.15	26.35	27.82	28.70
30 min	26.83	37.49	30.35	29.69	27.97	30.05	28.17	29.67	30.48
45 min	28.00	38.50	31.69	31.01	29.26	31.30	29.55	30.89	31.74
60 min	28.75	39.25	32.70	31.97	30.27	32.39	30.69	31.95	32.75
75 min	29.52	39.85	33.63	33.07	31.13	33.50	31.60	32.94	33.68
90 min	30.21	40.39	34.50	33.93	32.15	34.32	32.43	33.75	34.50
105 min	30.75	40.88	35.23	34.68	32.92	35.20	33.22	34.51	35.24
120 min	31.39	41.31	36.01	35.47	33.60	35.87	33.78	35.10	35.88
135 min	31.67	41.67	36.62	36.12	34.34	36.54	34.36	35.85	36.50
150 min	32.14	42.02	37.29	36.77	35.04	37.20	35.02	36.43	37.11
165 min	32.67	42.28	37.80	37.36	35.66	37.71	35.73	37.03	37.65
180 min	32.89	42.52	38.26	37.79	36.30	38.19	36.29	37.50	38.12
195 min	33.30	42.87	38.81	38.34	36.99	38.65	36.96	38.00	38.66
210 min	33.53	43.07	39.17	38.76	37.42	39.08	37.34	38.44	39.04
225 min	33.61	43.33	39.57	39.17	38.04	39.46	37.81	38.85	39.46
240 min	33.99	43.59	39.94	39.58	38.51	39.89	38.28	39.36	39.88
255 min	34.39	43.97	40.35	39.97	38.95	40.25	38.87	39.71	40.30
270 min	34.45	44.19	40.65	40.29	39.38	40.55	39.21	40.05	40.62
285 min	34.93	44.36	40.92	40.63	39.62	40.91	39.46	40.37	40.90
average	30.91	40.64	35.65	35.13	33.67	35.46	33.76	34.94	35.61

Table A-0-6 Temperature readings for chamber with PCM Walls and stage 2 heating element

PCM Floor and Walls	Temperature, °C								
	Amb H1	In C8	Out E7	Lf Fr G4	Lf Bck F9	Rt Fr B6	Rt Bck D10	Rt Mid A5	Room Average
start	20.67	21.02	20.39	20.36	20.40	20.66	20.61	20.62	20.58
15 min	26.81	36.74	29.62	29.14	28.13	28.93	26.81	28.93	29.76
30 min	28.45	38.38	31.33	30.64	29.73	30.43	28.32	30.45	31.33
45 min	29.53	39.30	32.52	31.86	30.63	31.55	29.48	31.53	32.41

60 min	30.30	40.03	33.54	32.80	31.62	32.48	30.39	32.50	33.34
75 min	30.99	40.71	34.55	33.79	32.38	33.47	31.23	33.46	34.23
90 min	31.57	41.12	35.35	34.65	33.19	34.20	31.94	34.22	34.95
105 min	32.08	41.55	36.17	35.47	34.06	35.06	32.87	35.07	35.75
120 min	32.61	42.02	36.94	36.30	34.87	35.79	33.62	35.79	36.48
135 min	33.09	42.25	37.59	37.04	35.66	36.68	34.53	36.68	37.20
150 min	33.31	42.46	38.17	37.62	36.25	37.24	35.27	37.23	37.75
165 min	33.71	42.80	38.78	38.23	37.00	37.88	36.05	37.85	38.37
180 min	34.12	43.19	39.30	38.86	37.57	38.56	36.75	38.56	38.97
195 min	34.49	43.58	39.87	39.43	38.24	39.10	37.44	39.11	39.54
210 min	34.63	43.89	43.37	39.93	38.87	39.60	38.06	39.61	40.48
225 min	34.96	43.93	40.66	40.29	39.34	39.99	38.53	40.00	40.39
240 min	35.20	44.30	41.02	40.72	39.70	40.34	38.99	40.33	40.77
255 min	35.59	44.54	41.34	41.04	40.14	40.78	39.45	40.78	41.15
270 min	35.81	44.75	41.70	41.40	40.47	41.03	39.86	41.03	41.46
285 min	35.92	44.78	41.85	41.56	40.63	41.32	40.11	41.32	41.65
average	32.19	41.07	36.70	36.06	34.94	35.75	34.02	35.75	36.33

Table A-0-7 Temperature readings for chamber with PCM Floor and Walls and stage 2 heating element

PCM Full	Temperature, °C								
	Amb H1	In C8	Out E7	Lf Fr G4	Lf Bck F9	Rt Fr B6	Rt Bck D10	Rt Mid A5	Room Average
start	20.08	20.96	19.60	19.73	19.67	19.58	19.84	19.94	19.90
15 min	25.73	36.03	29.04	28.41	26.63	28.38	26.38	28.22	29.01
30 min	27.15	37.64	30.58	29.95	28.18	29.94	27.75	29.69	30.53
45 min	28.13	38.62	31.60	30.99	29.01	31.03	28.74	30.61	31.51
60 min	29.05	39.36	32.54	31.87	29.91	31.96	29.70	31.64	32.42
75 min	29.67	39.95	33.41	32.74	30.84	32.89	30.35	32.30	33.21
90 min	30.39	40.43	34.09	33.42	31.31	33.64	30.93	33.05	33.84
105 min	30.95	40.77	34.78	34.04	31.97	34.37	31.54	33.75	34.46
120 min	31.52	41.40	35.55	34.91	32.63	35.19	32.32	34.49	35.21
135 min	31.97	41.71	36.21	35.56	33.51	35.89	33.04	35.11	35.86
150 min	32.37	42.18	36.99	36.29	34.40	36.61	33.94	35.90	36.62
165 min	32.65	42.47	37.63	37.00	34.94	37.34	34.64	36.56	37.23
180 min	33.13	42.80	38.20	37.60	35.69	37.91	35.24	37.17	37.80
195 min	33.55	43.04	38.73	38.20	36.37	38.50	35.94	37.73	38.36
210 min	33.87	43.37	39.28	38.80	36.90	39.02	36.56	38.34	38.90
225 min	34.20	43.66	39.77	39.33	37.58	39.58	37.26	38.93	39.45
240 min	34.34	43.80	40.14	39.78	38.17	39.94	37.89	39.41	39.87
255 min	34.63	44.11	40.57	40.22	38.73	40.41	38.48	39.89	40.34
270 min	34.92	44.46	40.97	40.57	39.34	40.76	38.95	40.24	40.76
285 min	35.27	44.64	41.31	41.00	39.66	41.14	39.42	40.69	41.12
average	31.18	40.57	35.55	35.02	33.27	35.20	32.95	34.68	35.32

Table A-0-8 Temperature readings for chamber with PCM full and stage 2 heating element

PCM Full plus Windcatcher	Temperature, °C								
	Amb H1	In C8	Out E7	Lf Fr G4	Lf Bck F9	Rt Fr B6	Rt Bck D10	Rt Mid A5	Room Average
start	19.79	19.58	19.14	19.17	19.10	19.03	19.28	19.35	19.24
15 min	24.79	35.73	26.48	25.61	24.01	25.05	23.58	25.21	26.52
30 min	26.31	37.43	28.18	27.29	25.62	26.55	25.20	26.35	28.09
45 min	27.40	28.59	28.41	28.48	26.67	27.88	26.34	27.55	27.70
60 min	28.36	39.19	30.26	29.34	37.32	28.66	26.89	28.45	31.44
75 min	28.84	39.86	31.04	30.10	28.11	29.58	27.68	29.44	30.83
90 min	29.66	40.40	31.81	30.84	28.72	30.34	28.23	30.14	31.50
105 min	30.33	40.87	32.43	31.43	29.37	30.98	29.00	30.22	32.04
120 min	30.74	41.33	33.07	32.01	29.98	31.72	29.47	31.12	32.67
135 min	31.27	41.76	33.69	32.71	30.51	32.44	30.04	32.24	33.34
150 min	31.75	42.09	34.34	33.31	31.06	33.11	30.73	32.95	33.94
165 min	32.01	42.47	34.92	33.89	31.64	33.87	31.31	33.16	34.47
180 min	32.47	42.72	35.51	34.59	32.28	34.50	31.86	34.12	35.08
195 min	32.78	43.06	36.12	35.18	32.88	35.18	32.55	34.64	35.66
210 min	33.08	43.30	36.67	35.83	33.64	35.79	33.18	34.88	36.18
225 min	33.59	43.69	37.30	36.42	34.28	36.48	33.78	35.88	36.83
240 min	33.73	43.95	37.85	37.04	34.99	37.08	34.45	36.75	37.44
255 min	33.97	44.15	38.30	37.55	35.64	37.57	35.08	37.11	37.91
270 min	34.32	44.31	38.70	37.98	36.34	38.03	35.62	37.65	38.38
285 min	34.82	44.62	39.12	38.35	36.97	38.45	35.97	38.05	38.79
average	30.50	39.96	33.17	32.36	30.96	32.11	30.01	31.76	32.90

Table A-0-9 Temperature readings for chamber with PCM full plus windcatcher and stage 2 heating element

No PCM	Temperature, °C								
	Amb H1	In C8	Out E7	Lf Fr G4	Lf Bck F9	Rt Fr B6	Rt Bck D10	Rt Mid A5	Room Average
start	18.50	19.56	18.87	18.87	18.83	18.71	19.05	19.09	19.00
15 min	22.12	27.34	24.16	23.75	22.93	23.68	23.21	23.76	24.12
30 min	23.08	28.26	25.33	24.96	24.22	24.92	24.43	24.98	25.30
45 min	23.71	28.88	26.20	25.86	25.19	25.81	25.35	25.86	26.16
60 min	24.24	29.31	26.87	26.53	25.86	26.49	26.06	26.51	26.80
75 min	24.68	29.66	27.39	27.08	26.49	27.03	26.66	27.08	27.34
90 min	25.13	30.01	27.88	27.58	26.92	27.57	27.13	27.55	27.80
105 min	25.47	30.33	28.29	28.01	27.41	27.96	27.61	28.00	28.23
120 min	25.79	30.55	28.61	28.35	27.80	28.29	27.95	28.33	28.56
135 min	26.08	30.79	28.92	28.64	28.08	28.60	28.25	28.63	28.84
150 min	26.37	31.00	29.19	28.92	28.43	28.90	28.56	28.93	29.13

165 min	26.59	31.22	29.44	29.16	28.61	29.17	28.81	29.16	29.37
180 min	26.81	31.37	29.61	29.37	28.83	29.33	28.99	29.33	29.55
195 min	27.04	31.54	29.80	29.56	29.04	29.54	29.20	29.55	29.75
210 min	27.18	31.65	29.98	29.73	29.22	29.70	29.36	29.71	29.91
225 min	27.37	31.80	30.14	29.91	29.37	29.87	29.55	29.88	30.07
240 min	27.55	32.01	30.30	30.08	29.57	30.06	29.75	30.06	30.26
average	25.16	29.72	27.71	27.43	26.87	27.39	27.05	27.44	27.66

Table A-0-10 Temperature readings for empty chamber (No PCM) with stage 1 heating element and room located closer to fan

PCM Full plus Windcatcher	Temperature, °C								
	Amb H1	In C8	Out E7	Lf Fr G4	Lf Bck F9	Rt Fr B6	Rt Bck D10	Rt Mid A5	Room Average
start	19.45	19.75	18.89	18.70	18.64	18.57	18.88	19.00	18.92
15 min	21.98	27.69	22.87	22.33	21.67	22.13	21.40	22.28	22.91
30 min	22.89	28.85	24.01	23.44	22.70	23.23	22.44	23.41	24.01
45 min	23.57	29.46	24.78	24.26	23.50	24.13	23.29	24.22	24.80
60 min	24.05	29.98	25.40	24.88	24.15	24.64	23.91	24.78	25.39
75 min	24.63	30.38	25.94	25.40	24.61	25.19	24.41	25.32	25.89
90 min	24.93	30.68	26.30	25.78	25.09	25.55	24.79	25.67	26.27
105 min	25.35	30.97	26.68	26.14	25.41	26.00	25.13	26.02	26.62
120 min	25.62	31.21	26.98	26.45	25.71	26.27	25.49	26.31	26.92
135 min	25.97	31.46	27.25	26.74	25.98	26.53	25.78	26.60	27.19
150 min	26.20	31.70	27.51	26.97	26.26	26.86	26.02	26.84	27.45
165 min	26.41	31.90	27.77	27.22	26.45	27.12	26.20	27.08	27.68
180 min	26.65	32.06	27.93	27.44	26.66	27.34	26.44	27.28	27.88
195 min	26.95	32.28	28.20	27.66	26.84	27.56	26.56	27.49	28.08
210 min	27.08	32.46	28.42	27.87	27.07	27.75	26.77	27.70	28.29
225 min	27.27	32.64	28.61	28.10	27.26	28.08	26.99	27.94	28.52
240 min	27.45	32.70	28.77	28.27	27.44	28.21	27.19	28.15	28.68
average	25.09	30.36	26.25	25.74	25.02	25.60	24.81	25.65	26.21

Table A-0-11 Temperature readings for chamber with PCM full plus windcatcher with stage 1 heating element and room located closer to fan

No PCM	Temperature, °C								
	Amb H1	In C8	Out E7	Lf Fr G4	Lf Bck F9	Rt Fr B6	Rt Bck D10	Rt Mid A5	Room Average
start	18.00	18.12	18.06	18.14	18.18	17.96	18.46	18.37	18.18
15 min	24.64	34.72	28.48	27.73	26.18	27.66	26.27	27.49	28.36
30 min	26.52	36.96	31.03	30.28	28.82	30.16	28.69	30.00	30.85
45 min	27.81	38.11	32.66	31.90	30.45	31.94	30.42	31.71	32.46
60 min	28.75	38.94	33.90	33.19	31.80	33.28	31.89	32.96	33.71
75 min	29.45	39.55	34.82	34.09	32.75	34.19	32.83	33.90	34.59
90 min	30.18	40.34	35.80	35.11	33.85	35.16	33.87	34.90	35.58

105 min	30.82	40.75	36.45	35.84	34.58	35.87	34.63	35.61	36.25
120 min	31.41	41.33	37.18	36.50	35.35	36.57	35.40	36.29	36.95
135 min	31.87	41.75	37.66	37.10	35.81	37.18	35.94	36.83	37.47
150 min	32.27	42.01	38.10	37.50	36.40	37.52	36.41	37.31	37.89
165 min	32.78	42.37	38.54	37.91	36.84	37.98	36.83	37.69	38.31
180 min	33.12	42.65	38.87	38.29	37.17	38.40	37.21	38.07	38.66
195 min	33.51	42.99	39.27	38.69	37.56	38.75	37.55	38.44	39.03
210 min	33.75	43.23	39.56	39.00	37.89	39.07	37.88	38.74	39.34
225 min	34.08	43.58	39.86	39.31	38.15	39.40	38.22	39.06	39.65
240 min	34.39	43.81	40.16	39.59	38.49	39.66	38.50	39.36	39.94
average	30.20	39.48	35.32	34.72	33.54	34.75	33.59	34.51	35.13

Table A-0-12 Temperature readings for empty chamber (No PCM) with stage 2 heating element and room located closer to fan

PCM Full plus Windcatcher	Temperature, °C								
	Amb H1	In C8	Out E7	Lf Fr G4	Lf Bck F9	Rt Fr B6	Rt Bck D10	Rt Mid A5	Room Average
start	19.47	19.82	18.88	18.43	18.45	18.34	18.58	18.69	18.74
15 min	24.36	36.23	26.42	25.56	23.88	25.07	23.33	25.13	26.52
30 min	25.81	37.82	28.20	27.20	25.54	26.70	24.96	26.80	28.18
45 min	26.87	38.78	29.41	28.49	26.61	27.94	26.09	27.92	29.32
60 min	27.62	39.55	30.35	29.37	27.47	28.70	26.96	28.74	30.16
75 min	28.37	40.21	31.17	30.18	28.29	29.70	27.66	29.51	30.96
90 min	29.04	40.65	31.87	30.84	29.05	30.37	28.35	30.17	31.61
105 min	30.08	41.40	32.95	31.93	29.74	31.54	29.38	31.31	32.61
120 min	30.39	41.74	33.54	32.49	30.49	32.23	29.85	31.74	33.15
135 min	30.76	42.16	34.14	33.14	30.84	32.87	30.38	32.30	33.69
150 min	31.20	42.45	34.62	33.67	31.58	33.40	30.92	32.84	34.21
165 min	31.60	42.79	35.25	34.25	32.00	34.11	31.38	33.48	34.75
180 min	31.90	43.04	35.79	34.82	32.62	34.76	32.01	34.06	35.30
195 min	32.46	43.40	36.36	35.36	33.25	35.28	32.62	34.65	35.85
210 min	32.47	43.62	36.88	35.98	33.74	35.92	33.13	35.21	36.35
225 min	32.79	43.90	37.38	36.48	34.43	36.52	33.68	35.76	36.88
240 min	33.02	44.12	37.86	37.02	35.05	37.08	34.32	36.34	37.40
average	29.31	40.10	32.42	31.48	29.59	31.21	29.03	30.86	32.10

Table A-0-13 Temperature readings for chamber with PCM full plus windcatcher with stage 2 heating element and room located closer to fan

No PCM	Humidity, %								
	Amb H1	In C8	Out E7	Lf Fr G4	Lf Bck F9	Rt Fr B6	Rt Bck D10	Rt Mid A5	Room Average
start	54.06	54.63	51.25	52.59	52.31	51.56	51.35	52.65	52.33
15 min	41.59	27.01	34.41	36.89	39.68	36.14	38.97	38.24	35.90
30 min	40.53	26.33	32.78	35.12	37.61	34.26	36.90	36.45	34.21
45 min	40.05	26.13	31.82	34.03	36.49	33.13	35.78	35.37	33.25

60 min	39.37	25.86	30.87	33.12	35.49	32.24	34.59	34.25	32.35
75 min	38.99	25.98	30.47	32.65	34.61	31.82	33.90	33.79	31.89
90 min	38.57	25.83	29.91	32.04	33.85	31.19	33.18	33.14	31.31
105 min	38.11	25.66	29.40	31.49	33.09	30.68	32.48	32.55	30.76
120 min	37.47	25.37	28.87	30.93	32.58	30.12	31.84	31.96	30.24
135 min	37.00	25.08	28.40	30.41	31.95	29.61	31.26	31.40	29.73
150 min	36.57	24.90	28.09	30.03	31.56	29.27	30.96	31.09	29.41
165 min	36.14	24.79	27.82	29.77	31.09	29.05	30.54	30.75	29.12
180 min	35.78	24.60	27.48	29.41	30.73	28.72	30.12	30.42	28.78
195 min	35.54	24.41	27.24	29.16	30.45	28.48	29.85	30.20	28.54
210 min	35.02	24.16	26.90	28.75	30.05	28.08	29.37	29.76	28.15
225 min	34.68	23.93	26.69	28.50	29.89	27.73	29.23	29.50	27.93
240 min	34.16	23.58	26.24	28.11	29.44	27.36	28.84	29.11	27.52
255 min	34.06	23.56	26.14	27.97	29.34	27.25	28.68	28.98	27.42
270 min	33.42	23.20	25.69	27.53	28.79	26.81	28.14	28.52	26.95
285 min	33.04	23.15	25.43	27.22	28.52	26.59	27.70	28.19	26.69
average	37.71	26.41	29.79	31.79	33.38	31.00	32.68	32.82	31.12

Table A-0-14 Humidity readings for empty chamber (No PCM) with stage 2 heating element

PCM Walls Only	Humidity, %								
	Amb H1	In C8	Out E7	Lf Fr G4	Lf Bck F9	Rt Fr B6	Rt Bck D10	Rt Mid A5	Room Average
start	47.26	32.92	42.06	45.57	47.23	44.73	46.18	45.90	43.51
15 min	41.20	25.67	34.25	36.80	39.50	35.20	38.89	37.66	35.42
30 min	40.76	25.39	33.53	36.00	38.84	34.47	38.08	36.86	34.74
45 min	40.37	25.37	33.03	35.46	38.18	33.91	37.22	36.40	34.23
60 min	39.72	25.13	32.32	34.71	37.33	33.12	36.27	35.52	33.49
75 min	39.34	25.00	31.67	33.84	36.85	32.30	35.42	34.78	32.84
90 min	38.63	24.78	30.85	33.04	35.63	31.43	34.80	33.99	32.07
105 min	38.24	24.54	30.16	32.44	34.71	30.85	33.79	33.39	31.41
120 min	37.77	24.40	29.65	31.76	34.31	30.25	33.62	32.86	30.98
135 min	37.41	24.28	29.12	31.10	33.43	29.69	33.02	32.25	30.41
150 min	36.98	24.10	28.48	30.46	32.72	29.00	32.40	31.65	29.83
165 min	36.59	24.06	28.06	29.91	32.08	28.57	31.69	31.05	29.35
180 min	36.07	23.86	27.63	29.40	31.28	28.07	30.92	30.53	28.81
195 min	35.70	23.65	27.14	28.96	30.50	27.68	30.24	29.99	28.31
210 min	35.54	23.51	26.79	28.53	30.10	27.33	29.75	29.64	27.95
225 min	35.42	23.41	26.45	28.16	29.47	27.03	29.38	29.26	27.59
240 min	35.00	23.24	26.10	27.82	28.98	26.64	28.94	28.76	27.21
255 min	34.65	23.03	25.81	27.48	28.58	26.32	28.33	28.44	26.85
270 min	34.52	22.87	25.56	27.17	28.10	26.07	27.93	28.09	26.54
285 min	34.03	22.76	25.30	26.91	27.87	25.83	27.73	27.83	26.32
average	37.76	24.60	29.70	31.78	33.78	30.42	33.23	32.74	30.89

Table A-0-15 Humidity readings for chamber with PCM Walls and stage 2 heating element

PCM Floor and Walls	Humidity, %								
	Amb H1	In C8	Out E7	Lf Fr G4	Lf Bck F9	Rt Fr B6	Rt Bck D10	Rt Mid A5	Room Average
start	49.19	49.25	49.26	47.23	49.38	48.87	48.05	48.02	48.58
15 min	35.52	36.61	36.62	33.47	25.53	36.84	38.86	39.26	35.31
30 min	35.00	36.08	36.10	32.72	25.10	36.22	38.33	38.43	34.71
45 min	34.58	35.76	35.76	32.29	25.01	36.19	37.84	38.02	34.41
60 min	33.95	35.10	35.09	31.64	24.82	35.57	37.24	37.63	33.87
75 min	33.38	34.59	34.57	30.99	24.73	35.06	36.97	37.35	33.47
90 min	32.66	33.99	33.98	30.37	24.74	34.56	36.28	37.02	32.99
105 min	31.99	33.26	33.26	29.77	24.63	33.79	35.36	36.76	32.40
120 min	31.40	32.82	32.84	29.25	24.56	33.02	34.81	36.47	31.97
135 min	30.75	31.91	31.91	28.73	24.58	32.42	33.76	36.20	31.36
150 min	30.36	31.52	31.49	28.40	24.62	31.87	33.04	36.19	31.02
165 min	29.81	30.95	30.94	27.88	24.50	31.20	32.23	35.87	30.51
180 min	29.29	30.36	30.36	27.44	24.30	30.70	31.55	35.57	30.04
195 min	28.80	29.83	29.84	27.01	24.10	29.90	30.83	35.25	29.54
210 min	28.42	29.46	29.47	26.66	23.98	29.40	30.21	35.18	29.19
225 min	28.06	29.07	29.06	26.35	24.00	28.87	29.68	34.87	28.84
240 min	27.47	28.57	28.56	25.86	23.56	28.37	29.02	34.36	28.33
255 min	27.26	28.19	28.20	25.68	23.45	28.04	28.56	34.03	28.02
270 min	27.01	28.08	28.09	25.41	23.36	27.74	28.27	33.89	27.83
285 min	26.92	27.84	27.85	25.36	23.46	27.65	28.12	33.80	27.73
average	31.59	32.66	32.66	29.63	25.62	32.81	33.95	36.71	32.01

Table A-0-16 Humidity readings for chamber with PCM Floor and Walls with stage 2 heating element

PCM Full	Humidity, %								
	Amb H1	In C8	Out E7	Lf Fr G4	Lf Bck F9	Rt Fr B6	Rt Bck D10	Rt Mid A5	Room Average
start	51.51	51.07	52.05	53.31	53.25	52.39	52.42	53.83	52.62
15 min	43.89	27.68	36.57	39.05	42.36	38.19	42.38	40.27	38.07
30 min	43.34	27.17	35.95	38.44	41.84	37.46	41.99	39.67	37.50
45 min	42.84	26.85	35.43	37.85	41.34	36.76	41.51	39.27	37.00
60 min	42.10	26.70	34.91	37.44	40.79	36.29	40.58	38.64	36.48
75 min	41.60	26.55	34.28	36.80	40.13	35.55	40.39	38.15	35.98
90 min	41.08	26.36	33.69	36.12	39.68	34.87	39.94	37.48	35.45
105 min	40.53	26.29	33.03	35.51	38.93	34.01	39.29	36.77	34.83
120 min	39.82	25.96	32.29	34.71	38.13	33.33	38.40	36.01	34.12
135 min	39.54	25.80	31.59	33.89	37.18	32.56	37.50	35.33	33.41
150 min	39.05	25.47	30.76	33.04	35.97	31.77	36.17	34.33	32.50
165 min	38.63	25.33	30.15	32.31	35.23	30.96	35.26	33.59	31.83
180 min	38.22	25.16	29.54	31.62	34.42	30.33	34.57	32.93	31.22

195 min	37.48	24.94	28.90	30.87	33.44	29.74	33.65	32.22	30.54
210 min	37.40	24.77	28.47	30.33	32.61	29.24	32.86	31.53	29.97
225 min	36.59	24.42	27.77	29.59	31.82	28.49	31.86	30.77	29.25
240 min	36.53	24.34	27.41	29.14	31.06	28.12	31.08	30.24	28.77
255 min	36.06	24.00	26.87	28.54	30.26	27.53	30.17	29.60	28.14
270 min	35.75	23.78	26.47	28.19	29.62	27.15	29.76	29.30	27.75
285 min	35.37	23.72	26.22	27.89	29.35	26.94	29.33	28.98	27.49
average	39.87	26.82	32.12	34.23	36.87	33.08	36.96	35.45	33.65

Table A-0-17 Humidity readings for chamber with PCM full with stage 2 heating element

PCM Full plus Windcatcher	Humidity, %								
	Amb H1	In C8	Out E7	Lf Fr G4	Lf Bck F9	Rt Fr B6	Rt Bck D10	Rt Mid A5	Room Average
start	46.98	48.91	47.80	49.10	49.02	48.23	48.25	49.64	48.71
15 min	42.00	25.87	37.83	40.71	43.64	40.81	44.20	42.60	39.38
30 min	41.44	25.28	36.95	39.91	43.00	40.33	43.46	41.96	38.70
45 min	41.04	25.04	36.43	39.45	42.71	39.62	43.15	41.31	38.25
60 min	40.43	25.11	36.08	39.11	42.78	39.34	43.28	41.03	38.11
75 min	40.16	24.71	35.33	38.27	41.92	38.28	42.35	40.41	37.32
90 min	39.08	24.33	34.47	37.40	41.05	37.35	41.74	39.62	36.57
105 min	38.34	24.07	33.73	36.67	40.28	36.50	40.61	38.80	35.81
120 min	38.07	23.98	33.26	36.26	39.72	35.88	40.27	38.38	35.39
135 min	37.63	23.83	32.73	35.58	39.29	35.15	39.74	37.51	34.83
150 min	37.31	23.82	32.26	35.09	38.68	34.48	39.00	37.16	34.36
165 min	37.38	23.74	31.82	34.64	38.29	33.88	38.52	36.57	33.92
180 min	36.90	23.70	31.29	33.92	37.57	33.22	37.74	35.93	33.34
195 min	36.56	23.51	30.60	33.25	36.75	32.42	36.93	35.09	32.65
210 min	36.24	23.37	30.02	32.51	35.69	31.69	36.10	34.40	31.97
225 min	35.67	23.14	29.38	31.84	34.90	30.95	35.29	33.46	31.28
240 min	35.56	22.97	28.80	31.14	33.95	30.27	34.59	32.88	30.66
255 min	35.10	22.79	28.31	30.57	33.01	29.73	33.60	32.16	30.03
270 min	34.94	22.79	27.88	30.07	32.18	29.17	32.90	31.62	29.51
285 min	34.57	22.73	27.63	29.77	31.91	28.96	32.46	31.29	29.25
average	38.27	25.18	33.13	35.76	38.82	35.31	39.21	37.59	35.00

Table A-0-18 Humidity readings for chamber with PCM full plus windcatcher and stage 2 heating element

No PCM	Temperature, °C								
	Amb H1	In C8	Out E7	Lf Fr G4	Lf Bck F9	Rt Fr B6	Rt Bck D10	Rt Mid A5	Room Average
start	29.18	33.68	32.01	31.72	31.20	31.72	31.38	31.69	31.92

15 min	24.06	23.14	26.04	26.81	27.02	26.67	27.08	26.97	26.25
30 min	23.17	21.95	24.60	25.19	25.50	25.07	25.41	25.40	24.73
45 min	22.61	21.33	23.50	24.07	24.39	23.89	24.38	24.29	23.69
60 min	22.10	20.88	22.70	23.20	23.42	22.98	23.51	23.41	22.87
75 min	21.80	20.76	22.19	22.58	22.81	22.37	22.90	22.80	22.35
90 min	21.43	20.44	21.71	22.06	22.27	21.86	22.35	22.29	21.85
105 min	21.12	20.27	21.32	21.60	21.80	21.40	21.92	21.83	21.45
120 min	20.90	19.92	20.90	21.17	21.36	20.97	21.45	21.40	21.03
135 min	20.60	19.84	20.62	20.84	21.01	20.65	21.16	21.09	20.74
150 min	20.42	19.66	20.35	20.55	20.71	20.37	20.92	20.82	20.48
165 min	20.26	19.47	20.14	20.33	20.47	20.13	20.62	20.56	20.25
180 min	19.98	19.31	19.81	19.98	20.10	19.79	20.24	20.21	19.92
195 min	19.83	19.21	19.64	19.80	19.91	19.61	20.06	20.03	19.75
210 min	19.69	19.08	19.49	19.63	19.76	19.45	19.91	19.87	19.60
225 min	19.61	18.98	19.35	19.49	19.59	19.29	19.76	19.72	19.45
240 min	19.48	18.91	19.21	19.36	19.47	19.15	19.63	19.59	19.33
255 min	19.33	18.83	19.11	19.24	19.35	19.05	19.54	19.48	19.23
270 min	19.33	18.78	19.06	19.18	19.25	18.98	19.46	19.41	19.16
285 min	19.29	18.71	18.96	19.09	19.18	18.89	19.35	19.32	19.07
average	21.21	20.66	21.53	21.79	21.93	21.61	22.05	22.01	21.66

Table A-0-19 Temperature readings during solidification for empty chamber (No PCM)

PCM Walls Only	Temperature, °C								
	Amb H1	In C8	Out E7	Lf Fr G4	Lf Bck F9	Rt Fr B6	Rt Bck D10	Rt Mid A5	Room Average
start	29.69	33.24	33.08	32.91	32.65	32.94	32.69	32.88	32.91
15 min	27.08	26.02	28.73	29.13	29.16	29.10	29.25	29.24	28.66
30 min	26.42	25.07	27.53	27.86	27.98	27.85	28.07	28.03	27.48
45 min	25.86	24.44	26.61	26.88	27.04	26.87	27.08	27.09	26.57
60 min	25.35	24.08	25.94	26.16	26.27	26.11	26.35	26.34	25.89
75 min	24.92	23.70	25.32	25.48	25.65	25.44	25.64	25.67	25.27
90 min	24.59	23.26	24.76	24.91	25.08	24.85	25.08	25.10	24.72
105 min	24.26	23.03	24.34	24.46	24.62	24.39	24.63	24.67	24.31
120 min	24.01	22.80	23.95	24.05	24.20	23.98	24.22	24.25	23.92
135 min	23.70	22.59	23.61	23.71	23.85	23.63	23.87	23.90	23.59
150 min	23.56	22.45	23.28	23.39	23.49	23.30	23.54	23.57	23.29
165 min	23.37	22.28	23.01	23.13	23.24	23.04	23.29	23.32	23.05
180 min	23.14	22.21	22.80	22.90	22.96	22.78	23.03	23.07	22.82
195 min	23.01	22.04	22.60	22.70	22.76	22.59	22.84	22.86	22.63
210 min	22.80	21.99	22.42	22.50	22.54	22.40	22.66	22.68	22.46
225 min	22.64	21.82	22.27	22.37	22.40	22.27	22.52	22.51	22.31
240 min	22.57	21.74	22.15	22.24	22.26	22.15	22.38	22.43	22.19
255 min	22.48	21.57	22.03	22.10	22.13	22.04	22.24	22.27	22.05
270 min	22.32	21.47	21.91	22.01	22.00	21.93	22.14	22.17	21.95
285 min	22.22	21.43	21.83	21.93	21.91	21.86	22.05	22.10	21.87

average	24.20	23.36	24.41	24.54	24.61	24.48	24.68	24.71	24.40

Table A-0-20 Temperature readings during solidification for chamber with PCM Walls

PCM Floor and Walls	Temperature, °C								
	Amb H1	In C8	Out E7	Lf Fr G4	Lf Bck F9	Rt Fr B6	Rt Bck D10	Rt Mid A5	Room Average
start	30.96	32.98	30.87	31.15	30.85	30.14	30.00	28.58	30.65
15 min	27.61	25.19	27.70	27.34	27.71	27.56	27.71	25.98	27.03
30 min	26.45	24.15	26.55	26.08	26.55	26.39	26.59	24.97	25.90
45 min	25.61	23.60	25.73	25.29	25.74	25.60	25.79	24.58	25.19
60 min	25.00	23.16	25.18	24.65	25.19	24.99	25.25	24.17	24.66
75 min	24.45	22.78	24.63	24.14	24.64	24.52	24.72	23.84	24.18
90 min	23.98	22.46	24.15	23.69	24.16	24.04	24.26	23.43	23.74
105 min	23.58	22.17	23.75	23.30	23.75	23.65	23.86	23.20	23.38
120 min	23.24	22.00	23.44	22.96	23.44	23.33	23.54	22.96	23.10
135 min	22.93	21.81	23.14	22.69	23.14	23.03	23.25	22.70	22.82
150 min	22.68	21.62	22.88	22.42	22.88	22.79	23.00	22.53	22.59
165 min	22.44	21.47	22.65	22.20	22.66	22.60	22.78	22.36	22.39
180 min	22.21	21.34	22.43	22.00	22.44	22.35	22.53	22.14	22.17
195 min	22.06	21.22	22.28	21.84	22.29	22.18	22.40	22.00	22.03
210 min	21.92	21.09	22.13	21.70	22.13	22.05	22.28	21.90	21.90
225 min	21.80	21.07	22.04	21.59	22.04	21.91	22.13	21.70	21.78
240 min	21.72	20.96	21.92	21.50	21.92	21.84	22.09	21.65	21.70
255 min	21.65	20.91	21.86	21.41	21.86	21.76	22.01	21.51	21.62
270 min	21.58	20.81	21.80	21.35	21.81	21.70	21.94	21.42	21.55
285 min	21.37	20.60	21.59	21.14	21.60	21.49	21.73	21.21	21.34
average	23.66	22.57	23.84	23.42	23.84	23.70	23.89	23.14	23.49

Table A-0-21 Temperature readings during solidification for chamber with PCM Floor and Walls

PCM Full	Temperature, °C								
	Amb H1	In C8	Out E7	Lf Fr G4	Lf Bck F9	Rt Fr B6	Rt Bck D10	Rt Mid A5	Room Average
start	29.31	36.24	32.52	31.79	31.01	32.03	29.83	31.01	32.06
15 min	25.64	25.13	27.20	27.17	27.07	27.45	27.10	27.21	26.90
30 min	25.19	24.14	26.02	26.05	26.04	26.17	26.06	26.17	25.81
45 min	24.66	23.57	25.29	25.33	25.36	25.37	25.43	25.45	25.12
60 min	24.26	23.12	24.65	24.77	24.82	24.72	24.88	24.89	24.55
75 min	23.84	22.75	24.14	24.30	24.38	24.21	24.40	24.44	24.09
90 min	23.44	22.39	23.70	23.86	23.97	23.73	24.08	24.02	23.68
105 min	23.13	22.20	23.31	23.50	23.62	23.34	23.72	23.68	23.34
120 min	22.91	21.99	23.06	23.22	23.35	23.04	23.42	23.40	23.07
135 min	22.68	21.74	22.73	22.91	23.06	22.74	23.18	23.12	22.78
150 min	22.48	21.62	22.53	22.70	22.85	22.52	23.02	22.92	22.59
165 min	22.32	21.51	22.31	22.50	22.68	22.31	22.80	22.72	22.40

180 min	22.15	21.36	22.14	22.32	22.50	22.14	22.60	22.53	22.23
195 min	22.01	21.28	22.00	22.18	22.36	22.01	22.49	22.40	22.10
210 min	21.94	21.15	21.88	22.08	22.24	21.90	22.41	22.30	21.99
225 min	21.79	21.07	21.79	21.99	22.13	21.83	22.35	22.22	21.91
240 min	21.71	21.09	21.73	21.95	22.10	21.76	22.24	22.17	21.86
255 min	21.61	21.02	21.68	21.90	22.05	21.72	22.19	22.11	21.81
270 min	21.55	20.96	21.61	21.83	21.98	21.66	22.17	22.05	21.75
285 min	21.54	20.94	21.59	21.81	21.93	21.63	22.17	22.02	21.73
average	23.21	22.76	23.59	23.71	23.78	23.61	23.83	23.84	23.59

Table A-0-22 Temperature readings during solidification for chamber with PCM full

PCM Full plus Windcatcher	Temperature, °C								
	Amb H1	In C8	Out E7	Lf Fr G4	Lf Bck F9	Rt Fr B6	Rt Bck D10	Rt Mid A5	Room Average
start	29.15	30.40	31.95	31.85	31.45	31.82	31.58	31.82	31.55
15 min	26.96	26.93	29.53	29.70	29.67	29.67	29.96	29.74	29.31
30 min	26.52	25.72	28.34	28.80	28.81	28.73	29.11	28.88	28.34
45 min	26.01	24.99	27.45	27.92	27.98	27.81	28.25	28.05	27.49
60 min	25.57	24.43	26.75	27.16	27.23	27.04	27.48	27.34	26.78
75 min	25.16	24.07	26.15	26.59	26.67	26.42	26.88	26.77	26.22
90 min	24.79	23.75	25.64	26.00	26.08	25.85	26.34	26.19	25.69
105 min	24.38	23.52	25.16	25.51	25.62	25.36	25.85	25.72	25.25
120 min	24.12	23.27	24.77	25.09	25.21	24.92	25.46	25.29	24.86
135 min	23.88	23.06	24.40	24.69	24.80	24.54	25.05	24.92	24.50
150 min	23.63	22.85	24.06	24.34	24.44	24.18	24.72	24.56	24.16
165 min	23.44	22.69	23.75	24.02	24.12	23.87	24.38	24.25	23.87
180 min	23.23	22.55	23.49	23.73	23.85	23.57	24.05	23.96	23.60
195 min	23.06	22.38	23.24	23.48	23.57	23.30	23.83	23.69	23.36
210 min	22.93	22.27	23.02	23.26	23.33	23.08	23.62	23.46	23.15
225 min	22.76	22.17	22.83	23.02	23.10	22.87	23.43	23.25	22.95
240 min	22.64	22.03	22.63	22.83	22.90	22.67	23.22	23.04	22.76
255 min	22.51	21.96	22.48	22.67	22.72	22.52	23.01	22.88	22.61
270 min	22.41	21.84	22.34	22.52	22.58	22.36	22.93	22.71	22.47
285 min	22.33	21.77	22.22	22.40	22.42	22.25	22.78	22.60	22.35
average	24.27	23.63	25.01	25.28	25.33	25.14	25.60	25.46	25.06

Table A-0-23 Temperature readings during solidification for chamber with PCM full plus windcatcher